Study of Vehicle Dynamics with Planar Suspension Systems (PSS)

by

Jian Jun Zhu

A thesis
presented to the University of Waterloo
in fulfillment of the
thesis requirement for the degree of
Doctor of Philosophy
in
Mechanical Engineering

Waterloo, Ontario, Canada, 2011

AUTHOR'S DECLARATION

I hereby declare that I am the sole author of this thesis. This is a true copy of the thesis, including any required final revisions, as accepted by my examiners.

I understand that my thesis may be made electronically available to the public.

Abstract

The suspension system of a vehicle is conventionally designed such that the spring-damper element is configured in the vertical direction, and the longitudinal connection between the vehicle chassis and wheels is always very stiff compared to the vertical one. This mechanism can isolate vibrations and absorb shocks efficiently in the vertical direction but cannot attenuate the longitudinal impacts caused by road obstacles. In order to overcome such a limitation, a planar suspension system (PSS) is proposed. This novel vehicle suspension system has a longitudinal spring-damper strut between the vehicle chassis and wheel. The dynamic performance, including ride comfort, pitch dynamics, handling characteristics and total dynamic behaviour, of a mid-size passenger vehicle equipped with such planar suspension systems is thoroughly investigated and compared with those of a conventional vehicle.

To facilitate this investigation, various number of vehicle models are developed considering the relative longitudinal motions of wheels with respect to the chassis. A 4-DOF quarter-car model is used to conduct a preliminary study of the ride quality, and a pitch plane half-car model is employed to investigate the pitch dynamics in both the frequency and time domain. A 5-DOF yaw plane single-track half-car model along with a pitch plane half-car model is proposed to carry out the handling performance study, and also an 18-DOF full-car model is used to perform total dynamics study. In addition to these mathematical models, virtual full-car models are constructed in Adams/car to validate the proposed mathematical models. For the sake of prediction of the tire-ground interaction force, a radial-spring tire model is modified by adding the tire damping to generate the road excitation forces due to road disturbances in the vertical and longitudinal directions. A dynamic 2D tire friction model based on the LuGre friction theory is modified to simulate the dynamic frictional interaction in the tire-ground contact pitch.

The ride quality of a PSS vehicle is evaluated in accordance with the ISO 2631 and compared with that of a conventional vehicle. It is shown that the PSS system exhibits good potential to attenuate the impact and isolate the vibration due to road excitations in both the vertical and longitudinal directions, resulting in improved vehicles' ride and comfort quality. The relatively soft longitudinal strut can absorb the longitudinal impact and, therefore, can protect the components. The investigation of handling performance including the steady-state handling characteristics, transient and frequency responses in various scenarios demonstrates that the PSS vehicle is directionally stable

and generally has comparable handling behaviour to a similar conventional vehicle. The application of PSS in vehicles can enhance the understeer trend, i.e. the understeer becomes more understeer, neutral steer becomes slightly understeer, and oversteer becomes less oversteer. The total dynamic behaviour combining the bounce, pitch, roll and the longitudinal dynamics under various scenarios such as differential brake-in-turn and asymmetric obstacle traversing was thoroughly investigated. Simulation results illustrate that the PSS vehicle has a relatively small roll angle in a turning manoeuvre. In some cases such as passing road potholes, the PSS vehicle has a better directional stability.

Acknowledgements

The author would like to thank his supervisor Professor A. Khajepour and co-supervisor Professor E. Esmailzadeh from UOIT for providing the opportunity for this research, for their continued intellectual guidance, encouragement and financial support throughout the course of this research.

The author would also like to express his gratitude to Professor M. Ahmadian of Virginia Tech for serving as his external examiner and valuable helps. The author also thanks his PhD committee Professor J. McPhee, Professor S. Lambert and Professor F. Ismail for their valuable suggestions, advices and comments on the research and this manuscript.

The author wishes to thank members of the faculty and staff of the Department of Mechanical & Mechatronics Engineering, University of Waterloo for their time and assistance during the course of this work. The author is thankful to all the friends and colleagues for their help and valuable discussion. Special thanks to his colleague, Mr. Alireza Kasaiezadeh for his help in the construction of Adams/car model in the dissertation research.

Financial support provided by Natural Sciences and Engineering Research Council of Canada (NSERC) postgraduate scholarship, Ontario Graduate Scholarship (OGS), University of Waterloo President's Graduate Scholarship, and Toyota Motor Manufacturing Canada (TMMC) fellowship are gratefully acknowledged.

The author would like to express his thanks for the patience, sacrifice and support to his wife who was pursuing her own study during the same time. Sincere thanks also go to the author’s father and other family member in China for their preserving support. Finally the author wishes to mention his sons whose innocents demand made this work somewhat tougher, but who provided a lot of enjoyment during the completion of the thesis.

Table of Contents

List of Figures

List of Tables

.

Chapter 1
Introduction

1.1 Introduction to Planar Suspension Systems

The suspension system of a road vehicle refers to the assembly between a vehicle chassis or body and a wheel (including axle), via which the forces and moments generated in the tire-ground contact are transferred to the chassis. Vehicle suspension systems are designed to provide satisfactory requirements of the ride, road-holding, handling and directional performance. Different types of suspension systems, such as MacPherson, double wishbone and multi-link suspensions, have been adapted in passenger vehicles to realize the above mentioned objectives [1]. A spring damper element is invariably implemented in the suspension design to isolate the vehicle chassis or body from vibrations and to absorb shocks. The spring-damper elements are mainly configured in a vertical direction, although a small side-view inclination angle may exist between the vertical direction and the spring-damper strut axis [1, 2]. This type of construction and configuration has remained substantially unchanged for the past century. Such a design is actually a one dimensional configuration because it generally provides isolation mainly in the vertical direction to attenuate shock forces and disturbances.

Excitation of vehicle vibrations arises mainly due to road disturbance, wheel non-uniformity, and unbalanced powertrain [3]. Among these vibration resources, road disturbances are the primary input of interest in designing suspension systems, but where the vehicle designers have the least control. In many situations, road disturbances can impose contact forces on a tire in different directions rather than merely the vertical one [3, 4, 5]. Forsen [4] measured the wheel forces of a tractor unit using an instrumented hub, and found that the longitudinal force variations could be of a similar magnitude as those in the vertical direction when traversing a short cleat. These forces are transferred to the body via a path “tire-suspension-chassis” and can, in turn, induce vibrations in more than one direction. Multi-directional force variations result in vibration and shock that cannot be attenuated effectively by the conventional suspension systems as these do not have elastic elements in non-vertical direction.

To improve the ride quality and reduce the noise level, attempt has been made to explore the idea of lowering the longitudinal stiffness of suspensions by the automotive industry. The multi-link

suspension system as well as the flexible link elevated compliance suspension (FLECS) developed by Magneti Marelli are the outcomes of such efforts [1, 6]. However, the longitudinal stiffness of the aforementioned suspensions is still considerably high compared to the vertical stiffness. The multi-link suspension system requires high production and assembly costs and has a great sensitivity to wear of the link bearings [1]. The soft longitudinal stiffness in these suspensions is generally realized by several types of bushings whose stiffness rate are difficult to estimate. In addition, void bushings are also employed in suspension design to increase the longitudinal elasticity. The stiffness of rubber bushings can change with time and, therefore, the design objective cannot be maintained during the entire lifespan of suspensions. Tilt side-view arrangement of suspension strut [2] as shown in Figure 1-1, is another attempt to reduce the longitudinal vibration. In this suspension design concept, the stiffness and damping in the vertical and longitudinal directions are highly coupled. The improvement of vibration isolation in the longitudinal direction may deteriorate that in the vertical direction. When passing over a relatively large road obstacle, a vehicle with such suspensions may not be able to provide enough shock absorption capacity in both the vertical and longitudinal directions simultaneously.

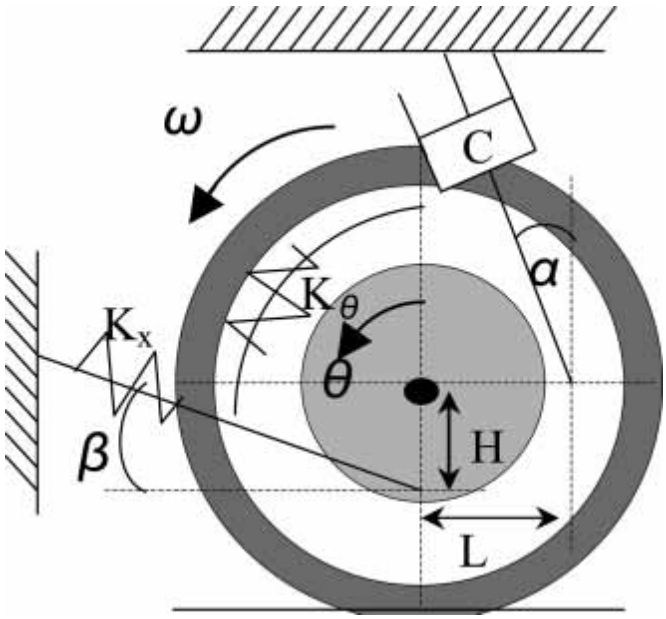

Figure 1-1: Tilt side-view arrangement of suspension strut [2]

In order to overcome the limitations of conventional suspensions in terms of shock absorption and vibration isolation along the longitudinal direction, we have proposed a novel planar suspension system (PSS) to improve the vehicle's dynamic behaviour. Its development is based on the idea that

the stiff longitudinal connection between the chassis and wheels is replaced by a nonlinear spring-damping strut so that the wheel can move 5~6 cm back and forth with respect to the chassis. While various implementation approaches could be possible, the implementation in this study is based on MacPherson suspension systems. Figure 1-2 illustrates the implementation of a planar suspension in a front MacPherson strut suspension and a rear dual-link MacPherson strut suspension. In the front planar suspension, a four- parallel bar mechanism is fixed to the upright of the conventional MacPherson suspension system. A longitudinal spring-damper strut is installed between the two diagonal ends of the four-bar linkage. The wheel hub is located at the center of one side of this linkage as shown. Such a mechanism can guarantee that the suspension longitudinal deflection is always within the wheel rotation plane. The longitudinal strut of front suspension can rotate about the kin-pin axis defined by the axis connecting the upper point of vertical strut and the outer point of control arm when steering operation is imposed. In the rear suspension, the rigid trailing arm is replaced by a spring-damper strut. In order to provide a good ability of vibration isolation as well as satisfy work space requirement under some conditions such as hard braking and quick driving, the longitudinal elasticity of the suspension is designed with such a characteristic that it is soft when the spring deflection is small, while very stiff when the spring deflection exceeds a certain value.

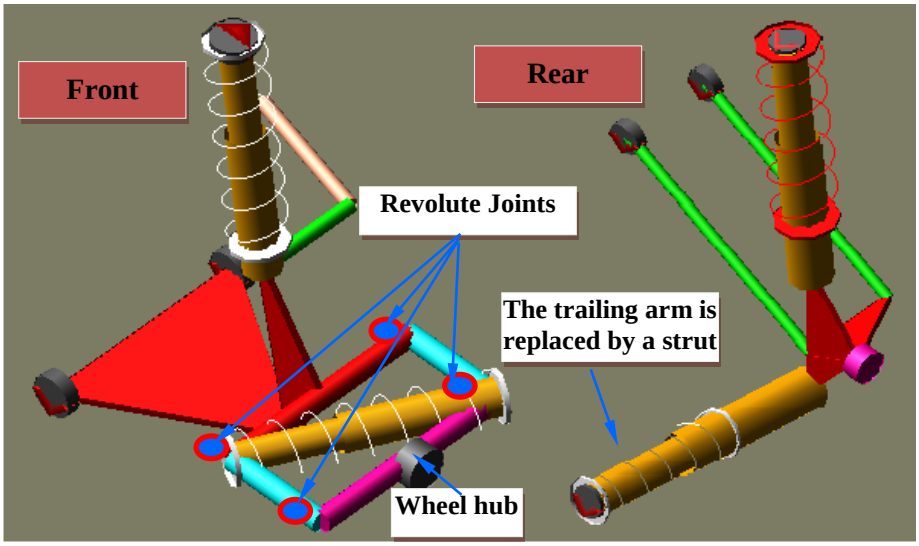

Figure 1-2: The realization of the planar suspension system

The planar suspension system (PSS) is a revolutionary concept that has the potential to increase comfort in many types of vehicles, including automobiles, trucks and off-road vehicles. It allows wheels to have vertical and longitudinal relative motions with respect to the vehicle chassis.

Therefore, the PSS is a two dimensional configuration. The longitudinal and vertical stiffness of a PSS system are rather independent of each other compared to other suspension concepts with low-longitudinal stiffness, such as the one shown in Figure1-1. It can be expected that a vehicle with such planar suspension systems can provide good ability to isolate vibrations and to absorb shocks induced by road irregularities in any direction within the wheel rotation plane. Especially for some off-road vehicles such as military vehicle which experience rough road condition at high speeds, the longitudinal impact and vibrations maybe a main concern for the health and ride comfort of the occupants. The PSS may provide a good prospective for these vehicles to improve the ride quality.

1.2 Objectives of the Dissertation Research

A PSS differs from a conventional suspension system, which has only a one-degree of freedom linkage mechanism along the strut axis, in that the PSS system comprises of two degrees of freedom, allowing the wheel to move in any direction within the wheel rotation plane. It is expected that the dynamic characteristics of a vehicle equipped with PSS will differ from those of a vehicle equipped with conventional suspension systems. Therefore, to explore its advantage or disadvantage and the feasibility of PSS concept, it is necessary to carry out a thorough investigation of the dynamic behaviour of a PSS vehicle. The scope of this dissertation research is to perform an in-depth study of the dynamic performance of a vehicle with PSS, including the ride quality for shock and vibration attenuation in both the vertical and longitudinal directions. Furthermore, the performance behavior for braking and acceleration, handling dynamics for directional control in steady-state and transient scenarios, vehicle stability and overall dynamics combining bounce, pitch, roll and yaw performance were investigated. This study will provide pivotal suggestions for the development of planar suspension systems.

The overall objective of this dissertation is to investigate the total dynamic characteristics of a vehicle equipped with PSS to explore the feasibility of this innovative concept. The possible implementations and detailed designs of a planar suspension system, however, is not the main focus of this study. A parallel dynamic study of a vehicle equipped with conventional suspension systems will also be conducted for the performance comparison between the PSS and the conventional suspension. The specific objectives of the research are:

- To develop a four DOF planar quarter-car model and perform preliminary ride comfort study. The responses of the chassis acceleration, suspension travel and road-holding capacity are investigated and compared with those of a conventional vehicle.

- To perform pitch dynamic study in both frequency and time domains. The frequency domain investigation is carried out using a linear 6-DOF half-car model accounting for motions in both vertical and longitudinal directions. The time domain study is conducted by a 9 DOF half-car vehicle model in cooperation with a nonlinear tire model. The transient friction between tires and road is taken into account. The responses are evaluated in accordance with ISO 2631 and compared with those of a conventional vehicle.
- To conduct the handling study and evaluate the directional behaviour of a PSS vehicle by studying the steady-state and transient steering response in terms of the yaw velocity and lateral acceleration based on a 11 DOF half-car handling model. A linearized study is also performed to explore the characteristics of handling response in the frequency domain.
- To investigate the traction/braking performance of a vehicle with PSS under some specific conditions such as differential braking, braking-in-turn and lane change. Comparison with a conventional vehicle is carried out.
- To develop an 18 DOF full-car vehicle model and investigate the total dynamics of a PSS vehicle, including the ride, performance, handling and roll characteristics. The dynamic behaviors of a PSS vehicle under some special conditions, such as differential braking and asymmetric road obstacles are investigated and compared with those of a similar conventional vehicle.
- To develop a virtual prototype of planar suspension system in Adams/car environment and implement the concept of PSS at the front and rear axles of a vehicle. The kinematics and compliances (K&C) analyses are carried out by several suspension analyses in Adams/car.
- To construct a full car model of a PSS vehicle in ADAMS and study the overall dynamic characteristics, including the ride quality, performance characteristics and handling behavior. The final investigation focuses on the vehicle acceleration response in both longitudinal and vertical directions, and the steering response to the steering input. The full ADAMS model would also be used to validate the proposed mathematic models.

1.3 Thesis Organization

This thesis consists of eight chapters. The present chapter is designed to introduce the basic features of the planar suspension systems, outline the overview, motivation and objectives of this research.

Chapter 2 presents a review of literature related to vehicle suspension design and vehicle dynamics. The fundamental issues, new achievements and the conventional models and approaches in the vehicle dynamic study are summarized. The new development in vehicle suspension design is also reviewed.

A preliminary study regarding the ride quality of a vehicle equipped with PSS is conducted in both frequency and time domains and presented in Chapter 3. A quarter-car model was developed and the longitudinal elasticity in the PSS is considered.

Chapter 4 presents the pitch dynamic study of the PSS vehicle. A linear pitch model with 6 DOF is proposed for the frequency domain study, and a nonlinear 9 DOF half-car model is developed to conduct the time domain investigation in the presence of isolated road obstacles and random road surface unevenness.

A model system, combining a half-car pitch plane model and a single-track yaw plane model, is developed in Chapter 5. This model, together with a dynamic 2D tire friction model, is employed to facilitate the handling performance study of the PSS vehicle. The steady-state handling characteristics of the PSS vehicle is investigated in this chapter following a general study of the tire-ground friction characters.

A thorough study of the handling performance for the PSS vehicle in frequency and time domains is presented in Chapter 6. The frequency and transient responses for various road maneuvers are predicted with different simulation conditions.

Chapter 7 presents the development of an 18 DOF full-car model and a virtual Adams/car model for the total vehicle dynamic study. The results from the two types of models are compared for validation. The overall dynamics, such as combined bounce, pitch, longitudinal and roll motions are investigated under various conditions.

The highlights and major conclusions drawn from this research together with recommendations for future work are finally presented in chapter 8.

Chapter 2
Literature Review

In general, the dynamic characteristics of a road vehicle may be described in terms of its ride comfort, performance characteristics and handling behaviour [7]. The formulation and analysis of the dynamic behavior of a vehicle with PSS require essential fundamental knowledge of various relevant subjects. These include inputs to a vehicle system from the road and driver's operation, the tire and ground contact mechanism, suspension design, ride comfort evaluation, handling control principle, vehicle stability requirement, and the vehicle modeling and simulation. The background materials related to these fields are reviewed in this chapter.

2.1 Automotive Suspension Design

The suspension design of a ground vehicle and its properties strongly influence a wide range of performance of that vehicle. Consequently, the suspension design plays a pivotal role in the dynamic performance of vehicles. The design of a road vehicle's suspension system is quite complex, since vehicles inevitably encounter a wide range of road conditions involving various surface roughness and discontinuities, loads and speeds. The ride and handling measures impose conflicting requirements for the suspension design [8, 9]. For a conventional vehicle, a soft and lightly damped suspension is desirable for attenuation and isolation of continuous vibrations arising from random road excitation. However, the interaction of the vehicle with abrupt road irregularities, such as bumps and potholes, requires relatively higher damping to suppress the induced oscillation. Satisfactory handling and directional control, on the other hand, require relatively hard and damped suspension [7]. The conventional suspension designs attempt to achieve a satisfactory comprise among these conflicting requirements.

The major objectives of the passenger vehicle suspension design were summarized by Sharp and Crolla [10]. The fundamental issues for heavy vehicle suspension design were reviewed by Cole [3], and the achievements in vehicle suspension design were presented by Ammon [11]. It is believed that ride comfort, suspension working space, road-holding capacity, directional controllability and stability, rollover stability, yaw stability, energy consumption, braking and traction are the main design criteria for a suspension system [3]. As discussed previously, these criteria impose conflicting requirements upon suspension design. Over the past several decades, a great deal of effort has been devoted to improving suspension design. Considerable improvements have been achieved through the

application of control techniques, which have been used in the development of controllable suspension systems, such as active and semi-active suspension systems [12-14]. Optimization was also widely carried out in vehicle suspension tuning to address many objectives and obtain a good compromise among the design criteria [15-18]. Advanced materials, such as electro rheological (ER) and magneto rheological (MR) fluids, were also used in the suspension system to achieve good stiffness and damping characteristics. New suspension mechanisms and configurations were also proposed to improve ride quality, enhance vehicle stability and reduce fuel consumption. Tilt side-view arrangement of suspension strut [2], as mentioned previously, is an attempt to improve the longitudinal ride quality. Maclaurin [19] developed a compound strut and planar six-bar linkage suspension to reduce kingpin axis offset and enhance control of camber angle change. To save the design space under the vehicle body, Carpiaux proposed an in-wheel suspension in which the spring and dampers are compact within the wheel rim [20]. It is notable that few of the published studies attempt a fundamental evaluation of the design alternatives. To date, research in the area has tended to focus on understanding and developing a single concept rather than on re-envisioning whole suspension design options.

According to [1], vehicle suspensions can be divided into three categories: (i) rigid axle suspensions with a rigid connection of the two wheels to an axle;(ii) independent wheel suspensions, in which the wheels are suspended independent of each other; and (iii) semi-rigid axle suspension, a form of axle that combines the characteristics of rigid axles and independent wheel suspensions. Among these suspensions, independent suspensions are the most widely used and well developed for ground vehicles as they can provide independent wheel motions, reduce the unsprung mass, and provide the possibility to lower the vehicle mass center, thereby improving the vehicle's stability [1].

2.2 Vehicles' Ride Comfort and Ride Dynamics

2.2.1 Ride Comfort Evaluation

The ride quality of a vehicle is concerned with the sensation of the passenger in a moving vehicle and is related to the vibration excited by the road surface irregularities. This vibration affects both the health and comfort of the vehicle's passengers. Numerous studies have been conducted in an attempt to establish ride comfort limits in terms of magnitude and frequency contents of vehicular vibration. The vibration exposure guidelines defined in ISO 2631 have been widely used to evaluate vehicle ride quality [21- 23]. Frequency weighted root-mean-square (RMS) acceleration is the basic evaluation

method provided by ISO 2631 and is frequently employed in vehicular ride quality assessments [17, 23]. ISO 2631 also provides additional vibration evaluation methods when the basic method is insufficient, such as the running RMS method and the fourth power vibration dose value (VDV) method. Running RMS method takes into account occasional shocks and transient vibration by use of a short integration time constant. VDV method is more sensitive to peaks than the basic evaluation method. VDV sometimes is used in vehicular ride evaluation [15, 23].

The Society of Automotive Engineers' manual describes the vertical vibration comfort limits for road transportation systems in relation to Janeway's comfort criterion, which is based on the data for sinusoidal vibration of a single frequency. This comfort criterion specifies the limits in terms of peak jerk, which is referred to as the third order derivative of displacement with respect to time, peak acceleration and peak velocity, as [24, 25]: peak jerk not greater than 12.6 $m.s^{-3}$ for frequency not greater than 6 Hz; peak acceleration not exceeding 0.33 $m.s^{-2}$ for frequency greater than 6 Hz but not exceeding 20 Hz; peak velocity not exceeding 0.0027 m/s for frequency in the range of 20 ~ 60 Hz. These limits can be used to establish the comfort zone in terms of peak acceleration responses as a function of the frequency. It is evident from this function that the human body is most sensitive to vertical vibrations in the 4 to 8 Hz frequency range [25]. This can serve as one of the design requirements for the vehicle suspension system. Extensive studies have shown that the body or sprung mass natural frequency of bounce motion is around 1Hz for modern vehicles and the unsprung bounce natural frequency is about 10Hz. This confirms that the natural frequency is outside the frequency range to which the human body is most sensitive.

The ride diagram is another ride comfort evaluation method proposed by Strandemar and Thorvald [26] as a novel method for truck ride evaluation. The basic idea is to separate the transient accelerations from the stationary vibrations in order to present a more complete image of the nature as well as the severity of driver vibrations. This is done using an algorithm where the acceleration time history is divided into segments based on sign changes in the time derivative. The segments are then classified as either "transient" or "stationary" segments, depending on whether peak-to-peak changes exceed the RMS value of the entire measuring period. The root mean square value of each segment is computed and the values in each category are summed to obtain a "transient" value and a "stationary" value.

Rauh [27] summarized the development of ride comfort and handling for advanced passenger vehicles. Most of the reported literatures only took into consideration the vertical vibration in the ride

comfort assessments, although ISO suggests that vibrations along multiple axles should be taken into account [21, 28]. Recently, attention has been paid on the role of the vibrations in the non-vertical directions in the passenger comfort. Attempts have been made to reduce the longitudinal vibration transmitted to passengers [2, 29]. However, these attempts are very preliminary and no significant improvement has been reported.

2.2.2 Road Irregularity Description

Since vehicular vibrations influencing ride comfort are mainly induced by the road surface irregularities, it is necessary to establish the description of a road profile as an input in the ride comfort evaluation of automobiles. Road irregularities are described in terms of the elevation profile along the wheel path. For in-plane vehicle vibrations, road irregularities can be exhibited in the form of either isolated abruptness or distributed random unevenness.

Isolated road abruptness refers to bump and pothole, and is always described by a half-wavelength sinusoidal function with respect to the position along the road. This description plays an important part in the study of vertical vibration for a vehicle system. A single road obstacle can induce not only tire-ground impact which is very damageable to vehicle components and annoying to passenger's comfort, but also can induce roll motion and disturb the vehicle moving direction. Therefore, such a type of road irregularity is frequently used in the optimization of suspension configuration design [18], control design [18], ride comfort studies [30] and roll stability investigation [52]. The excitation frequency of the sinusoidal description is proportional to the vehicle forward speed and inversely proportional to the wavelength. The profile in terms of the elevation of a road obstacle is expressed mathematically as [25]:

$$z = Z_o \sin(\frac{2\pi}{\lambda} x) = Z_o \sin(\frac{2\pi}{\lambda} vt) \tag{2.1}$$

where z is the elevation of the road surface at an arbitrary position (x); Z_o is the amplitude or height; λ is the wavelength of the obstacle; and v is the forward speed of the tire.

While the road profile description in the form of an isolated irregularity could provide a basis for comparative evaluation of various designs, it could not serve as a valid basis for studying the actual ride behavior since surface profiles are rarely of simple forms. With the improvement of measurement technologies, more and more in-dept studies of road profiles have been undertaken by both on-road measurements and theoretical studies [31]. The random characteristic of road surfaces is believed to

be statistically stationary; therefore, the characteristics of an entire road can be represented by a portion of the road surface [7]. The statistic properties of the surface profile in a vertical plane are often assumed to be the same as those in any parallel plane. In other words, the random characteristic is ergodic [7]. These two points can simplify the description of road profile significantly. One of the most widely used road representations is the Power Spectral Density (PSD) function, which plots road unevenness amplitudes versus spatial frequency. In vehicle dynamic studies, there are many approaches defining the PSD of road profiles [7, 25, 32]. The most popular and most easily understood approach is given by Wong [7]. ISO provides a standard of classification of road roughness in terms of PSD, such as very good (A), good (B) and average (C) road classes. Road profile measurement is a fundamental approach to acquire the necessary data for vehicle dynamics investigation, and therefore is frequency conducted by the research institutes and automotive industry [31, 33].

The representation of road roughness by PSD is readily used in ride studies in the frequency domain [17, 18]. However, this kind of description cannot be used in the time domain when random input is necessary. Approaches for generating a sample of random inputs in terms of profile elevation are proposed in [15, 34, 35]. Modeling and simulation using generated random road profiles as input can provide a relatively intrinsic understanding of the vehicle dynamic behaviors.

2.2.3 Vehicle Modelling

Computer modeling and simulation play an important role in the study of vehicle dynamics. A great number of models, from simple to complex, have been proposed to investigate vehicle dynamic behavior. The vehicle models integrate various components of the vehicle, namely, the vehicle body or chassis, wheels and the suspension system. The reported models also range from simple one-dimensional (1-D) model representations to highly complex three-dimensional (3-D) formulations.

Despite extensive use over many years, the two-mass quarter-car model continues to be a useful tool for understanding the basic vibration behavior of vehicle suspensions. In the present, a quarter-car model is frequently used in suspension control design [13, 36, 37], comfort evaluation [38] and suspension parameter optimization [18]. The quarter-car model can be used to study the basic vibration characteristics of a vehicle, such as natural frequency and mode shape, and to predict the bounce response for both the chassis and wheel. However, this model is too simple to predict the real response of a car to road excitations in non-vertical directions. Coupling between left and right, and front and rear wheels cannot be investigated by quarter-car models.

Half-car pitch plane models with either 2-DOF or 4-DOF have been widely used to investigate vehicle pitch dynamics. The 4-DOF half-car pitch plane model can predict the bounce response of the wheels and chassis as well as the pitch response of the chassis [39, 42], while the 2-DOF half-car pitch plane model can only predict the pitch and bounce response of the chassis [25]. Because the reported studies state that the human body is more sensitive to pitch motion [7], ride comfort evaluation based on half-car pitch plane models may result in an assessment that more accurately reflects the feeling of the human body. High order half-car pitch models were also occasionally reported in the literatures. A 7-DOF model proposed by Steven and Liu [40] takes into account the vertical, longitudinal and pitch motions of sprung mass, the vertical and spin motions of the front and rear wheels. This model was used to carry out vehicle suspension and performance evaluation. Another 7-DOF model proposed by Ju and Lin [41] takes into account the vertical, longitudinal and pitch motions of sprung mass, the vertical and longitudinal motions of the front and rear wheels. This model was employed to analyze vehicle–bridge dynamic interactions due to vehicle braking and acceleration.

Single-track or bicycle yaw-plane model is another type of half-car model used to study the handling performance of a vehicle [43, 44, 45, 46]. The simplest yaw-plane half –car model is a 2-DOF handling model in which the lateral and yaw motions are taken into account on the assumption that the vehicle forward velocity is constant or the longitudinal acceleration is very small [43, 44, 47]. The commonly-used vehicle model for handling study has 3 DOFs. Such a model can account for the longitudinal, lateral and yaw motions of vehicle [45, 48], but neglects the tire mass (unsprung mass) and cannot model the relative longitudinal motions between the chassis and tires of a PSS vehicle. The effect of suspension property and the roll motion on the handling performance is also neglected.

A great deal of effort has been devoted to developing complex models. Bouazara *et al.* proposed a 3-D full-car model to study vehicle safety and comfort, in which the vertical, pitch and roll motions were taken into account [49]. The finite element (FE) approach was employed to develop a full-car model in which the chassis is regarded as a plate. High frequency vibrations can be investigated using such kind of models; however, the computation cost is very expensive because of the large scale of DOFs [30]. Kim and Ro proposed an accurate full-car ride model using model reducing techniques [50]. This approach involves linearization of a full-car multibody dynamics (MBD) model to obtain a large-order vehicle model. In order to simplify the simulation, the states of the model are divided into two groups (i.e. ride and handling) depending on their effects on the ride quality and handling

performance. The singular perturbation method is then applied to reduce the model size. Most models focus on the vertical motion in ride comfort studies; however, fewer models take longitudinal motion into account. As an exception, S. L. Koo e*t. al*. [51] developed a simple longitudinal vehicle model to study the effect of longitudinal dynamics on ride quality. In this model, a fixed pitch center is assumed such that the vehicle body has a pure pitch motion with respect to the unsprung mass.

The simple full-car model is a 6-DOF model which neglects the effect of wheels and suspension systems [52, 53]. An 8-DOF model, which has 4 DOFs for the chassis velocities (longitudinal, lateral, roll and yaw) and one DOF at each wheel representing wheel spinning dynamics [54, 55,56], ignores the effect of suspension and wheel mass. The most upper order full-car model reported in literatures is the 14-DOF model which can predict vehicle pitch and heave motions [57, 58, 59], but cannot model the relative longitudinal motions between the chassis and wheels. Up to date, it is difficult to find an analytical full-car model in the reported literatures which takes into consideration the effect of the suspension longitudinal compliance although some commercial software package such as Adams/car has such a function. An important point should be mentioned is the introduction of roll center in the development of full-car models. While very few models do not contain the roll center [57], most 14-DOF full-car model take into consideration the effect of vehicle roll center [58, 59, 60]. Recently, with the development of computational technology, the commercial software packages based on multibody dynamics, such as Adams, MapleSim, CarSim and MotionView, have continuously developed for vehicle dynamic modeling and simulation. These packages provide more accurate and fast tools for the vehicle dynamics investigation, and thus widely used in the research and development of auto-industry [61-65].

In the modeling and simulation of vehicle dynamics, an issue regarding non-linearity is often involved, regardless of the type of model used. Non-linearity mainly arises due to the damping element in the suspension system and the tire-ground contact. However, other factors, such as friction and elasticity in the compliance and linkage of suspension, may also induce nonlinearity. As one main improvement, advanced control technologies are applied to the vehicle suspension system to satisfy the conflicting design requirements. For example, the damper is always designed such that it has a large damping coefficient in the extension stroke but a small damping coefficient in the compression stroke [66]. Also, dampers usually exhibit piecewise linear behaviour [25]. Such nonlinearity should be taken into consideration by using an appreciative model when high simulation accuracy is required.

2.3 Pitch Dynamics of Automobiles

While the bounce and roll dynamics of passenger vehicles have been extensively reported in the literature, relatively few studies have explored the pitch dynamic responses. The lack of a significant amount of study in this area may be due to the relatively small wheelbase of passenger cars. However, it is reported that the human body is more sensitive to pitch motion than bounce [7, 67, 68]. To a great extent, the pitch motion of a vehicle significantly influences the entire dynamic performance, which includes the ride, handling, suspension stroke and dynamic tire loads. This level of influence is partially attributed to the coupling between the vertical and pitch motions. Furthermore, the pitch motion can cause longitudinal dynamic motion of the vehicle in cases where the mass center of chassis is not located at the middle point of wheelbase. Passenger cars are generally designed to achieve a front/rear load distribution ratio and dynamic index (k^2/ab) close to unity [7, 67], where k is the radius of gyration of the sprung mass in pitch, and a and b are the longitudinal distances from the center of gravity (c.g.) to the front and rear wheel centers, respectively.

Wheelbase filtering is a unique phenomenon of vehicle pitch dynamics and is an important topic in frequency domain study. Wheelbase filtering refers to the correlation between front and rear excitation, which has received a significant amount of attention in vehicle pitch studies [21, 39, 68]. Wheelbase filtering takes place when a two-axle vehicle follows a path and both sets of wheels (i.e. front and rear) pass over the same road unevenness but at different times. The excitation of the rear wheel is the same as that of the front wheel but there is a time delay that is proportional to the wheelbase and inversely proportional to the speed. To minimize pitch motion, it has been suggested that the equivalent front and rear suspension should be designed such that the natural frequency of the front end of the vehicle is slightly smaller than that of the rear end [7]. This smaller natural frequency at the front end would ensure that both ends of the vehicle move in phase within a short time after the front end is excited and the vehicle merely bouncing. The study conducted by Sharp [39] illustrates this point. Sharp's results indicate that any pitching excited by the front axle input is largely cancelled by the response to the rear axle input at high speed.

Pitch dynamic study plays an important role in vehicle design activity due to the use of suspension tuning for minimizing motions in pitch. Sharp [39] stated that such tuning can bring a marked advantage in pitch suppression with very little disadvantage in terms of body accelerations. Odhams and Cebon [69] performed a tuning of a pitch-plane model of a passenger car with a coupled

suspension system. The results of this work implied that pitch tuning can lead to optimal suspension parameters that can suppress pitch motion.

2.4 Handling and Directional Stability

The handling performance of a ground vehicle refers to its response to a driver's steering commands and environmental inputs. The driver's steering commands are in the form of the tire steering angle, which is controlled by the steering wheel and other mechanisms. Environmental inputs involve the lateral force exerted on the vehicle by wind and road disturbances. There are two basic issues in vehicle handling: directional control and directional stability. The first issue concerns the vehicle's response in terms of yaw velocity and lateral acceleration to the steering input. The second issue refers to the ability of a vehicle to stabilize its direction of motion against external disturbances [7].

Directional control concerns the motion response of a vehicle to the driver's maneuvering. There has been a great deal of studies into the vehicle's handling characteristics under steady-state conditions [70, 71] and in transient periods [72-76]. The understeer coefficient, K_{us}, is an important variable used to describe the steady-state handling characteristics and defined as:

$$K_{us} = \frac{W_f}{C_{\alpha f}} - \frac{W_r}{C_{\alpha r}} \tag{2.2}$$

where W_f and W_r are the front and rear vertical wheel loads, respectively; $C_{\alpha f}$ and $C_{\alpha r}$ are the front and rear concerning stiffness, respectively.

There are three types of behaviors associated with steady-state handling characteristics: (i) understeer with an understeer coefficient greater than zero; (ii) neutral steer with an understeer coefficient equal to zero; and (iii) oversteer with an understeer coefficient less than zero. Among these three types of behaviors, oversteer is the least desirable from the directional stability point of view. It is considered desirable for a road vehicle to have a small degree of understeer up to a certain level of lateral acceleration (such as 0.4g) with increasing understeer beyond this point [8]. A handling diagram is a well-known tool for evaluating steady-state handling characteristics using the slope of the curve which is associated with the understeer coefficient. Frendo e*t. al* stated that such a definition of understeer coefficient may be inadequate, and proposed a new concept of handling surface together with a new definition of understeer gradient, which is the gradient of the handling surface and therefore, a vector [48]. Specific values of K_{us} may be calculated by the dot product of **w** and **t,** which represent the understeer gradient vector and the direction vector of a specified handling

curve, respectively [48, 77]. The reported study shows that the roll motion can induce the lateral wheel load transfer and, therefore, can influence the understeer coefficient due to wheel load transfer causing nonlinear lateral wheel forces [48]. Chu and Jones proposed a criterion to demonstrate how handling behavior is changed in the high lateral acceleration region. This criterion accounts for the effect of roll stiffness ratio, tire cornering stiffness and tire property coefficients [74].

Transient response characteristic is another major interest in handling studies. It is referred to as the period between the application of the steering input and the attainment of steady-state motion. The desired transient behavior is that the response approaches the steady-state motion within a minimum time and oscillation. The study of the transient handling response requires an appropriate vehicle model. A popular model is a half-car bicycle handling model in which it is assumed that the two tires in the front and the rear have same properties [78]. This model can provide a basic understanding of the transient response of vehicle motion to the steering input, but cannot account for the wheel load lateral transfer and the influence of roll motion. A more realistic vehicle handling model generally includes: a handling model to predict handling responses, such as lateral acceleration and yaw velocity; a tire model to predict lateral and longitudinal tire force; and a vehicle model to model the vehicle motions necessary to predict the force terms [48, 77]. However, such a model can be highly nonlinear and prohibitively expensive in computational cost. Another approach to investigate the transient handling response is handling tests. The objectives of these tests in the majority of the reported literature focus on the yaw rate and lateral acceleration response to step or sinusoidal steering input. Handling tests were also conducted by some researchers to identify physical parameters, such as concerning stiffness, which are difficult to obtain [79].

Another issue is directional stability, which concerns the ability of a vehicle to return to its original state after a short perturbation. It can be demonstrated that a vehicle is always directionally stable when it has understeer characteristic; however, when in the state of oversteer, the vehicle is directionally stable only when the speed of the vehicle is under a critical speed [7].

A few studies in frequency domain have been reported on vehicle handling performance [61, 98, 99]. Starkey [98] conducted a frequency domain investigation to study the effect of vehicle design parameters on the handling response characteristics. Xia and Law [99] performed a linearized analysis of handling qualities to investigate front wheel and four wheel steering handling behaviour. All these reported frequency analysis of vehicle handling behaviour is based on the assumption that

the front and rear tires are rigidly attached to the chassis and cannot move backward and forward with respect to the chassis.

2.5 Tire Modelling

Tires are key components of a vehicle and function to support the vehicle body; cushion the vibration and shock from the road surface irregularities in cooperation with suspension; and generate driving, braking, and lateral force and moment for cornering. Most vehicle tires are pneumatic tires, while some are solid. With the exception of the aerodynamic force applied to the vehicle body at high speed, all external forces and moments are generated by tire-ground contact. Therefore, an appropriate and effective tire model for the description of tire-ground interaction is crucial in the vehicle dynamic modeling and simulation in order to obtain accurate simulation results. Rauh and Mössner-Beigel [92] presented an overview on the most challenging tasks of today and tomorrow for tire simulation success in complete vehicle environments. Lutz *et al.* summarize the tire modeling requirements and model categories [78]. The selection of a tire model is dependent on the purpose, condition or assumption and accuracy requirement of the simulation.

The interaction between a tire and a road mainly refers to two aspects. One is the elastic deformation which contributes to the tire-ground contact force passing through the tire center. An appropriate approach to model this aspect of tire-ground interaction is the fundamental of durability analysis [80, 93]. When tire runs on a flat road, the contact force only has a vertical component. When tire runs on an uneven road, the contact force has a vertical and a longitudinal component. Another aspect is the tire-ground friction which contributes the lateral and longitudinal friction forces when a relative slip exists in the contact patch. The tire-ground friction forces are attributed to hysteresis and adhesion according to [67]. An accurate prediction of the friction force is the basis of vehicle performance and handling study.

In the modeling of tire-ground interaction due to elastic deformation, a linear point tire-ground contact model is simple and widely-used in ride comfort studies. This model assumes that the vertical tire load is proportional to tire deflection. However, the linear point tire-road contact model cannot predict the contact force in the longitudinal direction when the wheel passes over uneven roads. According to drum tests and computer simulations, tire elasticity is non-linear. The tire-ground contact patch can also develop non-vertical components in case of the existence of road discontinuities. The linear point model is inaccurate for short wavelength road unevenness. Therefore,

many kinds of in-plane nonlinear tire models have been proposed [81-85]. The radial spring tire model is a frequently used nonlinear model that assumes that the tire deflection only occurs in a radial direction and does not account for shear deformation along the circumferential direction [97]. This model can predict the vertical and longitudinal contact force with good accuracy [81], but cannot account for other important factors, such as air pressure of a pneumatic tire and shear deformation in a tangential direction. The rigid ring tire model has a low computational cost and takes into account air pressure and side wall stiffness. It can be used to simulate tire-ground contact in cases of short wavelength unevenness. However, this model needs the effective road plane elevation, effective forward slope of the road plane and the effective rolling radius as inputs [82]. These effective values are not easily obtained in the case of road irregularities. The flexible ring tire model does not require the above mentioned effective inputs in advance, but it is very time-consuming in computation [82]. Other in-plane tire models were also developed. Harth proposed an in-plane tire-obstacle interaction model based on the assumption that the vertical tire behavior depends fundamentally on air contained in the tire, while other factors, such as tire structure, bending membrane effect, *etc*, are negligible [83]. Kim e*t al*. developed a two-dimensional tire model that is composed of a rigid ring, a 6-DOF spring/damper element, a static circular beam, and residual springs in the radial direction [84]. This model can be used for ride or impact simulations as well as for general handling simulations; however, it requires a number of parameters which are not easily verified. The FE model was also developed to account for tire behavior in the vertical plane [85].

The second aspect in tire modeling is how to predict friction forces. Generally, the friction can be only along the longitudinal direction in braking and traction operation, or along both the longitudinal and lateral direction. It is a tough task to simulate the tire-ground adhesion or friction behaviour. Through the decades, numerous tire-ground friction models have been proposed [86- 88]. A very popular theory states that the relationship between tractive (or brake) effort and slip (or skid) is linear when there is a small slip (or brake skid) but non-linear when the slip (or skid) exceeds a critical value. This theory is presented by Wong [7] in *Theory of Ground Vehicles*. Another popular model is the Magic Formula presented by Pacejka [88, 89]. This model is actually an empirical formula used to describe the relationship between longitudinal/cornering forces and slip (skid)/cornering slip angle. The short wavelength intermediate frequency tire (SWIFT) model is another famous model that can predict the longitudinal slip force [90]. This model features a rigid belt ring in cooperation with the Magic Formula. Gipser [91] developed a flexible ring tire model (FTire), which is widely used and generally accepted today for ride comfort, handling, and road load prediction. This model mainly

serves as a sophisticated force element in multi-body systems (MBS) and finite element (FE) environments and can be used to predict the vibration along all three directions up to about 150 Hz [91]. However, most of these models are essentially static models and only represent rather artificial "curve fitting" procedures to experimental data, but do not interpret the physiological phenomena that give rise to the friction forces and moments. The literature implies that the steady state condition is rarely true in reality, especially when the vehicle passes through continuous successive states during cornering and acceleration/braking maneuvers. Dynamic models, on the other hand, can capture transient effects and are of interest when a vehicle is under large variations of states. Thus, a number of dynamic tire-ground friction models have been proposed [86, 87], but few of them are reported to be applied in the vehicle dynamics simulation. Among these models, the 2D Average Lumped LuGre model, in which the distribution properties of a normal contact force in the contact patch is taken into account, is a good representative. This model is proposed recently by Velenis *et al* [87] to describe the longitudinal/lateral friction forces between tires and ground with good accuracy and less computation-cost in the dynamic state.

In this chapter, the necessary background for the vehicle dynamics study is reviewed. From next Chapter, the dynamic study of a vehicle with planar suspension will be carried out with different models, from a simple quarter-car model to a complex full-car model.

Chapter 3
Study of Ride Dynamics

3.1 Overview

The ride dynamics of a ground vehicle deals with the vibration excited by road surface irregularities and its effect on passengers. As discussed in the previous chapter, the ride comfort evaluation methods provided by ISO 2631 state that the human body is sensitive to vibration acceleration and frequency [28], which are usually obtained by either computer simulation or real-time measurements. Simulation models have evolved from simple models, such as a quarter-car model, to complex ones, such as full car and FE vehicle models. Among these models, the quarter-car model continues to be a useful platform for understanding the basic vibration behavior of a vehicle and for evaluating the ride comfort [13, 36-38].

The unique mechanism and configuration of a PSS system have a special feature of the longitudinal connection. It can be expected that the ride dynamics of a PSS vehicle can be quite different from that of a conventional vehicle. Therefore, the ride dynamics of a vehicle with PSS will be preliminarily investigated using a quarter-car model. The commonly-used quarter-car model cannot predict the motion in vehicle heading or longitudinal direction and, therefore, cannot be applied to the modeling of a PSS vehicle directly. A new planar quarter-car model with 4 DOFs is therefore proposed to predict the motion responses in both the vertical and longitudinal directions. The ride dynamic study will be conducted in both frequency and time domain. The results of this study will be compared with those of a conventional vehicle.

3.2 Analysis and Comparison with a Conventional Vehicle in the Frequency Domain

In this study, the model is based on the front part of a mid-size conventional passenger car, as described in reference [25], and its parameters are listed in Table 3-1. The suspension vertical elasticity of a PSS system is identical to that of a conventional vehicle so that the vertical dynamics of the two types of vehicles are similar. To provide a good capability of vibration isolation as well as to satisfy work available space requirement under some conditions such as hard braking, the longitudinal springs are designed with such a characteristic that it is softer when the spring deflection

is small while it is stiff when the spring deflection reaches a certain value, for example, 5~6 cm. The suspension longitudinal force is determined by the following equations:

$$F = \frac{k_o}{d_r^2}\Delta x^3 + k_o \Delta x \tag{3.1}$$

$$k = \frac{dF}{d\Delta x} = 3k_o\left(\frac{\Delta x}{d_r}\right)^2 + k_o \tag{3.2}$$

where k is the dynamic spring stiffness which is state-dependent, and Δx is the spring deflection; d_r is a parameter to control the upper bound of the spring deflection; k_o is equal to the corresponding vertical spring stiffness ($k_{sf(r)}$) of a planar suspension system, and F is the spring force. Figure 3-1 illustrates the nonlinear spring characteristics with ko = 20 kN/m and d_r = 5 cm.

Table 3-1: Parameters of conventional vehicle (mid-size car) [253]

Total Mass (kg)	Tire Mass (kg)		Suspension vertical stiffness k_s (kN/m)		Suspension damping coefficient c_s (kN.s/m)		Tire stiffness k_t (KN/m)	Tire damping coefficient c_t (kN.s/m)
	Front	Rear	Front	Rear	Front	Rear		
1150	57/2	47.6/2	35.7/2	23.8/2	3.311/2	2.207/2	175	0.5

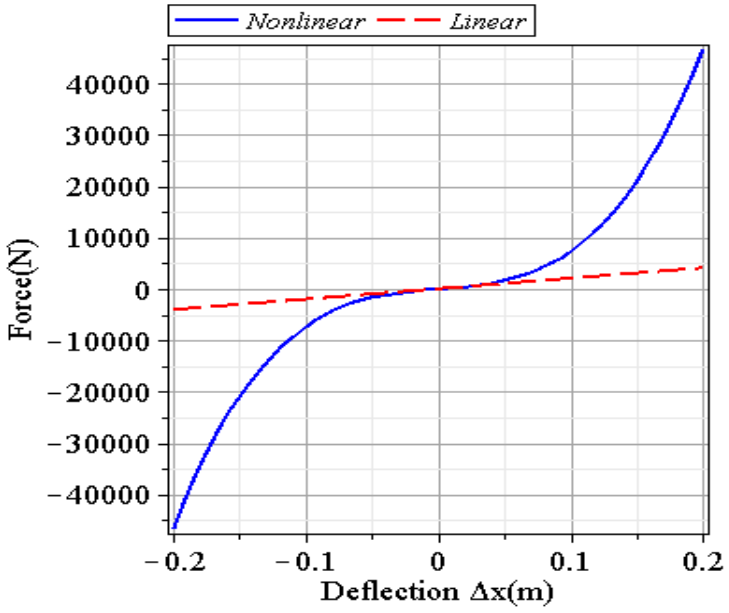

Figure 3-1: Nonlinear longitudinal spring characteristics

3.2.1 Quarter-Car Vehicle Model

In this study, a planar linear quarter-car vehicle model combined with a linear point tire-ground contact model is firstly proposed for the frequency domain study. The vehicle system is modeled as two independent subsystems in the vertical and longitudinal direction.

The proposed linear quarter-car model is illustrated in Figure 3-2. The vehicle chassis is modeled as sprung mass, which includes the mass of wheel axle. The wheel is represented by unsprung mass. Sprung and unsprung masses are connected by a vertical spring-damping element (k_s, c_s) and horizontal spring-damping element (k_{ls}, *cls*). The tire-ground contact is modeled as an unsprung spring-damping element (k_u, c_u). The longitudinal connection between the tire and external excitation is assumed to be very rigid and is represented by a very stiff spring element (k_{lu}). It is assumed to be 10 MN/m. The quarter-car model is formulated as a 4-DOF dynamic system including: the bounce (z_s) and the longitudinal motion (x_s) of the chassis (sprung mass), and the bounce (z_u) and the longitudinal motion (x_u) of the wheel (unsprung mass).

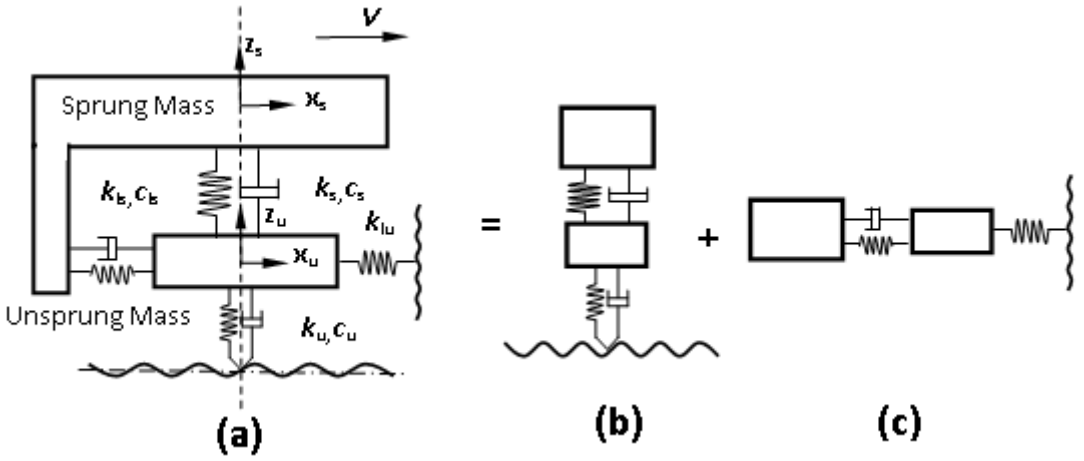

Figure 3-2: Quarter car model with PSS suspension

This study assumes that this quarter-car model (Figure 3-2(a)) is a superposition of two independent systems (Figure 3-2 (b) and (c)). There is no coupling between the two independent systems. This assumption is only used for comparison between a PSS vehicle and a conventional vehicle. The nonlinearity of the longitudinal suspension imposes a difficulty on the frequency analysis. In order to overcome such a difficulty, the longitudinal spring is linearized at the point where there is no longitudinal deflection. The longitudinal stiffness at this point is k_o, which is

assumed as same as the vertical stiffness. The system represented by Figure 3-2 (a) thus becomes a linear system.

The equation of motion for the vertical motion is as follows:

$$\begin{bmatrix} m_s & 0 \\ 0 & m_u \end{bmatrix}\begin{Bmatrix} \ddot{z}_s \\ \ddot{z}_u \end{Bmatrix}+\begin{bmatrix} c_s & -c_s \\ -c_s & c_s+c_u \end{bmatrix}\begin{Bmatrix} \dot{z}_s \\ \dot{z}_u \end{Bmatrix}+\begin{bmatrix} k_s & -k_s \\ -k_s & k_s+k_u \end{bmatrix}\begin{Bmatrix} z_s \\ z_u \end{Bmatrix}=\begin{bmatrix} 0 \\ c_u \end{bmatrix}\dot{z}_o+\begin{bmatrix} 0 \\ k_u \end{bmatrix}z_o \tag{3.3}$$

And the equation of motion for the longitudinal motion is as follows:

$$\begin{bmatrix} m_s & 0 \\ 0 & m_u \end{bmatrix}\begin{Bmatrix} \ddot{x}_s \\ \ddot{x}_u \end{Bmatrix}+\begin{bmatrix} c_{ls} & -c_{ls} \\ -c_{ls} & c_{ls}+c_{lu} \end{bmatrix}\begin{Bmatrix} \dot{x}_s \\ \dot{x}_u \end{Bmatrix}+\begin{bmatrix} k_{ls} & -k_{ls} \\ -k_{ls} & k_{ls}+k_{lu} \end{bmatrix}\begin{Bmatrix} x_s \\ x_u \end{Bmatrix}=\begin{bmatrix} 0 \\ c_{lu} \end{bmatrix}\dot{x}_o+\begin{bmatrix} 0 \\ k_{lu} \end{bmatrix}x_o \tag{3.4}$$

where z_o and x_o are the vertical and longitudinal components of the road excitation, respectively, and are assumed to be independent with each other. In equation (3.4), the damping coefficient, c_{lu}, is zero.

3.2.2 Analysis of Response to Frequency Input

The transmissibility (gain) is defined as the ratio of the magnitude of response to the magnitude of road excitation. The derivation of the transmissibility will take the vertical motion for example. The transmissibility for longitudinal motion can be obtained in the same way. The transfer function, taking the vertical direction as example, can be derived from equations (3.3).

Equation (3.3) can be re-written in the following form:

$$M\ddot{Z}+C\dot{Z}+KZ=Z_o \tag{3.5}$$

where M, C and K are mass, damping and stiffness matrix, respectively, and Z is the response vector and Z_o is the input vector. Assuming the road excitation is sinusoidal, i.e. $z_o e^{i\omega t}$, then Z_o can be written as:

$$Z_o=\begin{bmatrix} 0 \\ c_u \end{bmatrix}\dot{z}_o+\begin{bmatrix} 0 \\ k_u \end{bmatrix}z_o=\begin{bmatrix} 0 \\ i\omega t c_u+k_u \end{bmatrix}z_o e^{i\omega t} \tag{3.6}$$

The following equation can then be obtained from equation (3.5):

$$Z(\omega)=\left[-\omega^2 M+i\omega C+K\right]^{-1}\begin{bmatrix} 0 \\ i\omega t c_u+k_u \end{bmatrix}z_o(\omega)=Hz_o(\omega) \tag{3.7}$$

where H is the displacement response transfer function matrix. The transfer function for acceleration response is as follows:

$$H_{acc}(\omega) = -\omega^2 H(\omega) \tag{3.8}$$

In fact, the proposed model and analysis method can also be applied to a conventional vehicle because there always exists a longitudinal connection (i.e. trailing arm or joints) between the suspension and the chassis, as shown in Figure 3-3. This type of connection is always implemented by joints with robber bushings, which can transmit longitudinal motion and forces, and can be treated as a longitudinal spring element with a very large stiffness. The reported studies state that, for a conventional suspension, the longitudinal stiffness, which is provided generally by bushing stiffness, is approximately 20~50 times that of the suspension vertical stiffness [95, 96]. The value of k_{ls} for the conventional vehicle is assumed to be 30 times that of the vertical one in the present study. The longitudinal damping for the conventional vehicle is due to the rubber elements and friction in the linkages. Its coefficient is assumed to be 2 kN.s/m.

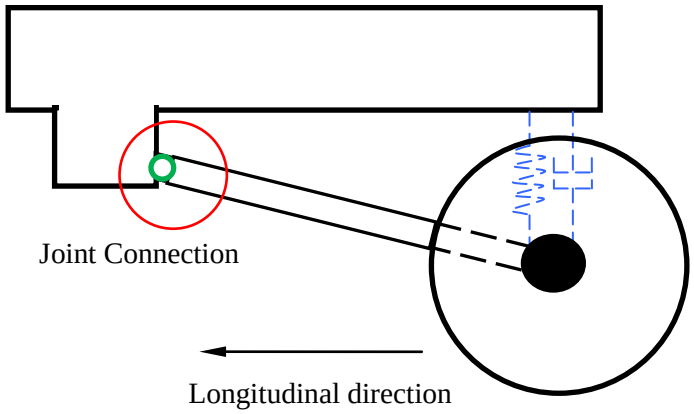

Figure 3-3: Conventional vehicle suspension and chassis connection in longitudinal direction

ISO/TC 108 WG9 categorizes roads in several classes according to the degree of road roughness. Roughness is usually described in terms of its power spectral density (PSD) against the circular spatial frequency. The circular spatial frequency (in cycle/m) can be switched to a temporal frequency (in Hz) by multiplying the vehicle speed. The PSD of road irregularities at speed of 60 km/h for class A, B, C, D are illustrated in Figure 3-4. The effect of speed on the PSD of road irregularity is shown in Figure 3-5 (class C, average), which indicates that an increase of speed can increase PSD value of road excitation at the same frequency. The input used in this study is an ISO class C (average) road.

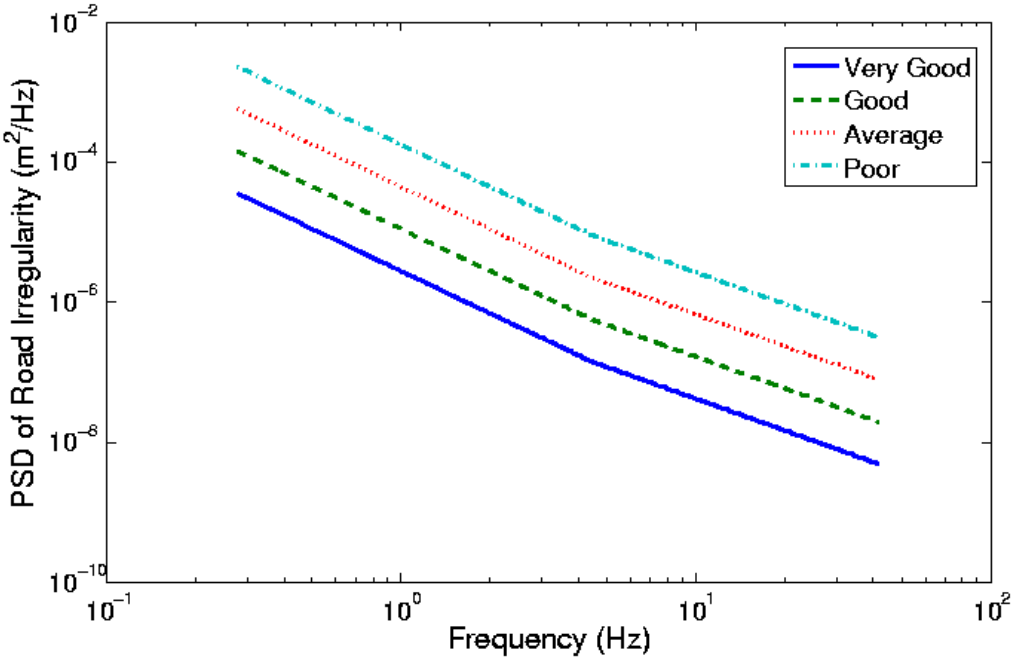

Figure 3-4: PSD of road roughness for ISO class A, B, C and D (60 km/h)

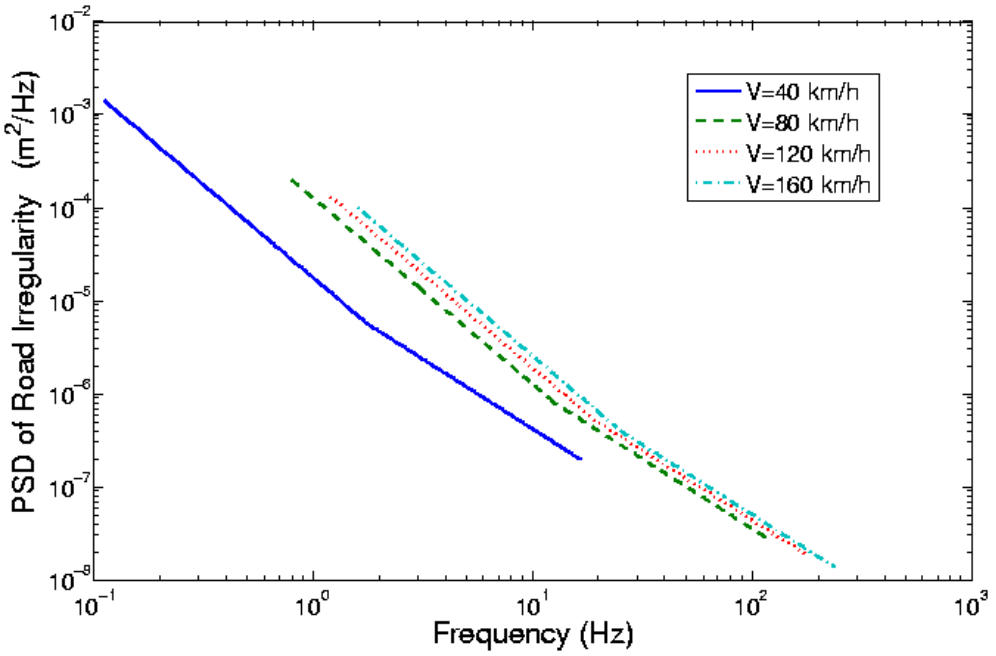

Figure 3-5: Effect of vehicle speed on PSD of road excitation (Class C, average)

The chassis vertical acceleration response to Class C (average) road excitation is studied at different vehicle speeds, as shown in Figure 3-6. The results show that the chassis acceleration response increases with increasing vehicle speed; this effect is particularly significant at the first resonant frequency. Due to the same parameters in the vertical direction, the vertical accelerations of the PSS and conventional vehicles are supposed to be identical.

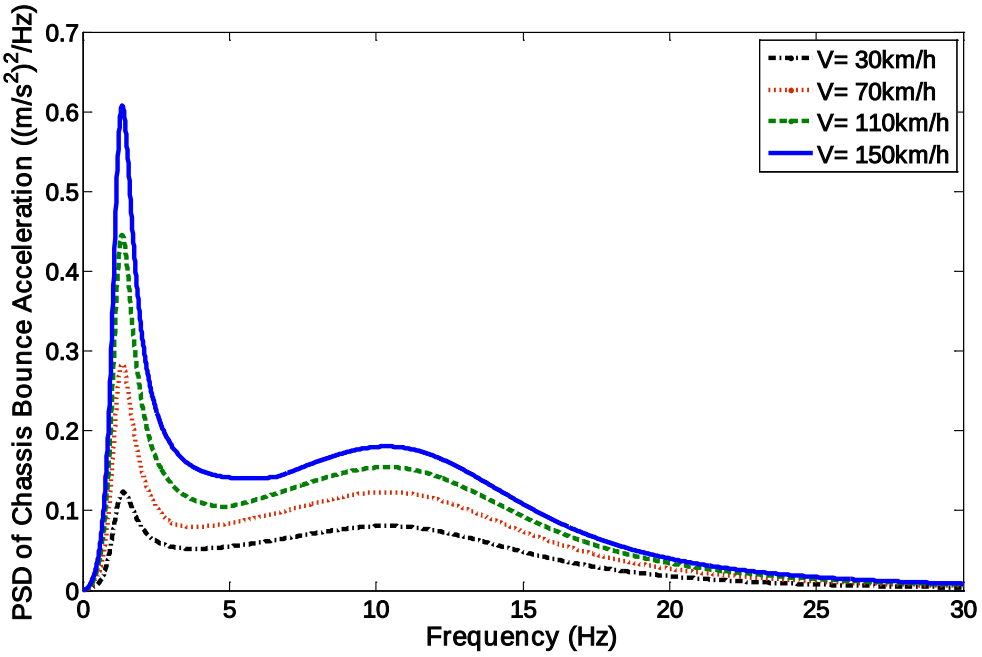

Figure 3-6: Chassis vertical acceleration response of PSS vehicle
(Road: class C, average)

Figure 3-7 illustrates a comparison of the chassis longitudinal acceleration response at a simulation speed 100 km/h. The longitudinal input used here is assumed to be ISO class *C* road roughness but the mean-square magnitude is half truncated to 32×10^{-6} m^2. Of course, ISO does not provide description for the road longitudinal input. The road assumption herein is just for comparison. As discussed previously, the model to simulate longitudinal motion of a conventional vehicle is the same as that for the PSS vehicle; however, the parameters used are different from those of the conventional vehicle. The results show that the response of the PSS vehicle is improved due to the introduction of a longitudinal spring-damping element between the chassis and wheel. The vibration along this direction is significantly cushioned, and the first resonant frequency is shifted from about 9Hz to around 1Hz. The peak value at this frequency is reduced significantly. Based on the simulation

results, it can be concluded that, with the same input, the acceleration response of the PSS vehicle along the longitudinal direction is much smaller than that of the convention vehicle.

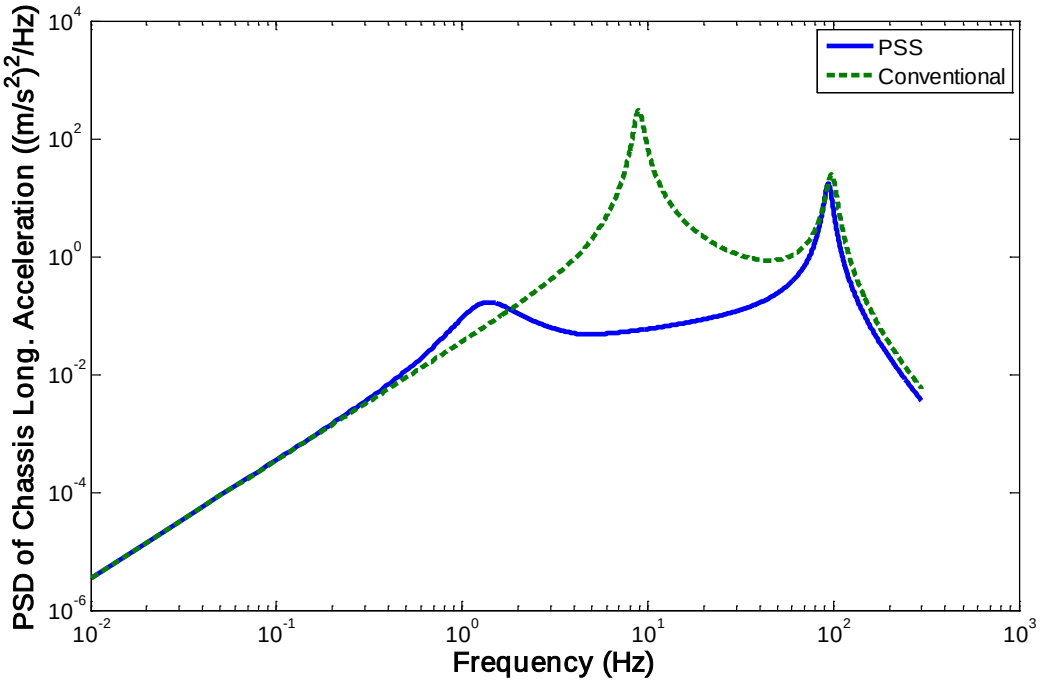

Figure 3-7: Comparison of chassis longitudinal acceleration response (Speed: 100km/h)

3.3 Time Domain Analysis

3.3.1 Integration of Tire Model to the Quarter-Car Model

Vehicle Model

A 4-DOF quarter-car model, as shown in Figure 3-8, is developed to study the dynamic behavior of a vehicle equipped with PSS in time domain. The vehicle chassis is modeled as a sprung mass, while the wheel is represented by an unsprung mass. The sprung and unsprung masses are connected by a PSS system represented by a linear vertical spring-damping element (k_s, c_s) and a nonlinear longitudinal spring-damping element (k_{ls}, c_{ls}). The stiffness coupling between the vertical and longitudinal spring-damping elements is neglected. The model has four degrees of freedom, consisting of bounces of sprung and unsprung mass (z_s and z_u), and the longitudinal motions of sprung and unsprung mass (x_s and x_u). The vehicle model interacts with the ground through a radial spring tire model discussed in the next sub-section. F_{bz} and F_{bx} are the vertical and longitudinal dynamic

interaction forces between the tire and ground. In this model, only the translational motions are considered and it is assumed there is no rotational motion.

The equation of motion for vertical motion is as follows:

$$\begin{bmatrix} m_s & 0 \\ 0 & m_u \end{bmatrix} \begin{Bmatrix} \ddot{z}_s \\ \ddot{z}_u \end{Bmatrix} + \begin{bmatrix} c_s & -c_s \\ -c_s & c_s \end{bmatrix} \begin{Bmatrix} \dot{z}_s \\ \dot{z}_u \end{Bmatrix} + \begin{bmatrix} k_s & -k_s \\ -k_s & k_s \end{bmatrix} \begin{Bmatrix} z_s \\ z_u \end{Bmatrix} = \begin{bmatrix} -m_s g \\ -m_u g \end{bmatrix} + \begin{bmatrix} 0 \\ F_b \end{bmatrix} \tag{3.9}$$

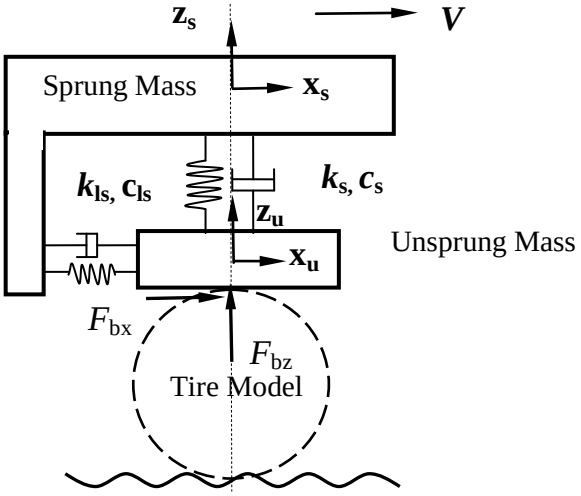

Figure 3-8: Quarter car model with PSS suspension

The equation of motion for longitudinal motion is as follows:

$$\begin{aligned} m_s \ddot{x}_s &= F_{ls} \\ m_u \ddot{x}_u &= F_{bx} - F_{ls} \end{aligned} \tag{3.10}$$

where the forces F_{bz} and F_{bx} applied on the unsprung mass are calculated based on the dynamic response of the vehicle model and the tire model at every time instance. F_{ls} is the longitudinal suspension force, and can be calculated based on equation (3.1) by adding damping as follows:

$$F_{ls} = \frac{k_o}{d_r^2}(x_u - x_s)^3 + k_o(x_u - x_s) + c_{ls}(\dot{x}_u - \dot{x}_s) \tag{3.11}$$

where d_r is assumed to be 5 cm in this study.

Tire Model

When a vehicle runs on a non-even road, the road applies a contact force to tires with components in both the vertical and longitudinal directions. A number of tire-ground contact models have been

developed for predicting these forces [81, 82, 97]. Among these models, a radial spring tire model is relatively accurate and with lower computational-cost according to reference [82]. This model is therefore selected and modified to include damping in this study. The outputs of the contact model are contact forces, contact patch length and effective tire radius.

The tire-road interaction in the vertical plane is represented by continuously distributed radial spring-damping elements symmetric to the wheel center. This model takes into account the stiffness and damping of tires. The road is assumed to be rigid. The tire deformation only takes place in the radial direction. The shear deformation along the circumferential direction is neglected. As shown in Figure 3-9, the contact patch is designated by the angle envelop (α_f, α_r). The radially distributed spring-damping elements are assumed to be linear. The stiffness and damping coefficients of radial spring-damping element, K_t and C_t (unit: N/m.rad and N.s/m.rad) are constant and are defined as the magnitude of force required to produce unit radial deformation of the spring and relative speed change within unit angle, respectively. The contact force is developed by radial interpenetration of the tire into the road. The elemental radial deflection, δ_i, at an angle α_i, leads to radial spring force dF, as shown in Figure 3-9, such that:

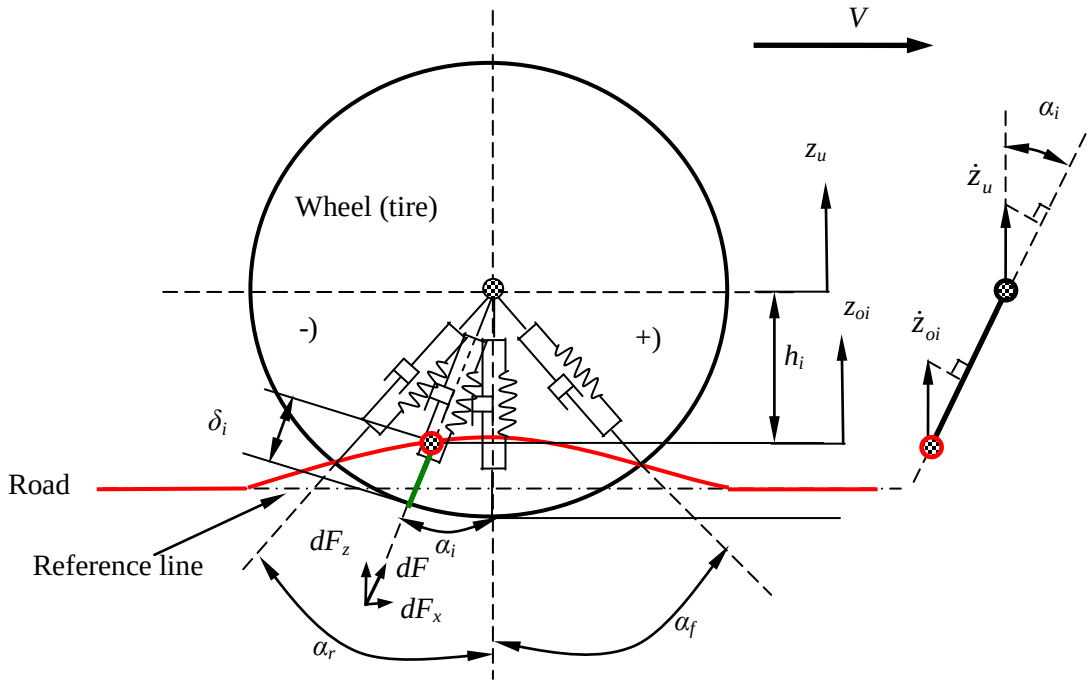

Figure 3-9: Radial spring tire-ground contact model

$$dF = \begin{cases} (C_t d\alpha_i)\Delta v_i + (K_t d\alpha_i)\delta_i & \delta_i > 0 \\ 0 & \delta_i \le 0 \end{cases} \tag{3.12}$$

where α_i is the angle between the vertical centerline of wheel plane and an arbitrary contact point within the contact patch, and $d\alpha_i$ is a small angle infinitesimal at angle α_i. Δv_i is the relative speed between two ends of the spring-damper element. For an instantaneous i^{th} radial spring-damping element, the elemental radial deflection or tire-road overlap δ_i can be expressed as:

$$\delta_i = R - \frac{R_e}{\cos\alpha_i} \tag{3.13}$$

where R is the nominal tire radius and R_e is the effective rolling radius of a loaded tire

$$R_e = R + z_u - z_{oi} \tag{3.14}$$

where z_u is the displacement of the tire center or the unsprung mass and z_{oi} is the road elevation of an arbitrary contact point within the contact patch.

The term Δv_i in equation (3.12) represents the relative velocity between two ends of the radial spring-damping element. As illustrated in Figure 3-9, it is readily to write:

$$\Delta v_i = (\dot{z}_{oi} - \dot{z}_u)\cos\alpha_i \qquad \text{for constant } \alpha_i \tag{3.15}$$

Performing integration over the contact patch (α_f, α_r) results in the contact forces in vertical and longitudinal direction as follows:

$$\begin{aligned} F_{bz} &= \int_{\alpha_r}^{\alpha_f} (C_t \Delta v_i + K_t \delta_i)\cos\alpha_i d\alpha_i \\ F_{bx} &= -\int_{\alpha_r}^{\alpha_f} (C_t \Delta v_i + K_t \delta_i)\sin\alpha_i d\alpha_i \end{aligned} \tag{3.16}$$

The above equation is valid where δ_i is not less than zero (i.e. does not lose contact). When losing contact, the contact force generated by the individual spring-damping element is zero. The relationship between the static wheel load and the tire deflection on a flat road is plotted in Figure 3-10. This figure shows that the linear point contact model overestimates the wheel-ground normal contact load for a small deflection but underestimates it for a large deflection compared to the radial-spring tire model.

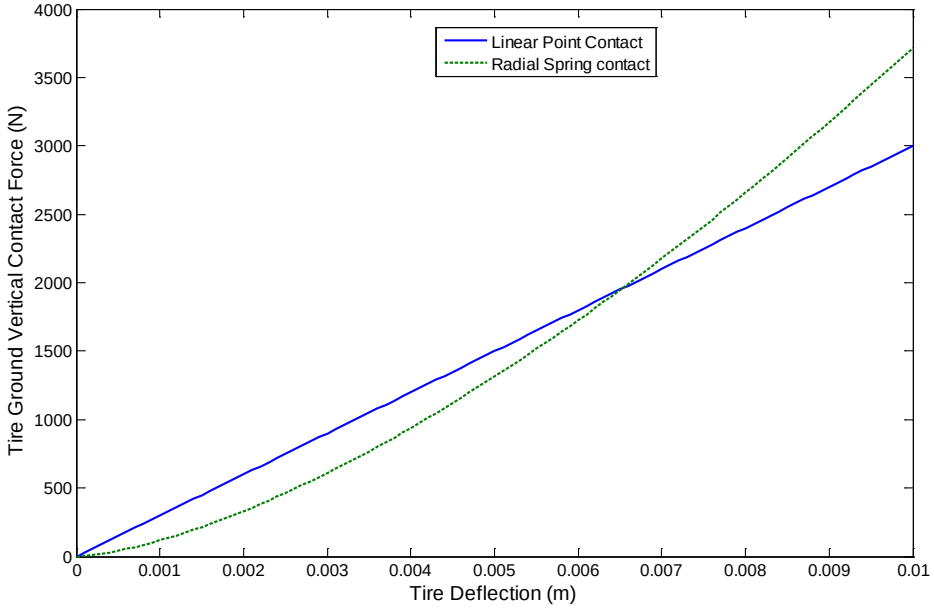

Figure 3-10: Tire-ground vertical static contact force vs. tire deflection

The contact patch length and effective tire rolling radius are needed in the calculation of tire-ground friction forces. For a flat road, the front and rear contact angles are equal, but their signs are opposite, i.e,

$$\begin{aligned} \alpha_r &= -\alpha_f = -\alpha_t \\ \alpha_t &= \cos^{-1}\frac{R-\delta_o}{R} = \cos^{-1}\frac{R-(z_o-z_u)}{R} \end{aligned} \tag{3.17}$$

Equation (3.16) changes to the following form by some manipulations:

$$\begin{aligned} F_{bz} &= 2K_t R(\sin\alpha_t - \alpha_t\cos\alpha_t) - C_t\dot{z}_u(\cos\alpha_t\sin\alpha_t + \alpha_t) \\ F_{bx} &= 0 \end{aligned} \tag{3.18}$$

The contact patch length and effective tire rolling radius for a flat road can be obtained from the following equations:

$$\begin{aligned} L_c &= 2R\sin\alpha_t \\ R_e &= R\cos\alpha_t \end{aligned} \tag{3.19}$$

3.3.2 Simulation Results

The model assembly of a quarter-vehicle and tire is employed to simulate the system dynamic motion when the vehicle passes over a 400 mm long, 150 mm high sinusoidal speeding bump with no driving force and rolling resistance. The model system has a constant speed before the wheel touches the bump. The value of sprung mass is assumed to be one quarter of the vehicle excluding the unsprung mass. Other parameters use the values listed in Table 3-2.

Table 3-2: Parameters for the conventional and PSS vehicles [25]

Type	Total Mass(kg)	Tire Mass(kg)	k_s (KN/m)	c_s (KN.s/m)	k_{ls}/k_s (KN/m)	c_{ls} (KN.s/m)	k_t *(ku)* (KN/m)	c_t (c_u) (KN.s/m)	*R*(m)
Conventional	1150	28.5	35.7/2	3.311/2	30	2	175	0.5	0.313
PSS	1150	28.5	35.7/2	3.311/2		3.311/2	175	0.5	0.313

Figures 3-11 and 3-12 illustrate the time histories of the displacement and velocity responses with a simulation speed of 8 km/h, respectively. It can be seen that when the tire passes over the bump, the bounce motion of the chassis is larger than the bump height while that of unsprung mass is close to the bump height. The excessive motion at the chassis level is due to the vertical suspension elasticity. In the longitudinal direction, the slop of the displacement plot starts to reduce when the tire touches the bump, which means the longitudinal velocity of both sprung and unsprung mass decreases after the wheel touches the obstacle. This can also be found in the velocity time history as shown in Figure 3-12. The longitudinal velocity approaches a minimum value for both the sprung and unsprung masses when the wheel-ground contact point is located at the top of the bump. After passing the top point of the bump, a longitudinal acceleration is obtained and the speed increases. Further study shows that there exists a critical initial speed below which the vehicle cannot pass the bump.

Figures 3-13 and 3-14 illustrate the time history of tire-ground contact force and chassis acceleration, respectively. When the tire hits the bump, the chassis experiences a vertical and a longitudinal contact force, and consequently obtains an upward and a backward acceleration. During the tire approaches to the top of the bump, the contact forces decrease gradually in both the vertical and longitudinal directions. The acceleration responses correspondingly decrease to a minimum

value. After passing over the top of the bump, the tire drops downward and experiences a forward contact force. As a result, the sprung mass obtains a forward and a downward acceleration response.

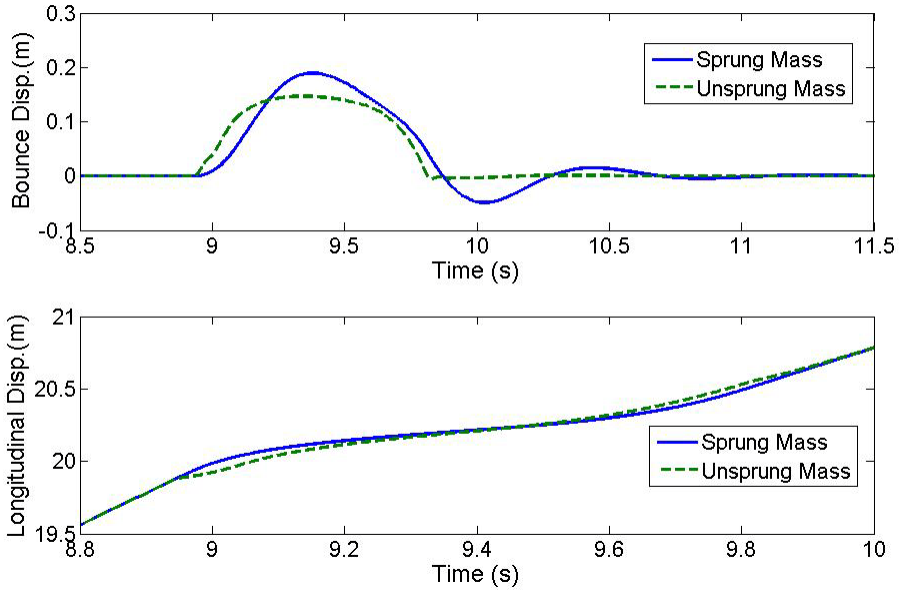

Figure 3-11: Sprung and unsprung mass displacement response of PSS vehicle (speed: 8 Km/h)

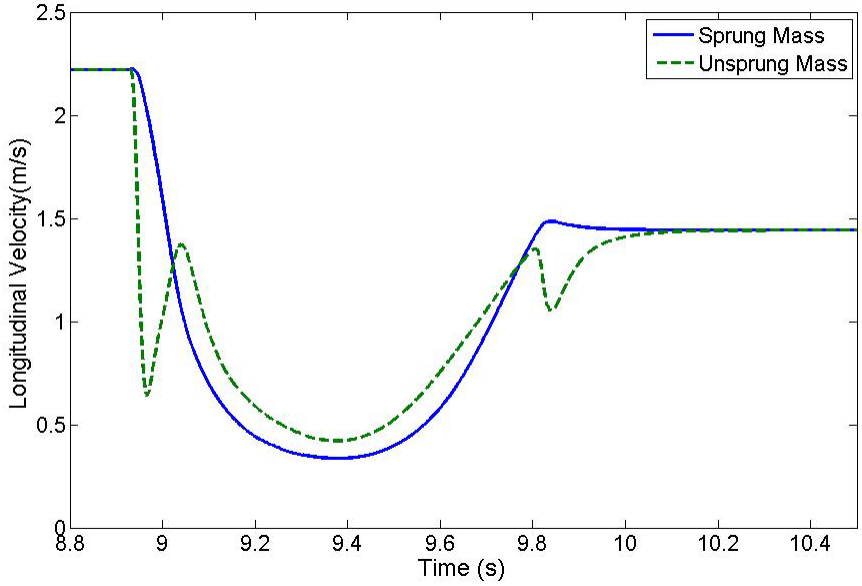

Figure 3-12: Longitudinal velocity response of PSS vehicle (speed: 8 Km/h)

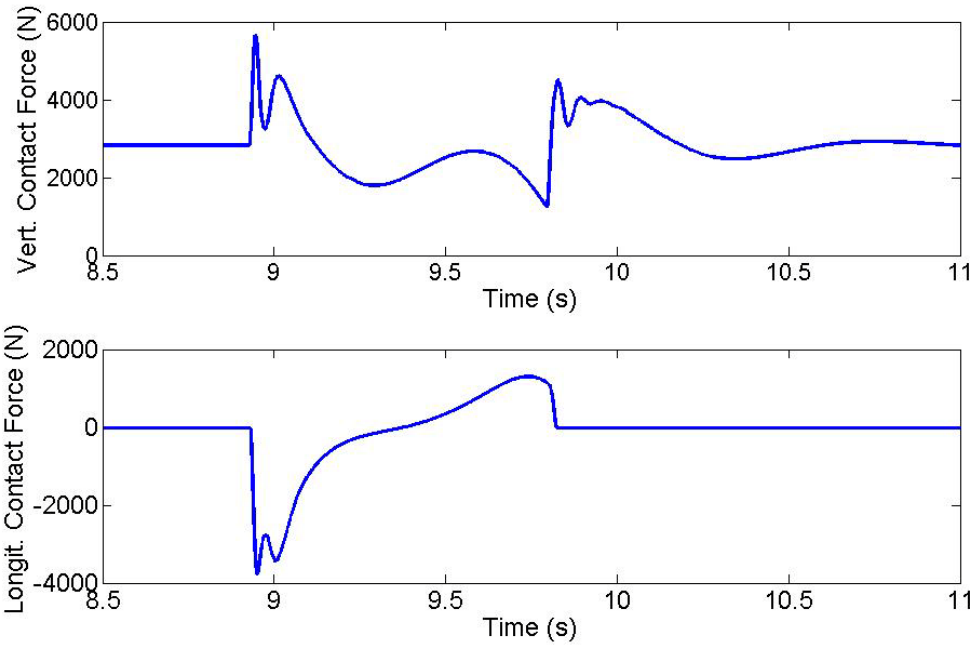

Figure 3-13: Time history of tire-ground contact force (speed: 8 Km/h)

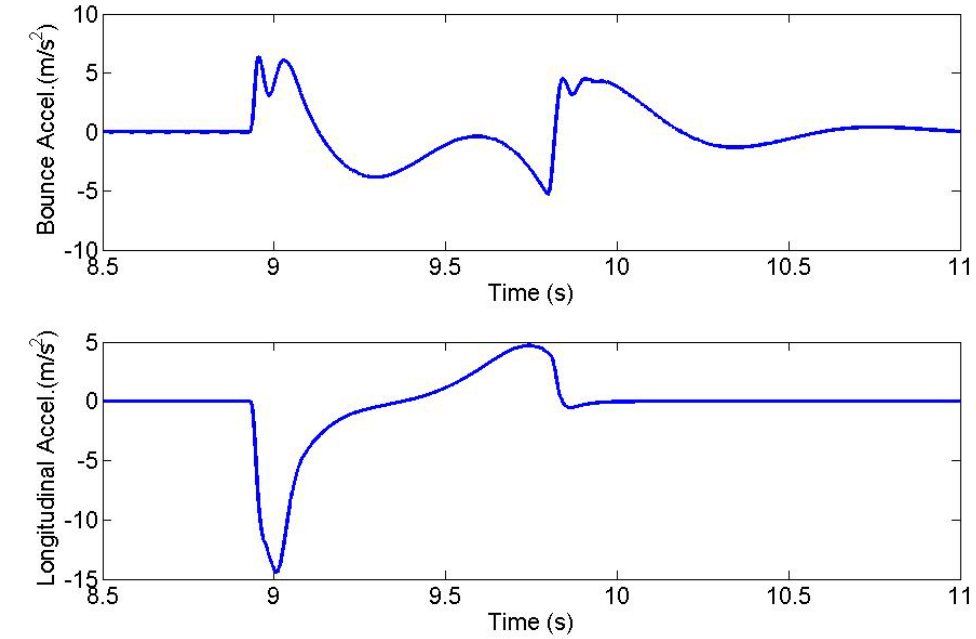

Figure 3-14: Time history of chassis (sprung mass) acceleration response (speed: 8Km/h)

The suspension longitudinal deflection, which determines the design space, is predicted as shown in Figure 3-15. The results imply that, due to the longitudinal spring between sprung and unsprung mass in the PSS system, a larger suspension travel space (7cm) is needed and the position of the wheels will not maintain a fixed point with respect to the chassis, and therefore the wheelbase can vary with the operation condition.

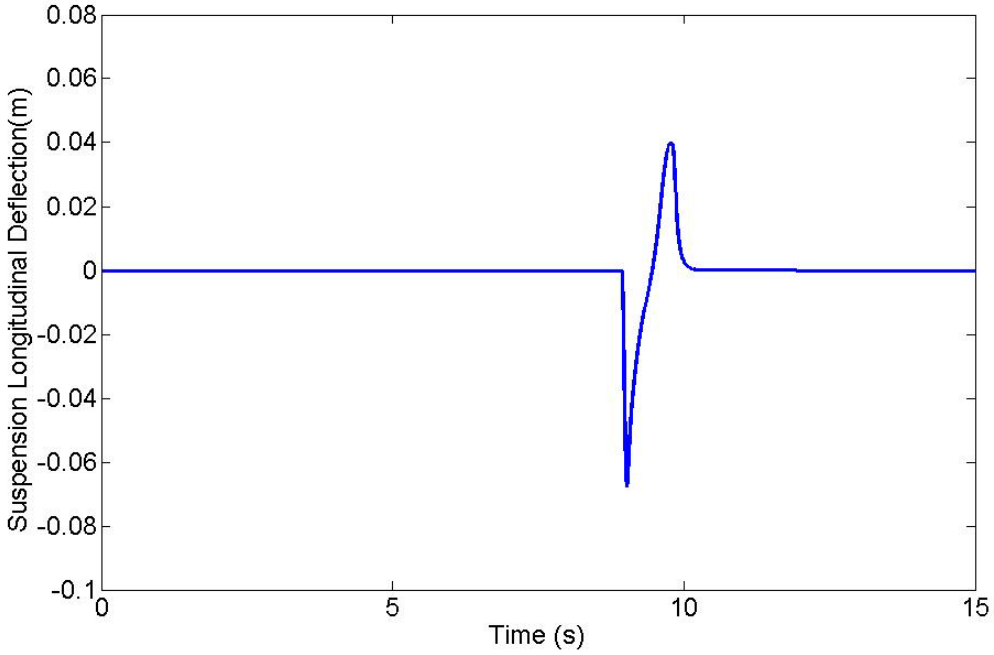

Figure 3-15: Time history of suspension longitudinal response (speed: 8 Km/h)

The planar dynamic performance of the conventional vehicle is also investigated and a comparison between the PSS vehicle and the conventional vehicle is carried out at 20 Km/h. The parameters of the conventional vehicle are listed in Table 3-2. Figure 3-16 depicts the time history of the velocity response when passing over the same obstacle. The results show that the velocity decrease in the PSS vehicle is slightly larger than that of the conventional vehicle after passing over the same bump. This means that the kinetic energy loss of the PSS vehicle is slightly larger. Such an energy loss can be related to the longitudinal damping in the suspension system. Meanwhile, the magnitude of the transient unsprung velocity of the PSS vehicle is much larger than that of a conventional vehicle, which means the relative longitudinal motion between the chassis and wheel in the PSS vehicle are more evident than that in the conventional vehicle. The evident relative longitudinal motion is due to the soft longitudinal stiffness in the planar suspension system.

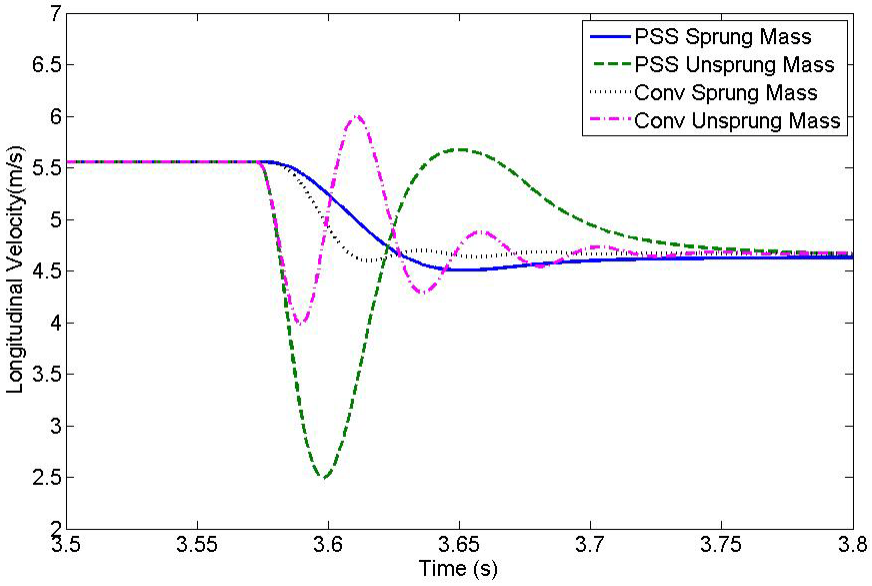

Figure 3-16: Comparison of sprung and unsprung mass velocity response between PSS and conventional vehicles (speed: 20 Km/h)

The time history of the chassis acceleration response for both the PSS vehicle and the conventional vehicle is plotted in Figure 3-17. In the vertical direction, the acceleration response of the PSS vehicle is smaller than that of the conventional vehicle due to the small passing speed of the PSS vehicle (see Figure 3-16). In the longitudinal direction, the chassis acceleration of the PSS vehicle is much smaller than that of the conventional vehicle due to the soft longitudinal connection in the planar suspension system. The results demonstrate that the shock-attenuation ability can be significantly improved by the implementation of a PSS. Meanwhile, the planar suspension system can also improve the vertical ride quality of a vehicle.

For a good understanding of the acceleration response, the dynamic tire ground contact forces are also predicted and plotted in Figure 3-18. It can be seen that once the tire touches the bumps, the vertical tire contact force increases rapidly to a peak value, and then starts to drop. This drop of the PSS vehicle takes place earlier than that of a conventional vehicle. The peak value of the vertical contact force in the PSS vehicle is slightly smaller than that of the conventional vehicle. This may be related to the backward relative motion of the wheel with respect to the chassis in the PSS vehicle. After the wheel passes the top of the bump, the tire loses contact to the road for both vehicles. A time delay in the contact force response exists in the PSS vehicle compared to the conventional vehicle.

This time delay may be related to the relatively large longitudinal motion in the PSS vehicle due to the soft longitudinal stiffness.

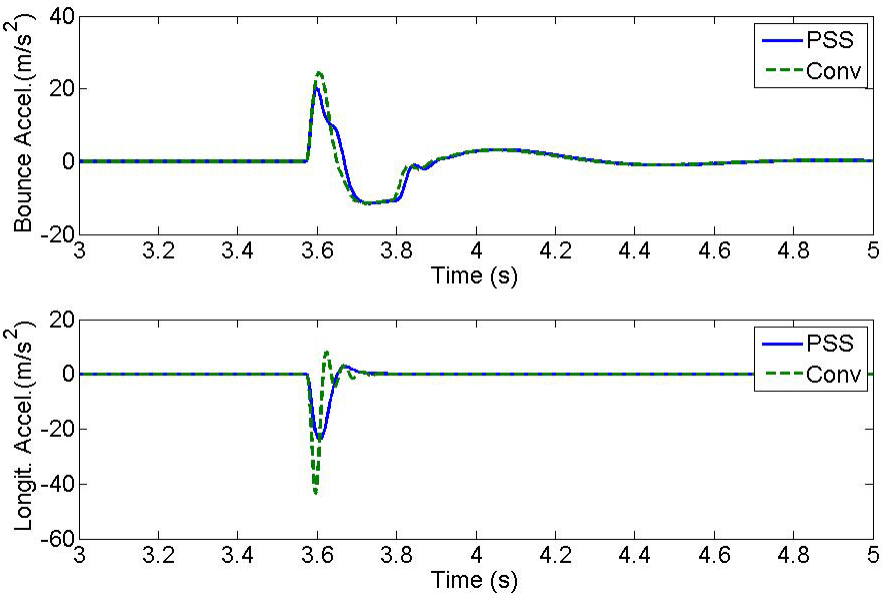

Figure 3-17: Comparison of sprung and unsprung mass acceleration response between PSS and conventional vehicles (speed: 20 Km/h)

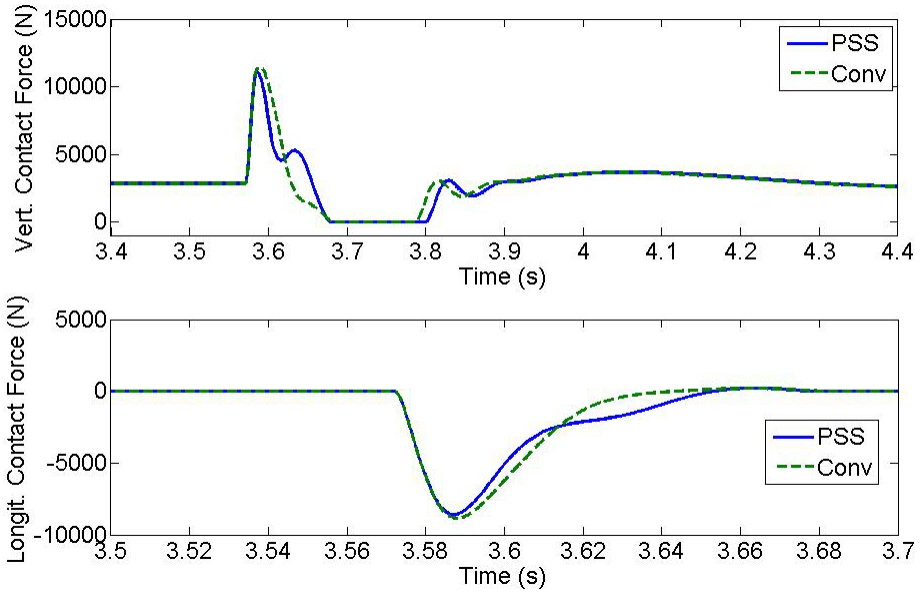

Figure 3-18: Dynamic tire-ground contact forces of PSS and conventional vehicles (Speed: 20 Km/h)

Figure 3-19 illustrates the suspension longitudinal forces of the PSS and conventional vehicles. As expected, the longitudinal suspension force in the PSS vehicle is much smaller than that of the conventional vehicle. This has an engineering value that PSS can perform as a main protector of the vehicle and their suspensions. For instance, one of the most disturbing situations happens in spring after the frost leaves the ground. A numerous big chunks of pavement creating puddles or potholes with very aggressive edges may occur. These puddles are very dangerous for the vehicle suspensions because they damage the alignment of the wheels and bend the suspension components. The PSS can be used to reduce the effects of the puddles on the vehicle components.

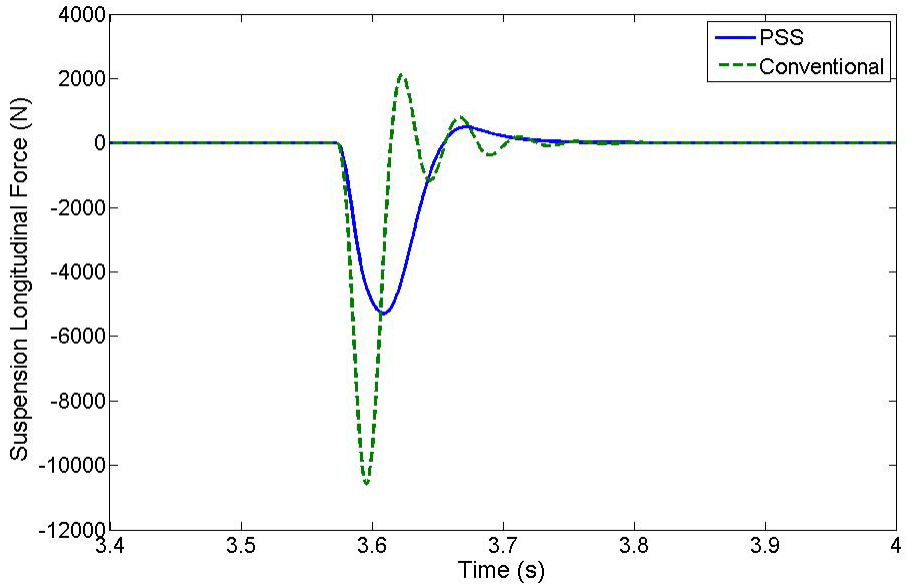

Figure 3-19: Comparison of suspension longitudinal force when passing over the bump

3.4 Summary

In this chapter, a 4-DOF quarter-car model was proposed to carry out a preliminary study of the ride quality of a vehicle equipped with planar suspension system (PSS) in frequency and time domain. This model takes into account the vertical and longitudinal motions of the sprung and unsprung masses. A linear tire-ground contact model was employed in the frequency domain study, while a radial spring contact model was used to predict the transient tire-ground contact forces in the time domain investigation. The tire damping neglected in the reported radial spring tire model was added in this study.

The dynamic response of a PSS vehicle due to road excitation was investigated and compared with that of a conventional vehicle. In this study, the simulation parameters were assumed identical in both the PSS and conventional vehicles except those in terms of the longitudinal suspension elasticity. The frequency domain study showed that, while the vertical acceleration responses of the PSS and Conventional vehicles were identical, the longitudinal acceleration responses of the PSS vehicle was much smaller than that of the conventional vehicle when frequency is below 100 Hz. Due to the softer longitudinal spring-damping element, the vibration along this direction can be sufficiently cushioned, and the first resonant frequency is shifted from about 10Hz to around 1Hz. The peak value at this frequency is reduced significantly. The results of time domain study demonstrated that the longitudinal acceleration of the PSS vehicle due to an isolated road bump was much smaller than that of the conventional vehicle. Meanwhile, the vertical acceleration response of the PSS vehicle was smaller than that of a conventional one. A time delay was observed between the transient responses of a PSS vehicle and a conventional vehicle. The vehicle speed drop due to the road bump in the PSS vehicle is slightly larger than that in the conventional vehicle. Based on these simulation results, it can be concluded that the planar suspension system can substantially improve the ride quality of an automobile. Particularly, the shock-attenuation ability along the longitudinal direction can be significantly improved by the implementation of PSS. In addition, the PSS can also reduce the longitudinal force in the suspension links and joints, and in turn protect these components from damage.

Chapter 4
Pitch Dynamics Study

4.1 Overview

Road unevenness can excite dynamic motions in both the vertical and longitudinal directions. It has been shown that the human body may be more sensitive to pitch motion than to other types of motions [7]. Few studies have explored pitch dynamic responses in passenger cars. It is expected that pitch motion plays an important role in ride quality of a PSS vehicle because it couples the vertical and longitudinal motions. Due to the special mechanisms of the PSS, the pitch dynamics of a vehicle with the PSS may exhibit some unique characteristics.

In this study, two kinds of pitch plane half-car models are developed to investigate the pitch dynamics of a PSS vehicle. The first model is a completely linear system with 6 DOFs where the tire-ground contact is modeled as a linear point contact. The nonlinear longitudinal spring in the PSS is linearized at a point with zero deflection. This linear model is used to perform the frequency domain study. The second model is a 9-DOF nonlinear model for the timed domain study, being validated with an Adams/car model. The nonlinearities arising from the suspension longitudinal strut, tire deflection and the tire-ground frictions are taken into account. The time domain investigation is conducted in terms of the responses to a single isolated road obstacle as well as the random road unevenness. Comparisons between the PSS and conventional vehicles in both frequency and time domains are carried out.

4.2 Study of Pitch Dynamics in Frequency Domain

4.2.1 Vehicle Model

The frequency domain study is carried out based on a linear 6-DOF pitch plane half-car model, as illustrated in Figure 4-1. The chassis is represented by a sprung mass, while the two wheels are modeled as unsprung mass. The sprung and unsprung masses are connected by a planar suspension system (PSS) represented by a vertical spring-damping element ($k_{sf(r)}$, $c_{sf(r)}$) and a longitudinal spring-damping element ($k_{lsf\ (r)}$, $c_{lsf\ (r)}$). The subscripts *f* and *r* represent the front and rear, respectively. The vertical spring-damping element is linear while the longitudinal is nonlinear. The tires are modeled by linear spring damping elements ($k_{uf(r)}$, $c_{uf(r)}$) and the tire-ground contact is modeled as a single point contact, as shown. The motion of the system is described by seven variables: the chassis bounce (z_s),

pitch (φ_s) and longitudinal motion (x_s), the front wheel bounce (z_{uf}) and longitudinal motion (x_{uf}), the rear wheel bounce (z_{ur}) and longitudinal motion (x_{ur}). In the frequency domain study, it is assumed that the front wheel has a constant forward speed. Among these motions, the front wheel longitudinal movement is specified by a constant speed, i.e. a kinematics constraint for the front wheel longitudinal motion is specified and x_{uf} is a dependent variable, hence the system has six independent variables or degrees of freedom. This model neglects the effect of the rolling resistance and aerodynamic forces.

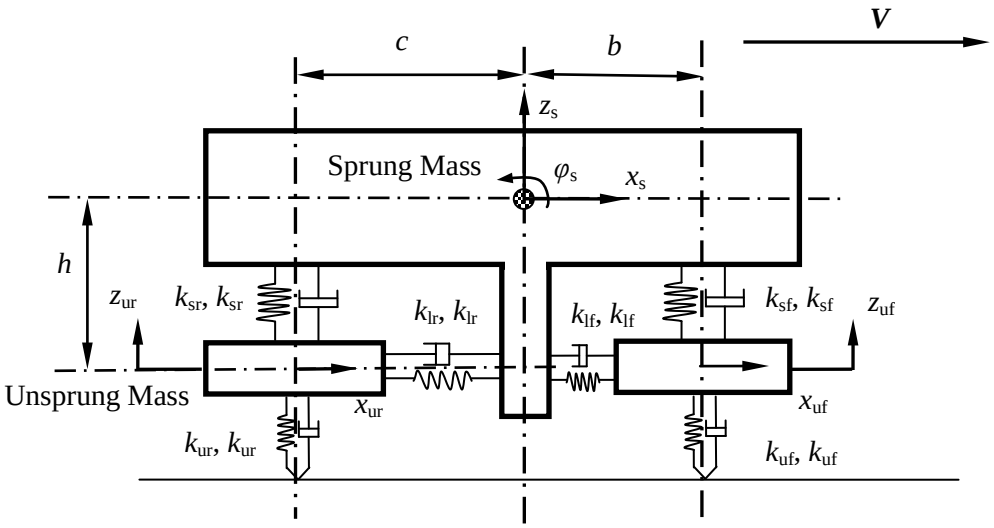

Figure 4-1: 6-DOF pitch plane half-car vehicle model

The longitudinal spring in the formulation of vehicle model is linearized at the point where the deflection is zero, i.e. $\Delta x=0$ in equation (3.2). By applying Newton's second law, the equation of motion can be written as follows:

$$\begin{aligned} &M\ddot{Z} + C\dot{Z} + KZ = F \\ &x_{uf} = vt \end{aligned} \tag{4.1}$$

where M, C and K are the mass, damping and stiffness matrices, respectively,

$$M = \begin{bmatrix} m_s & & & & & \\ & I_s & & & & \\ & & m_{uf} & & & \\ & & & m_{ur} & & \\ & & & & m_s & \\ & & & & & m_{ur} \end{bmatrix}$$

$$C = \begin{bmatrix} c_{sf}+c_{sr} & c_{sf}b-c_{sr}c & -c_{sf} & -c_{sr} & 0 & 0 \\ c_{sf}b-c_{sr}c & b^2c_{sf}+c^2c_{sr}+h^2(c_{lf}+c_{lr}) & -bc_{sf} & cc_{sr} & h(c_{lf}+c_{lr}) & -hc_{lr} \\ -c_{sf} & -bc_{sf} & c_{sf}+c_{uf} & 0 & 0 & 0 \\ -c_{sr} & cc_{sr} & 0 & c_{sr}+c_{ur} & 0 & 0 \\ 0 & h(c_{lf}+c_{lr}) & 0 & 0 & c_{lf}+c_{lr} & -c_{lr} \\ 0 & -hc_{lr} & 0 & 0 & -c_{lr} & c_{lr} \end{bmatrix}$$

$$K = \begin{bmatrix} k_{sf}+k_{sr} & k_{sf}b-k_{sr}c & -k_{sf} & -k_{sr} & 0 & 0 \\ k_{sf}b-k_{sr}c & b^2k_{sf}+c^2k_{sr}+h^2(k_{lf}+k_{lr}) & -bk_{sf} & ck_{sr} & h(k_{lf}+k_{lr}) & -hk_{lr} \\ -k_{sf} & -bk_{sf} & k_{sf}+k_{uf} & 0 & 0 & 0 \\ -k_{sr} & ck_{sr} & 0 & k_{sr}+k_{ur} & 0 & 0 \\ 0 & h(k_{lf}+k_{lr}) & 0 & 0 & k_{lf}+k_{lr} & -k_{lr} \\ 0 & -hk_{lr} & 0 & 0 & -k_{lr} & k_{lr} \end{bmatrix}$$

Z is the system state vector and F is the system input vector. They are expressed in the following forms:

$$Z = \begin{Bmatrix} z_s & \phi_s & z_{uf} & z_{ur} & x_s & x_{ur} \end{Bmatrix}^T \tag{4.2}$$

$$F = \begin{Bmatrix} 0 & h(c_{lf}v + k_{lf}x_{uf}) & c_{uf}\dot{z}_{of} + k_{uf}z_{of} & c_{ur}\dot{z}_{or} + k_{ur}z_{or} & c_{lf}v + k_{lf}x_{uf} & 0 \end{Bmatrix}^T \tag{4.3}$$

where $z_{of(r)}$ are the road unevenness at the front (rear) wheel-ground contact.

In this study, the parameters for a PSS vehicle and a conventional one are based on a mid-size passenger car [25] and listed in Table 4-1.

4.2.2 Frequency Domain Response Analysis

It is known that the response of a linear dynamic system to a constant input exhibits a transient pattern and will eventually die off in the existence of damping in the system, and the system will reach to a new state of equilibrium. For the frequency analysis, only the dynamic part of the response is of interest, and hence the static part due to the front wheel velocity and displacement, v and x_{uf}, can be neglected. In this frequency analysis, it is, therefore, assumed that the vehicle is not moving. The input vector expressed in equation (4.3) can be then rewritten as:

$$F = \begin{Bmatrix} 0 & 0 & c_{uf}\dot{z}_{of} + k_{uf}z_{of} & c_{ur}\dot{z}_{or} + k_{ur}z_{or} & 0 & 0 \end{Bmatrix}^T \tag{4.4}$$

Table 4-1: Parameters of a conventional vehicle (mid-size car) [25]

	Conventional	PSS
Total Mass(kg)	1314	1314
I_s (kgm^2)	1630	1630
b (m)	1.06	1.06
C (m)	1.44	1.44
k_{sr} (kN/m)	23.8/2	23.8/2
k_{sf} (kN/m)	35.7/2	35.7/2
c_{sr} (kNs/m)	2.207/2	2.207/2
c_{sf} (kNs/m)	3.311/2	3.311/2
k_{tf}, k_{tr} (kN/m)	175	175
c_{tf}, c_{tr} (kNs/m)	0.5	0.5
$k_{lsf(r)}$/ksf(r)	20	
c_{ls} (KN.s/m)	3.00	
m_{ur} (kg)	71.5/2	71.5/2
m_{uf} (kg)	76.4/2	76.4/2
h (m)	0.25	0.25
Note: the parameter, k_o, representing the suspension longitudinal property for the PSS, and the damping are assumed as same as the vertical counterparts.		

In the analysis of vibration transmissibility or, response gain, two special cases are often considered, i.e, $z_{of} = z_{or} = z_{o,}$ which represents the pure bounce excitation; and $z_{of} = - z_{or} = z_{o,}$ which implies pure pitch excitation. Although these two cases can rarely be seen in reality, they can provide an insight into the vehicle pitch response characteristics.

Pure Bounce Excitation ($z_{of} = z_{or} = z_o$)

Pure bounce excitation implies that the inputs at the front and real wheels are completely in phase. Assuming the road excitation is sinusoidal, i.e, $z_o e^{i\omega t}$, equation (4.4) representing the input vector becomes:

$$\begin{Bmatrix} 0 & 0 & i\omega c_{uf} + k_{uf} & i\omega c_{ur} + k_{ur} & 0 & 0 \end{Bmatrix}^T z_o e^{i\omega t} \tag{4.5}$$

Then the response of equation (4.1) in the frequency domain can be obtained from:

$$Z(\omega) = \left[-\omega^2 M + i\omega C + K \right]^{-1} \begin{Bmatrix} 0 & 0 & i\omega c_{uf} + k_{uf} & i\omega c_{ur} + k_{ur} & 0 & 0 \end{Bmatrix}^T z_o(\omega)$$

or

$$Z(\omega) = [H] z_o(\omega) = \begin{bmatrix} H_1 & H_2 & H_3 & H_4 & H_5 & H_6 \end{bmatrix}^T z_o(\omega) \tag{4.6}$$

where the elements of *H* are the transmissibility (gains) corresponding to the individual DOF.

Figure 4-2 depicts the displacement response transmissibility in the case of pure bounce input. It shows that pure bounce input excites a large chassis bounce motion but small pitch motion. Resonance occurs at the chassis bounce and wheel bounce natural frequency for vertical motion. Only one resonance occurs in the longitudinal direction at approximately 1 Hz.

Figure 4-3 illustrates the comparison of the displacement response gain between the PSS vehicle and the conventional vehicle. As expected, the chassis bounce, pitch and wheel bounce responses are very close for the two types of vehicles because the suspension vertical and tire parameters are identical. In the longitudinal direction, when the input frequency is less than the chassis natural frequency (about 1 Hz), the chassis longitudinal displacement of the PSS vehicle is slightly larger than that of the conventional vehicle. However, when the excitation frequency is larger than the chassis natural frequency, the chassis longitudinal displacement response of the PSS vehicle is rather small compared to that of the conventional vehicle. In addition, the response of the conventional vehicle exhibits two peak values corresponding to the two natural frequencies, whereas that of the PSS vehicle only exhibits one peak value. Such a result implies that a PSS can isolate the chassis from the longitudinal vibration more efficiently than a conventional vehicle when the excitation frequency is above 1 Hz. In reality, the road excitation frequency to an automobile is much higher than the natural frequency; therefore, the PSS can provide better vibration isolation capacity in the longitudinal direction. For the rear wheel, the longitudinal response of the PSS vehicle is larger for the frequency being less than 4 Hz while is smaller above this frequency when compared to that of the conventional vehicle. It should be noted that the ‘longitudinal displacement’ refers to the dynamic part rather than the absolute distance.

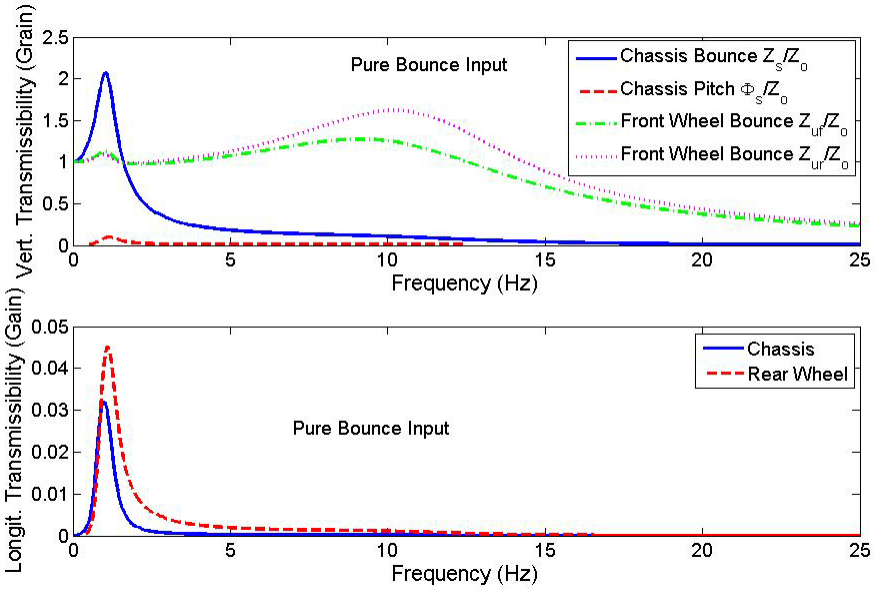

Figure 4-2: Displacement response transmissibility (gain) for pure bounce input

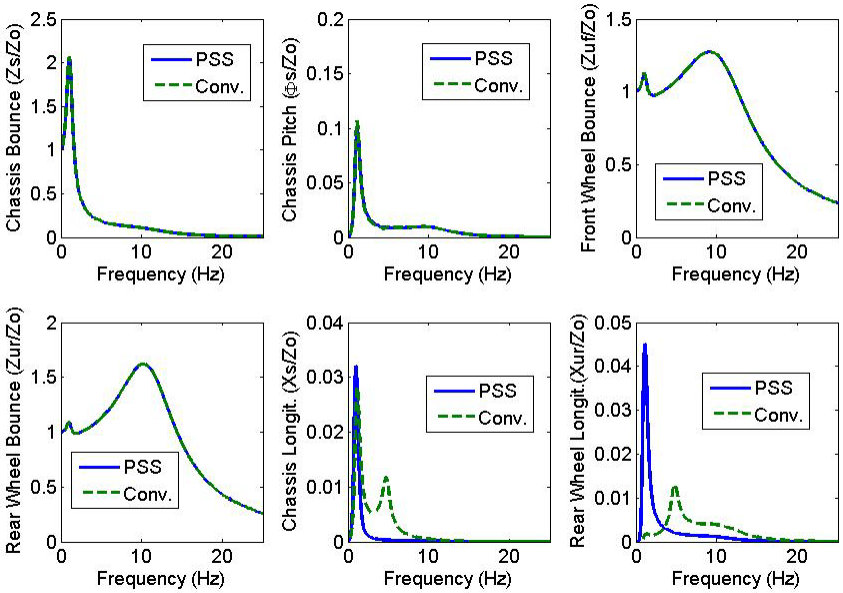

Figure 4-3: Comparison of displacement response transmissibility (gain) between PSS and conventional vehicles for pure bounce input

Pure Pitch Excitation (z_{of} = -z_{or} = z_o)

Pure pitch excitation is defined as the inputs at the front wheel and rear wheel are completely out of phase. Similar to the pure bounce case, the frequency response can be obtained by the following expression:

$$Z(\omega) = \left[-\omega^2 M + i\omega C + K\right]^{-1} \left\{0 \quad 0 \quad i\omega c_{uf} + k_{uf} \quad -i\omega c_{ur} - k_{ur} \quad 0 \quad 0\right\}^T z_o(\omega)$$

$$Z(\omega) = \left[H\right] z_o(\omega) = \left[H_1 \quad H_2 \quad H_3 \quad H_4 \quad H_5 \quad H_6\right]^T z_o(\omega) \tag{4.7}$$

where the elements of *H* are the transmissibility (gains) corresponding to the individual DOF.

Figures 4-4 and 4-5 illustrate the displacement transmissibility of the PSS vehicle and a comparison between the PSS and the conventional vehicles with respect to pure pitch input. Compared to the pure bounce input, pure pitch input excites a large pitch motion but a small bounce motion as shown in Figure 4-3. The longitudinal motion due to pure pitch input is also larger than that due to pure bounce motion because of serious pitch motion. Once again, Figure 4-5 shows the advantage of the PSS over the conventional suspension in its ability to cushion longitudinal vibrations above the chassis longitudinal natural frequency.

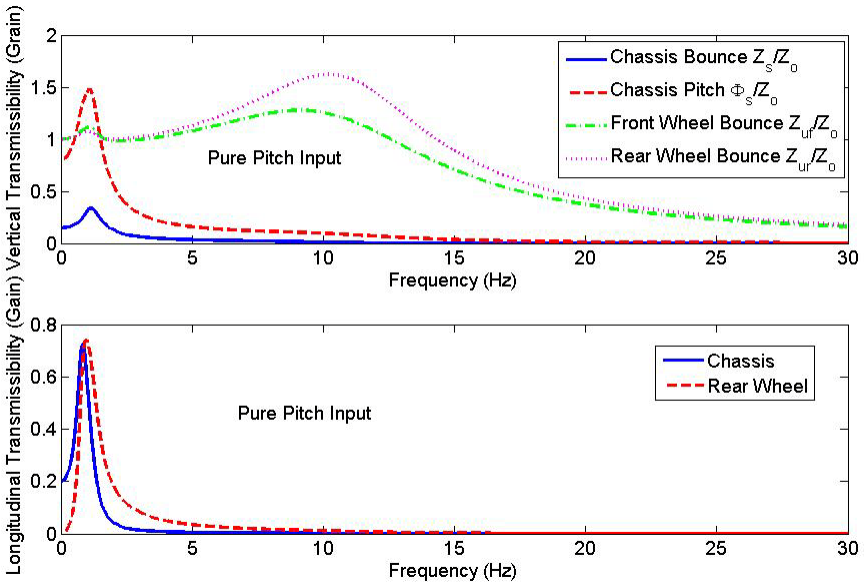

Figure 4-4: Displacement response transmissibility (gain) for pitch input

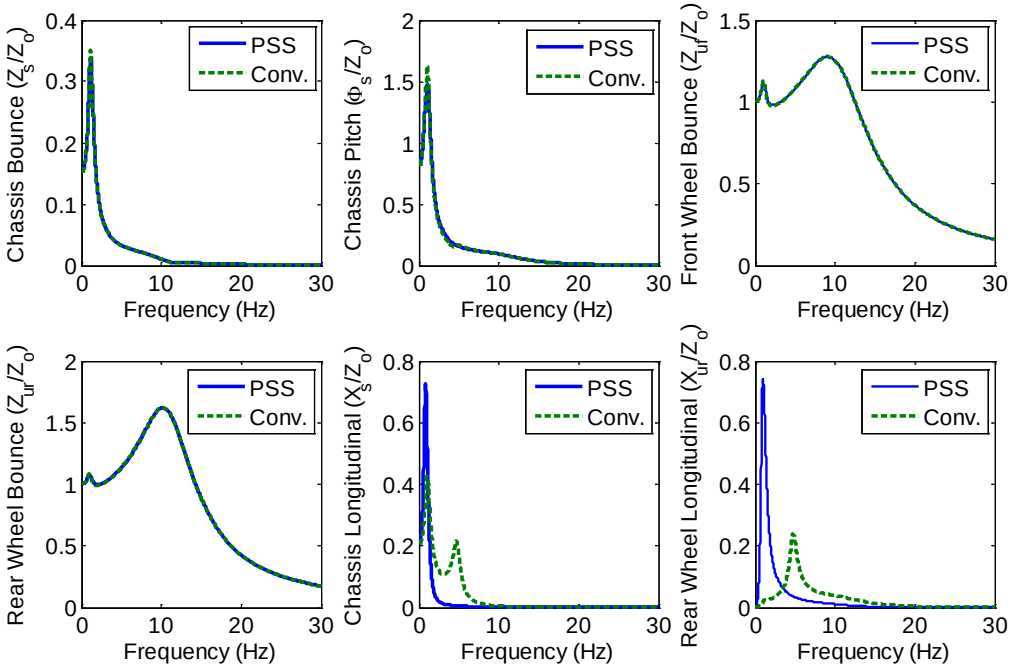

Figure 4-5: Comparison of response transmissibility (gain) between PSS and conventional vehicle for pure pitch input

4.3 Wheelbase Filtering of a Vehicle with PSS

Wheelbase filtering refers to the correlation between the front and rear excitation, which has received a great deal of attention in vehicle pitch studies [18, 39, 69]. This phenomenon takes place because, when a two-wheeled vehicle follows a path, both wheels will pass over the same road unevenness $z_o(t)$ but at different times. The excitation of the rear wheel is the same as the front wheel, but there is a time delay which is proportional to the wheelbase (b+c) and inversely proportional to the speed. The inputs at the front and rear wheels can be generally expressed as:

$$\begin{Bmatrix} z_{of} \\ z_{or} \end{Bmatrix} = \begin{Bmatrix} z_o(t) \\ z_o(t-\dfrac{b+c}{V}) \end{Bmatrix} \tag{4.8}$$

Then the input vector, F, becomes

$$F = \left\{ 0 \quad 0 \quad c_{uf}\dot{z}_o(t) + k_{uf} z_o(t) \quad c_{ur}\dot{z}_o(t-\frac{b+c}{V}) + k_{ur} z_o(t-\frac{b+c}{V}) \quad 0 \quad 0 \right\}^T \tag{4.9}$$

or in the frequency domain:

$$F = \left\{ 0 \quad 0 \quad (i\omega c_{uf} + k_{uf}) \quad (i\omega c_{ur} e^{-i\omega \frac{b+c}{V}} + k_{ur} e^{-i\omega \frac{b+c}{V}}) \quad 0 \quad 0 \right\}^T z_o(\omega) \tag{4.10}$$

The displacement response can be obtained from the following equation:

$$Z(\omega) = \left[-\omega^2 M + i\omega C + K \right]^{-1} \left\{ 0 \quad 0 \quad (i\omega c_{uf} + k_{uf}) \quad (i\omega c_{ur} e^{-i\omega \frac{b+c}{V}} + k_{ur} e^{-i\omega \frac{b+c}{V}}) \quad 0 \quad 0 \right\}^T z_o(\omega) \tag{4.11}$$

The transfer function matrix for the displacement response is as follows:

$$H(\omega) = \left[-\omega^2 M + i\omega C + K \right]^{-1} \left\{ 0 \quad 0 \quad (i\omega c_{uf} + k_{uf}) \quad (i\omega c_{ur} e^{-i\omega \frac{b+c}{V}} + k_{ur} e^{-i\omega \frac{b+c}{V}}) \quad 0 \quad 0 \right\}^T \tag{4.12}$$

And the transfer function matrix for the acceleration response is as follows:

$$H_{acc}(\omega) = -\omega^2 H(\omega) \tag{4.13}$$

Figure 4-6 depicts the chassis acceleration response transmissibility at 50 and 100 km/h for both the PSS and conventional vehicles. Similar to reports of [39], the results demonstrate that the response of the vehicle is modulated with a constant frequency $\Delta v = V/(b+c)$, and the maxima of the longitudinal and pitch accelerations correspond to the minima of bounce acceleration and vice versa. The results also indicate that the chassis bounce and pitch acceleration responses of the PSS vehicle are almost identical to those of the conventional vehicle because of the identical suspension vertical parameters. In the longitudinal direction, the chassis acceleration responses of the PSS vehicle are much smaller than those of the conventional vehicle, especially in the frequency range of 0~10 Hz, whose central value is corresponds to the natural frequency of chassis longitudinal motion (4.5 Hz).

To provide an insight into the difference between the PSS vehicle and the conventional vehicle in the interested frequency range, the acceleration response to Class C (average) road unevenness (as seen in Figure 3-4) at 100 km/h are predicted and plotted in Figure 4-7. As mentioned previously, the response of the PSS vehicle is generally superior to the conventional vehicle in the longitudinal direction and comparable in the vertical direction. A slight deviation of the pitch acceleration response is observed between these two types of vehicles in the frequency range of 1 ~8 Hz.

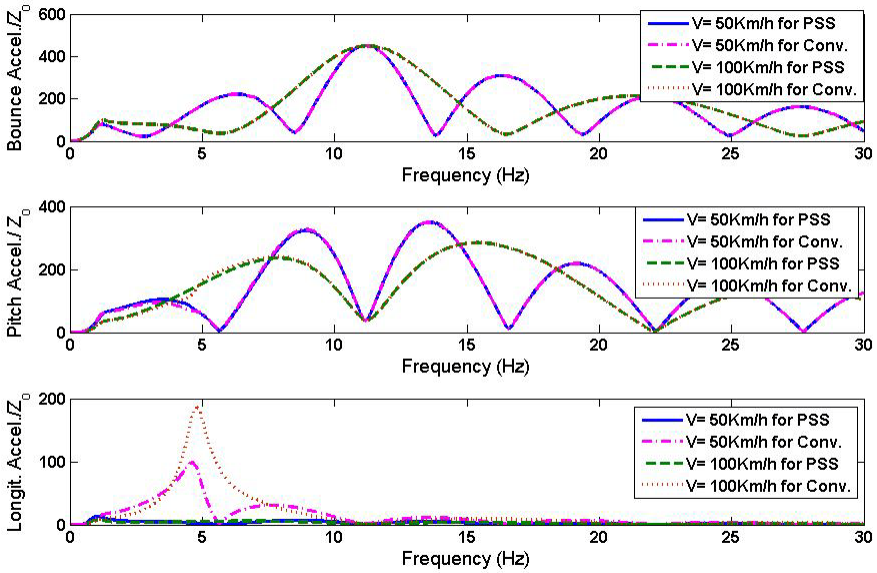

Figure 4-6: Chassis acceleration transmissibility of PSS and conventional vehicles

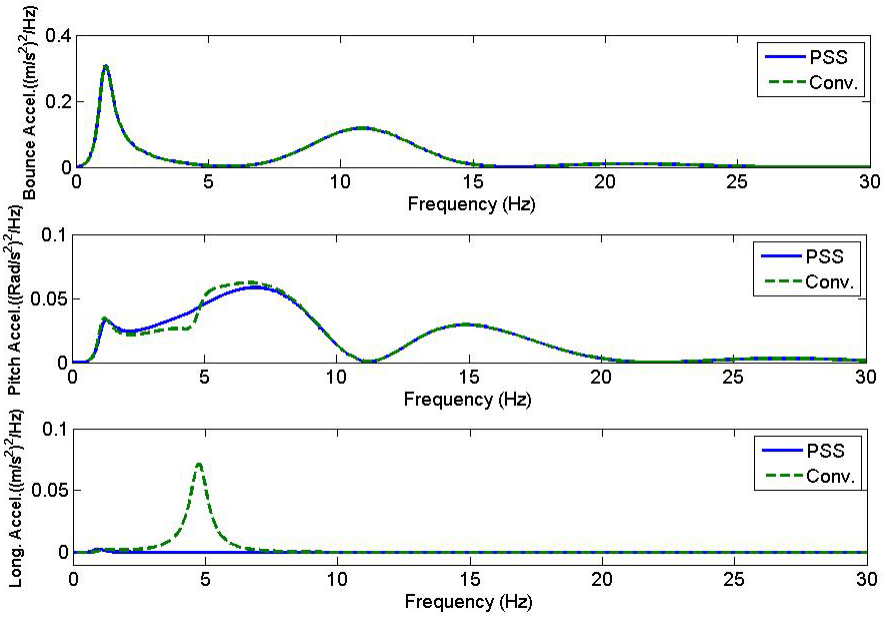

Figure 4-7: PSD of chassis acceleration response to average road roughness for PSS and conventional vehicles

The basic evaluation method using frequency weighted root-mean-squared (RMS) acceleration, as recommended by ISO 2631, is employed to assess ride comfort quantitatively. The frequency weighted root-mean-square of chassis acceleration is evaluated by ISO 2631 [28] as follows:

$$a_{ws} = \left[\int_{f_1}^{f_2} w^2 S_a(f) df \right]^{\frac{1}{2}} \tag{4.14}$$

where $S_a(f)$ is PSD of chassis acceleration response and w is the frequency weight factor. The frequency weight factor for the vertical vibration, pitch and the longitudinal vibration can be calculated, respectively, by [21]:

$$w_k = \begin{cases} 0.4 & 0.5 < f < 2Hz \\ \frac{f}{5} & 2 < f < 5Hz \\ 1 & 5 < f < 16Hz \\ \frac{16}{f} & 16 < f < 80Hz \end{cases}$$

$$w_d = \begin{cases} 1 & 0.5 < f \le 2 \\ \frac{2}{f} & 2 < f \le 80 \end{cases}, w_e = \begin{cases} 1 & 0.5 < f \le 1 \\ \frac{1}{f} & 1 < f \le 80 \end{cases} \tag{4.15}$$

where $w_{k,}$ w_d and w_e are the frequency weight factors for the vertical, longitudinal and pitch acceleration responses, respectively.

The term “ride” is commonly used in reference to tactile and visual vibrations (0.5~25 Hz). Vibrations with frequencies higher than 25 Hz, classified as noise, are not used in the evaluation of the ride quality. Therefore, in this evaluation, the integration range is 0.5~25Hz. The weighted roots-mean-square (RMS) accelerations, including the bounce, pitch and the longitudinal motions, were evaluated for both the PSS and conventional vehicles at a speed of 100 km/h as listed in Table 4.2. It can be concluded that, from a comfort point of view, the PSS vehicle is superior to the conventional vehicle in the longitudinal direction.

According to ISO 2631, the periodic, random and transient vibrations have effect on the health of seated persons in normal health exposed to whole-body vibration during travel, at work and during leisure activities. The effects of long-term high-intensity whole-body vibration can increase health risk to the lumber spine and the connected nervous system of the segments affected. With a lower

probability, vibration can also affect the digestive system, the genital/urinary system and the female reproductive organs. Meanwhile, ISO 2631 also states that vibrations affect the comfort of persons in normal health status. ISO 2631 gives the guidance applicable to vibration in the frequency range of 0.5Hz~80Hz in terms of health and comfort. The effect of multidirectional vibrations on health and comfort can be evaluated by the overall value of frequency weighted RMS acceleration, a_v, can be calculated by [28]:

$$a_v = (k_x^2 a_{wx}^2 + k_{ry}^2 \alpha_{wry}^2 + k_z^2 a_{wz}^2)^{\frac{1}{2}} \tag{4.16}$$

where $a_{wx,}$ a_{wz} are the frequency weighted RMS translational acceleration along the x and z directions while α_{wry} is the frequency weighted RMS rotational acceleration about the y axis (i.e. pitch motion). k_x, k_{ry} and k_z are the multiplying factors.

The multiplying factors can be selected in accordance with ISO 2631[28]. For seated persons, k_x and k_z can be selected as 1.4 and 1.0, respectively, when the effect of vibration on health is concerned. k_x, k_z at seat supporting surface are 1 when the effect of vibration on comfort is concerned; and if the rotational vibration is taken into account, the multiplying factor for pitch motion is 0.4 m/rad. Based on these values, the overall value of the weighted RMS acceleration, a_v, is calculated and listed in Table 4-2. It can be seen that the RMS value of the longitudinal acceleration of the PSS vehicle is much smaller than that of the conventional one while the RMS values of bounce and pitch accelerations are very close between the two types of vehicles. Table 4.2 further shows that for both health and comfort, the PSS vehicle is superior to the conventional vehicle.

Table 4-2: The weighted RMS of acceleration evaluated by basic evaluation method

	RMS of $\ddot{z}_s$ (m/s^2)	RMS of $\ddot{\varphi}_s$ (radian/s^2)	RMS of $\ddot{x}_s$ (m/s^2)	a_v (m/s^2) for health	a_v (m/s^2) for comfort
PSS	0.7954	0.1753	0.0392	0.7973	0.7995
Conventional	0.7954	0.1746	0.1379	0.8185	0.8103

4.4 Study of Pitch Dynamics in Time Domain

When running on a road, ground vehicles experience vibration due to road excitation in the form of either isolated irregularities, such as a bump or a pothole, or random distributed road unevenness. The

response of a PSS vehicle to these two kinds of excitations is important in the pitch dynamic study and thus discussed in this section.

4.4.1 Development of Vehicle Model

There are two factors in the longitudinal motion of a vehicle chassis when running on a road with irregularities. The first factor is the existence of pitch motion and the asymmetry of two wheels about the chassis mass center. The second factor is the longitudinal force transferred to the chassis from the tire when the tire encounters road obstacles. A linear point tire-ground contact model cannot generate the external input from the ground. A radial-spring tire model as described in Section 3.4, together with the Average Lumped LuGre model, is employed to generate the tire-ground contact force and the longitudinal friction force. The tire models are combined with the vehicle model to study the pitch dynamics in the time domain.

Vehicle model

The 6-DOF pitch plane model used in the frequency domain study is extended to a 9-DOF pitch plane half-car mode, as shown in Figure 4.8. The nine DOFs are the chassis vertical (z_s), pitch (φ_s), longitudinal motion (x_s), the front wheel vertical (z_{uf}), longitudinal (x_{uf}), spin motion (ω_{uf}), the rear wheel vertical (z_{ur}), longitudinal (x_{ur}), the spin motion (ω_{ur}). This model neglects the effect of rolling resistance and aerodynamic forces. It is worth noting that the spin motion of the two wheels should be considered so that the dynamic longitudinal tire-ground friction force can be taken into account. Otherwise the longitudinal force between the tires and ground only consist of the part due to tire deflection when passing over obstacles or unevenness, whereas the part of the tire-ground friction due to relative slip could be missed. This point will be discussed later.

The static height between the chassis mass center and tire center as seen in Figure 4-8 is signified by h. T_f and T_r represent the traction or braking torques applied to the front and rear tires, respectively. F_{zf} and F_{zr} stand for the normal contact forces applied to the front and rear tires, respectively; and F_{xfc} and F_{xrc} are the longitudinal contact forces due to tires' elastic deflections, and are applied to the centers of the front and rear tires, respectively. These forces can be predicted using the radial-spring tire model as presented in Section 3.4. F_{xft} and F_{xrt} are the longitudinal friction forces applied to the front and rear tires, respectively and can be predicted from an Average Lumped LuGre tire friction model discussed in later stage. The equations of motions are as follows:

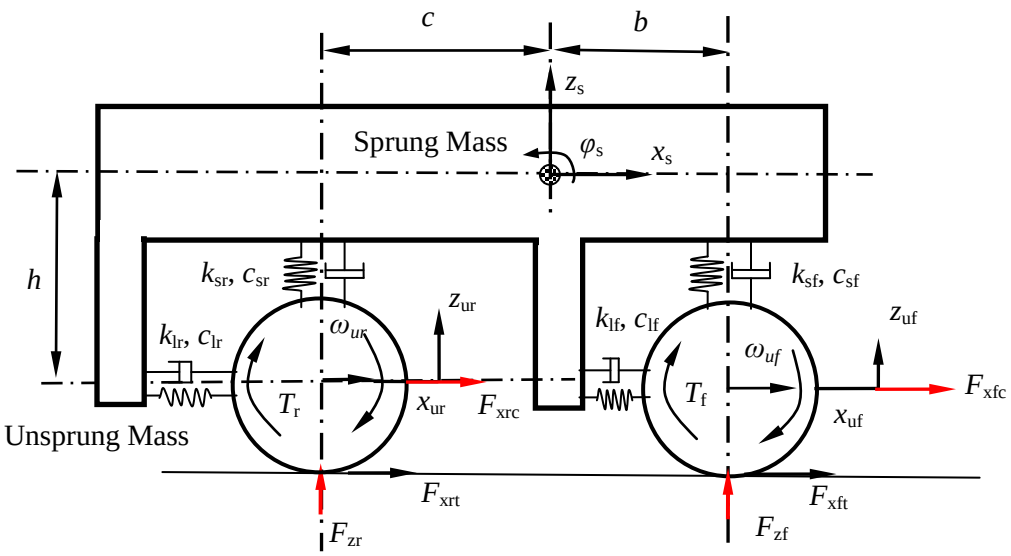

Figure 4-8: 9-DOFs two-dimensional planar half-car vehicle model

$$m_s\ddot{z}_s = -(c_{sf}+c_{sr})\dot{z}_s - \left[c_{sf}(x_{uf}-x_s) - c_{sr}(x_s-x_{ur})\right]\dot{\varphi}_s + c_{sf}\dot{z}_{uf} + c_{sr}\dot{z}_{ur} - (k_{sf}+k_{sr})z_s - \left[k_{sf}(x_{uf}-x_s) - k_{sr}(x_s-x_{ur})\right]\varphi_s + k_{sf}z_{uf} + k_{sr}z_{ur} - m_s g \tag{4.17-1}$$

$$I_s\ddot{\varphi}_s = -\left[c_{sf}(x_{uf}-x_s) - c_{sr}(x_s-x_{ur})\right]\dot{z}_s - \left[(x_{uf}-x_s)^2 c_{sf} + (x_s-x_{ur})^2 c_{sr}\right]\dot{\varphi}_s + (x_{uf}-x_s)c_{sf}\dot{z}_{uf} - (x_s-x_{ur})c_{sr}\dot{z}_{ur} - \left[k_{sf}(x_{uf}-x_s) - k_{sr}(x_c-x_{ur})\right]z_s - \left[(x_{uf}-x_s)^2 k_{sf} + (x_s-x_{ur})^2 k_{sr}\right]\varphi_s + (x_{uf}-x_s)k_{sf}z_{uf} - (x_s-x_{ur})k_{sr}z_{ur} + F_{lf}(h+z_s-z_{uf}) + F_{lr}(h+z_s-z_{ur}) \tag{4.17-2}$$

$$m_{uf}\ddot{z}_{uf} = c_{sf}\dot{z}_s + (x_{uf}-x_s)c_{sf}\dot{\varphi}_s - c_{sf}\dot{z}_{uf} + k_{sf}z_s + (x_{uf}-x_s)k_{sf}\varphi_s - k_{sf}z_{uf} - m_{uf}g + F_{zf} \tag{4.17-3}$$

$$m_{ur}\ddot{z}_{ur} = c_{sr}\dot{z}_s - (x_s-x_{ur})c_{sr}\dot{\varphi}_s - c_{sr}\dot{z}_{ur} + k_{sr}z_s - (x_s-x_{ur})k_{sr}\varphi_s - k_{sr}z_{ur} - m_{ur}g + F_{zr} \tag{4.17-4}$$

$$m_s\ddot{x}_s = F_{lf} + F_{lr} \tag{4.17-5}$$

$$m_{uf}\ddot{x}_{uf} = F_{xfc} - F_{lf} + F_{xft} \tag{4.17-6}$$

$$m_{ur}\ddot{x}_{ur} = F_{xrc} - F_{lr} + F_{xrt} \tag{4.17-7}$$

$$I_{uf}\dot{\omega}_{uf} = T_f - F_{xft}R_{ef} \tag{4.17-8}$$

$$I_{ur}\dot{\omega}_{ur} = T_r - F_{xrt}R_{er} \tag{4.17-9}$$

where F_{lf} and F_{lr} are the longitudinal forces of the front and rear suspension, and can be determined by the following equations:

$$\begin{aligned} F_{lf} = {} & \frac{k_{of}}{d_r^2}\left[x_{uf} - x_s - (h + z_s - z_{uf})\varphi_s - b\right]^3 + k_{of}\left[x_{uf} - x_s - (h + z_s - z_{uf})\varphi_s - b\right] \\ & + c_{lf}\left[\dot{x}_{uf} - \dot{x}_s - (h + z_s - z_{uf})\dot{\varphi}_s\right] \end{aligned} \tag{4.18-1}$$

$$\begin{aligned} F_{lr} = {} & \frac{k_{or}}{d_r^2}\left[x_{ur} - x_s - (h + z_s - z_{ur})\varphi_s + c\right]x_{ur}{}^3 + k_{or}\left[x_{ur} - x_s - (h + z_s - z_{ur})\varphi_s + c\right] \\ & c_{lr}\left[\dot{x}_{ur} - \dot{x}_s - (h + z_s - z_{ur})\dot{\varphi}_s\right] \end{aligned} \tag{4.18-2}$$

where d_r is a parameter to control the upper bound of the spring deflection and assumed to be 5 cm; and k_o is the nominal stiffness parameter of a planar suspension system, which is equal to the corresponding vertical spring stiffness.

As mentioned in Section 3.2, there always exist joints with rubber bushings between the suspension and the chassis, which can transfer longitudinal forces. These bushings can be treated as the longitudinal spring elements with large stiffness. Therefore, the proposed model can also be applied to a conventional vehicle.

It is necessary to point out that this vehicle model can also be employed to study the braking and traction performance as long as the braking or driving torques applied to the tires are given. However, it is assumed in this study that the vehicle has a constant forward speed before touch the road obstacles and there is no applied torque to the tires.

Tire-Ground Longitudinal Friction Model

To simulate the longitudinal tire-ground dynamic friction in the event that tires experience excessive speed changing when a tire traverses an obstacle or running off-road, the Average Lumped LuGre model proposed by Canudas-de-Wit [101] is employed in this study. This model takes into account the distribution properties of the normal wheel force in the contact patch, and can accurately capture the transient friction behaviour, as well as any velocity-dependent characteristics according to the reported simulation and experiment results [101].

The tire-ground friction force characteristic in the Average Lumped LuGre model is described by the following equations [101]:

$$\dot{\bar{z}}(t) = v_r - \frac{\sigma_o |v_r|}{g(v_r)} \bar{z}(t) - k(t) |\omega R_e| \bar{z}(t) \tag{4.19}$$

$$\mu(t) = \sigma_o \bar{z}(t) + \sigma_1 \dot{\bar{z}}(t) + \sigma_2 v_r \tag{4.20}$$

$$F_{xt}(t) = \mu(t) F_z \tag{4.21}$$

$$\text{with } g(v_r) = \theta \left[\mu_c + (\mu_s - \mu_c) e^{-\left|\frac{v_r}{v_s}\right|^{\alpha}} \right] \tag{4.22}$$

where $\bar{z}(t)$ is the mean internal dynamic friction state and the parameter θ in equation (4.22) captures the changes in the road characteristics. v_r is the relative velocity defined by:

$$v_r = R_e \omega - \dot{x}_u \tag{4.23}$$

where ω is the angular velocity of a tire and $\dot{x}_u$ is the linear forward velocity of the tire center. R_e is the effective rolling radius of the tire.

Model parameters σ_o, σ_1 and σ_2 are the stiffness, damping and viscous relative damping coefficients, respectively. $\mu(t)$ is the dynamic friction coefficient. F_{xt} and F_z are the friction and normal forces, respectively. The coefficient, $k(t)$, represents the dynamic distribution properties of the normal force. As suggested in reference [101], it can be chosen to be between $1/L_c$ and $2/L_c$ where L_c is the contact patch length. μ_c and μ_s are the Coulomb and static friction coefficients, respectively. v_s is the Stribeck relative velocity and α is a parameter to capture the steady-state friction/slip characteristic and its proposed value is 0.5 [101]. The parameters used for the tire model are listed in Table 4-3.

Table 4-3: Parameters for tire friction model

R (m)	σ_o (m^{-1})	σ_1 (s/m)	σ_2 (s/m)	μ_c	μ_s	v_s (m/s)	α	k
0.306	178	1	0.011	0.08	1.5	5.5	1/2	$1.5/L_c$

4.4.2 Response due to an Isolated Road Obstacle

In this study, an 850 mm long, 100 mm high single sinusoidal bump is used to model the road irregularity. This bump can be typically found in a speed-constrained zone. The responses of a vehicle with PSS and conventional suspension system to this road excitation are investigated using the 9-

DOF analytical vehicle model. In order to validate the result, the responses due to the same road excitation are also predicted by Adams/car virtual models as shown in Figure 4-9. The Adams full-car model of a PSS model, as well as that of a conventional model, consist of a body system, two suspension systems, two wheel systems and a brake system. The vehicle parameters are for a midsize passenger car. The mass property of sprung and unsprung masses, spring and damping rates, the vehicle dimensional are the same as the values of the analytical model, as listed in Table 4-1. For a conventional vehicle, the front suspension system is a MacPherson front suspension while the rear suspension is a dual-link MacPherson rear suspension. The vertical spring rates and damping coefficients are equal to those of the 9-DOF vehicle model. The bushings are used and the active mode is compliance so as to achieve some longitudinal elasticity. For a PSS vehicle, the suspension systems are developed by adding the longitudinal struts to the conventional MacPherson suspension system as schemed in Figure 1-2. The parameters for the tire friction model in Adams/car, which is actually Magic Formula, are modified according to Table 4-3 using the method discussed in reference [101].

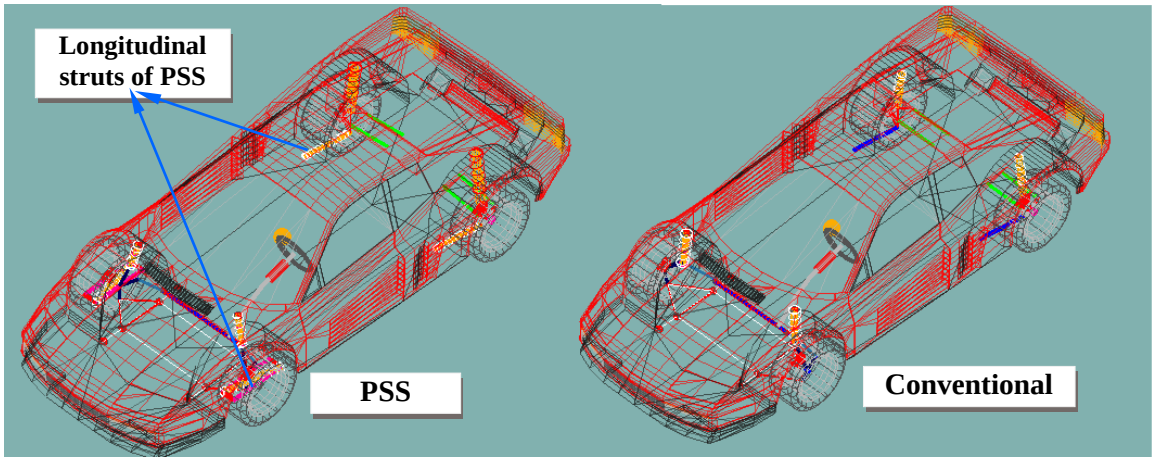

Figure 4-9: Virtual model of a PSS vehicle and a conventional vehicle

The simulation speed is 50Km/h. Figure 4-10 illustrates the time history of the acceleration responses of the PSS and conventional vehicles. The results clearly indicate that a bump can excite vibrations in both the vertical and longitudinal directions.

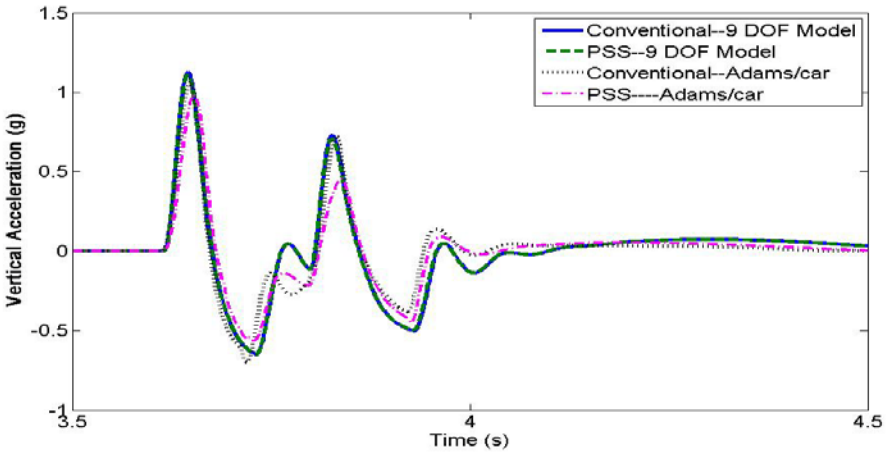

(a) Vertical

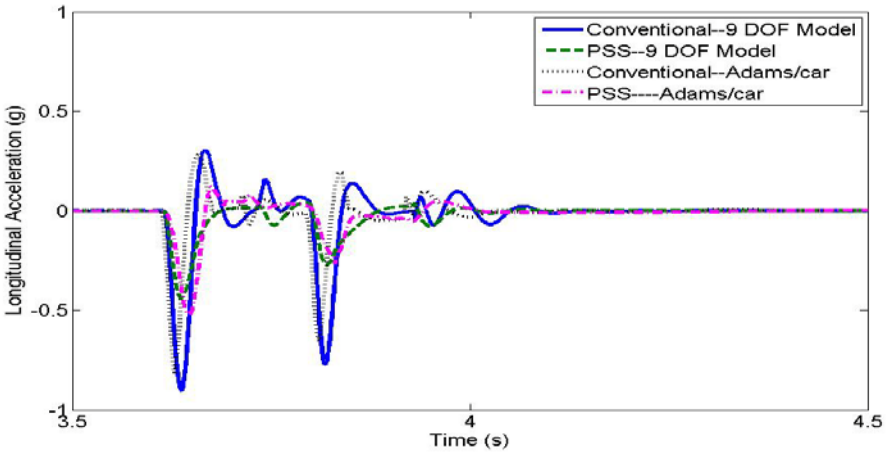

(b) Longitudinal

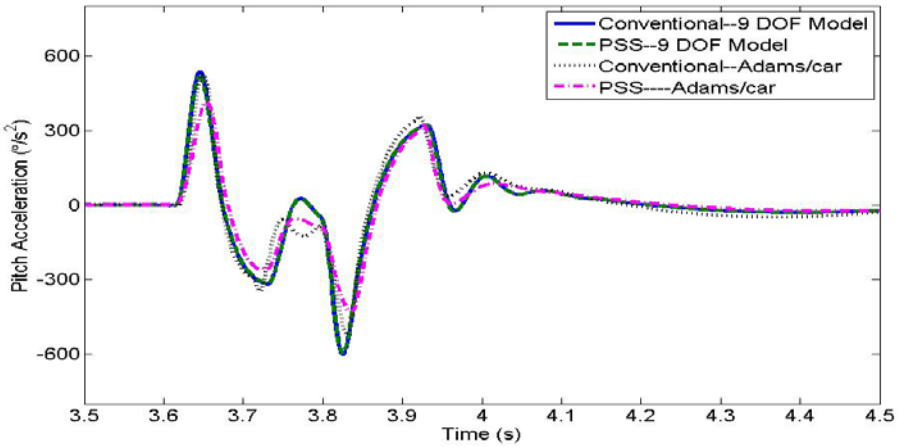

(c) Pitch

Figure 4-10: Time history of vehicle acceleration response to a single road bump

The vertical acceleration responses for the conventional vehicle obtained from two types of simulation models have a fairly good agreement, as shown in Figure 4-10(a), which demonstrates the fidelity of the proposed analytical 9-DOF model. For the PSS vehicle, a deviation is observed in the vertical acceleration response between the 9-DOF analytical model and the Adams/car model. This deviation is more obvious when the rear wheel hits the bump. The deviation results from the difference of suspension vertical stiffness in the 9-DOF model and the ride rate in Adams/car model. Because the vertical strut has to move towards the vehicle centerline to accommodate the parallel four-bar mechanism, the ride rate of a front PSS is smaller than the spring stiffness of the front suspension in 9 DOF model. Also, unlike the 9-DOF model, the longitudinal and vertical springs of PSS in the Adams/car model are completely coupled. Furthermore, the complexity of the Adams/car model may also induce some difference in the simulation response. Even though, the simulation results, obtained from either the 9-DOF analytical model or the Adams/car model, demonstrate that the vertical acceleration responses of the PSS and conventional vehicles to this single road bump are generally comparable.

Figure 10 (b) displays the longitudinal component of the acceleration responses. The responses of the two types of vehicles obtained from the 9-DOF vehicle model have shown a good agreement with those from Adams/car model although some differences are observed. The simulation results demonstrate that the planar suspension system has a significant improvement in absorbing the longitudinal shock induced by the road obstacle. The ride comfort of the vehicle with PSS has therefore shown improved. Figure 10 (c) portrays the pitch acceleration response. The result implies that the pitch responses are comparable for the two types of vehicles. The deviation is observed between the pitch acceleration of the PSS vehicle predicted from Adams/car model and that from the 9-DOF analytical model. This deviation can also be attributed to the difference of suspension vertical ride rate in the two types of vehicle models.

In order to have a better understanding of the vehicle behaviour when passing over a road bump, the tire-ground interaction forces are predicted and plotted in Figure 4-11. The simulation results imply that a road bump can induce an upward impact force as well as a backward impact force when the vehicle hits the bump. The results also indicate that both the front and rear tires lose contact after the tire passes over the bump top point at the assigned simulation speed. The contact forces of the PSS and conventional vehicles due to tire elastic deflection are identical in the vertical and longitudinal directions. The results further reveal that the longitudinal friction forces are generated in

the contact patch when tires transverse road obstacles, and therefore, must be taken into account in the modeling and simulation. That is the reason why the wheel spin motions should be considered in the formulation of the half–car model for the time domain study. Figure 4-11 also shows that the transient longitudinal friction forces are quite different between the PSS and conventional vehicles. This difference is attributed to the different relative longitudinal slips between the tire and the ground when the tires are traversing the bump.

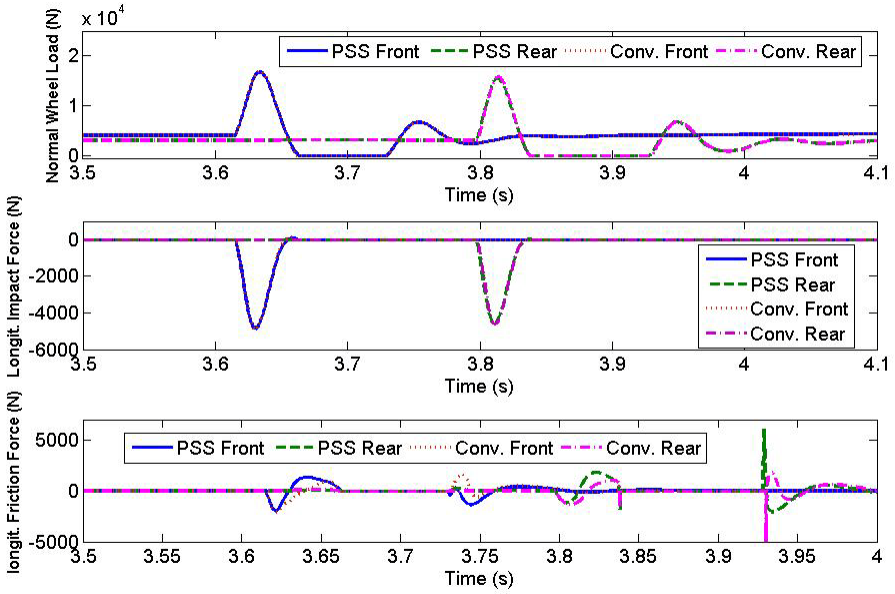

Figure 4-11: Time history of the tire force when traversing a road bump

The longitudinal strut travel space may be a concern arising from the replacement of the stiff trailing arm by a relatively soft longitudinal strut. The longitudinal deflection of the planar suspension system is thus investigated, as illustrated in Figure 4-12. It can be seen that, when the vehicle passes over the bump at 50Km/h, the maximum longitudinal compression is only 3.5 cm. This is because the maximum deflection is constrained by the nonlinear property of the longitudinal spring. When the deflection exceeds a certain value (5cm), d_r, the spring rapidly becomes very stiff.

In order to investigate how far a PSS can improve the longitudinal ride comfort compared to a conventional suspension, the simulation is conducted at different speeds and the peak values of longitudinal acceleration responses for the front and rear axles are predicted as illustrated in Figure 4-13. The results indicate that the PSS can reduce the vehicle longitudinal acceleration response at the entire simulation speed range. Such a reduction is not evident at very low speed whereas very

significant at high speed. This can be explained by the fact that the suspension system is actually in a static or quasi-static state at very low speed and the PSS cannot efficiently isolate the static tire-ground interaction.

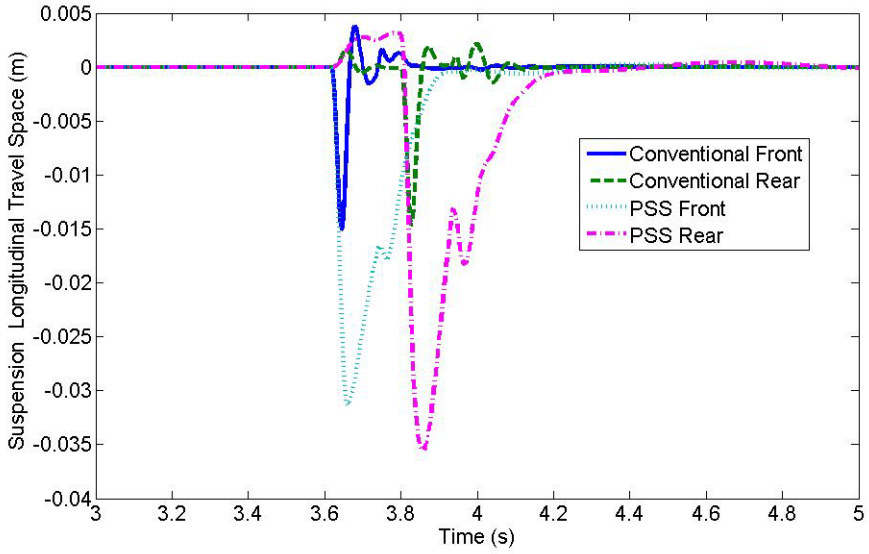

Figure 4-12: Time history of the suspension longitudinal deflection

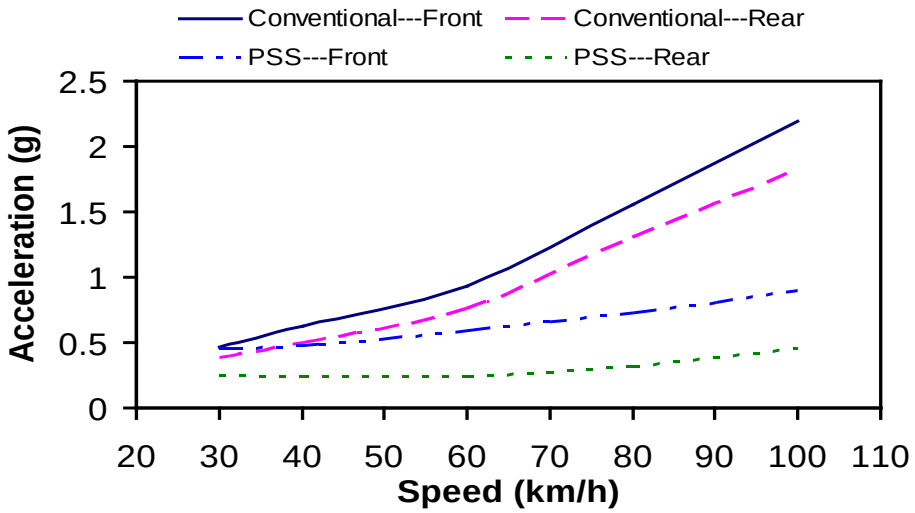

Figure 4-13: Peak value of longitudinal acceleration of a vehicle with PSS and conventional suspension system

Figure 4-14 illustrates the time history of the pitch response of the two types of vehicles due to a 200mm long, 150mm high road bump at 50km/h. it can be seen that while the responses ob the two types of the vehicles are very close, the PSS vehicle has a slightly larger pitch motion. This is due to the relatively soft longitudinal stiffness in the planar suspension system.

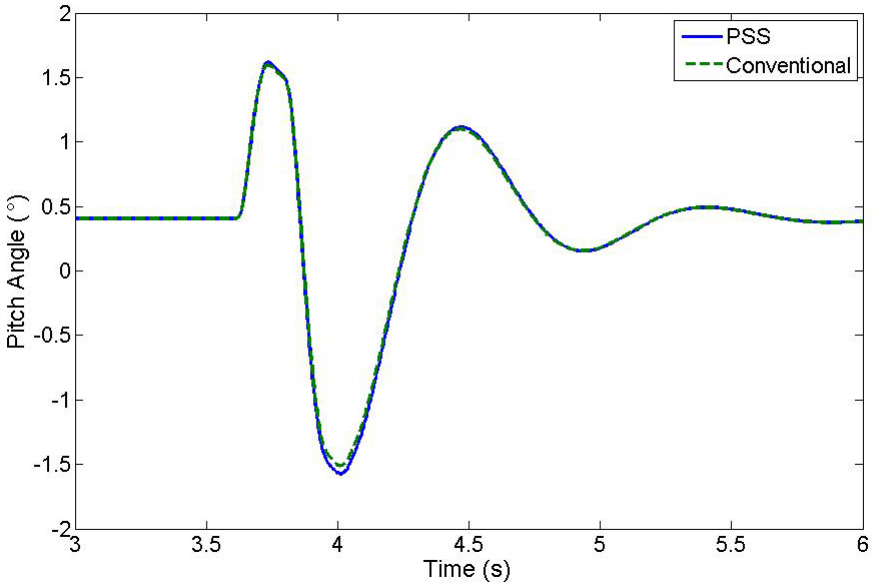

Figure 4-14: Time history of pitch angle of the PSS and conventional vehicles

4.4.3 Response due to Distributed Road Unevenness

A vehicle experiences vibration excitation on a rough road or an off-road where ground excitations have a wide range of frequency component. In order to explore the vibration isolating ability of a PSS vehicle in such a condition, the pitch dynamic behaviour of the PSS vehicle on an uneven road is investigated and compared with that of a similar conventional vehicle.

The ISO standard provides the road profile with power spectral density (PSD) of random elevations against spatial frequency. This kind of road description can be directly used in the frequency domain analysis, as presented in the previous section. However, for the pitch dynamics, the study in the frequency domain cannot completely illustrate the effect of the coupling between two wheels due to the existence of time lag. Many researchers transmitted such a road description to the random road unevenness from frequency domain to time domain [15, 16, 35]. In this study, samples of the road profiles are generated using the spectral representation method [15]. The random road elevation, z_o, can be expressed by:

$$z_o(x) = \sum_{n=1}^{N} s_n \sin(\Omega_n x + \phi_n) = \sum_{n=1}^{N} s_n \sin(n\Omega_o x + \phi_n) \tag{4.24}$$

where s_n is the magnitude of the harmonics excitation of frequency Ω_n ($n\Omega_o$) and can be evaluated from the selected road spectra as follows:

$$s_n = \sqrt{2S_g(\Omega_n)\Delta\Omega} = \sqrt{2S_g(n\Omega_o)\Delta\Omega} \tag{4.25}$$

where S_g is the road power spectral density (PSD) and $\Delta\Omega$ is the spatial frequency increase step and can be calculated by:

$$\Delta\Omega = \frac{2\pi}{L} \tag{4.26}$$

where L is the length of the road segment considered. Ω_o is selected equal to 0.01. The phases φ_n are treated as random variables, following a uniform distribution in the interval [0 2π].

The aforementioned method of selecting the road excitation history requires knowledge of the power spectral density of the road profile. Figure 4-15 shows the specific forms of three typical road profiles for a 100 m long segment corresponding to the spectra of three classes of roads, i.e., good, average and poor quality roads shown in Figure 3-4, as examples in the numerical calculations performed in this study. Although it seems that the fundamental shape of the road is harmonic, Figure 4-15 describes the uneven characteristics of the different types of roads. Therefore, this method is used to generate the random profile [15].

In this study, a 100 m long road segment with class C profile is used as the input to investigate the pitch dynamic performance of the PSS vehicle due to the random excitation. The simulation speed is 100 km/h. For the random response study, only the chassis bounce, pitch and the longitudinal acceleration are evaluated.

The comparison of the acceleration response between a PSS and a conventional vehicle are predicted and plotted in Figure 4-16. The chassis bounce and pitch accelerations of the PSS vehicle are almost identical to those of the conventional vehicle. The difference cannot be determined from the figure. However, the difference of chassis longitudinal acceleration is very significant. Compared to the conventional vehicle, the chassis longitudinal acceleration of the PSS vehicle is very small.

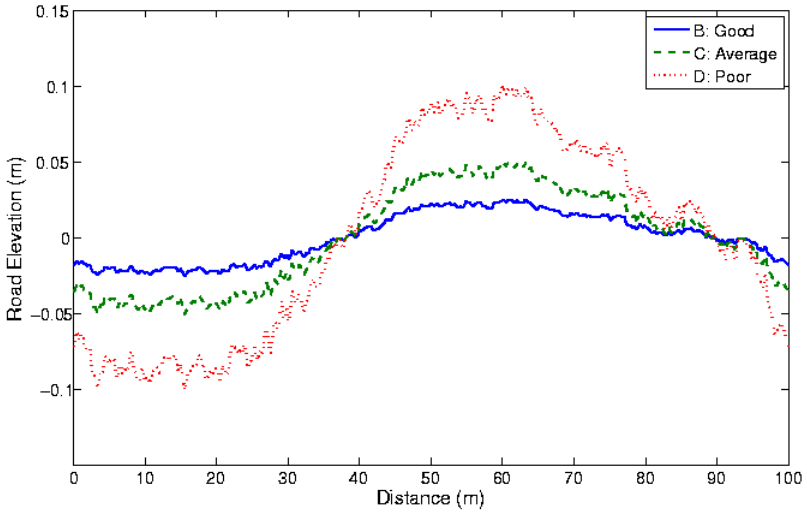

Figure 4-15: Description of road profile in elevation of good, average and poor road quality

Frequency weighting is performed to the acceleration response in accordance with ISO 2631. This weighting can be conducted using signal filters. The transfer functions of these filters are defined and presented in Annex-A of ISO 2631-1. The values of the weighting factors at different frequencies (i.e. the magnitudes of transfer functions vs. frequency) are plotted in Figure 4-17. It should be noted that the unit of the weighting factors is *dB*. W_k, W_d, W_e represent the frequency weighting for the bounce motion (translation along *z* direction), longitudinal motion (translation along *x* direction) and the pitch motion (rotation about *y* axis), respectively. The time history of frequency-weighted acceleration can be obtained by filtering the signals of acceleration response illustrated in Figure 4-16. After the acceleration responses are frequency-weighted, the mean square values of the frequency-weighted acceleration can be readily calculated using the method described by ISO 2631.

The frequency weighted mean square values of the acceleration response during the period when the vehicle is running on a 100 m road segment with the random unevenness are evaluated using the basic method as listed in Table 4-4. The results show that, in the vertical direction, the RMS of acceleration response of the PSS vehicle is close to that of the conventional vehicle, whereas the RMS of the pitch acceleration of the PSS vehicle is somehow larger. However, the difference is very small and can be neglected. In the longitudinal direction, the RMS of the acceleration response of the PSS vehicle is very small compared to that of the conventional vehicle due to the soft longitudinal connection between the sprung and unsprung masses. The overall frequency-weighted acceleration is

also calculated using equation (4-16) and listed in Table 4-4. The evaluation results indicate that the PSS vehicle improves for both health and comfort compared with the conventional vehicle.

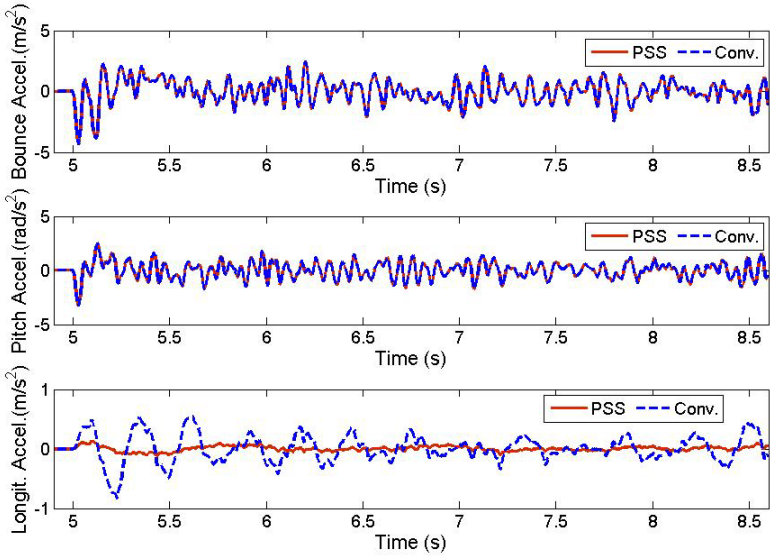

Figure 4-16: Comparison of chassis acceleration for the PSS and conventional vehicles

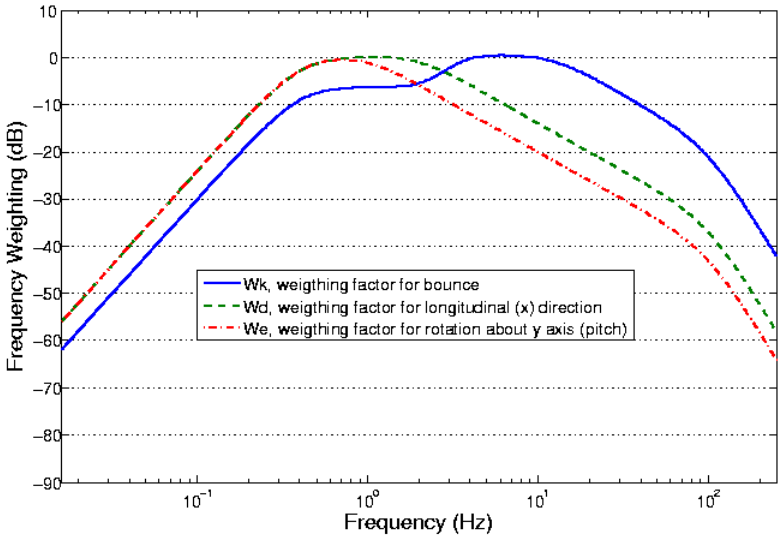

Figure 4-17: Frequency weighting factor vs. frequency

Table 4-4: Root mean square (RMS) value of the frequency weighted acceleration response at 100km/h

	RMS of Bounce (m/s^2)	RMS of Pitch (rad/s^2)	RMS of Long. (m/s^2)	a_v (m/s^2) for health	a_v (m/s^2) for comfort
PSS	0.7958	0.1483	0.0357	0.7974	0.7988
Conventional	0.7959	0.1455	0.1307	0.8167	0.8087

The simulation conditions, such as the road roughness and simulation speed, for the frequency and time domain study are identical. Therefore, it is interesting to find that the RMS values of the frequency weighted acceleration response evaluated in time domain shown in Table 4-4, are very close to those evaluated in the frequency domain, as listed in Table 4-2. The evaluation results obtained from the two approaches, especially in the vertical direction, are almost identical. Small differences exist in the results in terms of the pitch and longitudinal motions. The difference in the pitch and longitudinal motions are due to the fact that the external longitudinal excitation due to the random road roughness cannot be accounted for by the linear point tire model used in the frequency study. However, the differences are very small and can be neglected. In other word, it can be concluded that the evaluation results obtained in the frequency and time domains have a good consistence. The results also indicate that the method for the generation of random road profile is effective.

The Adams/car models are also used to predict the vehicle longitudinal acceleration responses due to the random road excitation at 50km/h, as shown in Figure 4-18. The road description used in the Adams/car model is *MDI_2D_uneven.rdf* provided in the MD Adams/car package. Figure 4-18 reflects a significant improvement of the PSS system compared to the conventional suspension system in isolating vibrations along the longitudinal direction. The longitudinal acceleration response of the vehicle with PSS is much smaller than that of the vehicle with the conventional vehicle. Although bushings are widely used in the construction of the conventional suspension Adams model, the vibration isolation ability is still very weak compared to that of the planar suspension system.

In order to thoroughly investigate the effect of PSS on ride quality, the ride quality of the PSS vehicle at different speeds is evaluated. Previous study demonstrates that the proposed 9-DOF analytical vehicle model is effective to simulate the vehicle behaviour on an uneven road. However, it was also found that the simulation is very time-consuming using this model compared with using

Adams/car model. Therefore, the investigation is conducted using Adams/car package. The road model used in the investigation is *MDI_2D_uneven.rdf*. Using the approach discussed previously, the RMS values of the frequency weighted acceleration responses, as well as the overall values, are evaluated at 30, 50, 80 km/h, as listed in Table 4-5.

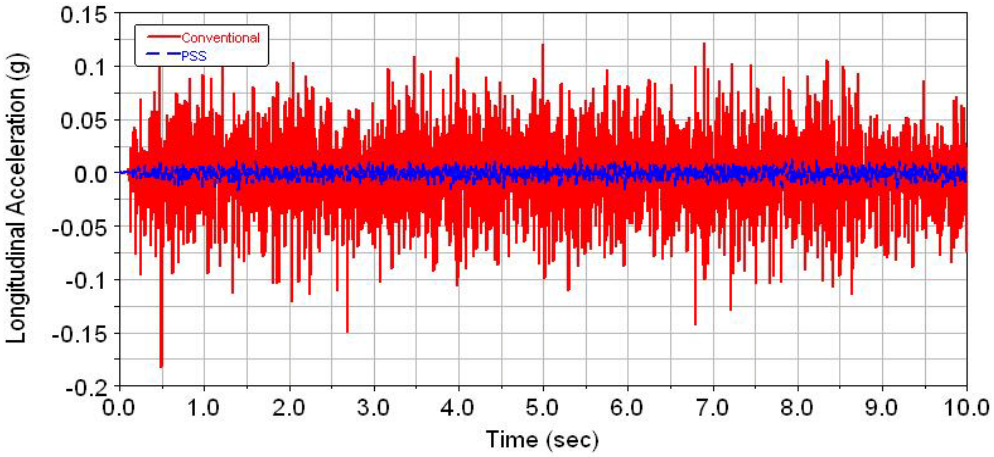

Figure 4-18: Time history of vehicle longitudinal acceleration response to random road unevenness (*MDI_2D_uneven.rdf*)

Table 4-5: Root mean square (RMS) of the frequency weighted acceleration response at various speed

		RMS of Vertical (g)	RMS of Pitch (rad/s^2)	RMS of Long. (g)	a_v (g) for health	a_v (g) for comfort
PSS	30km/h	0.0097	0.0155	**0.00039**	0.0097	0.0098
	50km/h	0.0083	0.0139	**0.00046**	0.0083	0.0083
	80km/h	0.0073	0.0125	**0.00063**	0.0074	0.0074
Conv.	30km/h	0.01	0.0144	**0.0016**	0.0102	0.0101
	50km/h	0.0099	0.0136	**0.0032**	0.0109	0.0104
	80km/h	0.0083	0.0116	**0.0028**	0.0092	0.0088

The result indicates that the overall value of weighted RMS acceleration of the PSS vehicle is smaller than that of the conventional one. The vibration isolation capacity of the PSS vehicle is much better than that of the conventional vehicle, especially in the longitudinal direction. There should be no surprise that the RMS values of frequency weighted acceleration in any direction, as well as the

overall values of weighted RMS acceleration, do not increase with an increase in the vehicle speed. The reason is that the frequency of random excitation increases with the vehicle speed and the high frequency components of the responses are filtered in frequency weighting. Compared with the results shown in Table 4-4, the improvement of the PSS vehicle in terms of the vertical response presented in Table 4-5 over the conventional vehicle is relatively larger, and consequently the overall results shown in Table 4-5 exhibit more improvement than those shown in Table 4-4. The relatively small vertical response of the PSS vehicle obtained from Adams/car model is attributed to the small ride rate as discussed previously.

4.5 Summary

In this chapter, a linear half car model with 6 DOFs was first proposed to perform the frequency domain study. In this model, the tire-ground contact was modeled as a linear point contact. The nonlinear longitudinal spring in a PSS was linearized at the point with zero deflection. The dynamic frequency response of a PSS vehicle to the frequency input was investigated and compared with those of a similar conventional vehicle. These frequency responses were used to evaluate the ride quality based on the basic evaluation method provided by ISO 2631. The evaluation results indicate that for both health and comfort, the PSS vehicle is superior to the conventional vehicle. A significant improvement has achieved in terms of vibration isolation in the longitudinal direction.

In addition, a nonlinear 9-DOF half-car pitch plane vehicle model was developed to facility the time domain study incorporating a radial-spring tire-ground contact model and an Average Lumped LuGre tire dynamic friction model. This vehicle model was validated with Adams/car virtual model. The vertical, longitudinal and pitch acceleration responses of the PSS vehicle as well as the conventional vehicle to the road excitations, including a single bump and random unevenness, were investigated. These responses were used to evaluate the ride quality. The evaluation exhibits good potential for the implementation of the planar suspension system in ground vehicles. The investigation results demonstrate that a significant improvement of shock attenuation and vibration isolation can be obtained in the longitudinal direction through the application of the PSS. The ride quality of the PSS vehicle can thus be improved.

Chapter 5
Handling Dynamics Study: Model Development and Steady-State Characteristics

5.1 Overview0

The handling performance of a ground vehicle involves directional control and directional stability. The directional behaviour of a vehicle is mainly controlled by the lateral force generated at the tire-ground contact patch and the location of the front and rear tires with respect to the gravity center of the vehicle. Meanwhile, the lateral force is determined by the relative tire-ground slippages, tire-ground contact condition and the vehicle weight distribution at the front and rear tires, etc. The soft longitudinal connection of a vehicle equipped with planar suspension systems (PSS) can induce relative longitudinal motion between the chassis and tires. This relative motion may influence not only the vehicle weight distribution (wheelbase) but also the tire-ground relative slippages. These relative slippages significantly influence the longitudinal and lateral forces, and can further influence the handling behaviour. Such an influence may determine the feasibility of the design concept of the PSS. Therefore, it is necessary to investigate the handling behaviour including directional control and directional stability of a vehicle equipped with PSS.

The commonly-used vehicle model for handling study is a half-car single-track model (or bicycle model) with three DOFs (longitudinal, lateral and yaw motions of a vehicle) [45, 48]. This model, however, neglects the axle mass (unsprung mass) and suspension effect, and cannot model the relative longitudinal motions between the chassis and tires of the PSS vehicle. In this study, a single-track handling model system, consisting of a vehicle sub-model and tire sub-model, is developed. The vehicle sub-model includes a pitch plane and a yaw plane models so that the bounce, pitch, lateral and longitudinal motions are taken into account. The tire sub-model consists of a radial spring contact model and a dynamic 2D friction model which can generate the transient longitudinal and lateral adhesion or friction forces. The total number of degrees of freedom (DOF) in the model system is 15, among which 11 DOFs describe the vehicle dynamic motions and 4 DOFs model the front and rear tires' dynamic friction behaviour. This model is used to investigate the coupling between the traction (or braking), handling, pitch and the bounce motions of a vehicle with PSS. The schematic diagram of the model system is illustrated in Figure 5-1.

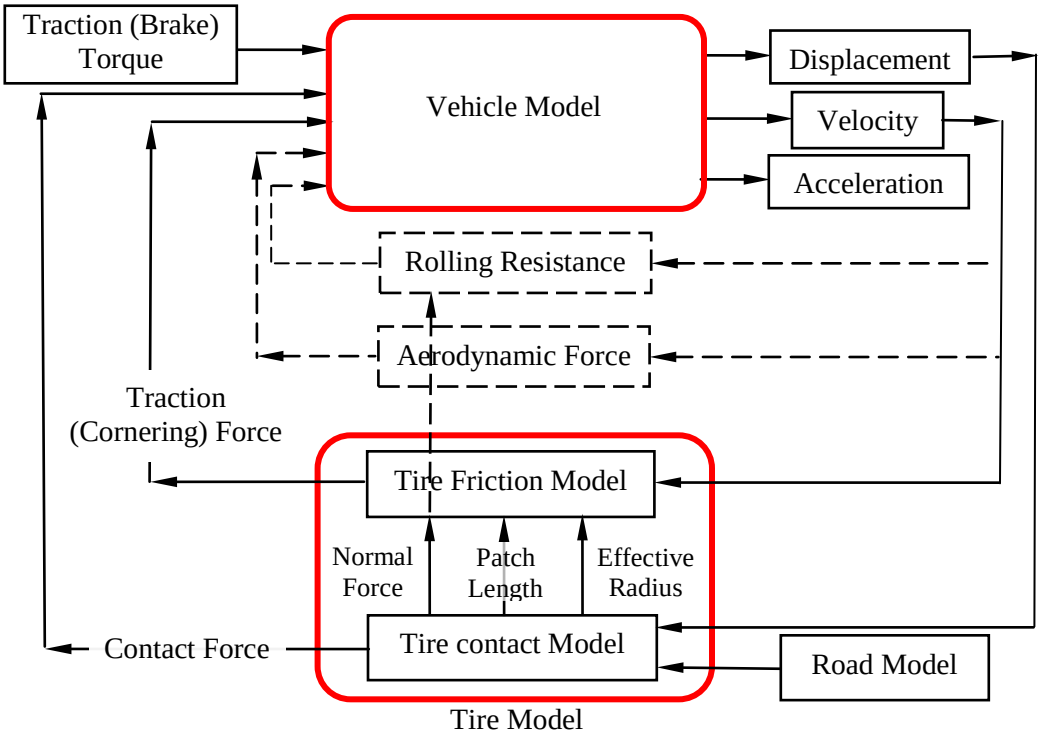

Figure 5-1; Overall model layout for the handling performance of a ground vehicle

The study of vehicle handling generally involves three issues: the steady-state steering response, frequency steering response and the transient steering response. In this chapter, the formulation of simulation model is first presented followed by the steady-state handling performance study of a vehicle with planar suspension systems. The other two issues are discussed in the next chapter. The developed model and corresponding approach are also applied to a similar conventional vehicle for the sake of comparison.

5.2 2D Average LuGre Dynamic Tire Friction Model

An accurate prediction of the tire-ground friction force by an appropriate tire friction model is the crucial element of a vehicle handling simulation model. Therefore, the tire friction modeling is first discussed in this section.

Through the decades, numerous tire-ground friction models have been proposed [86, 87, 88]. Among these models, the most commonly used one is the semi-empirical Magic Formula presented by Pacejka [88]. However, this model is essentially a static model generally used to reproduce the experimental tire friction curves according to the longitudinal and side slip at a constant vehicle speed

or tire angular velocity. The steady-state condition is rarely true in reality, especially when the tires pass through continuous successive states during cornering and acceleration/braking maneuvers. Dynamic models, on the other hand, can capture transient effects and are of interest when a vehicle is under large variations of states. Thus, a number of dynamic tire-ground friction models have been proposed [86, 87], but few of them are reported to be successfully applied to the vehicle dynamics simulation. Among these models, the 2D Average Lumped LuGre model, recently proposed by Velenis *et al* [87], is a good representative. This model is actually the expansion of the dynamic tire longitudinal friction model presented in Section 4.3. This 2D tire friction model can simulate the coupling of the friction forces in the longitudinal and lateral directions with good accuracy in the dynamic state. Therefore, this model is employed and modified to model the 2D friction/adhesion behaviors in this study. The effective tire rolling radius, the contact patch length and the normal wheel load are time variant instead of constant as assumed in reference [87].

The LuGre Dynamic friction theory assumes that friction is generated due to the interaction forces between the microscopic bristles in the contact area, as illustrated in Figure 5-2. The dynamic friction forces between the tire and ground in the longitudinal (x) and lateral (y) directions, $F_i(t)$, are governed by the following [87]:

$$\begin{aligned} \dot{\bar{z}}_i(t) &= v_{ri} - C_{oi}(\vec{v}_r)\bar{z}_i(t) - k_i(t)\left|\omega R_e\right|\bar{z}_i(t) \\ \mu_i(t) &= \sigma_{oi}\bar{z}_i(t) + \sigma_{1i}\dot{\bar{z}}_i(t) + \sigma_{2i}v_{ri} \qquad i = x, y \\ F_i(t) &= F_n(t)\mu_i(t) \end{aligned} \tag{5.1}$$

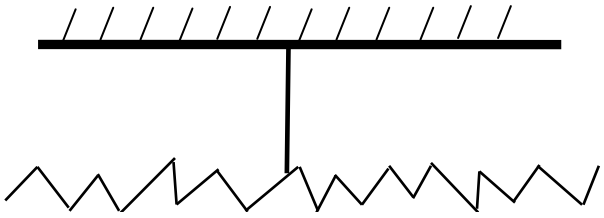

Figure 5-2: Microscopic view of dynamic friction

where $F_n(t)$ and $F_i(t)$ are the normal wheel load and tire friction force in the i direction, respectively; $\mu_i(t)$ is the dynamic friction coefficient in the i direction. $\bar{z}_i(t)$ is a variable representing the mean internal dynamic friction state; v_{ri} is the tire-ground slip velocity in i direction. R_e is the effective tire rolling radius and ω is the tire angular velocity. Parameters σ_{oi}, σ_{1i} and σ_{2i} are the stiffness coefficient,

damping coefficient and the relative viscous damping coefficient, respectively. v_s is the Stribeck relative velocity and γ is a parameter to capture the steady state friction/slip characteristic.

In equation (5.1), the variables, C_{oi}, are determined by

$$C_{oi}(\vec{v}_r) = \frac{\lambda(\vec{v}_r)\sigma_{oi}}{\mu_{ki}^2} \tag{5.2}$$

$$\text{with } \lambda(\vec{v}_r) = \frac{\left\| M_k^2 \vec{v}_r \right\|}{g(\vec{v}_r)} \text{ and } \vec{v}_r = \begin{bmatrix} v_{rx} \\ v_{ry} \end{bmatrix} \tag{5.3}$$

where v_{rx} and v_{ry} are the tire relative slip velocities along the longitudinal and lateral direction, and are defined as follows:

$$\begin{aligned} v_{rx} &= \omega R_e - v\cos(\alpha) \\ v_{ry} &= -v\sin(\alpha) \end{aligned} \tag{5.4}$$

where α is the side slip angle and v is the overall velocity of the tire.

$$g(\vec{v}_r) = \theta \left[\frac{\left\| M_k^2 \vec{v}_r \right\|}{\left\| M_k \vec{v}_r \right\|} + \left(\frac{\left\| M_s^2 \vec{v}_r \right\|}{\left\| M_s \vec{v}_r \right\|} - \frac{\left\| M_k^2 \vec{v}_r \right\|}{\left\| M_k \vec{v}_r \right\|} \right) e^{-\left(\frac{\left\| \vec{v}_r \right\|}{v_s}\right)^{\gamma}} \right] \tag{5.5}$$

where θ is a parameter to capture the changes in the road characteristics: θ =1, 0.8 and 0.2 signifies dry, wet and icy road conditions, respectively. Therefore, this friction model can be used to simulate the vehicle behaviour in the split-μ traction, braking and the cornering manoeuvre just by changing the value of θ.

$$M_s = \begin{bmatrix} \mu_{sx} & 0 \\ 0 & \mu_{sy} \end{bmatrix} \quad \text{and} \quad M_k = \begin{bmatrix} \mu_{kx} & 0 \\ 0 & \mu_{ky} \end{bmatrix} \tag{5.6}$$

where μ_{si} and μ_{ki} are the static and kinetic friction coefficient, respectively.

The term, $k_i(t)$, in equation (5.1), describes the distribution characteristics of the normal wheel load along the tire-ground contact patch and is very computationally-expensive [87] by the existing tire contact mode, for example, the radial spring model. Velenis [87] have suggested that $k_i(t)$ can be approximated in such a way that the steady-state solution of the tire-ground friction force calculated by the distributed LuGre friction model is the same as that predicted from the lumped LuGre friction

model, which neglects the effect of distribution characteristics of normal load. This model takes into account the advantage of both the lumped and the distributed LuGre model. That is why this model is called the Average Lumped LuGre model. The value of $k_{i(t)}$ in the steady-state can be calculated from the following expression by setting the derivative of mean internal dynamic friction state, $\bar{z}_i(t)$ in first equation of Equation (5-1), equal to zero as follows:

$$k_{iss} = \frac{1}{|\omega R_e|}\left(\frac{v_{ri}}{\bar{z}_i^{ss}} - C_{oi}(\vec{v}_r)\right) \tag{5.7}$$

where ^{ss} stands for 'steady state'. According to the literature [87], a trapezoidal normal load distribution, as observed in Figure 5-3, is chosen to represent the normal load distribution characteristics in the contact patch and is described by

$$f_n = \begin{cases} \alpha_1 \xi & for\ 0 \le \xi \le \xi_L \\ f_{\max} & for\ \xi_L \le \xi \le \xi_R \\ \alpha_2 \xi + \beta_2 & for\ \xi_R \le \xi \le L \end{cases} \tag{5.8}$$

where L is the length of tire-ground contact patch. The meaning of the parameters, ζ, ζ_L, ζ_R and f_n can easily understood in Figure 5-3.

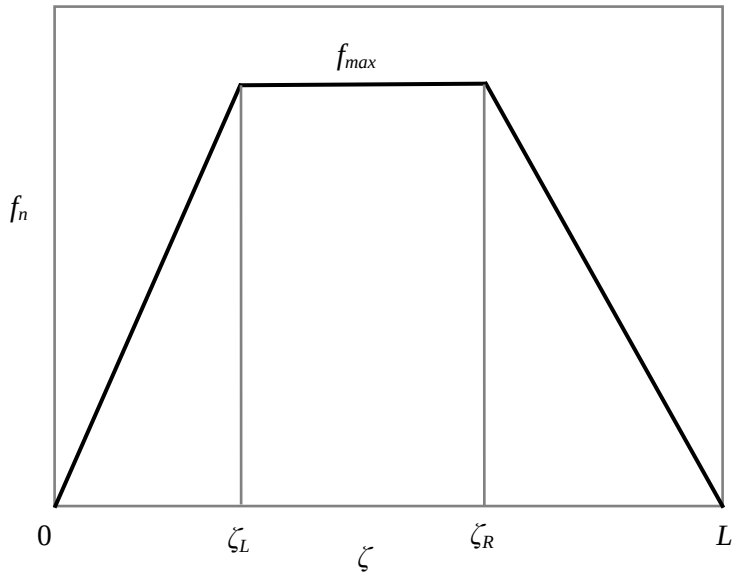

Figure 5-3: Trapezoidal load distribution

The relationship between the overall normal force, F_n, and f_{max}, can be described by the following equation:

$$F_n = \frac{L - \xi_L + \xi_R}{2} f_{\max} \tag{5.9}$$

The mean internal friction state variable in the steady state, $\bar{z}_i^{ss}$, is obtained from the following [87]:

$$\begin{aligned}
\bar{z}_i^{ss} = {} & \frac{1}{F_n} C_{1i}\alpha_1 \left[\frac{\xi_L^2}{2} + C_{2i}\xi_L e^{-\frac{\xi_L}{C_{2i}}} - C_{2i}^2 (1 - e^{-\frac{\xi_L}{C_{2i}}}) \right] \\
& + \frac{1}{F_n} C_{1i} f_{\max} \left[(\xi_L - \xi_R) + C_{2i} (e^{-\frac{\xi_R}{C_{2i}}} - e^{-\frac{\xi_L}{C_{2i}}}) \right] \\
& + \frac{1}{2F_n} C_{1i}\alpha_2 (L^2 - \xi_R^2) + \frac{1}{F_n} C_{1i}\beta_2 (L - \xi_R) \\
& + \frac{1}{F_n} C_{1i}\alpha_2 C_{2i} (L e^{-\frac{L}{C_{2i}}} - \xi_R e^{-\frac{\xi_R}{C_{2i}}}) \\
& + \frac{1}{F_n} C_{1i} C_{2i} (\beta_2 + \alpha_2 C_{2i}) (e^{-\frac{L}{C_{2i}}} - e^{-\frac{\xi_R}{C_{2i}}})
\end{aligned} \tag{5.10}$$

where $C_{1i} = \frac{\nu_{ri}\mu_{ki}^2}{\lambda(\nu_{ri})\sigma_{oi}}$, $C_{2i} = \frac{|\omega R_e|}{C_{oi}\lambda(\nu_{ri})}$. (5.11)

Once the mean internal friction state variable in steady-state ($\bar{z}_i^{ss}$) is determined, the value of *ki(t)* in the steady-state can be evaluated from equation (5.7). The 2D dynamic friction forces can be predicted using equation (5.1) at every time instant.

The friction forces in steady-state are always of interest in the tire-ground friction modeling. In the steady-state in which the angular, longitudinal and lateral velocities of a tire are constant, the tire-ground friction forces in the longitudinal and lateral direction can be calculated from the following equation [87]:

$$F_i^{ss} = F_n \mu_i^{ss} \qquad i = x, y \tag{5.12}$$

where μ_i^{ss} are the steady-state tire friction coefficient and given by

$$\mu_i^{ss} = \frac{-\sigma_{oi} C_{1i} \alpha_1}{F_n}\left[\frac{\xi_L^2}{2} + C_{2i}\xi_L e^{-\frac{\xi_L}{C_{2i}}} - C_{2i}^2(1-e^{-\frac{\xi_L}{C_{2i}}})\right]$$
$$\frac{-\sigma_{oi} C_{1i} f_{\max}}{F_n}\left[(\xi_R - \xi_L) + C_{2i}(e^{-\frac{\xi_R}{C_{2i}}} - e^{-\frac{\xi_L}{C_{2i}}})\right]$$
$$-\frac{1}{2F_n}\sigma_{oi} C_{1i}\alpha_2(L^2 - \xi_R^2) - \frac{\sigma_{oi} C_{1i}\beta_2}{F_n}(L-\xi_R) \qquad (5.12\text{-}1)$$
$$-\frac{\sigma_{oi} C_{1i}\alpha_2 C_{2i}}{F_n}(Le^{-\frac{L}{C_{2i}}} - \xi_R e^{-\frac{\xi_R}{C_{2i}}}) - \frac{\sigma_{oi} C_{1i} C_{2i}}{F_n}(\beta_2 + \alpha_2 C_{2i})(e^{-\frac{L}{C_{2i}}} - e^{-\frac{\xi_R}{C_{2i}}})$$
$$-\frac{\sigma_{2i} v_{ri}}{F_n}\left[\frac{1}{2}\alpha_1\xi_L^2 + f_{\max}(\xi_R - \xi_L) + \frac{1}{2}\alpha_2(L^2 - \xi_R^2) + \beta_2(L-\xi_R)\right]$$

Where C_{oi} and C_{2i} are given by equation (5-11).

Using the definition of longitudinal slip for the braking and acceleration cases, the longitudinal slip, *s*, takes the following form:

$$s = \begin{cases} \dfrac{v_{rx}}{\omega R_e} & \text{for } v\cos(\alpha) < \omega r, \text{ acceleration} \\ -\dfrac{v_{rx}}{v\cos(\alpha)} & \text{for } \omega r > v\cos(\alpha), \text{ braking} \end{cases} \qquad (5.13)$$

It is believed that the lateral elastic stiffness, σ_{oy}, is dependent on the wheel normal load and can be determined by [86]

$$\sigma_{oy} = \frac{p_3}{p_5 F_n + p_4} \qquad (5.14)$$

The parameters for the tire friction model are obtained from reference [86, 87] and listed in Table 5-1.

Table 5-1: Parameters for the tire friction model

σ_{ox}	555	μ_{sx}	1.35	σ_{1y}	1	σ_{2y}	0.025	p_3	5.7e5
μ_{kx}	0.75	μ_{sy}	1.4	v_s	3.96	$\zeta_{L/L}$	0.02	p_4	210.7
μ_{ky}	0.75	σ_{1x}	1	σ_{2x}	0.0007	$\zeta_{R/L}$	0.77	p_5	0.5

In order to study the friction characteristics in a situation where the longitudinal and lateral frictions are combined, the steady-state friction coefficients in two directions are studied using equation (5.12). In this investigation, it is assumed that the tire radius is 0.303 m, the length of contact patch is 0.2 m and the normal contact force is 2000 N according to the literature [87]. The plots of longitudinal and lateral friction coefficients with longitudinal slip at different constant values of side slip angle, and the plots of longitudinal and lateral friction coefficients with side slip angle at different constant values of longitudinal slip, as well as the friction ellipse plots, are calculated at a tire speed of 60 km/h and presented in Figures 5-4 and 5-5, respectively.

Several basic points can be drawn from these two figures. First, these figures are in qualitative agreement with the reported curves obtained by Magic formula [7, 88]. Secondly, the longitudinal and lateral tire frictions are highly coupled. For a constant side slip angle, large longitudinal friction can reduce the lateral friction. In other word, the traction/braking operation in a turning or concerning manoeuvre can reduce the lateral cornering force compared to a free cornering condition at same side slip angle. Meanwhile, for a constant longitudinal slip ratio, large lateral friction can reduce the longitudinal friction. Finally, in the steady-state, the tire friction forces are approximately linear with small slip but highly non-linear with a medium and large slip in both longitudinal and lateral directions. Figure 5-6 depicts the longitudinal and lateral friction coefficient changes in 3D with the longitudinal slip, *s*, and side slip angle, α.

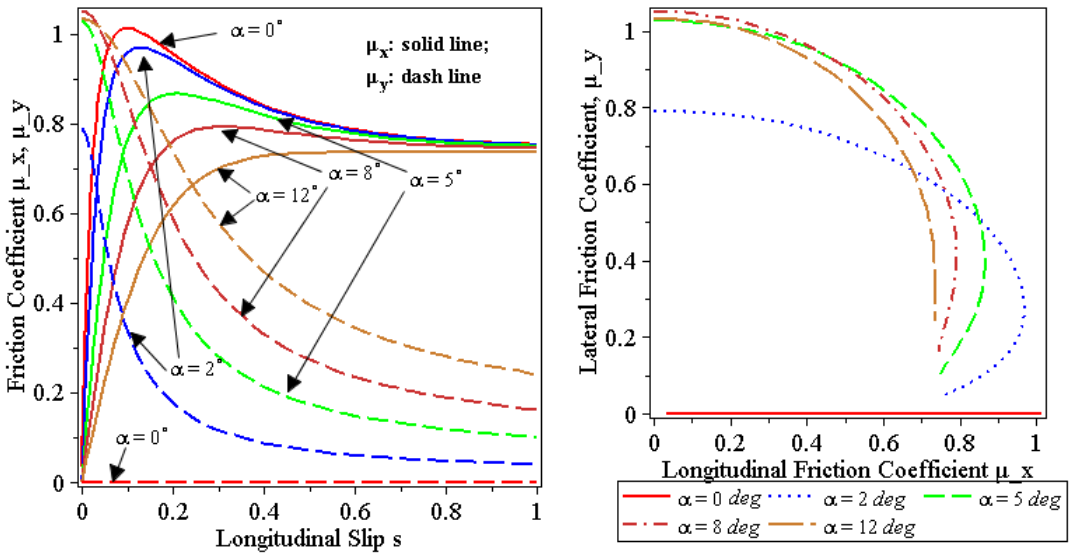

Figure 5-4: Longitudinal and lateral friction coefficients vs. longitudinal slip

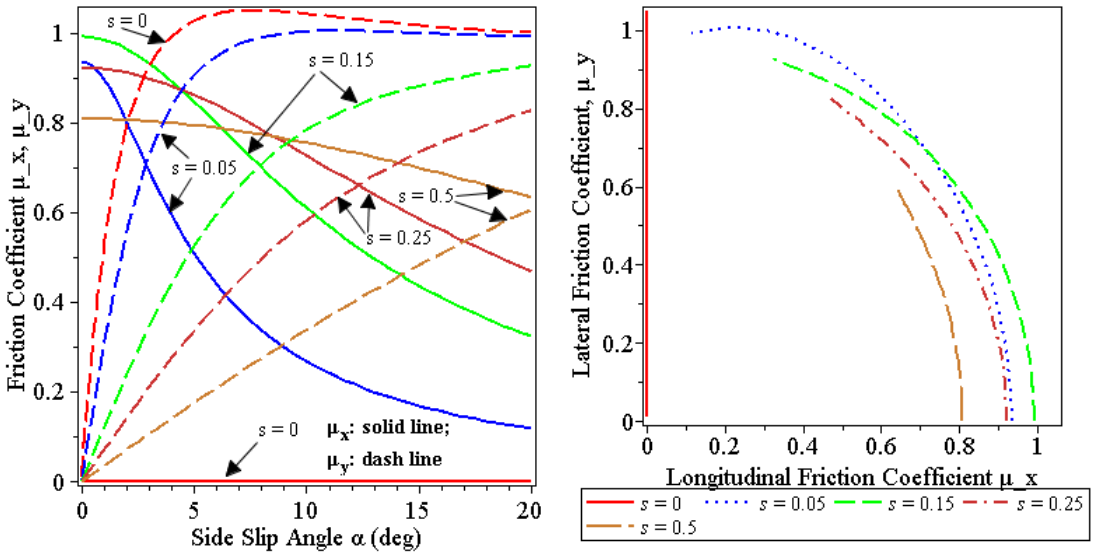

Figure 5-5: Longitudinal and lateral friction coefficients vs. side slip angle

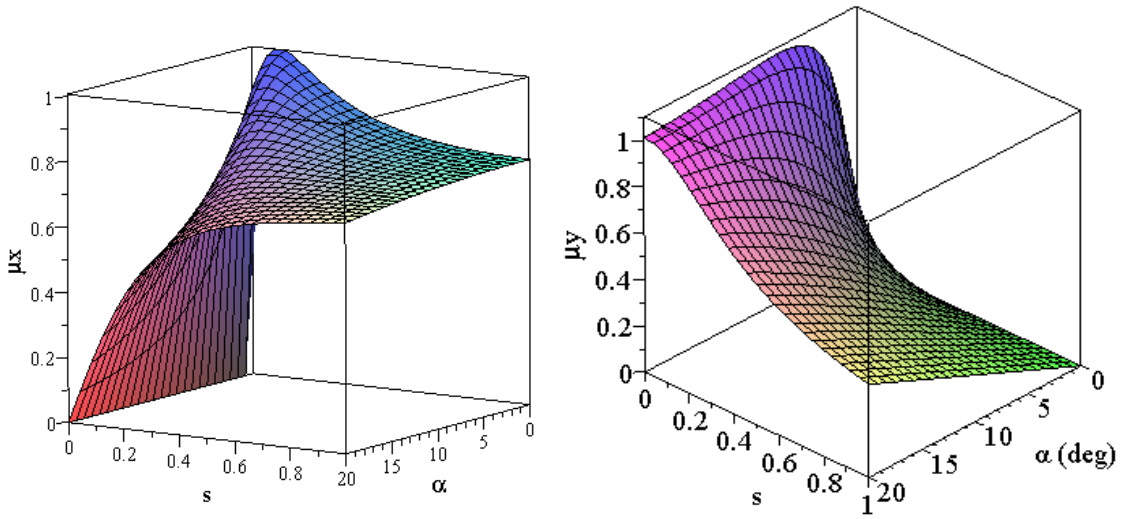

(a) Longitudinal (b) Lateral

Figure 5-6: Friction coefficients in (s- α) space

The effect of tire forward velocity on the longitudinal and lateral friction coefficients is shown in Figure 5-7. It can be seen that the tire friction in both directions is large at low velocity but small at high velocity. This velocity-dependency of tire-ground friction is more evident in the non-linear range and can influence the vehicle direction control and braking/traction control. It is therefore necessary

to seek new models such as LuGre tire friction model to predict the two-dimensional friction force in the vehicle handling and performance study.

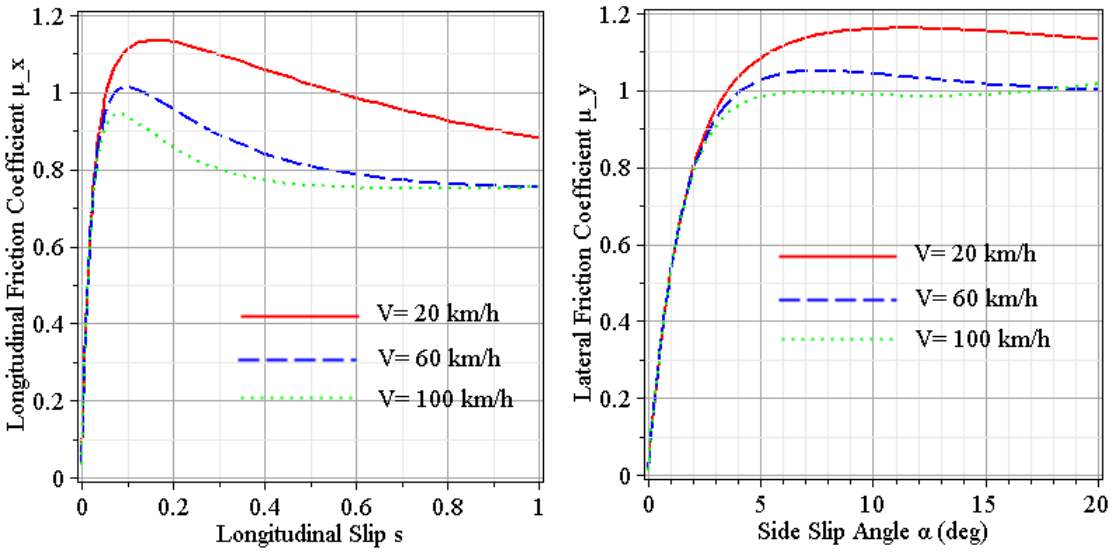

(a) Longitudinal (α = 0º) (b) Lateral (s=0.01)

Figure 5-7: Friction coefficients at different tire forward velocities

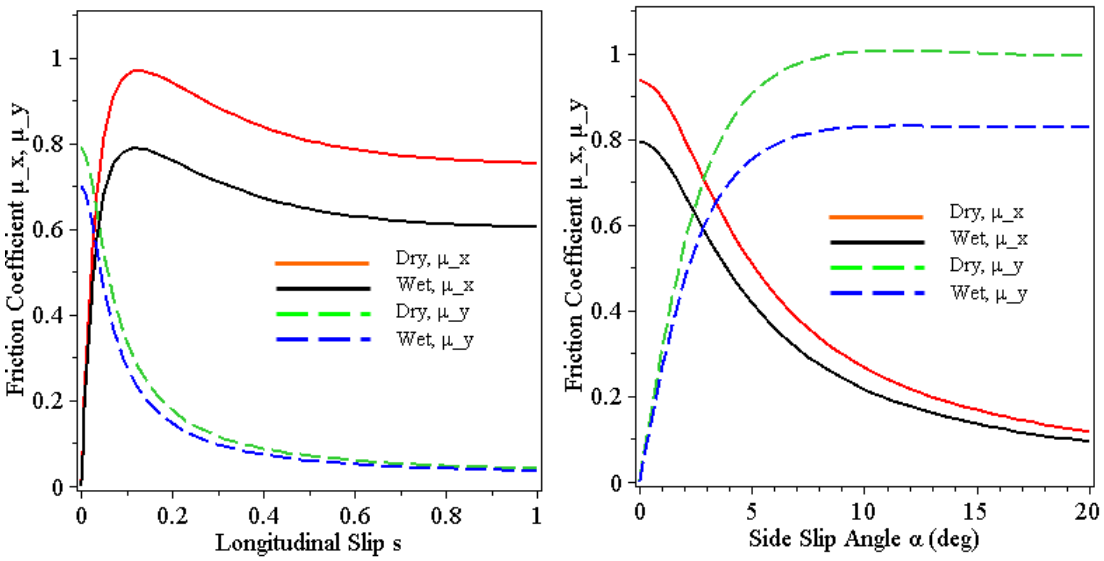

(a) slip angle = 2˚ (b) longitudinal slip = 0.05

Figure 5-8: Comparison of friction coefficient on dry and wet road in the steady-state

Figure 5-8 illustrates the steady-state friction coefficients in the longitudinal and lateral directions for dry and wet roads, respectively. It can be seen that the road dryness has significant influence on

the tire-ground friction even if the longitudinal slips or the side slip angles of the tire are identical under different road conditions. Once again, the commonly used tire friction models such as Magic formula cannot predict this phenomenon.

5.3 Development of a Half-Car Handling model

In this study, a front-wheel-steer (FWS) vehicle is employed to conduct the cornering simulation of a PSS vehicle. The model of the vehicle system consists of two subsystems. One is a half-car pitch plane model with 6 DOFs. It models the vehicle heave and pitch motions in the vertical plane and the spinning motions of the tires. The other subsystem is a single-track yaw plane model with 5 DOFs. This subsystem models the longitudinal, lateral and yaw motions of the vehicle, as well as the relative longitudinal motions between the chassis and each tire. This model is based on the assumption that the longitudinal and lateral friction characteristics, the normal wheel loads and the road conditions are identical in the left and right sides. The suspension elasticity in the two sides is also identical. Due to the different configurations and layouts, the vehicle models for a PSS vehicle and a conventional vehicle differ.

5.3.1 Formulation of the Half-Car Pitch Plane Sub-Model

In the half-car pitch plane sub-model, as shown in Figure 5-9, the chassis is represented by a sprung mass and the tires are modeled as unsprung masses. The sprung and unsprung masses are connected by PSS designated by a linear vertical spring-damper element ($k_{sf,r}$, $c_{sf,r}$) and a longitudinal spring-damper element ($k_{lf,r}$, $c_{lf,r}$). The subscripts f and r represent the front and rear. The coupling between the vertical and longitudinal spring-elements is neglected. The half-car pitch plane vehicle sub-model has 6 DOFs: the bounce (z_s) and pitch (φ_s) motions of the chassis, the bounce motions of the front tire (z_{uf}) and the rear tire (z_{ur}), and the spin motions of the front tire (θ_f) and the rear tire (θ_r). The height between the chassis mass center and the tire center is signified by h. T_f and T_r represent the driving and braking torques applied to the front and rear tires, respectively. F_{zf} and F_{zr} stand for the normal contact forces applied to the front and rear tires, respectively. F_{xfc} and F_{xrc} are the longitudinal contact forces applied to the front and rear tires, respectively. F_{xft} and F_{xrt} are the longitudinal friction forces applied on the front and rear tires, respectively.

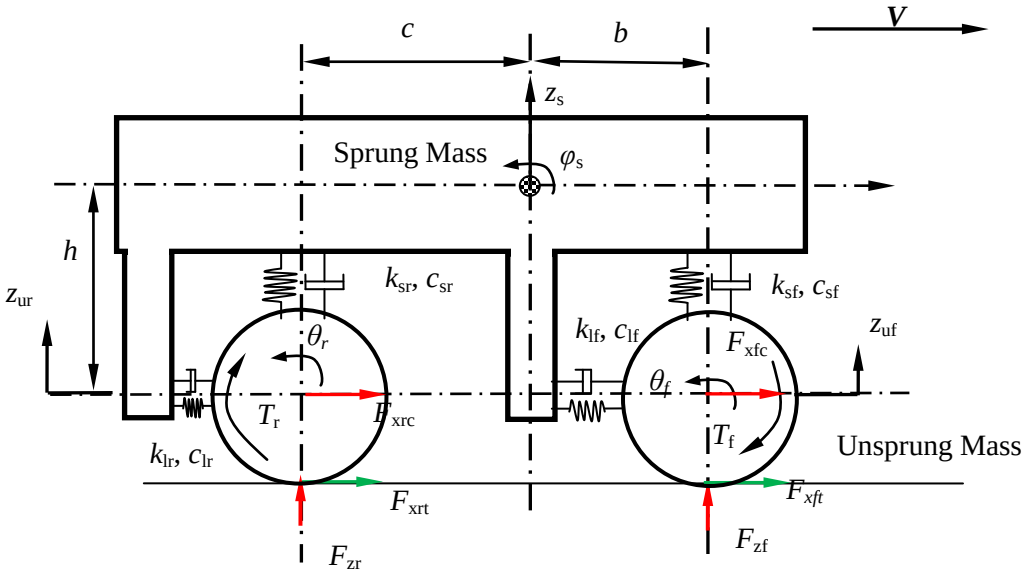

Figure 5-9: Two-dimensional half-car vehicle model

By applying Newton's second law, the equations of vertical motion can be written as follows:

$$M\ddot{Z} + C\dot{Z} + KZ = F \tag{5.15}$$

where M, C and K are the mass, damping and the stiffness matricies respectively. For a vehicle equipped with the planar suspension systems, they are

$$M = \begin{bmatrix} m_s & & & & & \\ & I_{sy} & & & & \\ & & m_{uf} & & & \\ & & & m_{uf} & & \\ & & & & I_{uf} & \\ & & & & & I_{ur} \end{bmatrix}$$

$$C = \begin{bmatrix} c_{sf}+c_{sr} & c_{sf}(b+x_{A1}\cos\delta_f)-c_{sr}(c-x_{B1}) & -c_{sf} & -c_{sr} & 0 & 0 \\ c_{sf}(b+x_{A1}\cos\delta_f)-c_{sr}(c-x_{B1}) & (b+x_{A1}\cos\delta_f)^2 c_{sf}+(c-x_{B1})^2 c_{sr} & -(b+x_{A1}\cos\delta_f)c_{sf} & (c-x_{B1})c_{sr} & 0 & 0 \\ -c_{sf} & -(b+x_{A1}\cos\delta_f)c_{sf} & c_{sf} & 0 & 0 & 0 \\ -c_{sr} & (c-x_{B1})c_{sr} & 0 & c_{sr} & 0 & 0 \\ 0 & 0 & 0 & 0 & 0 & 0 \\ 0 & 0 & 0 & 0 & 0 & 0 \end{bmatrix}$$

$$K=\begin{bmatrix} k_{sf}+k_{sr} & k_{sf}(b+x_{A1}\cos\delta_f)-k_{sr}(c-x_{B1}) & -k_{sf} & -k_{sr} & 0 & 0 \\ k_{sf}(b+x_{A1}\cos\delta_f)-k_{sr}(c-x_{B1}) & (b+x_{A1}\cos\delta_f)^2k_{sf}+(c-x_{B1})^2k_{sr} & -(b+x_{A1}\cos\delta_f)k_{sf} & (c-x_{B1})k_{sr} & 0 & 0 \\ -k_{sf} & -(b+x_{A1}\cos\delta_f)k_{sf} & k_{sf} & 0 & 0 & 0 \\ -k_{sr} & (c-x_{B1})k_{sr} & 0 & k_{sr} & 0 & 0 \\ 0 & 0 & 0 & 0 & 0 & 0 \\ 0 & 0 & 0 & 0 & 0 & 0 \end{bmatrix}$$

where δ_f is the steering angle of the front tire. x_{A1} and x_{B1} are the front and rear longitudinal suspension deflections, respectively. They represent the relative motions between the chassis and each tire. The definitions are given in the yaw plane vehicle sub-model and portrayed in Figure 5-10 in the next subsection. It should be noted that the longitudinal deflections occur in the plane of wheel rotation for the PSS.

Note that Z is the displacement vector and F is the input vector. They are expressed as following

$$Z=\begin{Bmatrix} z_s & \phi_s & z_{uf} & z_{ur} & \theta_f & \theta_r \end{Bmatrix}^T$$

$$F=\begin{Bmatrix} -m_s g & (F_{lsf}\cos\delta_f - F_{lsr})h & -m_{uf}g+F_{zf} & -m_{uf}g+F_{zr} & F_{xft}R_{ef}-T_f & F_{xrt}R_{er}-T_r \end{Bmatrix}^T$$

where F_{lsf} and F_{lsr} are the suspension longitudinal forces. R_{ef} and R_{er} are the effective rolling radii of the front and the rear tires and are evaluated from the radial-spring tire contact model. The torque is assumed to be positive clockwise such that the driving torque is positive, whereas the counter clockwise angular motion of tires is positive as shown in Figure5-9.

It is noteworthy to point out that only the tire-ground friction forces would generate torque with respect to the tire center; the longitudinal components of the contact forces, F_{xfc} and F_{xrc}, pass the wheel centers and do not generate torque.

As mentioned previously, the longitudinal elasticity always exists in a conventional suspension system and can be treated as a longitudinal spring with large stiffness. The pitch plane-half car model for a conventional vehicle can also be established in a similar approach. However, unlike the PSS, the possible longitudinal relative motions between the chassis and the tires (or the longitudinal deflections of the suspension system) in a conventional suspension occur in the chassis vertical plane. The expression of the mass matrix, M, is the same as that of the vehicle with planar suspension systems, but the damping and stiffness matrix are given in the following forms:

$$C=\begin{bmatrix} c_{sf}+c_{sr} & c_{sf}(b+x_{A1})-c_{sr}(c-x_{B1}) & -c_{sf} & -c_{sr} & 0 & 0 \\ c_{sf}(b+x_{A1})-c_{sr}(c-x_{B1}) & (b+x_{A1})^2c_{sf}+(c-x_{B1})^2c_{sr} & -(b+x_{A1})c_{sf} & (c-x_{B1})c_{sr} & 0 & 0 \\ -c_{sf} & -(b+x_{A1})c_{sf} & c_{sf} & 0 & 0 & 0 \\ -c_{sr} & (c-x_{B1})c_{sr} & 0 & c_{sr} & 0 & 0 \\ 0 & 0 & 0 & 0 & 0 & 0 \\ 0 & 0 & 0 & 0 & 0 & 0 \end{bmatrix}$$

$$K=\begin{bmatrix} k_{sf}+k_{sr} & k_{sf}(b+x_{A1})-k_{sr}(c-x_{B1}) & -k_{sf} & -k_{sr} & 0 & 0 \\ k_{sf}(b+x_{A1})-k_{sr}(c-x_{B1}) & (b+x_{A1})^2k_{sf}+(c-x_{B1})^2k_{sr} & -(b+x_{A1})k_{sf} & (c-x_{B1})k_{sr} & 0 & 0 \\ -k_{sf} & -(b+x_{A1})k_{sf} & k_{sf} & 0 & 0 & 0 \\ -k_{sr} & (c-x_{B1})k_{sr} & 0 & k_{sr} & 0 & 0 \\ 0 & 0 & 0 & 0 & 0 & 0 \\ 0 & 0 & 0 & 0 & 0 & 0 \end{bmatrix}$$

The input vector, *F*, is modified as follows:

$$F=\begin{Bmatrix} -m_s g & (F_{lsf}-F_{lsr})h & -m_{uf}g+F_{zf} & -m_{uf}g+F_{zr} & F_{xft}R_{ef}-T_f & F_{xrt}R_{er}-T_r \end{Bmatrix}^T$$

5.3.2 Formulation of the Single-Track Yaw Plane Sub-Model

In the formulation of the yaw plane sub-model, as illustrated in Figure 5-10, two coordinate frames are used to describe the yaw plane motions of a vehicle. The first coordinate frame (*XOY*) is the global frame, while the second one (*xoy*) is fixed to and moving with the chassis so that the yaw mass moment of inertia of the chassis is constant during the cornering manoeuvre.

The yaw plane model for a vehicle with PSS is shown in Figure 5-10 (a). The chassis is represented by a rigid body, and the front tire is modeled as a rigid body attached to a slider. This slider can only translate with respect to a body that is controlled by the steering system. The steering input is the angle (δ_f) between the chassis longitudinal centerline and the tire. The rear wheel is modeled as a rigid body attached to another slider which can only move backward and forth, and cannot rotate with respect to the chassis. Point A_1 and point B_1 represent the mass centers of front and rear wheels, respectively, while point A and point B signify the points on the chassis and at which the front and rear wheels connect to the chassis via the longitudinal suspension. The suspension longitudinal deflection locates in the wheel rotation plane. When there is no longitudinal deflection,

points A_1 and A, points B_1 and B coincide. The absolute longitudinal, lateral and yaw velocities of the chassis mass center are V_x, V_y and Ω_z, respectively. They are described in the body fixed frame (xyz), and are observed in the global frame (*XOY*). x_{A1} and x_{B1} are the relative longitudinal motion between the chassis and two wheels.

As illustrated in Figure 5-10 (a). F_{xf} and F_{xr} represent the total longitudinal forces acting on the front and rear tires. They have two components: one is due to the tire ground friction, and the other one is due to the road obstacles. F_{xo} is the external longitudinal force acting on the chassis. F_{yf} and F_{yr} are the lateral friction forces or cornering forces applied to the front and rear tires, and can be predicted from the LuGre tire friction model presented in previous section. The equations of motion for the vehicle yaw plane motions are derived as follows:

$$m_s a_{sx} + m_{uf} a_{ufx} + m_{ur} a_{urx} = F_{xf} \cos\delta_f - F_{yf} \sin\delta_f + F_{xr} + F_{xo} \tag{5.16-1}$$

$$m_s a_{sy} + m_{uf} a_{ufy} + m_{ur} a_{ury} = F_{yf} \cos\delta_f + F_{yr} + F_{xf} \sin\delta_f \tag{5.16-2}$$

$$I_{sz}\dot{\Omega}_z + I^o_{ufz}\dot{\Omega}_z + I^o_{urz}\dot{\Omega}_z = F_{xf} b \sin\delta_f + F_{yf}(b\cos\delta_f + x_{A1}) - F_{yr}(c - x_{B1}) \tag{5.16-3}$$

$$m_{uf} a_{ufx} \cos\delta_f + m_{uf} a_{ufy} \sin\delta_f = (F_{xf} - F_{lsf}) \tag{5.16-4}$$

$$m_{ur} a_{urx} = F_{xr} + F_{lsr} \tag{5.16-5}$$

where F_{lsf} and F_{lsr}, are the suspension longitudinal forces and can be calculated by

$$F_{lsf} = \frac{k_{lf}}{d_s^2}(x_{A1})^3 + k_{lf} x_{A1} + c_{lf} \dot{x}_{A1} \tag{5.17-1}$$

$$F_{lsr} = -\frac{k_{lr}}{d_s^2}(x_{B1})^3 - k_{lf} x_{B1} - c_{lf} \dot{x}_{B1} \tag{5.17-2}$$

a_{sx}, a_{ufx}, and a_{urx} are the longitudinal acceleration components of the chassis, front wheel and rear wheel, respectively; and a_{sy}, a_{ufy}, a_{ury} are the lateral acceleration components of the chassis, front wheel and rear wheel, respectively. They are

$$a_{sx} = \dot{V}_x - V_y \Omega_z$$

$$a_{ux} = \dot{V}_{xf} - V_y \Omega_z - x_{A1}\dot{\Omega}_z \sin\delta_f + \ddot{x}_{A1}\cos\delta_f - x_{A1}\ddot{\delta}_f \sin\delta_f - \Omega_z^2(x_{A1}\cos\delta_f + b)$$
$$- 2x_{A1}\Omega_z\dot{\delta}_f \cos\delta_f - 2\dot{x}_{A1}\Omega_z \sin\delta_f$$

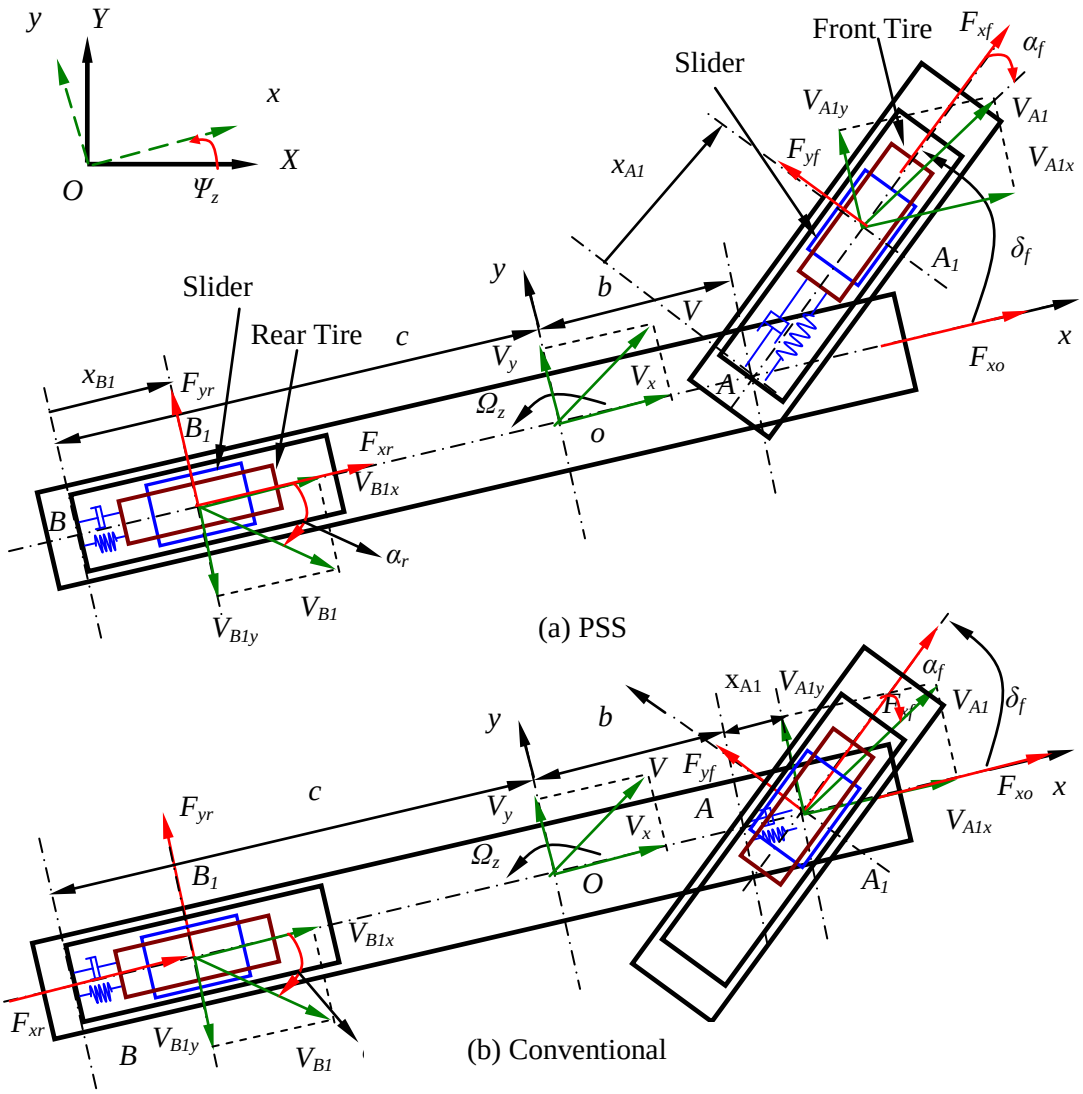

Figure 5-10: 5-DOF Single-track vehicle handling model

$$a_{urx} = \dot{V}_x - V_y\Omega_z + \ddot{x}_{B1} - (x_{B1} - c)\Omega_z^2$$

$$a_{sy} = \dot{V}_y + V_x\Omega_z$$

$$a_{ufy} = \dot{V}_y + V_x\Omega_z + \dot{\Omega}_z(x_{A1}\cos\delta_f + b) + x_{A1}\ddot{\delta}_f\cos\delta_f + \ddot{x}_{A1}\sin\delta_f - x_{A1}\Omega_z^2\sin\delta_f$$
$$- 2x_{A1}\Omega_z\dot{\delta}_f\sin\delta_f + 2\dot{x}_{A1}\Omega_z\cos\delta_f$$

$$a_{ury} = \dot{V}_y + V_x\Omega_z + (x_{B1} - c)\dot{\Omega}_z + 2\dot{x}_{B1}\Omega_z$$

$\boldsymbol{I}_{sz,}$ I^{o}_{ufz} and I^{o}_{urz} are the mass moment inertia of the sprung mass, front unsprung mass and rear unsprung mass with respect to the vertical axis through the chassis mass center (point *O*), respectively. I^{o}_{ufz} and I^{o}_{urz} are state-dependent and can be determined from

$$I^{o}_{ufz} = I_{ufz} + m_{uf}(b^2 + x^2_{A1} + 2bx_{A1}\cos\delta_f)$$

$$I^{o}_{urz} = I_{urz} + m_{ur}(x_{B1} - c)^2$$

where I_{ufz} and I_{urz} are the respective mass moment inertia of the front unsprung and rear unsprung masses with respect to the vertical axis through its mass center, respectively.

Unlike the case of a PSS vehicle, both the front and rear wheels in a conventional vehicle can only move backward and forward in the chassis longitudinal plane, as illustrated in Figure 5-10(b). The longitudinal suspension deflections can only occur in the *xoy* plane. The equations of motion for a conventional vehicle are established as

$$\begin{aligned} &m_s(\dot{V}_x - V_y\Omega_z) + m_u\left[\dot{V}_x - V_y\Omega_z + \ddot{x}_{A1} - (b + x_{A1})\Omega_z^2\right] \\ &+ m_{ur}[\dot{V}_x - V_y\Omega_z + \ddot{x}_{B1} - (x_{B1} - c)\Omega_z^2] = F_{xf}\cos\delta_f - F_{yf}\sin\delta_f + F_{xr} + F_{xo} \end{aligned} \tag{5.18-1}$$

$$\begin{aligned} &m_s(\dot{V}_y + V_x\Omega_z) + m_u\left[\dot{V}_y + V_x\Omega_z + (b + x_{A1})\dot{\Omega}_z + 2\dot{x}_{A1}\Omega_z\right] \\ &+ m_{ur}[\dot{V}_y + V_x\Omega_z + (x_{B1} - c)\dot{\Omega}_z + 2\dot{x}_{B1}\Omega_z] = F_{yf}\cos\delta_f + F_{yr} + F_{xf}\sin\delta_f \end{aligned} \tag{5.18-2}$$

$$\begin{aligned} &I_{sz}\dot{\Omega}_z + \left[I_{ufz} + m_{uf}(b + x_{A1})^2\right]\dot{\Omega}_z + \left[I_{urz} + m_{ur}(x_{B1} - c)^2\right]\dot{\Omega}_z \\ &= F_{xf}(b + x_{A1})\sin\delta_f + F_{yf}(b + x_{A1})\cos\delta_f - F_{yr}(c - x_{B1}) \end{aligned} \tag{5.18-3}$$

$$m_{uf}\left[\dot{V}_x - V_y\Omega_z + \ddot{x}_{A1} - (b + x_{A1})\Omega_z^2\right] = (F_{xf}\cos\delta_f - F_{lsf}) - F_{yf}\sin\delta_f \tag{5.18-4}$$

$$m_{ur}[\dot{V}_x - V_y\Omega_z + \ddot{x}_{B1} - (x_{B1} - c)\Omega_z^2] = F_{xr} + F_{lsr} \tag{5.18-5}$$

It is assumed that the longitudinal spring-damper elements in the conventional suspension system are linear. The front and rear longitudinal suspension forces, $F_{lsf(r)}$, are obtained using the following equations:

$$F_{lsf(r)} = k_{lf(r)} x_{A1} + c_{lf(r)} \dot{x}_{A1} \tag{5-19}$$

The side slip angles of the two tires for a vehicle with PSS, as defined in Figure 5-10 (a), can be determined from

$$\begin{aligned} \alpha_f &= \tan^{-1}\frac{V_{A1y}}{V_{A1x}} - \delta_f \\ &= \tan^{-1}\frac{V_y + x_{A1}(\Omega_z + \dot{\delta}_f)\cos\delta_f + \dot{x}_{A1}\sin\delta_f + \Omega_z b}{V_x + \dot{x}_{A1}\cos\delta_f - x_{A1}(\Omega_z + \dot{\delta}_f)\sin\delta_f} - \delta_f \end{aligned} \tag{5.20-1}$$

$$\alpha_r = \tan^{-1}\frac{V_{B1y}}{V_{B1x}} = \tan^{-1}\frac{V_y + (x_{B1} - c)\Omega_z}{V_x + \dot{x}_{B1}} \tag{5.20-2}$$

For a vehicle with a conventional suspension, the side slip angles of the two tires are

$$\alpha_f = \tan^{-1}\frac{V_{A1y}}{V_{A1x}} - \delta_f = \tan^{-1}\frac{V_y + \Omega_z(b + x_{A1})}{V_x + \dot{x}_{A1}} - \delta_f \tag{5.21-1}$$

$$\alpha_r = \tan^{-1}\frac{V_{B1y}}{V_{B1x}} = \tan^{-1}\frac{V_y + (x_{B1} - c)\Omega_z}{V_x + \dot{x}_{B1}} \tag{5.21-2}$$

The parameters of the PPS and convention vehicles used in this study are listed in Table 5-2.

Table 5-2: Vehicle parameters of a PPS and a conventional vehicle [25, 73]

	PPS	Conventional
Dimension L x W x H (m)	4.69 x 1.83 x 1.45	4.69 x 1.83 x 1.45
Total Mass (kg)	1300	1300
I_{sy} (kgm^2)	1630	1630
I_{sz} (kgm^2)	2000	2000
b (m)	1.0714	1.0714
c (m)	1.4286	1.4286
k_{sr} (kN/m)	23.8/2	23.8/2
k_{sf} (kN/m)	35.7/2	35.7/2
c_{sr} (kNs/m)	2.207/2	2.207/2
c_{sf} (kNs/m)	3.311/2	3.311/2

k_{tf}, k_{tr} (kN/m)	175	175
c_{tf}, c_{tr} (kNs/m)	0.5	0.5
$k_{lf(r)}$ /$k_{sf(r)}$		30
$c_{lf(r)}$		2.5 kN.s/m
m_{ur} (kg)	57/2	57/2
m_{uf} (kg)	47.6/2	47.6/2
h (m)	0.25	0.25
I_{ufy} (kgm^2)	2	2
I_{ufz} (kgm^2)	1.1	1.1
I_{ury} (kgm^2)	2	2
I_{urz} (kgm^2)	1.1	1.1

5.4 Analysis of Steady-State Handling Characteristics

Steady-state handling characteristics are very important to evaluate the handling performance of a vehicle. In this study, the steady-state handling responses in terms of the yaw velocity gain, lateral acceleration gain and the curvature response are derived from the proposed single-track handling model. The handling characteristics of a PSS vehicle and a similar conventional vehicle are investigated and compared in three cases: understeer, neutral steer and oversteer. Also, the effect of the longitudinal friction force on the steady-state handling performance is examined.

5.4.1 Derivation of Steady-State Steering Response

Steady-state handling performance refers to the directional behaviour of a vehicle during a turn in such a state that the state variables, such as the vehicle forward velocity and steering angles, remain constant. In other words, the derivative terms in equations describing the vehicle motions are zero. In this study, the analysis of the steady-state handling characteristic is based on the following assumptions:

(1) The steering angle and the side slip angles of the two tires are very small. Therefore, the following expressions hold:

$$\sin\delta_f \approx \delta_f, \cos\delta_f \approx 1, \sin\alpha_f \approx \alpha_f, \cos\alpha_f \approx 1, \sin\alpha_r \approx \alpha_r \text{ and } \cos\alpha_r \approx 1$$

(2) The value order of chassis lateral velocity and yaw rate is very small compared to that of the vehicle longitudinal velocity.

(3) High order terms, i.e. the products of small terms, such as the steering angle, side slip angles of two tires, chassis lateral velocity and yaw rate, are negligible;

(4) Equation (5.12) can be linearized and the lateral tire friction force is calculated from:

$$F_y = -C_\alpha \alpha \tag{5.22}$$

where C_α is the cornering coefficient of front or rear tire. This term is not constant but state-dependent and can be evaluated from equation (5.12) as

$$C_\alpha = \frac{\partial F_y(\alpha, s, v, F_n, L)}{\partial \alpha}\bigg|\alpha = 0 \tag{5.23}$$

Based on these assumptions, the equations of motion in the steady state are rewritten as

$$F_{xf} - F_{yf}\delta_f + F_{xr} = -F_{xo} \tag{5.24-1}$$

$$F_{yf} + F_{yr} + F_{xf}\delta_f = (m_s + m_{uf} + m_{rur})V_x\Omega_z \tag{5.24-2}$$

$$F_{xf} b\delta_f + F_{yf}(b + x^e_{A1}) - F_{yr}(c - x_{B1}) = 0 \tag{5.24-3}$$

$$\begin{array}{ll} F_{xf} - F_{lsf} = 0 & \text{for PSS} \\ F_{xf} - F_{lsf} - F_{yf}\delta_f = 0 & \text{for conventional} \end{array} \tag{5.24-4}$$

$$F_{xr} + F_{lsr} = 0 \tag{5.24-5}$$

Equations (5.24-1), (5.24-4) and (5.24-5) establish the equilibrium (steady) states of the longitudinal motions for the chassis, front tire and the rear tire with a constant forward velocity. Equations (5.24-2) and (5.24-3) describe the steady-state cornering motion of the chassis.

Substitution of equations (5.20) and (5.21) in equation (5.22) leads to the lateral friction force terms, F_{yf} and F_{yr}, in the steady state as

$$F_{yf} = C_{\alpha f}\left[\delta_f - \frac{V_y + \Omega_z(b + x_{A1})}{V_x}\right] \tag{5.25-1}$$

$$F_{yr} = -C_{\alpha r}\frac{V_y + (x_{B1} - c)\Omega_z}{V_x} \tag{5.25-2}$$

Substituting the force terms defined by equation (5.25) in equations (5.24-2) and (5.24-3) leads to the following:

$$\begin{bmatrix} \frac{C_{\alpha f} + C_{\alpha r}}{V_x} & mV_x + \frac{C_{\alpha f}(b + x_{A1}) - C_{\alpha r}(c - x_{B1})}{V_x} \\ \frac{C_{\alpha f}(b + x_{A1}) - C_{\alpha r}(c - x_{B1})}{V_x} & \frac{C_{\alpha f}(b + x_{A1})^2 + C_{\alpha r}(c - x_{B1})^2}{V_x} \end{bmatrix} \begin{bmatrix} V_y \\ \Omega_z \end{bmatrix} = \begin{bmatrix} C_{\alpha f} + F_{xf} \\ C_{\alpha f}(b + x_{A1}) + F_{xf} b \end{bmatrix} \delta_f \tag{5.26}$$

where m is the total mass of the vehicle including the chassis and two tires (m_s+m_{uf}+m_{ur}). It is evident that the above steady-state handling equations of the chassis are identical to the widely-used conventional steady-state handling equations when the longitudinal deflections (x_{A1}, x_{B1}) of the suspensions are equal to zero (the longitudinal friction force applied to the front wheel is zero in this case) [7].

Solving equation (5.26) leads to

$$\begin{aligned} \delta_f = & \frac{(b + c + x_{A1} - x_{B1})^2}{R\left[(b + c + x_{A1} - x_{B1}) + \frac{F_{xf}(b + c - x_{B1})}{C_{\alpha f}} - \frac{F_{xf} x_{A1}}{C_{\alpha r}}\right]} \\ & + \frac{V_x^2}{R} \frac{\left[m(c - x_{B1})C_{\alpha r} - m(b + x_{A1})C_{\alpha f}\right]}{\left[(b + c + x_{A1} - x_{B1}) + \frac{F_{xf}(b + c - x_{B1})}{C_{\alpha f}} - \frac{F_{xf} x_{A1}}{C_{\alpha r}}\right] C_{\alpha f} C_{\alpha r}} \end{aligned} \tag{5.27}$$

The suspension longitudinal deflections are zero when there is no longitudinal force applied to the two tires, and the above equation becomes

$$\begin{aligned} \delta_f &= \frac{(\mathrm{b+c})^2 C_{\alpha f} C_{\alpha r} + mV_x^2[cC_{\alpha r} - bC_{\alpha f}]}{R(\mathrm{b+c})C_{\alpha r} C_{\alpha f}} \\ &= \frac{\mathrm{b+c}}{R} + \frac{V_x^2}{R}\left(\frac{mc}{LC_{\alpha f}} - \frac{mb}{LC_{\alpha r}}\right) \end{aligned} \tag{5.28}$$

This expression is the same as the widely-used steady-state handling equation where the longitudinal forces are neglected [7]. Although equations (5.26) and (5-28) are similar to those appear in the literature, the significance is that the cornering stiffness, $C_{\alpha f}$ and $C_{\alpha r}$, are not constant but a

function of the normal wheel load, the contact patch length, the longitudinal slip, the side slip angle, the tire forward velocity and the longitudinal force.

In the steady-state handling study, the yaw velocity gain, lateral acceleration and curvature response are of the most interests, and are always examined. Because $\Omega_z = V_x/R$, the yaw velocity gain, G_{yaw}, defined as the ratio of the steady-state yaw velocity to the steer angle, can be evaluated by

$$G_{yaw} = \frac{\Omega_z}{\delta_f} = \frac{V_x\left\{\left[(b+c+x_{A1}-x_{B1})C_{\alpha f} + F_{xf}(b+c-x_{B1})\right]C_{\alpha r} - F_{xf}C_{\alpha f}x_{A1}\right\}}{(b+c+x_{A1}-x_{B1})^2 C_{\alpha f}C_{\alpha r} + mV_x^2\left[(c-x_{B1})C_{\alpha r} - (b+x_{A1})C_{\alpha f}\right]} \tag{5.29}$$

The lateral acceleration gain, G_{acc}, defined as the ratio of the steady-state vehicle lateral acceleration to the steer angle, can be derived from equation (5.27) as

$$G_{acc} = \frac{V_x^2/gR}{\delta_f} = \frac{a_y/g}{\delta_f} = \frac{V_x^2\left[(b+c+x_{A1}-x_{B1})C_{\alpha f}C_{\alpha r} + F_{xf}(b+c-x_{B1})C_{\alpha r} - F_{xf}C_{\alpha f}x_{A1}\right]}{g(b+c+x_{A1}-x_{B1})^2 C_{\alpha f}C_{\alpha r} + g\ V_x^2 m\left[(c-x_{B1})C_{\alpha r} - (b+x_{A1})C_{\alpha f}\right]} \tag{5.30}$$

The curvature response, defined as the ratio of the steady-state curvature to the steer angle, is expressed by the following:

$$\frac{1/R}{\delta_f} = \frac{(b+c+x_{A1}-x_{B1})C_{\alpha f}C_{\alpha r} + F_{xf}(b+c-x_{B1})C_{\alpha r} - F_{xf}C_{\alpha f}x_{A1}}{(b+c+x_{A1}-x_{B1})^2 C_{\alpha f}C_{\alpha r} + mV_x^2\left[(c-x_{B1})C_{\alpha r} - (b+x_{A1})C_{\alpha f}\right]} \tag{5.31}$$

5.4.2 Study of steady-state handling Responses

Equation (5.27) indicates that the longitudinal friction force and the suspension longitudinal deflection influence the vehicle steady-state handling characteristics. Figure 5-11 shows the relationship between the required steering angle, the longitudinal force and the vehicle velocity of an understeer vehicle with PSS and conventional suspension systems.

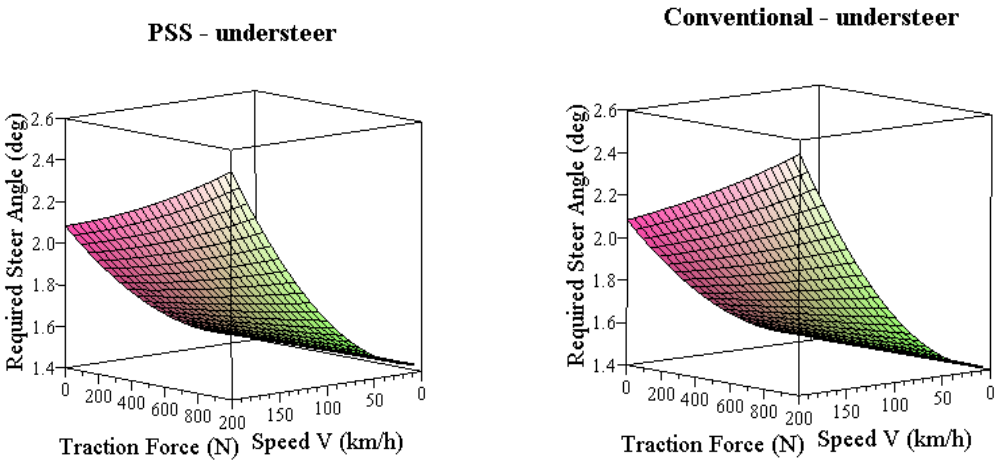

Figure 5-11: Required steering angle of a PSS vehicle

Equation (5.28) implies that there is no difference in the steady-state handling characteristics between a PSS vehicle and a conventional vehicle when no traction or braking forces are involved. However, in reality, a longitudinal friction force is always applied to the tires to balance the external longitudinal force, F_{xo}. Although such external forces are out of the control of engineer, it should be taken into account in the vehicle development. At least, their influence on the steady-state handling performance of a vehicle, especially a PSS vehicle, should be investigated and well-understood. Generally, the longitudinal friction force can be either a forward traction force or a backward braking force. These two scenarios are studied in this section.

The steady-state handling characteristics are often classified as understeer, neutral steer and oversteer. In general, for a vehicle whose tires are identical and the wheelbase parameter b is larger than c, as shown in Figure 5-9, its steady-state handling characteristic is understeer. The steering characteristic becomes neutral steer when b and c are equal, and oversteer if b is less than c [7].

5.4.2.1 Steady-State Handling Performance Involving a Traction Force

This subsection presents the investigation of the steady-state handling performance of a vehicle with PSS in the conditions where a traction force is applied to the front tire in order to compensate the drag forces so as to maintain a constant forward speed in a turning. It is assumed that the vehicle negotiates a curve with a constant radius (100m) in a steady-state condition. The investigation is carried out in two conditions: (i) F_{xf} = 200 N and (ii) F_{xf} = 800 N. The first value may represent a common driving

situation while the second one may represent a steady driving condition on a curved road up a hill. Also, the free handling behaviour with $F_{xf} = 0$ is investigated as a baseline.

The relationship between the required steering angle and the vehicle speed with various traction forces is shown in Figure 5-12. It is evident that the required steering angle, for both the PSS and the conventional vehicles, increases by increasing the speed for the understeer vehicles. The difference in the required steering angle between the two types of vehicles is very small. For the vehicles with neutral steer characteristic, the PSS vehicle requires a larger steering angle at lower speeds, but a smaller steering angle at high speeds than the conventional vehicle. For the vehicles with oversteer characteristic, the required steer angle decreases with an increase in the vehicle speed. The PSS vehicle requires larger steering angles at lower speeds and smaller steering angles at high speeds than the conventional vehicle. Figure 5-12 also implies that the tractive friction force applied to the front tire can lead to an increase in the required steer angle. A large tractive friction force results in a need of large steering angle. The effect of the longitudinal elasticity in the suspension system has little influence on the required steering angle when the tractive friction force is small, but a slight influence when the longitudinal force is relatively large. Even when the longitudinal force is relatively large (800N), the difference in the required steering angle between the two types of vehicles is negligible. Therefore, it can be concluded that a PSS does not induce a significant difference in the required steering angle compared with that of a conventional suspension system in the same steady-state cornering condition.

Figure 5-13 depicts the yaw velocity gain characteristics of the two types of vehicles. It can be seen that the yaw velocity generally increases as the vehicle speed increased, and when the traction force increases, the yaw velocity is decreased. This means that the longitudinal traction force at the front tire can enhance the understeer behaviour and mitigate the oversteer characteristic. Meanwhile, the yaw responses of the PSS and the conventional vehicles to the same steering input are almost identical in all the understeer, neutral steer and the oversteer conditions.

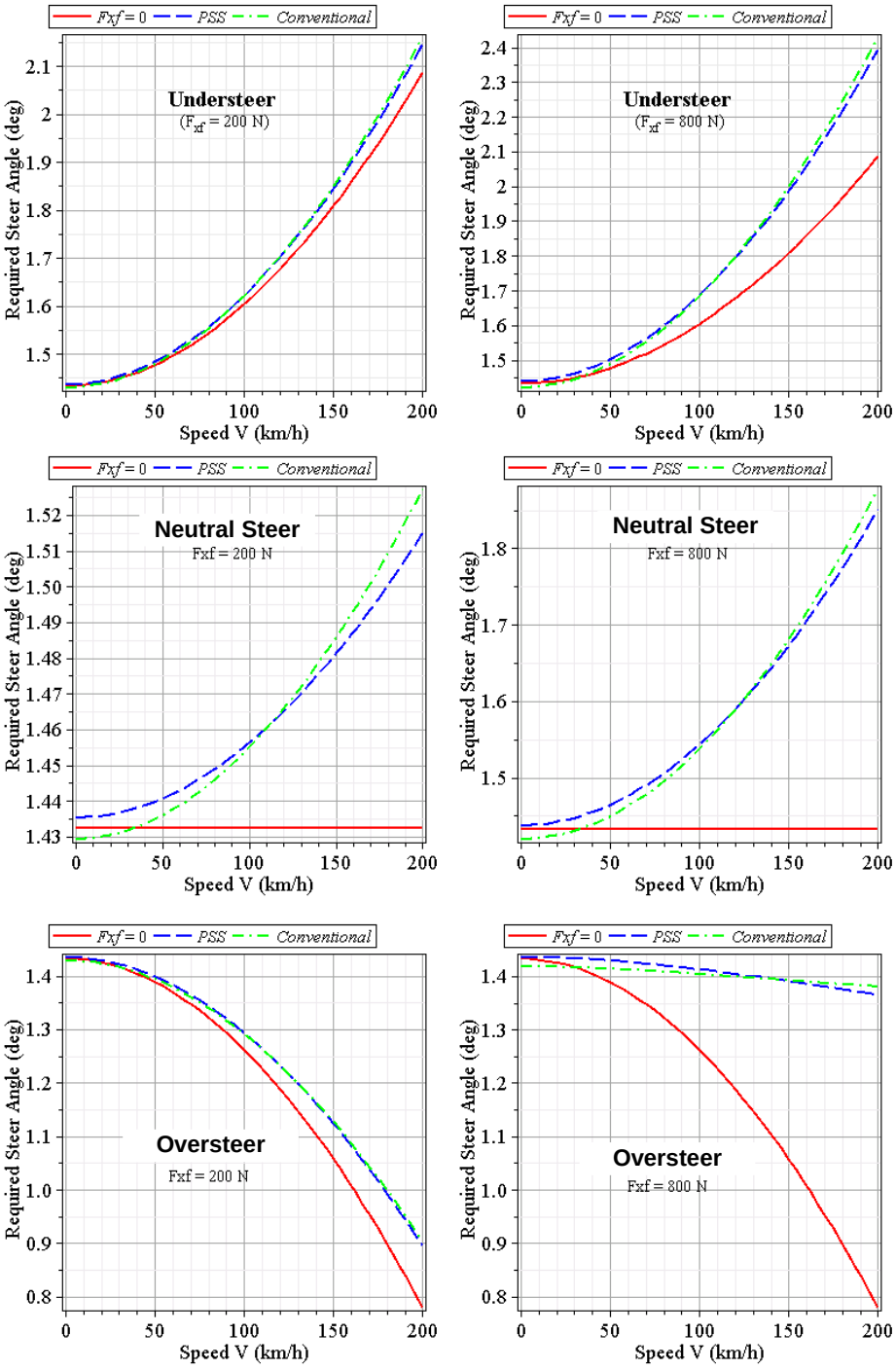

Figure 5-12: The required steering angle at different speeds (traction case)

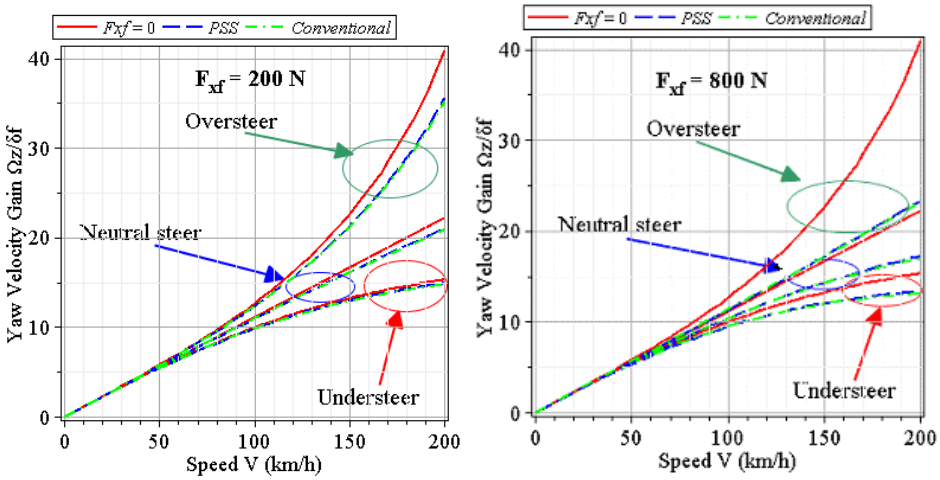

Figure 5-13: Yaw velocity gain (rad/s/rad) of a vehicle with PSS and conventional suspension

The lateral acceleration gains, defined by equation (5.30), of a vehicle with PSS and conventional suspension system are displayed in Figure 5-14 with the understeer, neutral steer and the oversteer characteristics, respectively. It can be seen that an increase in the vehicle speed can increase the lateral acceleration. The lateral acceleration increases rapidly especially for the oversteer case when the speed is high. This occurs because the high vehicle speed is close to the critical speed of an oversteer vehicle. Figure 5-14 clearly shows that the traction force can enhance the understeer trend. The larger the longitudinal traction force, the smaller the lateral accelerations are for a vehicle with both the PSS and conventional suspension. The results shown in Figure 5-14 indicate that there is little difference between a PSS vehicle and a similar conventional one in terms of the lateral acceleration response to the same handling input.

Figure 5-15 portrays the curvature response, defined by equation (5.31), of a PSS vehicle and a conventional vehicle with the understeer, neutral steer and the oversteer characteristics, respectively. The curvature response decreases with an increase in the vehicle speed for the vehicles with the understeer characteristic, whereas increases for the vehicles with the oversteer behaviour. The vehicle speed has little effect on the curvature response for a neutral steer vehicle, and the longitudinal traction force can reduce the curvature response. Similar to the yaw velocity and lateral acceleration responses, the difference of the curvature response between a PSS vehicle and a conventional vehicle is negligible.

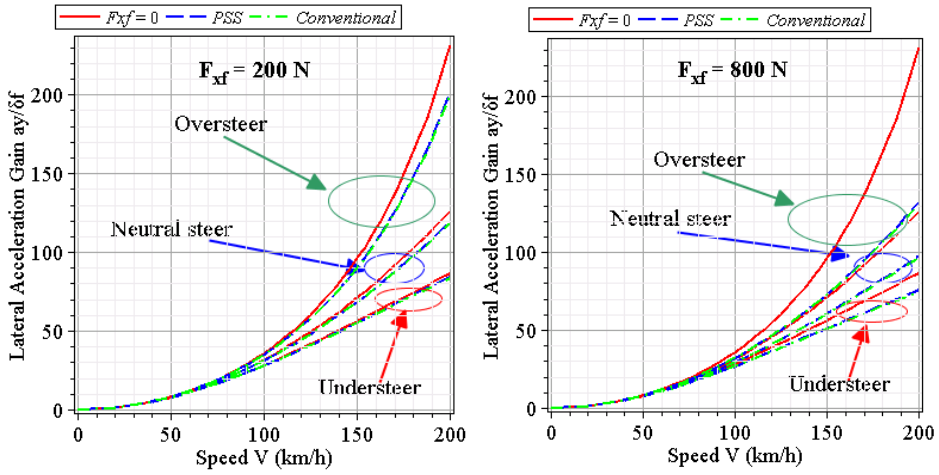

Figure 5-14: Lateral acceleration gain (g/rad) of a vehicle with PSS and conventional suspension

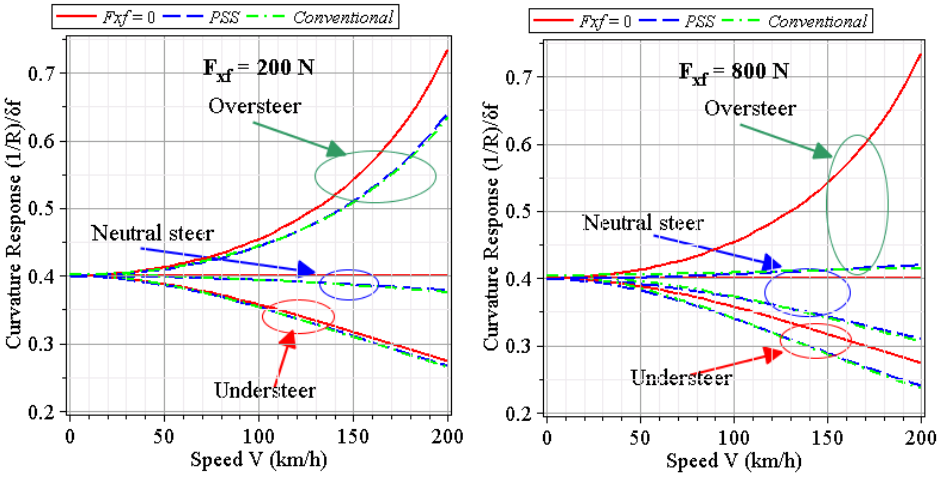

Figure 5-15: Curvature response (1/m/rad) of a vehicle with PSS and conventional suspension

5.4.2.2 Steady-State Handling Performance Involving a Braking Force

The steady-state handling characteristic of a PSS vehicle in a case where the braking force has to be applied is now studied and compared with that of a conventional vehicle. In this study, the braking ratio is assumed to be 6:4, i.e. 60% of braking force is applied to the front wheel and 40% to the rear wheel.

Figure 5-16 illustrates the relationship between the required steering angle and vehicle speed with different braking forces. For vehicles with the understeer characteristic, an increase in the speed

increases the required steering angle. The braking force has little influence on the required steering angle of a conventional vehicle, whereas it can increase that of a PSS vehicle. For the vehicle with the neutral steer characteristic, the required steer angle is constant when there is no longitudinal force. The existence of the braking force changes the neutral steer to somewhat understeer, and such changes are more evident for a PSS vehicle. For the vehicles with the oversteer characteristic, a higher speed requires a smaller steering angle. The existence of the braking forces can reduce the required steering angle. This reduction is more evident for a PSS vehicle. It can be concluded that the application of the longitudinal braking forces can induce the understeer trend for vehicles, and this trend is more evident for the PSS vehicle.

Figure 5-17 demonstrates the yaw velocity gains, defined by equation (5.29), of a vehicle with PSS and conventional suspension in the steady-state with braking forces. The results signify that the yaw velocity generally increases with an increase in the vehicle speed. For both the PSS vehicle and conventional vehicle with any of understeer, neutral steer and oversteer characteristic, the backward braking force applying to the two tires can reduce the yaw velocity gain compared with that of a free turning in which there is no longitudinal force. The larger the longitudinal forces are, the larger the reduction is. The reduction in the yaw velocity gain, caused by the braking force, is influenced by the suspension longitudinal elasticity. For the PSS vehicle, this reduction is larger than that of the conventional vehicle. From this point of view, the longitudinal braking force may increase the critical speed of an oversteer vehicle. The PSS vehicle may be more advantageous than a conventional vehicle in terms of the directional stability in the existence of braking forces.

The lateral acceleration gain, defined by equation (5.30), for both the PSS and conventional vehicles is examined and plotted in Figure 5-18. An increase in the vehicle speed can increase the lateral acceleration as indicated. Similar to the yaw velocity gain, the lateral acceleration can be reduced by braking forces. Compared with the conventional vehicle, the effect of the braking forces in the PSS vehicle is more evident.

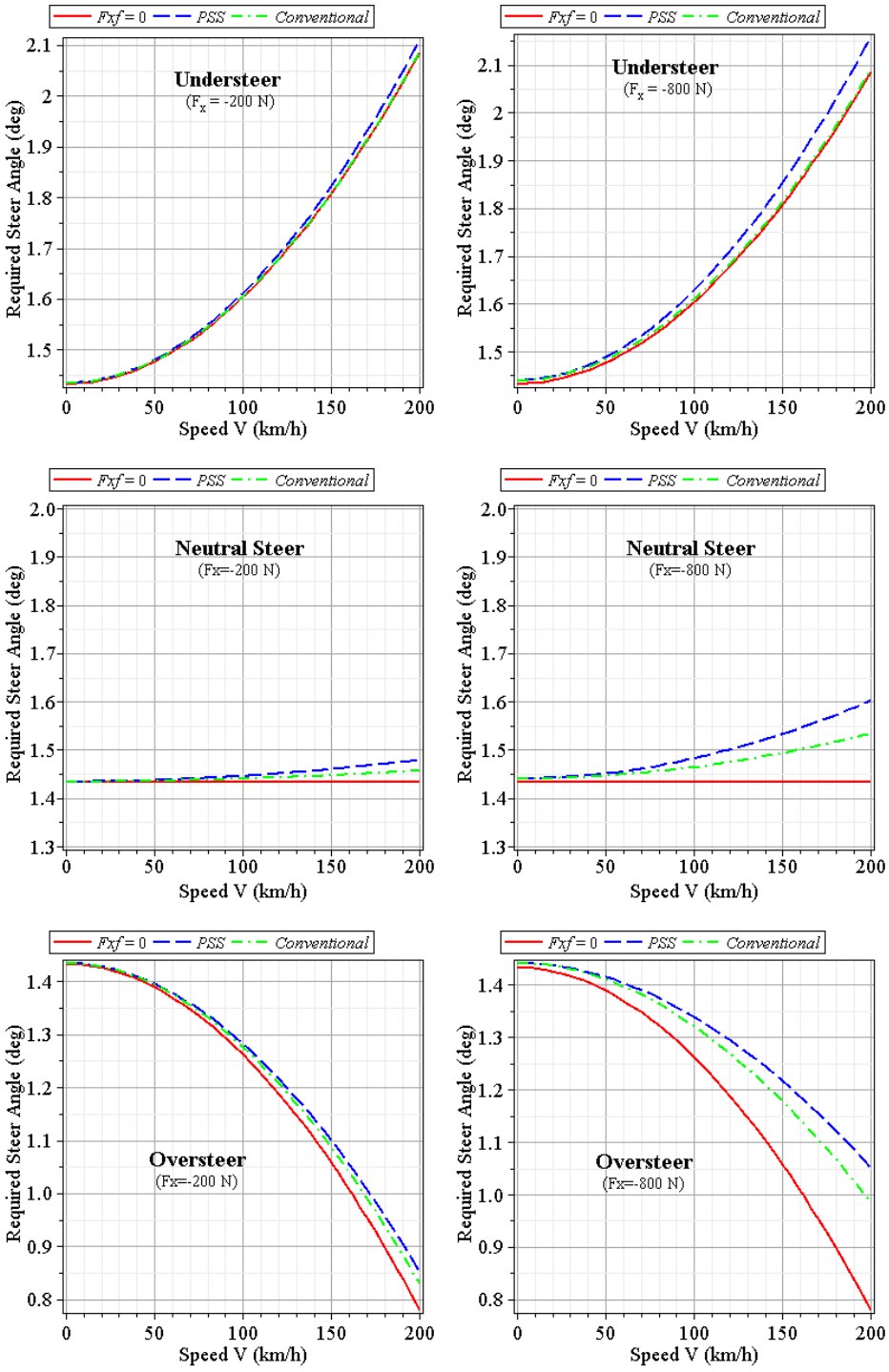

Figure 5-16: Required steering angle at different speeds (braking case)

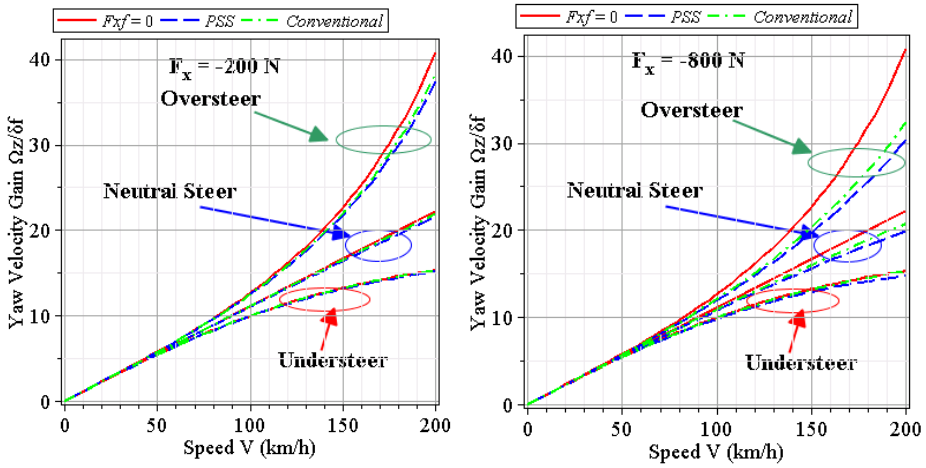

Figure 5-17: Yaw velocity gain (rad/s/rad) of a vehicle with PSS and conventional suspension

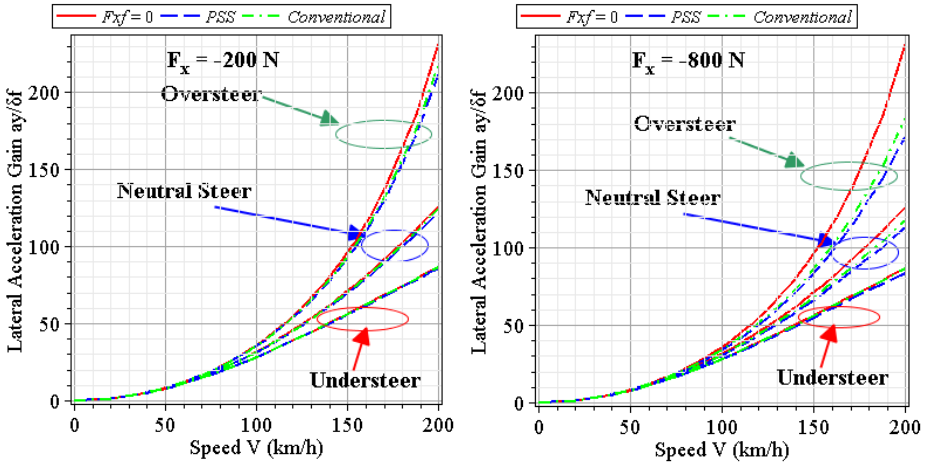

Figure 5-18: Lateral acceleration gain (g/rad) of a vehicle with PSS and conventional suspension

Figure 5-19 depicts the curvature response, defined by equation (5.31), of a PSS and a conventional vehicle. The curvature response decreases with the increase in the speed for the vehicles with the understeer characteristic, but increases for the vehicles with the oversteer characteristic. The vehicle speed has little effect on the curvature response of a neutral steer vehicle when the braking force is small. The figure also shows that the braking forces can reduce the curvature response, especially when the forces are relatively large. Compared to the conventional vehicle with stiff longitudinal connections, the reduction in the curvature response of the PSS vehicle is relatively large.

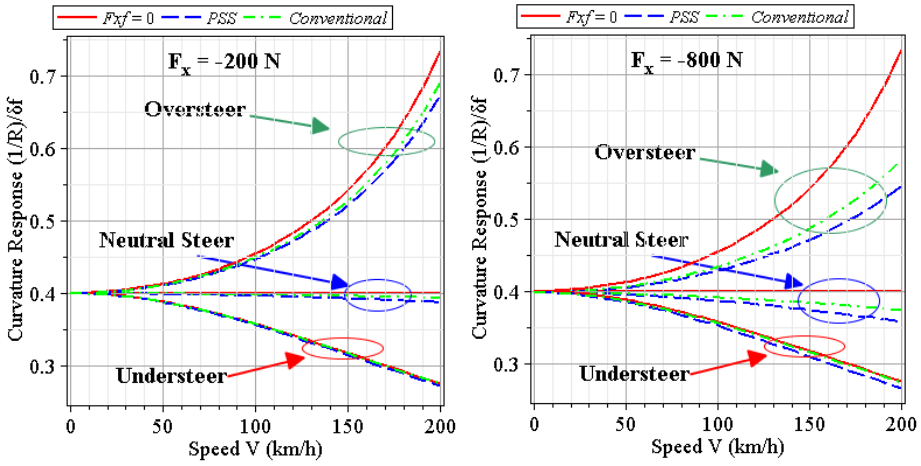

Figure 5-19: Curvature response (1/m/rad) of a vehicle with PSS and conventional suspension

5.5 Summary

A handling model system consisting of a 5-DOF single-track yaw plane sub-model and a 6-DOF half-car pitch plane sub-model was developed incorporating a 2D dynamic tire-ground friction model to study the handling performance of a PSS vehicle. This model system accounts for the relative motions between the wheels and chassis, and takes into account the coupling between the longitudinal and lateral friction forces. This model can be used to investigate the effect of suspension longitudinal compliance on the vehicle bounce, pitch and the handling dynamics.

In this chapter, a study regarding the steady-state handling characteristics of the PSS vehicle was carried out in conditions where a forward and a backward friction forces exist. The vehicles were assigned the understeer, neutral steer and the oversteer handling characteristics, respectively. Throughout the investigation, it was concluded that, while the PSS vehicle exhibits a similar steady-state handling performance to the conventional vehicle, the application of PSS in vehicles can enhance the understeer trend in the presence of longitudinal braking or traction forces, i.e. understeer becomes more understeer, neutral steer becomes slightly understeer and oversteer becomes less oversteer. The longitudinal force can enhance the understeer trend of the PSS vehicle more than that of the conventional vehicle.

Chapter 6
Handling Dynamics Study: Time and Frequency Domain Responses

6.1 Overview

In last chapter, an 11-DOF model system for a vehicle equipped with PSS was developed, and the handling characteristics in the steady-state were investigated in different scenarios. However, the relative motions between the chassis and tires occurs most possibly when the state of wheels changes such as braking or traction, or when wheels experience external disturbances such as road obstacles. The transient handling behaviour may be more important. As in many other vibrating systems, a phase shift can build up for a vehicle between a steering input and the corresponding directional output as input frequencies changes. The steering input may entail various frequencies, from low frequency made by normal drivers to high frequency by professional drivers [80]. On the other hand, due to the existence of the relative motions, the directional stability of a vehicle with PSS is a crucial concern and plays a pivotal role in the feasibility of the planar suspension system. The frequency domain study of a PSS vehicle, therefore, needs to be carried out.

The handling performance study of a PSS vehicle in time domain and frequency domain is presented in this chapter. The parameters used are the same as those used in the previous chapter, as listed in Table 5-2. In the time domain study, the transient handing response is predicted using the proposed analytical model in various scenarios. In the frequency domain investigation, the nonlinear model system is first linearized. The directional stability of the PSS vehicle is examined by an eigenvalue analysis of the linearized system. The frequency handling responses of a PSS vehicle, in terms of yaw velocity gain and lateral acceleration gain, are predicted and analyzed under the conditions where the wheels with and without traction forces. The corresponding response of a similar conventional vehicle is also predicted in both the time and frequency domains for comparison.

6.2 Study of Handling Performance in Time Domain

Due to possible wheelbase changes and the resulting variation in the vehicle weight distribution, the transient response of a PSS vehicle to handling demand may exhibit different characteristics from that of a conventional vehicle in handling maneuvers. Therefore, a time domain study of the handling performance is carried out. The real-time responses of the PSS vehicle in four scenarios, including a

turning on a bumpy road, a turning combined with braking, a turning combined with acceleration, and a lane change with acceleration, are predicted and studied using the proposed vehicle model. The results are also compared with those of a similar conventional vehicle using the same approach.

The trajectory is an important measure of a vehicle's directional behaviour. In this study, the trajectory of a vehicle refers to the trajectory of the chassis mass center, and is defined by the coordinate of the chassis mass center in the global coordinate system (X_s, Y_s). As denoted in Figure 5-10, it is assumed that the yaw angle of the chassis or the x axis, ψ_z, is measured from the chassis original position that coincides with the X axis of the global system. It can be readily calculated from

$$\psi_z(\mathrm{t}) = \int_0^{\mathrm{t}} \Omega_z(\tau)\mathrm{d}\tau \tag{6.1}$$

The lateral and longitudinal velocities of the chassis mass center in the global coordinate system (ZYZ), V_X and V_Y, can be derived from the knowledge of the corresponding ones in the body-fixed coordinate system (xyz), V_x and V_y, as the following:

$$\begin{Bmatrix} V_X(t) \\ V_Y(t) \end{Bmatrix} = \begin{bmatrix} \cos\psi_z(t) & -\sin\psi_z(t) \\ \sin\psi_z(t) & \cos\psi_z(t) \end{bmatrix} \begin{Bmatrix} V_x(t) \\ V_y(t) \end{Bmatrix} \tag{6.2}$$

Then the coordinate of the chassis mass center in the global system, X_s and Y_s, which define the vehicle's position, are

$$\begin{aligned} X_s(t) &= \int_0^t V_X(\tau)d\tau \\ Y_s(t) &= \int_0^t V_Y(\tau)d\tau \end{aligned} \tag{6.3}$$

6.2.1 Validation of the Proposed Handling Model

The proposed simulation model for handling study has not been validated. In order to investigate the model fidelity, a validation for the conventional vehicle is first carried out with the reported study conducted by Shim and Ghike based on a 14-DOF full-car model for a J-turn manoeuvre at 50 km/h [58]. Their results were validated with CarSim and Adams/Car. Figure 6-1 illustrates the reported study data in the J turn. The results in terms of the lateral acceleration and yaw rate are obtained from the proposed analytical model in the present study for a conventional vehicle and superposed on the reported results, as the green dash line shown in Figure 6-1. It can be seen that the results obtained

from different models correlate with a good agreement. The slight difference may be due to the fact that Shim's results are obtained form a full-car model where the roll motion and the wheel load lateral transfer are considered, whereas there are no roll motion and wheel load lateral transfer in the half-car model.

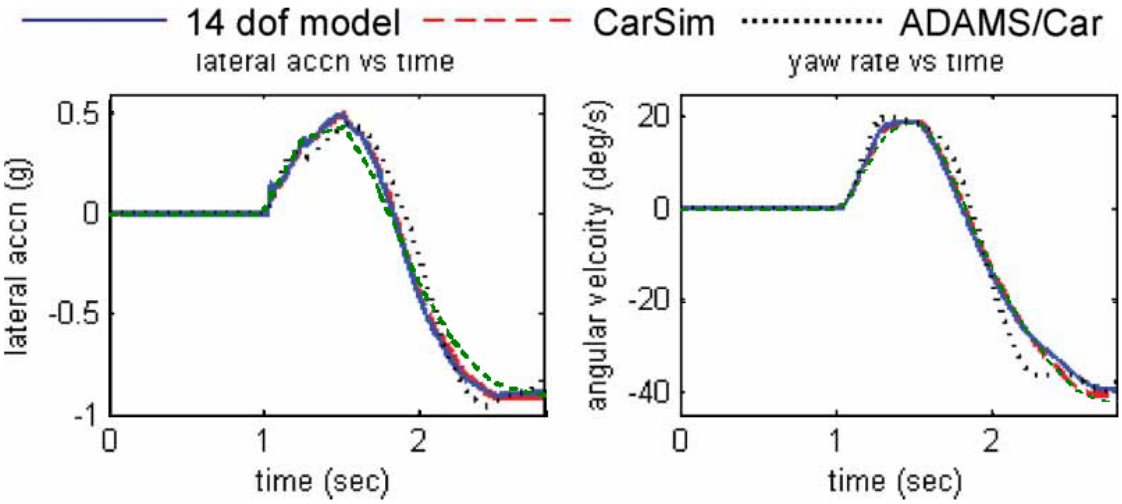

Figure 6-1: Comparison of the lateral acceleration and yaw rate of a conventional vehicle with the reported data [58] in a J-turn (green dash line represents the result of this study)

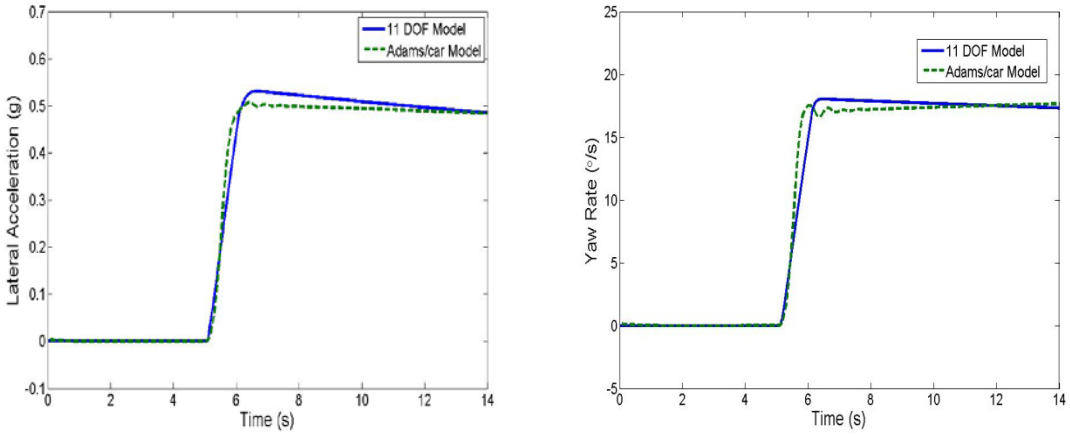

Figure 6-2: Comparison of the lateral acceleration and yaw rate of a PSS vehicle from different models in a step steering

The proposed 11-DOF analytical model for the PSS vehicle is also validated with an Adams/car model in which PSS is constructed as illustrated in Figure 4-9. The validation is carried out at 60 km/h with a 3º step steering input. The lateral acceleration and yaw rate responses of the PSS vehicle are predicted using the two types of models, and plotted in Figure 6-2. It can be seen that the results

obtained from the 11-DOF half-car analytical model are generally in good agreement with those obtained from the Adams/car model. The slight deviation is due to the fact that the Adams/car model is a full-car model with much complexity. The difference between tire models may also contribute to this deviation.

6.2.2 Case Ⅰ: Turning on a Bumpy Road

In this case, it is assumed that a vehicle commences to turn with an initial speed of 50 km/h. The steering input is a 5° step steering angle. During the turning, the vehicle undergoes a bump excitation which is 200 mm long and 100 mm high. Figure 6-3 depicts the vehicle trajectories of the PSS and conventional vehicles. The results indicate the turning path for a constant steering angle almost maintains a circle despite of the bump disturbance. Figure 6-3 implies that, the trajectories of the two types of vehicles almost coincide with each other during the entire manoeuvre.

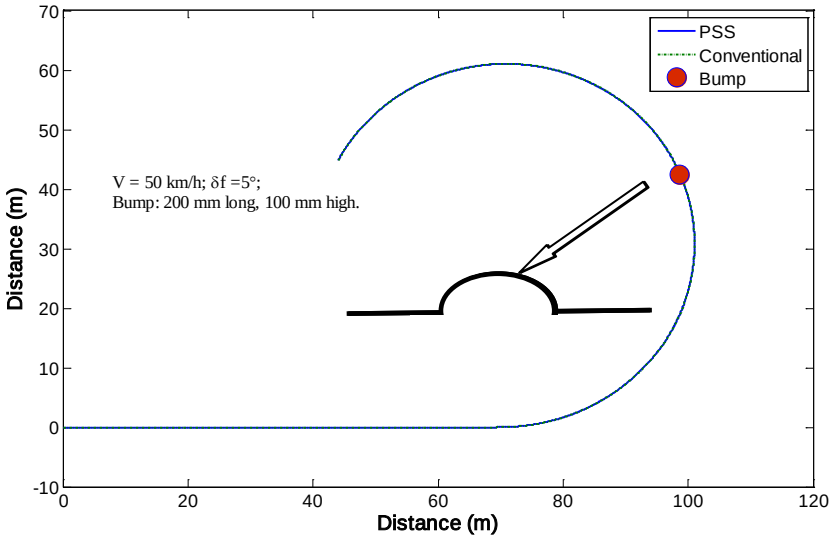

Figure 6-3: Vehicle trajectory of a step steering input turning

The velocity and acceleration responses of the chassis are illustrated in Figures 6-4 and 6-5, respectively. It can be seen from Figure 6-4 that the velocity components of the PSS vehicle are almost as same as those of a conventional vehicle. There is no significant difference in the lateral and yaw velocities between the two types of vehicles when the vehicles hit the bump. The bump-induced variation of the longitudinal velocity, namely the vehicle speed of a PSS vehicle, is somewhat less than that of a conventional vehicle. Figure 6-5 demonstrates that the bounce and lateral accelerations of the PSS vehicle are very close to those of a conventional vehicle. However, significant

improvement is achieved in the longitudinal direction for the PSS vehicle. The bump-induced longitudinal acceleration of the PSS vehicle is much smaller than that of the conventional vehicle without any compromise in the handling performance.

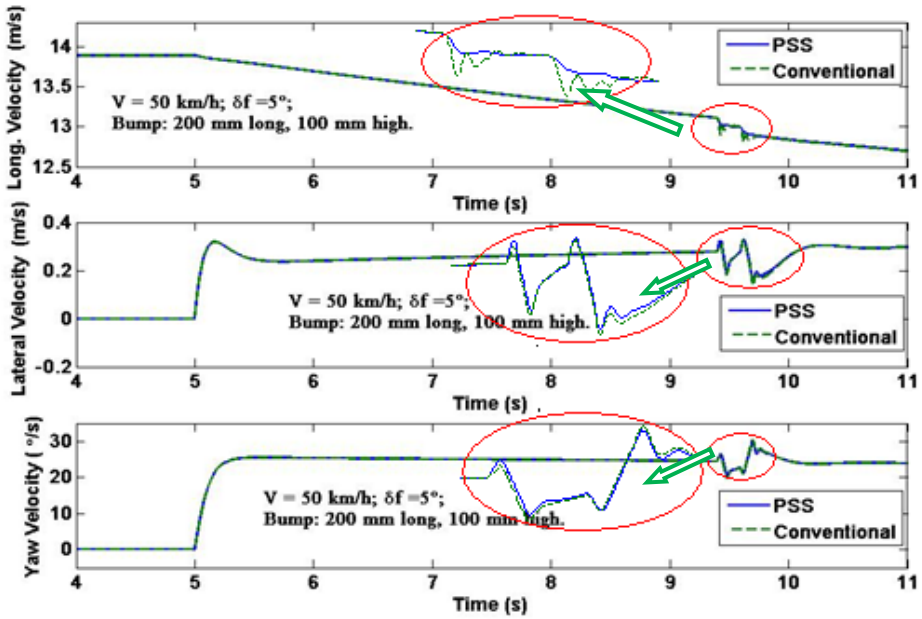

Figure 6-4: Time history of chassis velocity components for a turning on a bumpy road

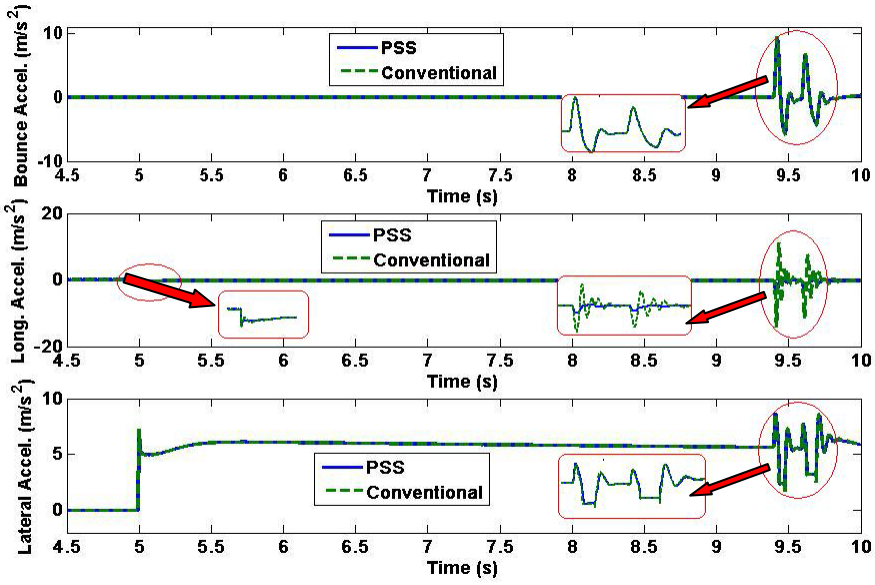

Figure 6-5: Time history of chassis acceleration components for a turning on a bumpy road

In order to have a good understanding of the vehicle's motion during the turning on a bumpy road, the dynamic tire-ground contact forces developed at the tire-ground contact patch due to this bump are predicted and plotted in Figures 6-6. The force plots show that the tires lose contact at the simulation speed when passing over the given size bump. There is little force difference in the vertical and longitudinal directions between the PSS vehicle and the conventional vehicle, except a time delay for the PSS vehicle. This time delay is obviously induced by the soft longitudinal strut in the PSS.

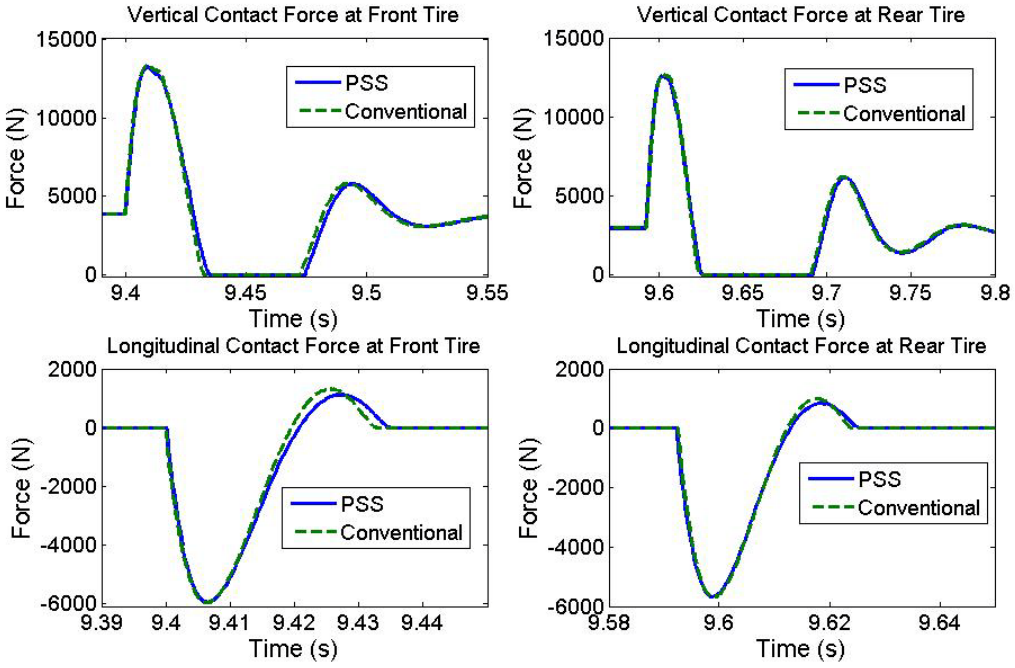

Figure 6-6: Time history of tire-ground contact forces

It is interesting to see from Figure 6-7 that the longitudinal and lateral friction forces are developed when a vehicle passes over a bump during a turning. It can be understood that the wheel forward velocity decreases when it hits a bump, whereas the angular velocity of the wheel does not change simultaneously. Therefore, a slip velocity is developed between the tire and road, generating the friction forces. It is readily understood that the changes of the wheel normal load induced by the bump can also contribute to the undulations of the friction forces. Due to the fact that the tires in the PSS vehicle and those in the conventional vehicle undergo different tire forward velocity changes when hitting a bump, the excessive friction forces developed at the tire-ground contact patch exhibit different pattern in the longitudinal direction. However, Figure 6-7 shows that the lateral friction forces of the two types of vehicles are very close even when hitting the bump.

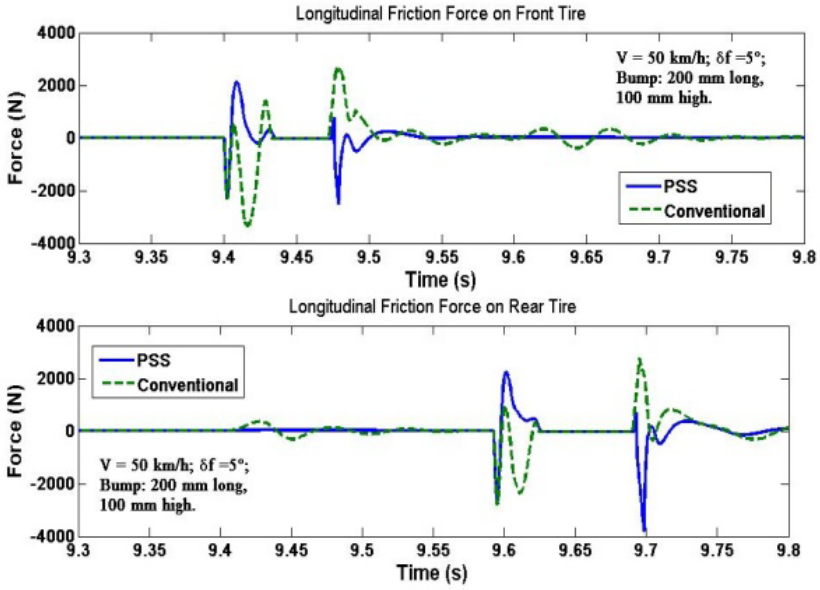

(a) Longitudinal

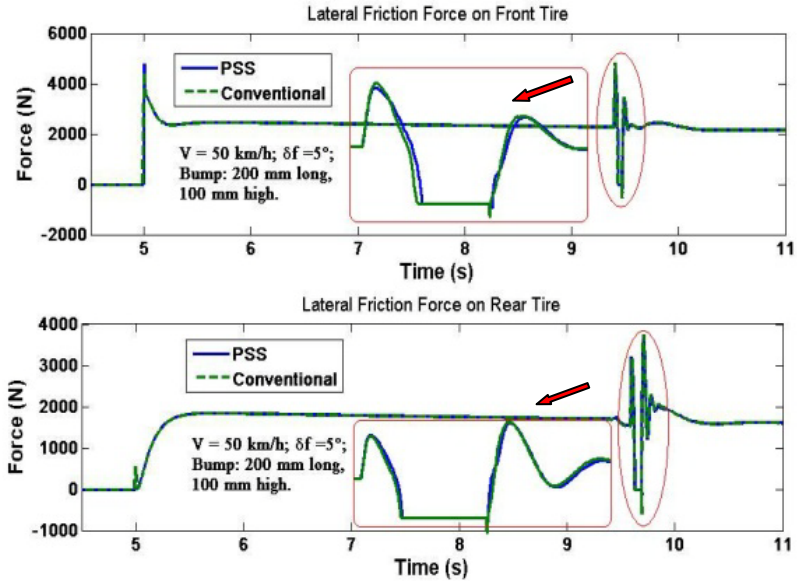

(b) Lateral

Figure 6-7: Time history of the tire friction forces

The suspension longitudinal forces, shown in Figure 6-8, indicate that the longitudinal forces transmitted to the vehicle body via the PSS are relatively small compared to those via a conventional suspension. To some extent, the vehicle body, suspension linkages and the joints experience less impact damages when the PSS vehicle encounters large road obstacles.

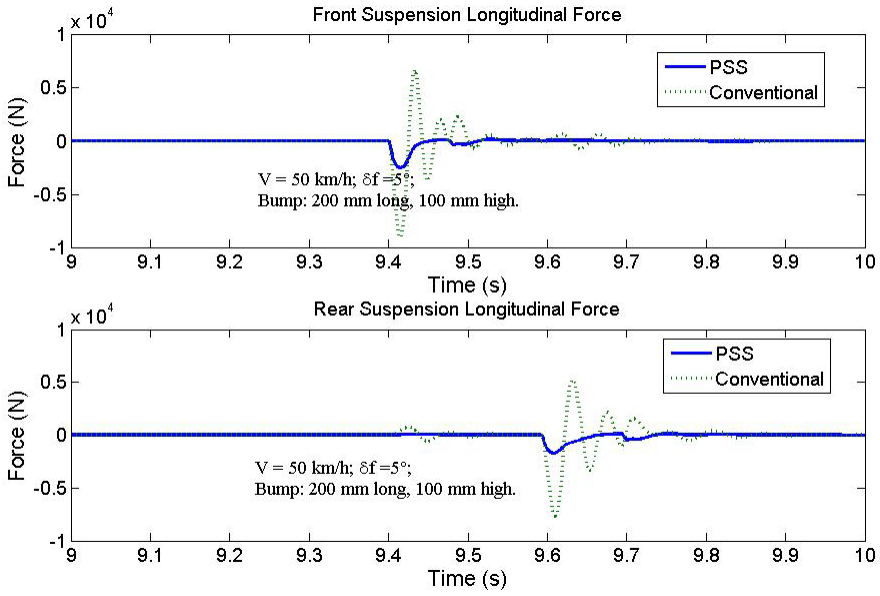

Figure 6-8: Time history of the suspension longitudinal forces

A concern regarding the suspension working-space may arise when the tires traverse road obstacles. Therefore, the longitudinal suspension deflections of the PSS vehicle are predicted and compared with those of the conventional vehicle, as plotted in Figure 6-9. The results show that the suspension longitudinal deflections of the PSS vehicle are considerably larger than those of the conventional vehicle due to the soft longitudinal connection. However, the deflection is less than 3 cm in the simulation condition, which means that no excessive design space is required in the longitudinal direction.

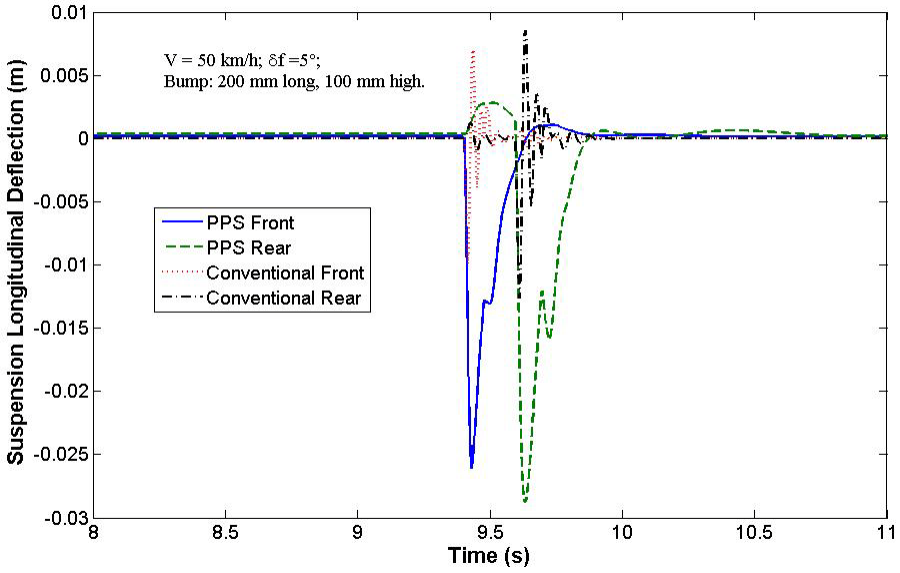

Figure 6-9: Time history the suspension longitudinal deflection

6.2.3 Case Ⅱ: Turning Combined with Braking

A braking-in-turn manoeuvre is explored using the proposed analytical model with an initial vehicle speed of 100 km/h. The steering input and the braking torque, illustrated in Figure 6-10, are applied simultaneously. The braking torque is applied to the front and rear tires with such a ratio that the applied braking torque is proportional to the static wheel load.

The time history of the chassis velocity components are plotted in Figure 6-11. In the longitudinal direction, the velocity decreases and exhibits no difference between the PSS and conventional vehicles. However, the lateral and yaw velocities of the PSS vehicle are quite different from those of the conventional vehicle. The lateral and the yaw velocities of the PSS vehicle are comparatively small. This difference corresponds to the relative motions between the wheels and chassis. In the braking manoeuvre, the wheels in the PSS vehicle develop a relative longitudinal velocity with respect to the vehicle body. This longitudinal velocity can influence the relative slip velocity defined by equation (5.4) and results in larger longitudinal friction force. As discussed previously, the longitudinal friction can reduce the lateral friction force. Such a relative longitudinal motion in a conventional vehicle is very small. Therefore, the lateral friction force in the PSS vehicle is slightly smaller than that in the conventional vehicle; and the lateral motion of the PSS vehicle is smaller than that of the conventional vehicle.

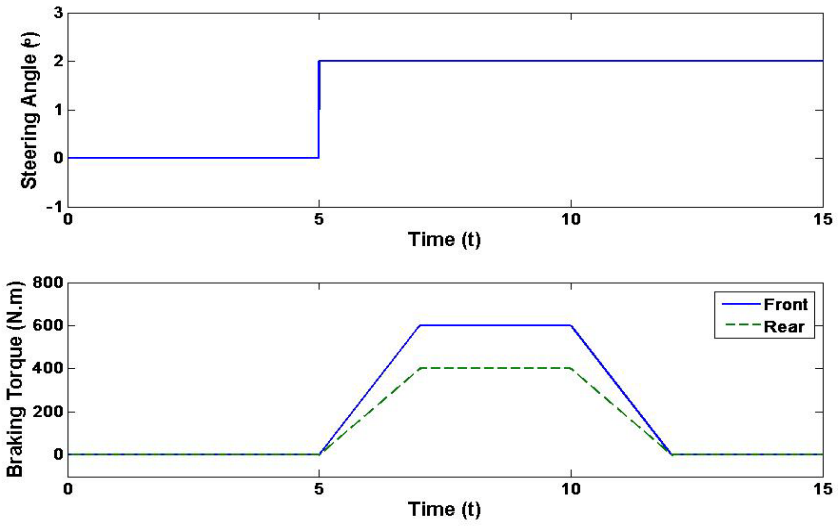

Figure 6-10: Steering and braking torque inputs in a combining operation

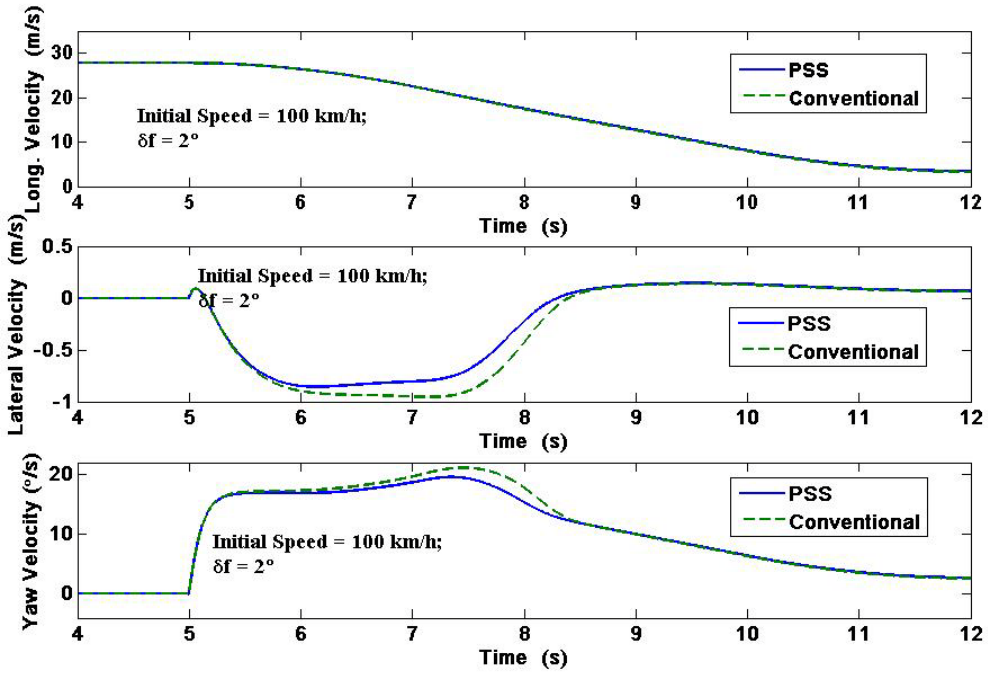

Figure 6-11: Time history of the chassis velocity components

The chassis acceleration responses are plotted in Figure 6-12. At the instant when the braking torque first increases and then decreases, a vertical acceleration is generated. The magnitude of this vertical acceleration of the PSS vehicle is larger than that for the conventional vehicle, possibly due to

the larger pitch motion of the PSS vehicle. However, the vertical accelerations are generally very small and negligible. The longitudinal acceleration of the two types of vehicles are very close, whereas the lateral acceleration of the PSS vehicle is slightly small when compared with that of the conventional vehicle.

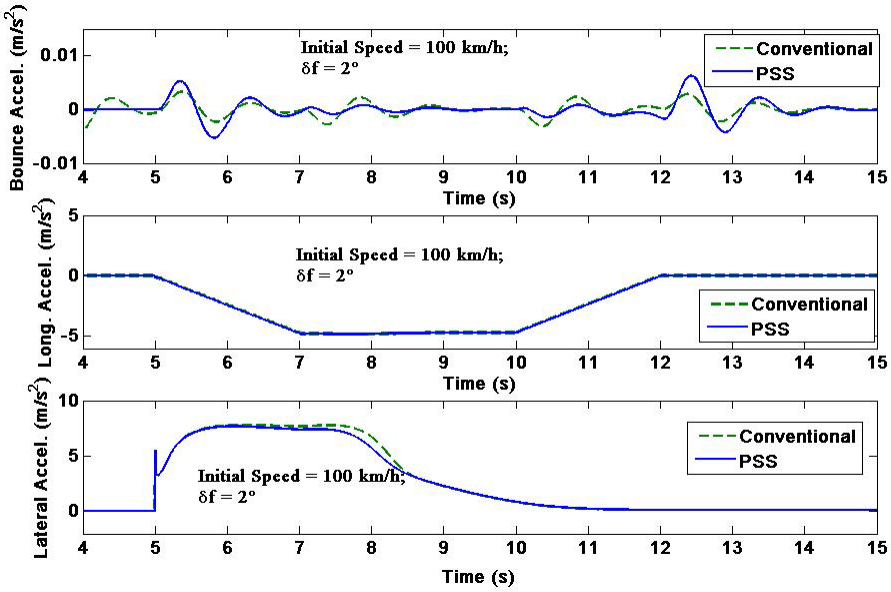

Figure 6-12: Time history of the chassis acceleration components

The trajectories of the two types of vehicles are plotted in Figure 6-13. It is clear that the path radius of the PSS vehicle gradually becomes larger in the turning than that of the conventional vehicle, i.e., the vehicle with PSS exhibits more understeer characteristic in a turning combined with a braking operation. This may be related to the changes in the wheelbase and the weight distribution of the vehicle with PSS. Because of the stiff longitudinal suspension stiffness in the conventional suspension, the weigh distribution remains almost unchanging. Such a characteristic of the PSS vehicle is controversial. It may be an advantage when stability is preferable in some situations such as this brake-in-turn manoeuvre. On the contrary, it is undesirable when a rapid turning response is needed in an obstacle-avoidance manoeuvre. However, the path variation shown in Figure 6-12 is very small and can be neglected.

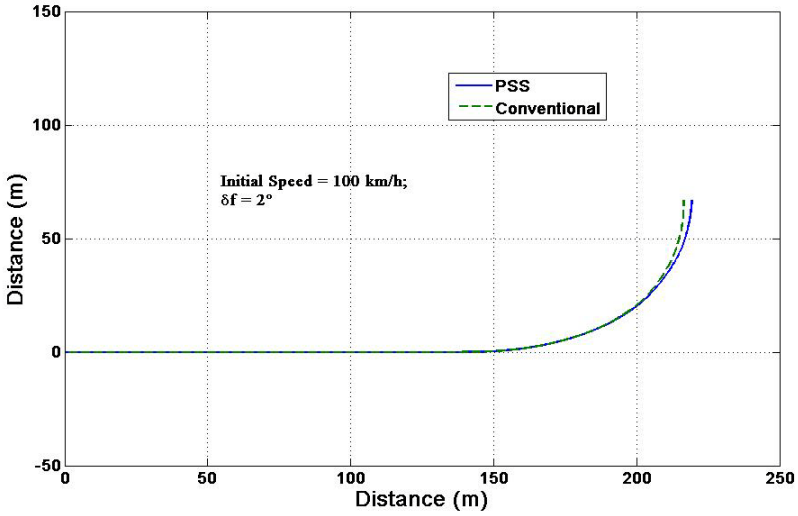

Figure 6-13: Vehicle trajectory in a braking-in-turn operation

Figure 6-14 illustrates the normal wheel loads at the front and the rear tires. In this combined operation, the normal wheel load is transferred to the front wheel from the rear wheel. This is actually induced by the braking operation. This figure also shows that the normal wheel load transfer of the PSS vehicle is larger than that of a conventional vehicle, may be due to wheelbase changes.

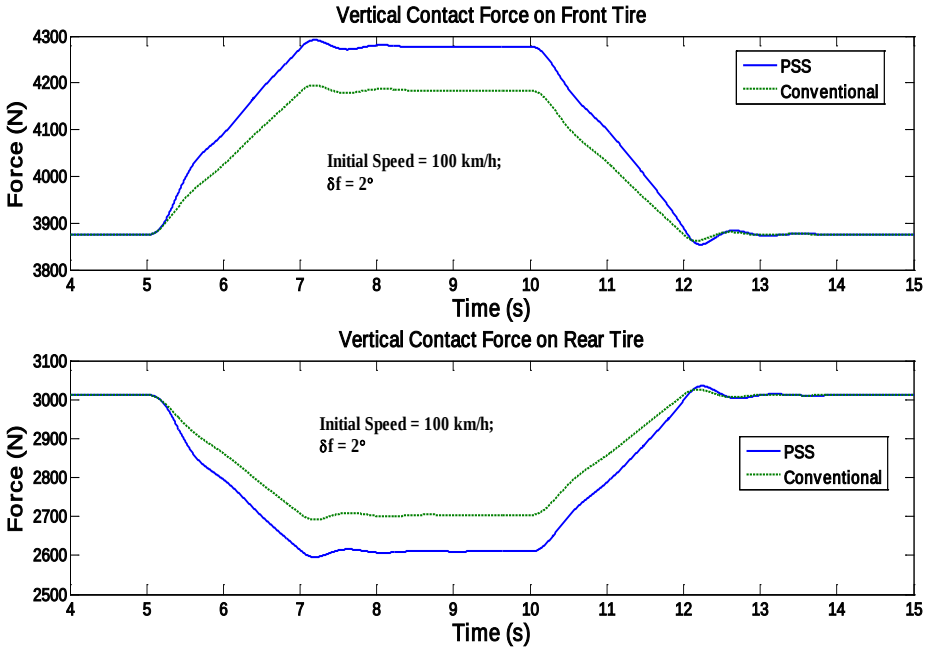

Figure 6-14: Time history of the normal wheel load

6.2.4 Case Ⅲ: Turning Combined with Acceleration

A combination of turning and acceleration maneuvers is studied with an initial vehicle speed of 20 km/h. The steering input and the driving torque, as shown in Figure 6-15, are applied at the same time. The driving torque is solely applied to the front tire.

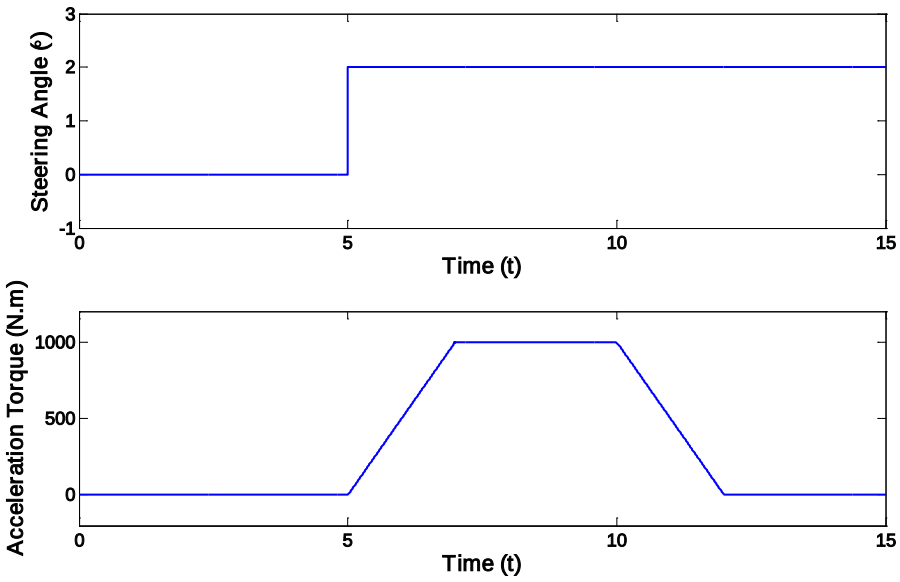

Figure 6-15: Steering and driving torque inputs in a combining operation

The time history of the chassis velocity components is illustrated in Figure 6-16. In the longitudinal direction, there is no difference between the PSS vehicle and the conventional vehicle. The lateral and yaw velocities of the PSS and conventional vehicles are close at the beginning of the operation. When the driving torque starts to reduce, the lateral velocity has a peak and the yaw velocity has a dip. This is due to the fact that, in a two-dimensional friction, the lateral friction force can increase when the longitudinal tractive friction force decreases. The suddenly increased lateral force results in a rapid directional response. The difference between the PSS and conventional vehicles is due to the different dynamic normal load at the front wheel. Because of the extension of the front suspension, the front wheel of the PSS vehicle moves far away to the gravity center, and the front wheel load becomes smaller than that of a conventional vehicle, and so are the lateral cornering forces at the front wheel. This is why the yaw velocity of a PSS vehicle is always slightly smaller than that of the conventional vehicle during the manoeuvre.

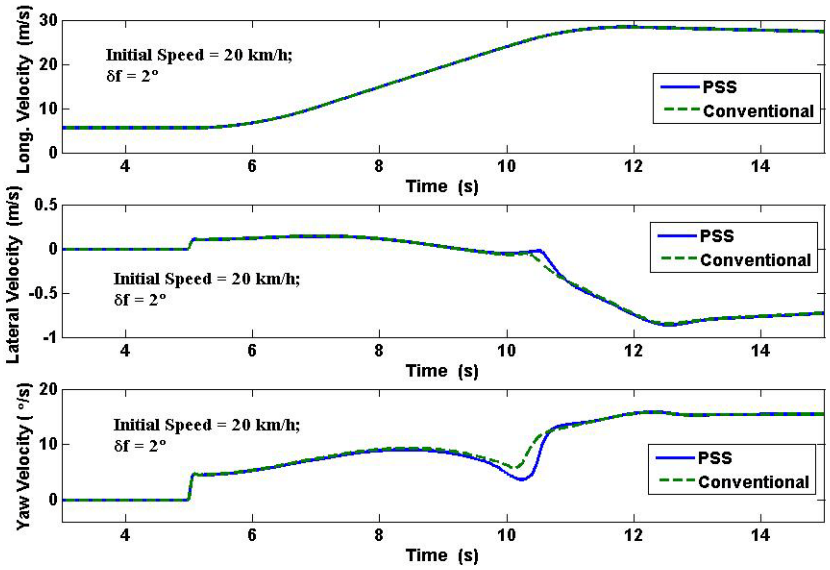

Figure 6-16: Time history of the chassis velocity components

The chassis acceleration responses are plotted in Figure 6-17. When the driving torque increases and then decreases, a vertical acceleration is generated and its magnitude of the PSS vehicle is larger than that of the conventional vehicle, as in the braking-in-turn manoeuvre. However, the vertical accelerations are generally small and negligible. The longitudinal and lateral acceleration responses of the two types of vehicles are very close in the course except when the driving torque starts to decrease.

The trajectories of the two types of vehicles are plotted in Figure 6-18. It can be seen that, during the operation, the radius of the path for the PSS vehicle becomes larger than that of the conventional vehicle. In other words, the PSS vehicle becomes more understeer in a turning combined with an acceleration operation. This is similar to the braking-in-turn case.

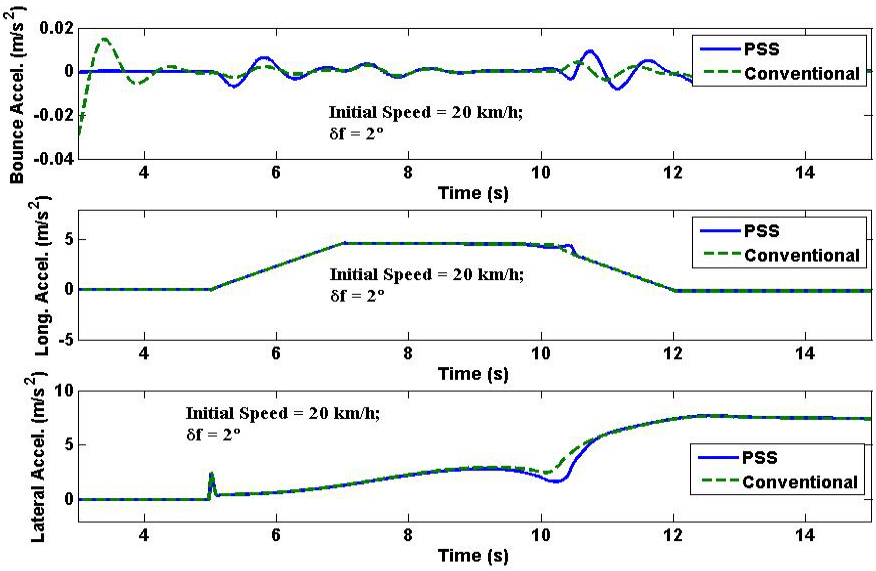

Figure 6-17: Time history of the chassis acceleration components

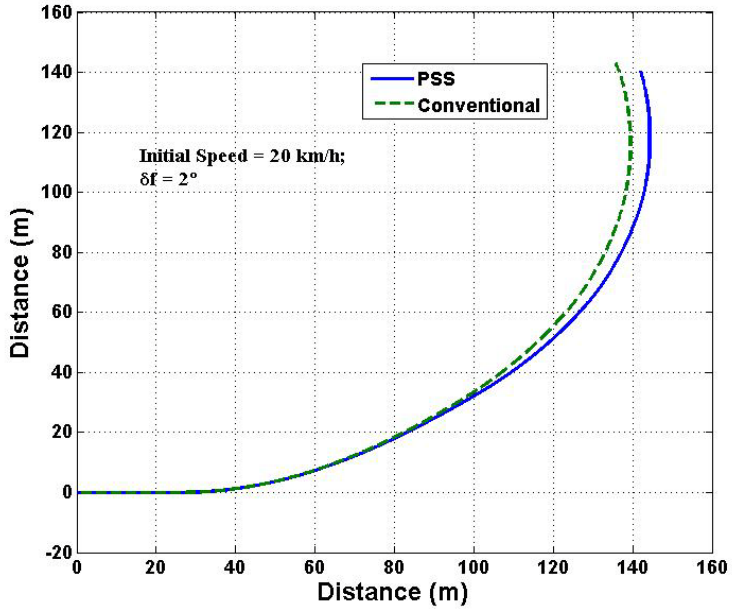

Figure 6-18: Vehicle trajectory in an acceleration-turning combined

6.2.5 Case Ⅳ: Lane Change Manoeuvre

In this study, a lane change, combined with an acceleration operation, is studied. Figure 6-19 illustrates the trajectory of the two types of vehicles for a lane change combined with an acceleration operation, as well as the trajectories for a pure lane change without any other input. The figure shows

that the trajectories of the PSS and conventional vehicles are very close although that of the vehicle with PSS is somehow inside when combined with an acceleration operation. This difference is induced by the difference in the suspension longitudinal deflection. The trajectories of the two types of vehicles are almost the same during pure lane change manoeuvre.

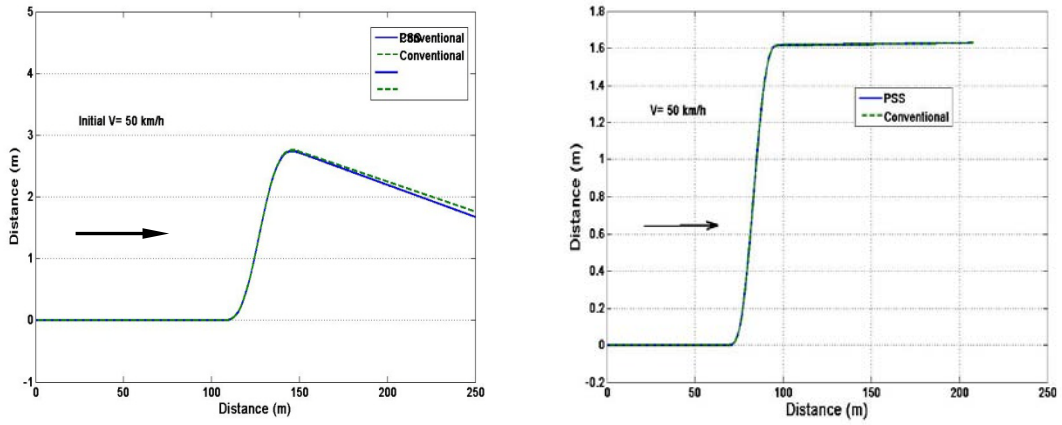

(a) Lane change combined with acceleration (b) Lane change with no other input

Figure 6-19: Trajectory for a lane change

Figure 6-20 depicts the time history of the chassis velocity components. Clearly, the velocity components of the vehicle with PSS are very close to those of the vehicle with conventional suspension. In addition, the results imply that a high vehicle speed results in a large lateral velocity. Figure 6-21 shows the acceleration response of the combined operation. The results indicate that the bounce acceleration of the vehicle with PSS, although very small, is larger than that of the vehicle with conventional suspension at the beginning and end of the acceleration operation. This may be due to the difference of the coupling between the bounce and pitch for the two types of vehicles. The longitudinal acceleration determined mainly by the traction input, and the lateral acceleration induced primarily by the steering input, are very close between these two types of vehicles.

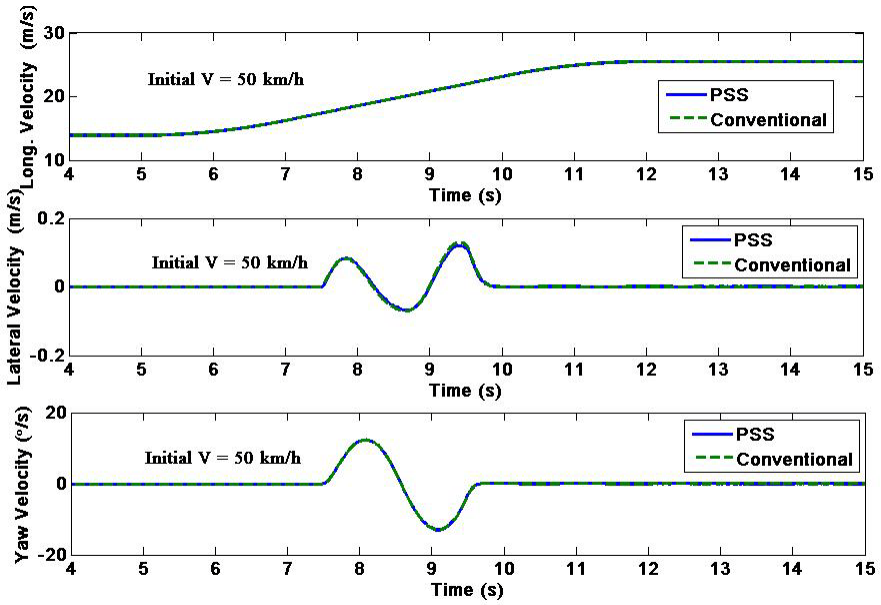

Figure 6-20: Time history of the chassis velocity components in a lane change

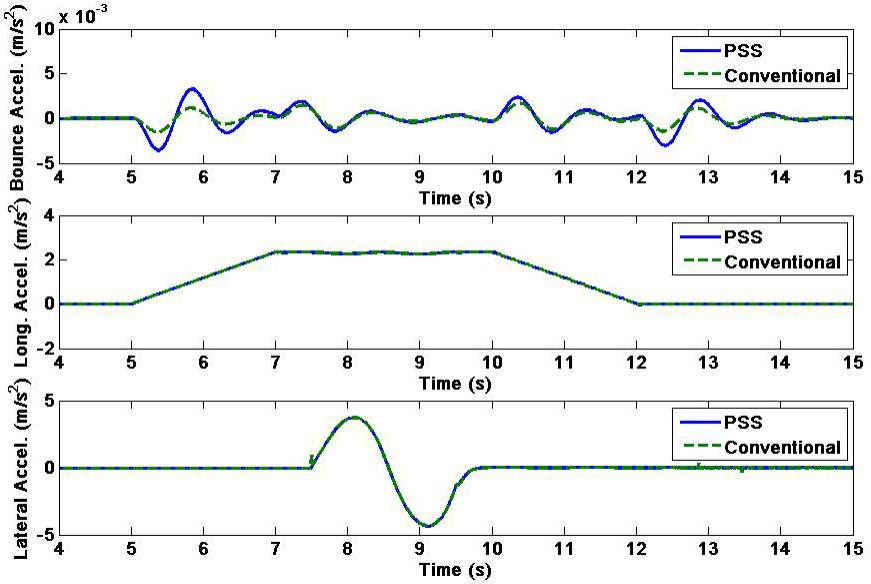

Figure 6-21: Time history of the chassis acceleration components in a lane change

6.3 Study of Handling Performance in Frequency Domain

The directional stability is an important issue in the vehicle handling study, and the frequency handling response of a vehicle plays an important role in the evaluation of a vehicle's handling

performance. Therefore, a frequency domain study of handling performance for a PSS vehicle is carried out.

In this study, the proposed vehicle model is linearized at operation points to obtain the frequency domain transformation of the linearized system from input to output. The directional stability of a PSS vehicle is examined by an eigenvalue analysis of the linearized system. The frequency handling responses of a PSS vehicle, in terms of a yaw velocity gain and a lateral acceleration gain, are predicted and analyzed. These responses are also compared with those of a similar conventional vehicle to assess the handling performance of the planar suspension system in frequency domain.

6.3.1 Linearization of System Equations

The vehicle model system presented in Section 5.3 is highly nonlinear. The nonlinearity arises from the nonlinear longitudinal components of the suspension system, the state-dependent stiffness and damping matrices of the pitch plane sub-model, the coupling between the pitch and yaw plane motions, and the nonlinear friction between tires and the ground. In order to perform a frequency domain study, the system model is first linearized.

The model system, described by equation (5.15) for the pitch plane motions and equation (5.16) or (5.18) for the yaw plane motions, is rewritten in the state space form as:

$$\dot{X}(t) = f\left[X(t), U(t)\right] \tag{6.4}$$

where ***X(t)*** is the state vector as follows:

$$\mathrm{X(t)} = \left\{ \dot{z}_s \quad \dot{\phi}_s \quad \dot{z}_{uf} \quad \dot{z}_{ur} \quad \dot{\theta}_f \quad \dot{\theta}_r \quad z_s \quad \phi_s \quad z_{uf} \quad z_{ur} \quad V_x \quad V_y \quad \Omega_z \quad \dot{x}_{A1} \quad \dot{x}_{B1} \quad x_{A1} \quad x_{B1} \right\}^T \tag{6.5}$$

This state vector describes the motions of the vehicle model system. Note that θ_f and θ_r, representing the rotational motions of two tires, are not needed.

U(t) is input vector containing the input variables, including the road irregularity, driving/braking torque and steering angular input, as follows:

$$U(t) = \left\{ \dot{z}_{of} \quad \dot{z}_{or} \quad z_{of} \quad z_{or} \quad T_f \quad T_r \quad \ddot{\delta}_f \quad \dot{\delta}_f \quad \delta_f \right\}^T \tag{6.6}$$

Equation (6.4) can be linearized at an operation point, $\boldsymbol{X_o}$, with a reference input, $\boldsymbol{U_o}$, in the following form:

$$\dot{X}(t) = f(X_o, U_o) + A(X - X_o) + B(U - U_o) \tag{6.7}$$

where ***A*** is a *17×17* matrix and ***B*** is a *17×9* matrix as follows:

$$A = \left[\frac{\partial f}{\partial X}\right]_{X_o, U_o} \text{ and } B = \left[\frac{\partial f}{\partial U}\right]_{X_o, U_o} \tag{6.8}$$

When the operation point is an equilibrium point at which the system is linearized, the following expression holds:

$$\mathrm{f}(\mathrm{X_o}, \mathrm{U_o}) = 0 \tag{6.9}$$

Let $X^{'} = X - X_o$, *and* $U^{'} = U - U_o$, then

$$\dot{X}^{'} = AX^{'} + BU^{'} \tag{6.10}$$

The crucial task of the system linearization is to determine the equilibrium point. This point can be obtained by setting all the time derivatives in equation (6.4), excluding the angular velocities of the two tires ($\dot{\theta}_{\mathrm{fo}}$ and $\dot{\theta}_{\mathrm{ro}}$), to zero and solving for ***X*** with a certain set of values of $\mathbf{U}_{\mathrm{o}}$.

Equation (6.10) represents a time invariant linear system. The frequency domain transformation from $U^{`}(\omega)$ to $\boldsymbol{X}^{`}(\omega)$ are established as follows:

$$X^{'}(\omega) = (i\omega I - A)^{-1} BU^{'}(\omega) \tag{6.11}$$

It can be seen from equation (6.5) that the 12th element of $\boldsymbol{X}^{'}(\omega)$ is the response of the lateral velocity variation, and the thirteenth element is the response of the yaw velocity variation, that is,

$$\begin{aligned} V_y^{'}(\omega) &= (V_y - V_{yo})(\omega) = X^{'}(\omega)[1 \quad 2 \\ \Omega_z^{'}(\omega) &= (\Omega_z - \Omega_{zo})(\omega) = X^{'}(\omega)[1 \quad] \end{aligned} \tag{6.12}$$

In the vehicle handling analysis, the lateral acceleration (a_y) response is always of paramount interest, but is not a state variable of the system. However, the lateral acceleration can be attained by the following expression:

$$a_y = \dot{V}_y + V_x \Omega_z \tag{6.13}$$

The frequency response of the acceleration is easily obtained from the above relationship as follows:

$$a_y(\omega) = i\omega V_y(\omega) + V_x \Omega_z(\omega) \tag{6.14}$$

The steady-state 2D friction forces predicted using equation (5.12) are nonlinear with respect to the longitudinal slip, *s*, and side slip angle, α, and thus cannot be applied to the frequency study. Therefore, equation (5.12) needs to be linearized as follows:

$$F_i^{SS}(\alpha, s) = F_n[\mu_i^{SS}(\alpha_o, s_o) + \frac{\partial \mu_i^{SS}(\alpha_o, s_o)}{\partial \alpha}(\alpha - \alpha_o) + \frac{\partial \mu_i^{SS}(\alpha_o, s_o)}{\partial s}(s - s_o)] \tag{6.15}$$

where (s_o, α_o) are the point where the linearization is performed. The close form of the partial derivative terms may not exist. A secant linearization method is used to obtain these terms in this study.

The purpose of this study is to investigate the frequency response of a vehicle due to a frequency input in the neighborhood of an equilibrium point. The investigation is performed in two scenarios: (i) the external longitudinal force applied to the vehicle, F_{xo}, is zero; and (ii) the external longitudinal force applied to the vehicle, F_{xo}, is constant and forward. Owing to the complexity of the model system, the Maple symbolic computation tool is employed to perform the simulation.

6.3.2 Turning on a Straight Flat Road without Longitudinal Friction Force

When there are no road irregularity and external longitudinal force, a vehicle can keep a steady-state or equilibrium state without any torque and steering inputs. The reference input vector, $\boldsymbol{U}_o$, is equal to *zero.* Substituting $\boldsymbol{U}_o$ in equation (6.4) and solving for $\boldsymbol{X}$ can result in $\boldsymbol{X}_o$. It should be noted that the derivative elements in $\boldsymbol{X}_o$, excluding the angular velocities of the two tires ($\dot{\theta}_{fo}$ and $\dot{\theta}_{ro}$), are equal to zero and the longitudinal velocity of the chassis, V_x can be arbitrarily assigned in steady-state. In this study, the speed is set as 80 km/h. The suspension longitudinal deflections are zero because there is no external longitudinal force. The lateral velocity and yaw velocity are zero, so only the bounce and pitch motions need to be determined. Thus, the linearized point is as follows:

$$\begin{aligned} X_o &= \left\{ \dot{z}_{so} \quad \dot{\phi}_{so} \quad \dot{z}_{ufo} \quad \dot{z}_{uro} \quad \dot{\theta}_{fo} \quad \dot{\theta}_{ro} \quad z_{so} \quad \phi_{so} \quad z_{ufo} \quad z_{uro} \quad V_{xo} \quad V_{yo} \quad \Omega_{zo} \quad \dot{x}_{A1o} \quad \dot{x}_{B1o} \quad x_{A1o} \quad x_{B1o} \right\}^T \\ &= \left\{ 0 \quad 0 \quad 0 \quad 0 \quad -\frac{V_x}{R} \quad -\frac{V_x}{R} \quad z_{so} \quad \phi_{so} \quad z_{ufo} \quad z_{uro} \quad V_x \quad 0 \quad 0 \quad 0 \quad 0 \quad 0 \quad 0 \right\}^T \end{aligned} \tag{6.16}$$

The point (s_o, α_o), where the linearization of the friction model is performed as in equation (6.15) for each tire, is (0, 0) in this case.

The stability of the linear system defined by equation (6.10) is first examined. This can be done by referring to the eigenvalues of matrix ***A***. According to the stability theory of a linear system, a system is asymptotically stable if the real part of every eigenvalue of ***A*** is negative, and bounded-input bounded-output (BIBO) stable if the real part of every eigenvalue of ***A*** is non-positive. The eigenvalues of matrix ***A*** for the PSS vehicle are calculated and listed in Table 6-1.

Table 6-1: Eigenvalues of the linearized system (matrix A) for a PSS vehicle

No	Eigenvalue	Frequency (Hz)	Damping Ratio
1	-841.00	133.85	
2	-511.18	84.58	
3	-45.65±75.80 i	14.08	0.516
4	-28.36±74.88 i	12.74	0.354
5	-1.83±6.27 i	1.04	0.280
6	-2.24±6.91 i	1.16	0.309
7	-11.47±10.57 i	2.48	0.735
8	-19.00±6.63 i	3.20	0.944
9	-12.54±4.21 i	2.05	0.956
10	-2.62×10^{-9}	4.49×10^{-10}	

It is evident from Table 6-1 that all of the eigenvalues have negative real part. Therefore, this system is stable at the linearization point ($\boldsymbol{X_o}$, $\boldsymbol{U_o}$).

The yaw velocity gain and phase lag, as well as the lateral acceleration gain and phase lag, of the PSS vehicle and the conventional vehicle are depicted in Figures 6-22 and 6-23, respectively. The investigation is carried out in the conditions of the vehicles with understeer, neutral steer, and oversteer characteristics. These steer characteristics are obtained by changing the distances between the vehicle gravity center and the two tires (*b* and *c*).

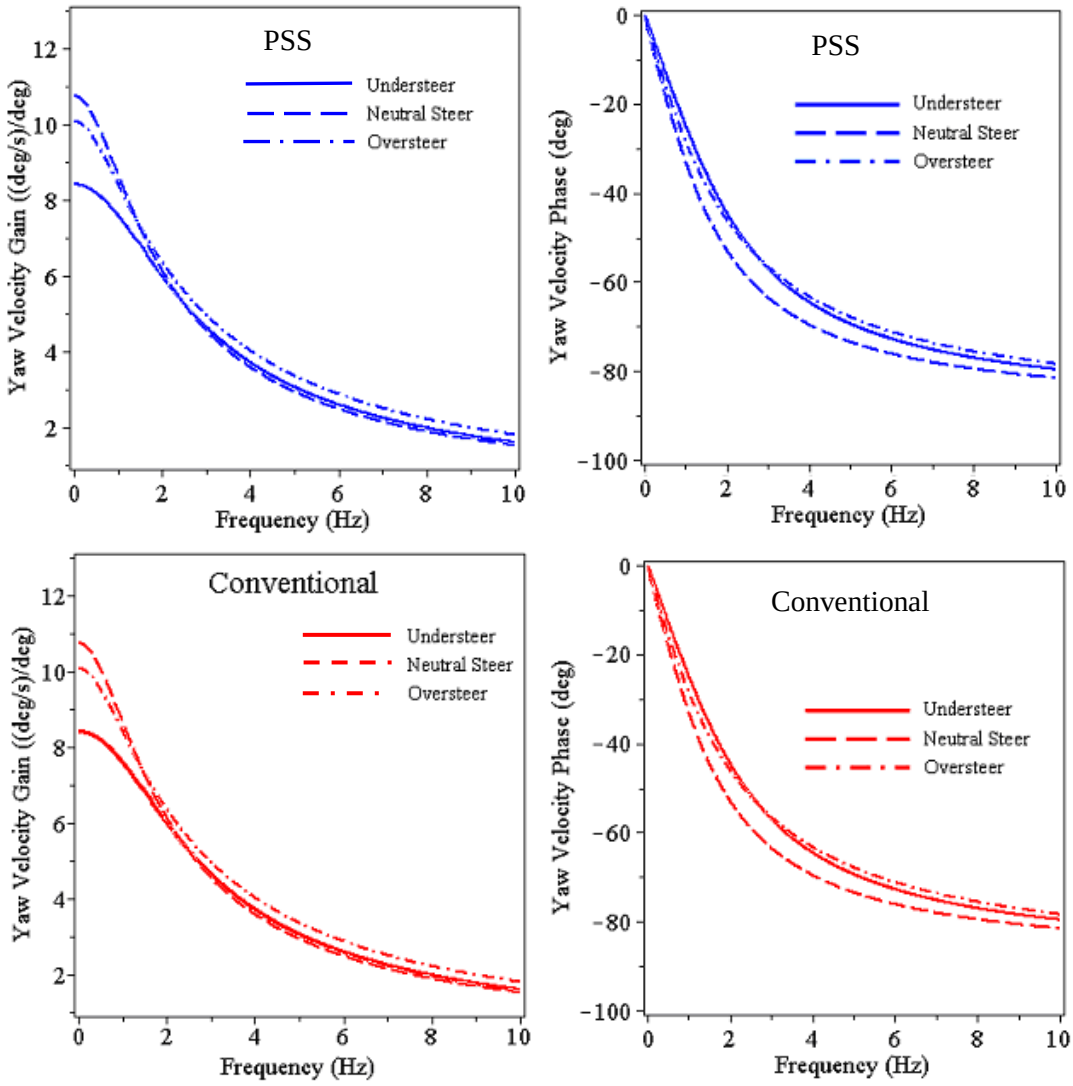

Figure 6-22: Frequency response of yaw velocity gain and phase lag

Figure 6-22 indicates that an increase in the steering frequency generally leads to a small yaw velocity response but a large phase lag. The results displayed in Figure 6-23 imply that an increase in the steering frequency first reduces the lateral acceleration response to a minimum value at a critical frequency, which is between 2 and 3 Hz. After this frequency, the lateral acceleration response increases for an increase in the steering frequency. It is evident from Table 6-1 that this critical frequency is actually the natural frequency of the steering motions. The phase angle exhibits the same pattern, but the critical frequency is somewhat small. The solutions shown in these two figures are consistent with those in the literatures [98, 99]. This implies the proposed model and method are effective. When the input frequency is zero, the responses are actually the steady-state responses,

which are consistent with the result obtained in Chapter 5. The results also indicate that the frequency response of yaw velocity and the phase lag for a PSS vehicle are almost the same as those of a conventional vehicle. In other words, the application of a soft connection between the sprung and unsprung masses in a PSS vehicle does not affect the handling performances when no external forces are applied.

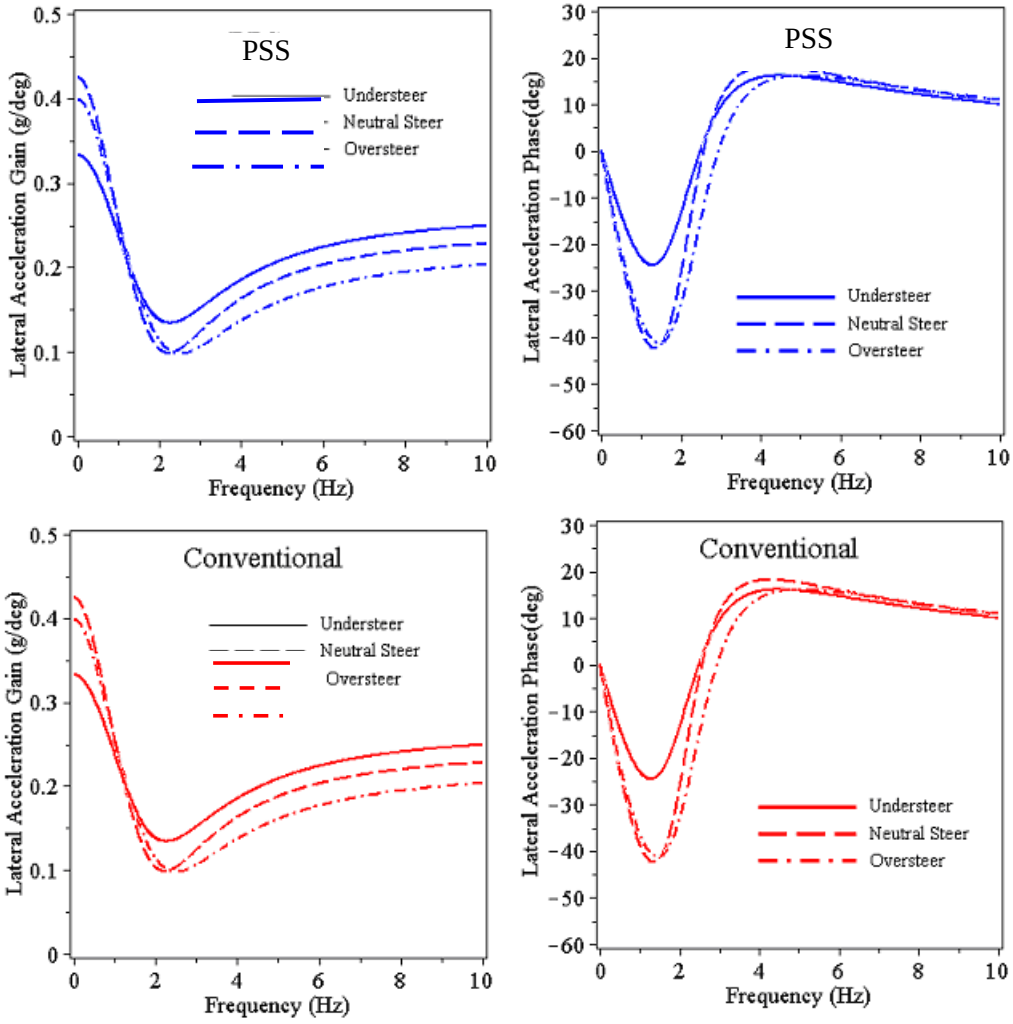

Figure 6-23: Frequency response of yaw velocity gain and phase lag

The frequency responses for an understeer PSS vehicle and a similar conventional vehicle at various speeds are displayed in Figure 6-24 and 6-25, respectively. They reflect the effect of the vehicle speed on the frequency responses. In general, the yaw velocity and lateral acceleration responses are small at a low speed, and are larger at a higher speed for these two types of vehicles. Partially in the frequency range between 0~3 Hz, the speed dependency of the yaw velocity and

lateral acceleration on the vehicle speed is very significant. However, such an effect becomes negligible at high frequency. Figure 6-24 and 6-25 also indicates that the frequency responses of these two types of vehicles are close at various speeds.

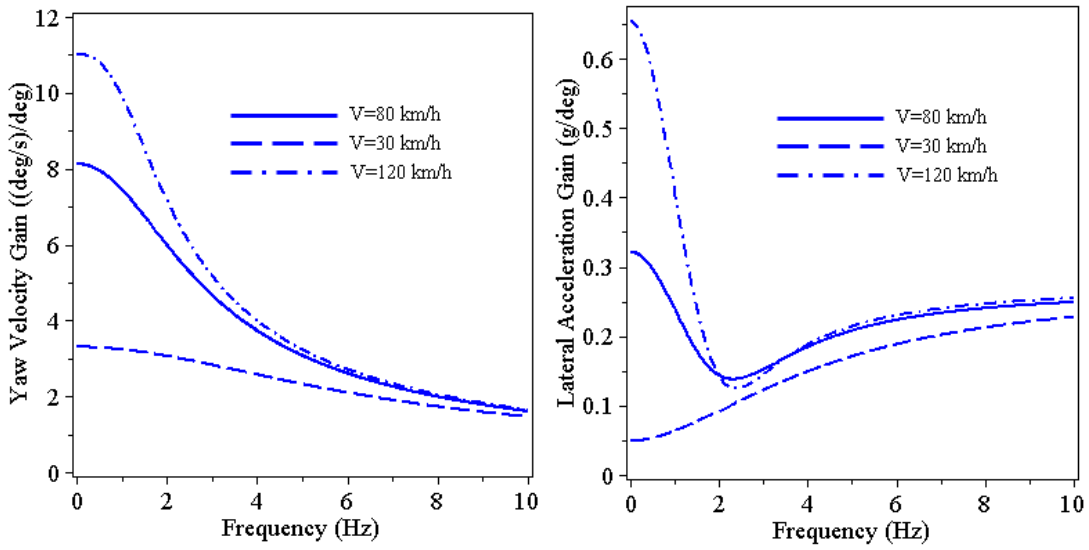

Figure 6-24: Effect of speed on frequency response of yaw velocity and lateral acceleration gains for a PSS vehicle

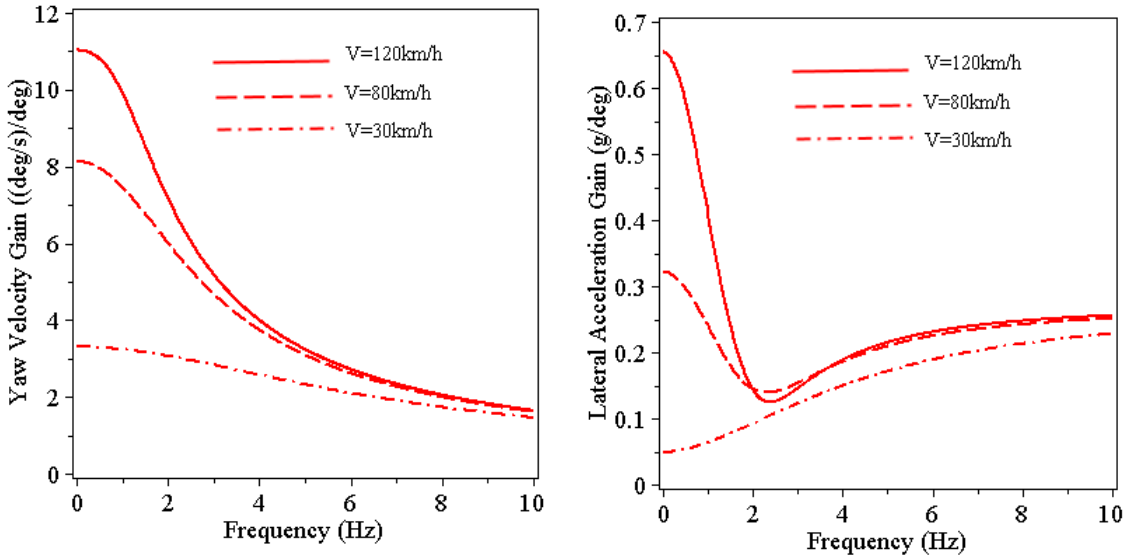

Figure 6-25: Effect of speed on frequency response of yaw velocity and lateral acceleration gains for a conventional vehicle

6.3.3 Turning on a Flat Road with Longitudinal Braking Force

In some cases, a braking force is needed to balance the external forward longitudinal force acting on a vehicle to maintain a steady state. In such cases, the suspension systems generate longitudinal deflections. The wheelbase and vehicle weight distribution at the front and rear wheels changes. As a result, the longitudinal and lateral friction forces also have to change.

In this study, the total longitudinal braking force needed to maintain a constant speed is assumed to be 300 N, with such a distribution ratio that the applied braking torque is proportional to the static wheel load. By knowing the suspension force which is equal to the braking force in the steady state, the front and rear longitudinal deflections of a PSS suspension are calculated by solving equation (5-17) for Δx with knowledge of the spring force F.

To obtain the required longitudinal braking force to balance the external force, the longitudinal slips, s_{fo}, at the front tire and, s_{ro}, at the rear wheel, are generated in the contact patch when the braking torque are applied. These longitudinal slips can be calculated from the tire model when the friction forces are known. Note the tire forward velocity is known. Having these two parameters, the angular velocity of the front (rear) wheel, $\dot{\theta}_{f(r)o}$, can be determined by the following equation:

$$\dot{\theta}_{f(r)o} = \frac{-V_x}{R_{ef(r)}(1 - s_{f(r)o})} \tag{6-17}$$

The point (s_o, α_o), where the linearization of the friction model is performed as in equation (6-15) for the front (rear) tire, is ($s_{f(r)o}$, 0) in this case.

After the vehicle model system is linearized at point ($\boldsymbol{X_o}$, $\boldsymbol{U_o}$). The eigenvalue analysis is performed at a speed of 80 km/h. The analysis results, as listed in Table 6-2, indicate the real parts of all the eigenvalues except the last one are negative. The real part of the last eigenvalue can be regarded as zero. This means the system is BIBO stable. The nonnegative eigenvalue may relate to the vehicle forward motion (V_x). It can be understood that, physically, the vehicle forward velocity cannot return its original value when it undergoes a disturbance but keep constant after the disturbance disappears.

Table 6-2: Eigenvalues of the linearized system (matrix A) for a PSS vehicle with braking force

No	Eigenvalue	Frequency (Hz)	Damping Ratio
1	-782.36+0.0 i	124.52	
2	-537.13+0.0 i	85.49	
3	-45.65±75.79 i	14.08	0.516
4	-28.36±74.88 i	12.74	0.354
5	-18.96±8.69 i	3.32	0.909
6	-1.83±6.29 i	1.04	0.280
7	-2.26±6.94 i	1.16	0.31
8	-11.49±10.60 i	2.49	0.735
9	-12.35±4.02 i	2.07	0.951
10	3.96×10^{-10}+0.0 i	6.31×10^{-11}	

Figure 6-26 illustrates the yaw velocity gain and phase lag. It is obvious that the yaw velocity responses of the two types of vehicles are very close when the steering frequency is less than 3 Hz. When the frequency increases, the yaw response of the PSS vehicle becomes greater than that of the conventional vehicle, and the difference becomes more significant with increasing the frequency. The phase magnitude of the conventional vehicle increases with an increase in the frequency, whereas that of the PSS vehicle first increases, and then decreases, with an increase in the frequency.

The frequency responses of the lateral acceleration and its phase are plotted in Figure 6-27. The results reflect that the lateral acceleration response exhibits the same pattern as the yaw velocity response. When the frequency is less than 3 Hz, the lateral accelerations of the two types of vehicles are fairly close. When the steering frequency is above this value, the lateral acceleration of the PSS vehicle is larger than that of the conventional vehicle. This can be explained by the fact that the side slip angle of the front tire in a PSS vehicle is influenced by the rate of steering angle, as indicated in equation (5.20-1). At high steering frequency, the side slip angles of front tire in a PSS vehicle are large, and result in large larger lateral friction forces. However, neither the side slip angles of the front tire nor the lateral friction force in a conventional vehicle are influenced by the steering frequency.

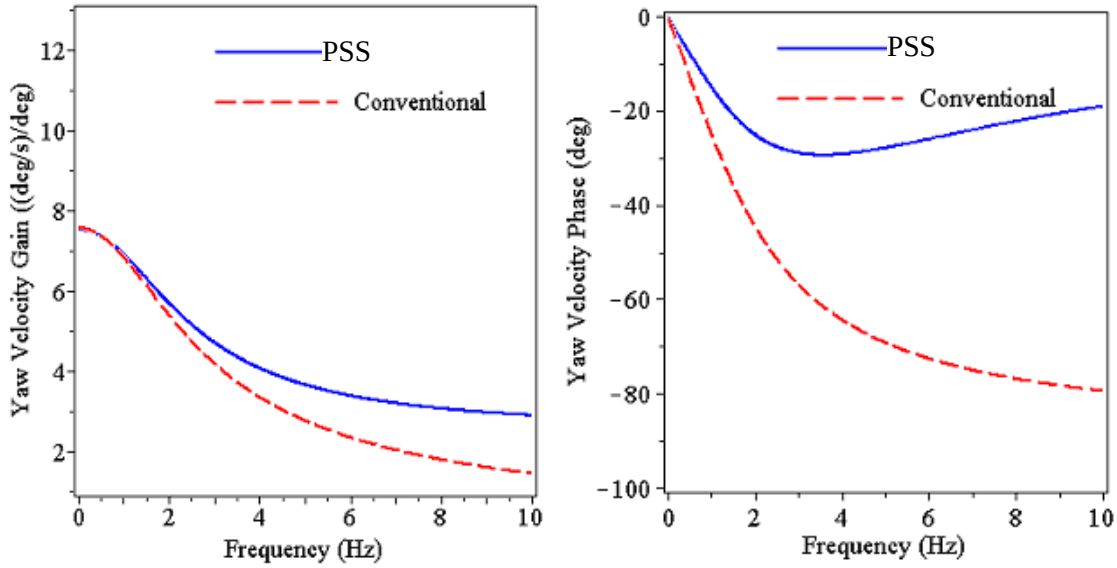

Figure 6-26: Frequency response of yaw velocity gain and phase lag

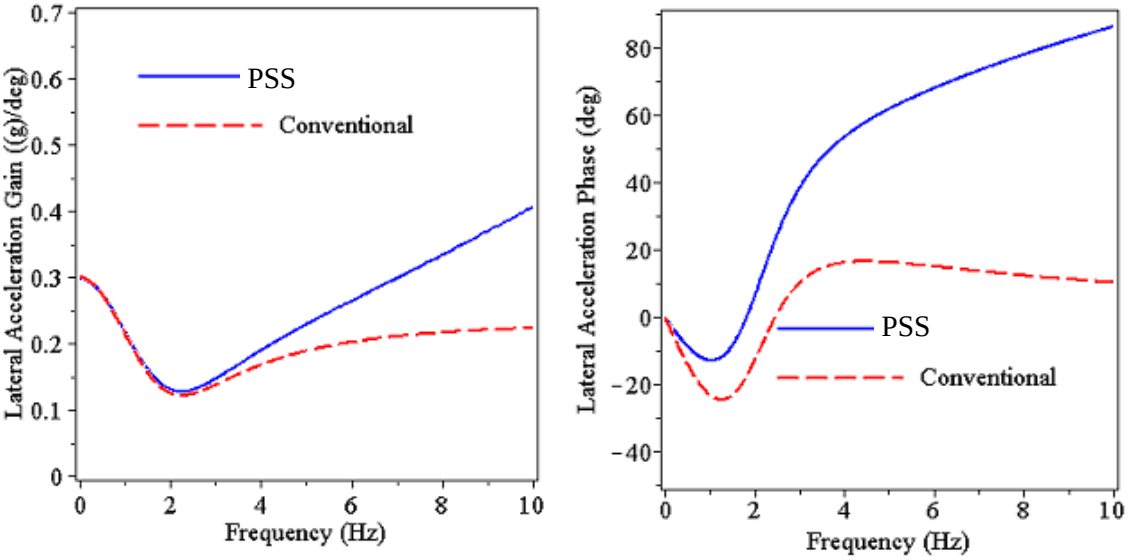

Figure 6-27: Frequency response of lateral acceleration gain and phase lag

It should be note that the lateral friction force will reach a maximum at a critical value of the side slip angle and cannot increase by further increasing the side slip angle. At the high frequency, where the side slip angle of the front tire in a PSS vehicle is large, the linearization of friction force represented by equation (6-16) cannot describe the relationship between the lateral force and slide slip

angle. Consequently, the response gains of the PSS vehicle illustrate in Figure 6-26 and 6-27 have low accuracy at high frequency.

6.4 Summary

In this chapter, the handling behaviour of a PSS vehicle was investigated in the time and frequency domains using the model system developed in Chapter 5.

In the time domain study, the dynamic handling response of a PSS vehicle was predicted and analyzed under different turning conditions, and compared with those of a conventional vehicle. The simulation results demonstrate that the planar suspension system can effectively absorb the longitudinal shock when a vehicle turns on a bumpy road, but does not induce any disadvantages regarding the handing performance. On the contrary, in some cases such as a turning combined with a braking operation where the stability is a major concern, the PSS vehicle exhibits more understeer behaviour, which means that the vehicle is more directionally stable. This is the unique property of the PSS regarding the effect on the handling characteristics. The result also indicated that the PSS can sufficiently absorb the longitudinal impact and reduce the longitudinal force, and therefore can protect the vehicle components from damage.

The frequency domain study was carried out by linearizing the dynamic system to investigate the system stability and frequency response. An eigenvalue analysis indicates that the vehicle is completely directionally stable. The investigation of the frequency response shows that the handling behaviour of the PSS vehicle is almost the same as that of the conventional vehicle when there is no longitudinal force in the suspension system. When the longitudinal braking forces exist, namely when the suspensions have longitudinal deflections, the two types of vehicle have similar handling responses when the steering input frequency is less than 3 Hz. At high frequency, the PSS vehicle is more sensitive to the directional excitation than the conventional vehicle, particularly in terms of the lateral acceleration. This is another effects of PSS on the handling characteristics.

Chapter 7
Total Dynamics Study

7.1 Overview

The ride quality, pitch dynamics and handling performance of a PSS vehicle have been studied in previous chapters. However, these studies were based on either a quarter-car model or a half-car model in which several simplifications are assumed. These models can only simulate a specific aspect of the dynamic behaviors of a PSS vehicle, but cannot investigate the total dynamics of the PSS vehicle. On the other hand, the overall dynamic performance is very important to evaluate the feasibility, merits and disadvantage of a new automobile suspension system. Due to the distinctive features of the planar suspension system, the total dynamic performance of a vehicle with such planar suspension systems is not clear and may differ from that of a conventional vehicle. Therefore, simulations based on a full-car vehicle model will be conducted in this chapter to thoroughly investigate the total dynamics of a PSS vehicle.

An appropriate vehicle model is the foundation to conduct a successful dynamic simulation. The simplest full-car model is a 6-DOF model which neglects the effect of wheels and suspension systems [52]. An 8-DOF model, which has four DOFs for the body velocities (longitudinal, lateral, roll and yaw) and one DOF at each wheel representing the wheel spin dynamics [54, 55], ignores the effect of suspension and wheel mass. The most upper order full-car model reported in literatures is the 14-DOF model which can predict the vehicle pitch and heave motions [57, 58], but cannot model the relative longitudinal motions between the body and wheels. While a few multibody dynamic (MBD) commercial software packages have been reported to simulate the compliance [102], it is difficult to find an analytical full-car model in the reported literatures which takes into account the effect of the suspension longitudinal compliance. For the aforementioned motivations, an 18-DOF full-car vehicle model is developed in this chapter. This model, in cooperation with a dynamic 2D tire-ground friction model which couples the longitudinal and lateral tire-ground friction together, can simulate the effects of the suspension longitudinal elasticity on the vehicle dynamic performance. In order to exhibit the implementation of the PSS in an automobile, and to validate the proposed mathematic full-car model, an Adams/car virtual model is developed.

In this chapter, the proposed mathematical full-car model, together with the Adams/car model, are employed to study the overall dynamics of the PSS vehicle. The coupling between the vehicle

motions along different axes is investigated in various conditions. The total dynamics of the PSS vehicle are first studied using the Adams/car model. After that, the dynamic behaviors of the PSS vehicle are investigated and analyzed in two special scenarios: (i) under differential braking condition; and (ii) negotiating asymmetric road excitations. In this study, the performances of a similar conventional vehicle under the same conditions are also investigated for the purpose of comparison.

7.2 Development of an 18-DOF Analytical Full-Car Model

In order to include the relative motion between wheels and the vehicle body in a PSS vehicle, an 18-DOF full-car vehicle analytical model is proposed in this study. In this model, one DOF is added to each wheel compared to the commonly-used 14-DOF full-car vehicle model reported in literatures.

It is known that, in a double wishbone or multilink suspension, the tire camber angle changes are very small compared to the roll angle of the body. However, for a MacPherson suspension, the wheel inclination angle changes close to the body roll angle [58]. Therefore, it is more accurate to consider the wheels remaining normal to the body instead of the ground in the vehicle modeling. In this study, it is assumed that the wheels always remain in the pitch plane of body, and there is no relative camber angel between vehicle wheels and body. It is further assumed that the longitudinal and vertical motions of the suspension system are completely decoupled.

The scheme of the 18 DOF full-car model for a PSS vehicle is illustrated in Figure 7-1. This model consists of 6 DOFs at the vehicle chassis center of gravity (CG), and 3 DOFs at each of four wheels. The chassis is represented by a rigid body with a chassis-fixed coordinate frame, *xyz*, attached to the center of gravity (frame 1) and the *x* axis is aligned in the longitudinal symmetric axis of the vehicle. *u*, *v* and *w* designate the forward, lateral and vertical velocities, respectively, of the chassis. ω_x, ω_y and ω_z represent the chassis roll, pitch and the yaw angular velocities, respectively. The attitude and position of the chassis-fixed frame, *xyz*, with respect to the global coordinate frame, *XYZ*, can be determined by successive coordinate transformations through the Euler angles as shown in Figure 7-1. Namely, the frame *xyz* is obtained by rotating the global frame *XYZ* first through yaw angle ψ about *Z* axis, second through the pitch angle φ about y' axis and then through the roll angle θ about *x* axis. Each wheel is represented by an unsprung mass with 3 DOFs, including the vertical and longitudinal relative motions (z_u and x_u) between chassis and wheels, and wheel spin (Ω_u). A wheel-fixed coordinate frame, $x'y'z'$ (frame 2), is attached to the center of wheel-ground contact patch. The

frame 2 is obtained by rotating the global frame through the yaw angle ψ about Z axis. In other words, the coordinate frame 1 is obtained by rotating the coordinate frame 2 first through the pitch angle φ about y' axis, and then through the roll angle θ about x axis. The relation between the coordinate frames is illustrated in Figure 7-1.

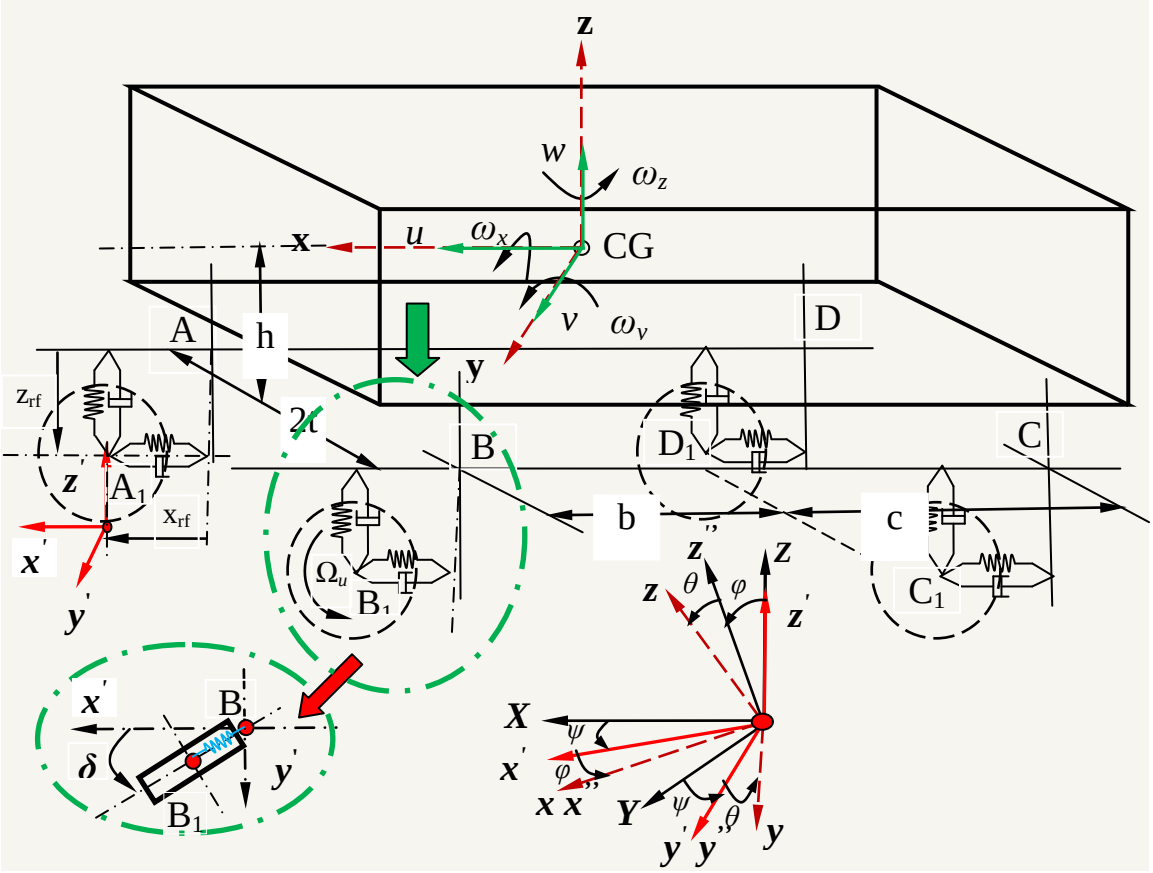

Figure 7-1: Schematic of 18-DOF full-car model for a vehicle with planar suspension and coordinate frames

By the assumption, the vertical suspension deflection of the PSS vehicle is always along the vertical direction or axis z of frame 1, and the longitudinal suspension deflection of the front suspensions are always within the wheel plane and can rotate together with the front wheel in a steering.

As mentioned previously, longitudinal elasticity always exists in the conventional suspension system due to implementation of rubber bushings. These bushings can transfer longitudinal motions and forces, and thus can be treated as a longitudinal spring element with very large stiffness. The distinguishing property of a conventional vehicle from a PSS one is in that the longitudinal deflection

of the front suspension remains in the vehicle pitch plane, i.e. *xz* plane of the coordinate frame 1, and it do not rotate with the front wheels in a steering operation, as depicted in Figure 7-2.

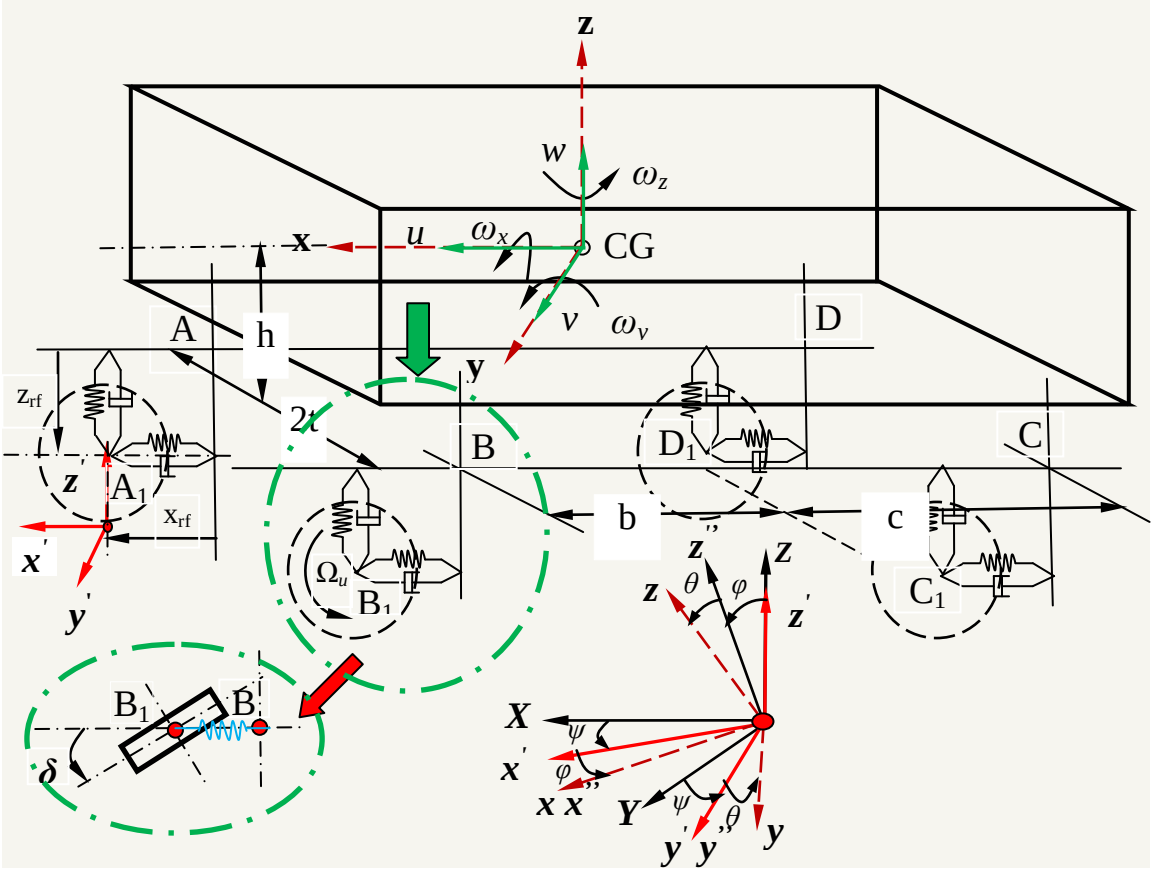

Figure 7-2: Schematic diagram of an 18-DOF full-car model for a conventional vehicle and coordinate frames (it is worthy to note the difference from Figure 7-1)

The center of front right wheel A_1, is connected to the chassis at the point A through the planar suspension system. Obviously these two points coincide when the suspension has no deflections. The distance of the center of gravity, *CG*, to the plane *ABCD* is *h*. The model is a multi-body system consisting of five rigid bodies. In order to establish the equations of the motion, the kinematic and kinetic analyses need to be carried out.

Kinematical Analysis

The respective translational and rotational velocities, **V** and **ω**, of the chassis gravity center, CG, in the frame 1 would take the following forms:

$$\mathbf{V} = \begin{Bmatrix} u \\ v \\ w \end{Bmatrix} \text{ and } \boldsymbol{\omega} = \begin{Bmatrix} \omega_x \\ \omega_y \\ \omega_z \end{Bmatrix} \tag{7.1}$$

The translational acceleration, **a**, of the chassis gravity center, CG, in frame 1 can be determined by

$$\mathbf{a} = \dot{\boldsymbol{V}} = \begin{Bmatrix} \dot{u} \\ \dot{v} \\ \dot{w} \end{Bmatrix} + \boldsymbol{\omega} \times \mathbf{V} = \begin{Bmatrix} \dot{u} + \omega_y w - \omega_z v \\ \dot{v} + \omega_z u - \omega_x w \\ \dot{w} + \omega_x v - \omega_y u \end{Bmatrix} \tag{7.2}$$

The velocity and acceleration at the four points (A, B, C and D) where the four wheels connect to the chassis in frame 1 can be derived by the following equation:

$$\mathbf{V_{ij}} = \mathbf{V} + \boldsymbol{\omega} \times \mathbf{r_{ij}}$$

$$\boldsymbol{a_{ij}} = \boldsymbol{a} + \dot{\boldsymbol{\omega}} \times \mathbf{r_{ij}} + \boldsymbol{\omega} \times \left(\boldsymbol{\omega} \times \mathbf{r_{ij}}\right) \tag{7.3}$$

where $i = \text{r(right) or l(left)}, j = \text{f(front) or r(rear)}$.

$$\mathbf{r_{rf}} = \begin{Bmatrix} b \\ -t \\ -h \end{Bmatrix}, \mathbf{r_{lf}} = \begin{Bmatrix} b \\ t \\ -h \end{Bmatrix}, \mathbf{r_{rr}} = \begin{Bmatrix} -c \\ -t \\ -h \end{Bmatrix}, \mathbf{r_{rl}} = \begin{Bmatrix} -c \\ t \\ -h \end{Bmatrix}$$

where *t* is half of the wheel track. *b* and *c* are the longitudinal distances from the chassis gravity center, *CG*, to the front and rear wheel connect points *A* (*D*) and *B*(*C*), respectively.

The velocity and acceleration of each wheel (unsprung mass), $\mathbf{V_{uij}}$ and $\mathbf{a_{uij}}$, in frame 1 can be obtained by the following equations:

$$\mathbf{V_{uij}} = \mathbf{V_{ij}} + \mathbf{V'_{uij}} + \boldsymbol{\omega} \times \mathbf{r_{uij}} \tag{7.4}$$

$$\boldsymbol{a_{ij}} = \boldsymbol{a_{ij}} + \mathbf{a'_{uij}} + \dot{\boldsymbol{\omega}} \times \mathbf{r_{gij}} + \boldsymbol{\omega} \times \left(\boldsymbol{\omega} \times \mathbf{r_{uij}}\right) + \mathbf{2}\boldsymbol{\omega} \times \mathbf{V'_{uij}} \tag{7.5}$$

where $\boldsymbol{\omega}$ is the angular velocity of frame 1 and $\mathbf{r_{uij}}$ is the position vector in frame 1 of the *ij* unsprung mass center with respect to the point (one of A, B, C, and D) on the chassis where the corresponding unsprung mass connect to the chassis. For a PSS vehicle, this position vector is expressed as

$$\boldsymbol{r_{uif}} = \begin{Bmatrix} x_{if} cos\delta_f \\ x_{if} sin\delta_f \\ -z_{if} \end{Bmatrix} \text{ and } \boldsymbol{r_{uir}} = \begin{Bmatrix} x_{ir} \\ 0 \\ -z_{ir} \end{Bmatrix} \tag{7.6}$$

where x_{ij} and z_{ij} are longitudinal and vertical suspension deflections, respectively, of the planar suspension measured in coordinate frame 1. The sign convention is that the extension of spring is positive. δ_f is the tire rotation about the vertical axis (z) of frame 1. It can be evaluated by the following equations:

$$\delta_f = \delta cos\varphi cos\theta \tag{7.7}$$

where δ is the front wheel steering angle about the vertical axis of frame 2 or global frame (Z axis). In fact, the above equation indicates that δ_f can be regarded equal to δ for small angular motion assumption.

For a conventional vehicle, the position vector in frame 1 of the *ij* unsprung mass center with respect to the point on the chassis where the unsprung mass connect to the chassis, $\mathbf{r_{uij}}$, takes the following form:

$$\mathbf{r_{uij}} = \begin{Bmatrix} x_{ij} \\ 0 \\ -z_{ij} \end{Bmatrix} \tag{7.8}$$

where $\boldsymbol{x_{ij}}$ and $\boldsymbol{z_{ij}}$ are longitudinal and vertical deflections, respectively, of the suspension measured in coordinate frame 1.

$\mathbf{V'_{uij}}$ and $\mathbf{a'_{uij}}$ are the relative velocity and acceleration in frame 1 between the unsprung mass center and the corresponding attaching point on the chassis. For the PSS vehicle as shown in Figure 7-3, the relative velocity and acceleration in frame 1 for front wheels are

$$\mathbf{V'_{uif}} = \begin{Bmatrix} \dot{x}_{if} cos\delta_f - x_{ij}\dot{\delta}_f sin\delta_f \\ \dot{x}_{if} sin\delta_f + x_{ij}\dot{\delta}_f cos\delta_f \\ -\dot{z}_{if} \end{Bmatrix} \text{ and } \mathbf{a'_{uif}} = \begin{Bmatrix} (\ddot{x}_{if} - x_{if}\dot{\delta}_f^2) cos\delta_f - x_{if}\ddot{\delta}_f sin\delta_f \\ x_{if}\ddot{\delta}_f cos\delta_f + (\ddot{x}_{if} - x_{if}\dot{\delta}_f^2) sin\delta_f \\ -\ddot{z}_{if} \end{Bmatrix} \tag{7.9}$$

The relative velocity and acceleration in frame 1 for rear wheels in the PSS vehicle are as:

$$\mathbf{V'_{uir}} = \begin{Bmatrix} \dot{x}_{ir} \\ 0 \\ -\dot{z}_{ir} \end{Bmatrix} \text{ and } \mathbf{a'_{uir}} = \begin{Bmatrix} \ddot{x}_{ir} \\ 0 \\ -\ddot{z}_{ir} \end{Bmatrix} \tag{7.10}$$

For a conventional vehicle, the relative velocity and acceleration in frame 1 between the unsprung mass center and the corresponding attaching point on the chassis, $\mathbf{V'_{uij}}$ and $\mathbf{a'_{uij}}$, are described by

$$\mathbf{V}_{\mathbf{uij}}^{'} = \begin{Bmatrix} \dot{x}_{ij} \\ 0 \\ -\dot{z}_{ij} \end{Bmatrix} \text{ and } \mathbf{a}_{\mathbf{uij}}^{'} = \begin{Bmatrix} \ddot{x}_{ij} \\ 0 \\ -\ddot{z}_{ij} \end{Bmatrix} \tag{7.11}$$

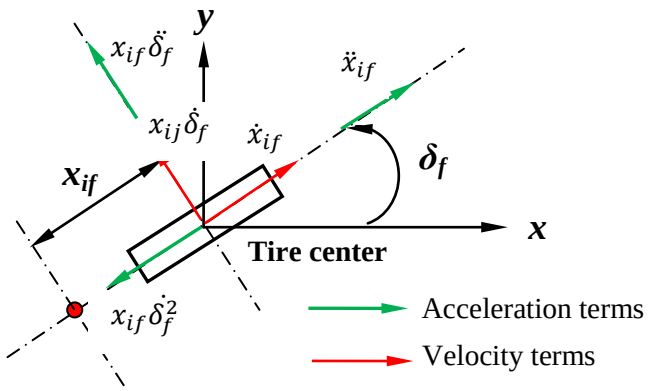

Figure 7-3: Relative velocity and acceleration components of the front wheels of a PSS vehicle in the coordinate frame 1 (xyz)

Through the above formulation, it can be seen that the derivation of the velocity and acceleration of the wheels is very complex and tedious. In this study, the Maple symbolic computation tool is employed for the formulation of these terms.

Kinetic Analysis

By neglecting the aerodynamic forces applied to the vehicle body, the external forces applied to the vehicle are generally from the tire-ground contact patch, and are transmitted to the body through the suspension systems. The forces applied to the wheels, taking the right side as example, are illustrated in Figure 7-4. F_{sxrf} and F_{szrf} are the longitudinal and vertical suspension forces that measured in frame 1. The vertical suspension is assumed to be linear and the suspension forces are determined by the following equation:

$$F_{szrf} = -k_{zrf} z_{rf} - c_{zrf} \dot{z}_{rf} \tag{7.12}$$

Considering the nonlinear spring characteristic of the PSS, discussed in previous chapters, the suspension longitudinal force of the PSS in frame 1, F_{sxrf}, can be determined by the following equations:

$$F_{sxrf} = \frac{k_o}{d_r^2} x_{rf}^3 + k_o x_{rf} + c_{xrf} \dot{x}_{rf} \tag{7.13-1}$$

where d_r is a parameter to control the upper bound of the spring deflection, which is considered as 5 cm in this study. k_o is the nominal stiffness parameter of a planar suspension system, which is equal to the corresponding vertical spring stiffness.

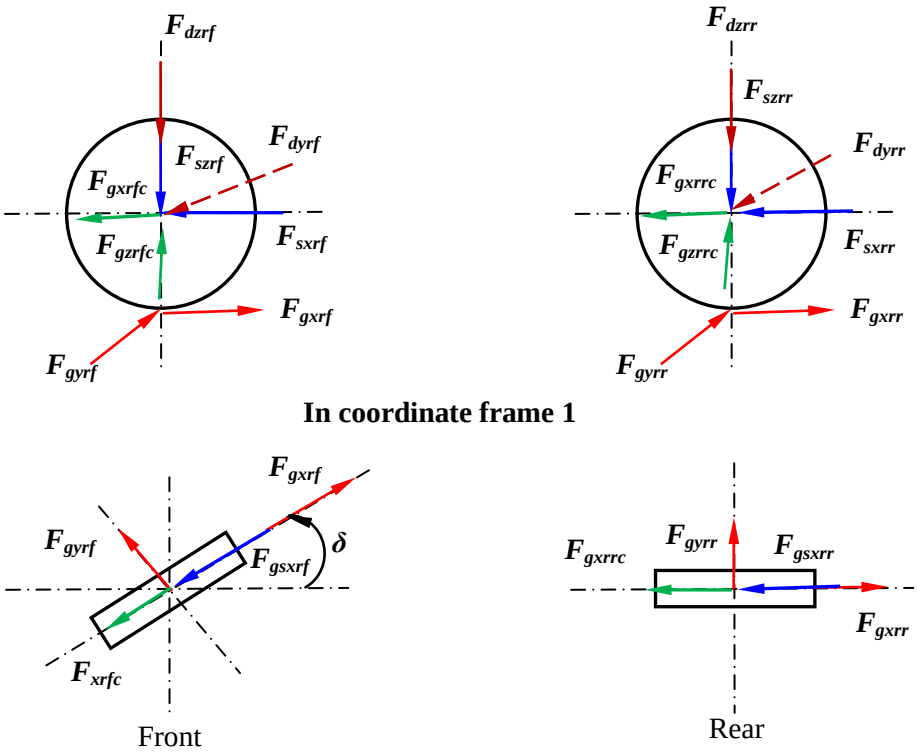

Figure 7-4: Forces applied to the unsprung masses in coordinate frames 1 and 2

The longitudinal force of the conventional suspension can be calculated by

$$F_{sxrf} = k_{xlf} x_{rf} + c_{xrf} \dot{x}_{rf} \tag{7.13-2}$$

Assume F_{gxrf} and F_{gyrf} are the longitudinal and lateral friction forces applied to the right front tire. They are generated in the contact patch and can be evaluated from the dynamic tire friction model discussed in Chapter 5. F_{gxrfc} and F_{gzrfc} are the longitudinal and vertical components of contact force applied to the right front tire, and can be predicted by the radial spring contact model presented in Chapter 3. These forces are developed in contact patch and measured in coordinate frame 2, x'y'z'. For convenience, all the force terms are transformed to frame 1 as follows:

$$\begin{Bmatrix} F_{xrf} \\ F_{yrf} \\ F_{zrf} \end{Bmatrix} = \boldsymbol{R} \begin{Bmatrix} F_{gxrf}cos\delta - F_{gyrf}sin\delta \\ F_{gyrf}cos\delta + F_{gxrf}sin\delta \\ 0 \end{Bmatrix} \text{ and } \begin{Bmatrix} F_{xrfc} \\ F_{yrfc} \\ F_{zrfc} \end{Bmatrix} = \boldsymbol{R} \begin{Bmatrix} F_{gxrfc}cos\delta \\ F_{gxrfc}sin\delta \\ F_{gzrfc} \end{Bmatrix} \tag{7.14}$$

where $\boldsymbol{R}$ is the transformation matrix from frame 2 to frame 1 and take the following form:

$$\boldsymbol{R} = \begin{bmatrix} 1 & 0 & 0 \\ 0 & \cos\theta & sin\theta \\ 0 & -sin\theta & \cos\theta \end{bmatrix} \begin{bmatrix} cos\varphi & 0 & -sin\varphi \\ 0 & 1 & 0 \\ sin\varphi & 0 & cos\varphi \end{bmatrix} \tag{7.15}$$

For the rear wheel, take the right side as example, the force terms transformed to the frame 1 can be written as follows:

$$\begin{Bmatrix} F_{xrr} \\ F_{yrr} \\ F_{zrr} \end{Bmatrix} = R \begin{Bmatrix} F_{gxrr} \\ F_{gyrr} \\ 0 \end{Bmatrix} \text{ and } \begin{Bmatrix} F_{xrrc} \\ F_{yrrc} \\ F_{zrrc} \end{Bmatrix} = R \begin{Bmatrix} F_{gxrrc} \\ 0 \\ F_{gzrfc} \end{Bmatrix} \tag{7.16}$$

The vertical and longitudinal forces are transmitted to the sprung mass through the suspension struts. The acting points of these two forces on the vehicle body can be easily determined. However, the lateral force transmitted to the unsprung mass is through the suspension links, and the acting point on the vehicle body is not easily to be determined. In the roll dynamic study, an imaginary point of roll center, is always introduced. Figure 7-5 shows the forces in the roll plane of, for example, the front suspension. This point is regarded as a pivot around which body roll occurs and the lateral forces are transferred from the axle to the sprung mass. In the formulation of the vehicle model, the front and rear roll centers are assumed to be fixed at the distances, h_{rcf} and h_{rcr}, respectively, below the sprung mass center CG along the negative z-axis of the chassis-fixed coordinate frame 1, as shown in Figure 7-5. $m_{uf}a_{urfy}$ is the lateral inertial force of the right front wheel and evaluated as follows:

$$m_{uf}a_{urfy} = F_{yrf} + F_{yrfc} - F_{dyrf} - m_{uf}gcos\varphi\sin\theta \tag{7.17}$$

where F_{dyrf} is the lateral force transmitted to the sprung mass in frame 1.

If the roll center is assumed to be in the ground plane, i.e. if the vehicle is a rigid instead of flexibly suspended one, the roll moment about the roll center along the longitudinal axis of frame 1 at, for example, the right front corner, is given as

$$\begin{aligned} M_{xrfo} = F_{yrf}\left(R_{erf} + z_{rf} + h\right) + \left(F_{yrfc} - m_{uf}gcos\varphi sin\theta\right)\left(z_{rf} + h\right) \\ - m_{uf}a_{gurfy}\left(z_{rf} + h\right) = F_{yrf}R_{erf} + F_{dyrf}\left(z_{rf} + h\right) \end{aligned} \tag{7.18}$$

and the load transfer through the suspension links due to the lateral, F_{dzrf}, equals to zero. When a roll center is taken into consideration as shown in Figure 7-5, the roll moment transferred to the sprung mass by the right front suspension is

$$M_{xrf} = F_{dyrf} h_{rcf} \tag{7.19}$$

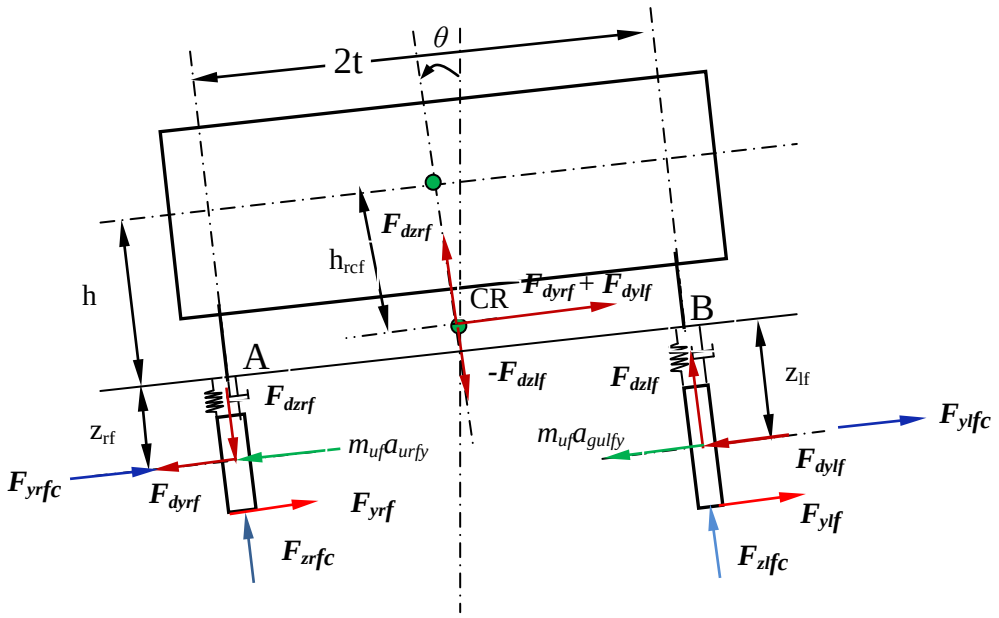

Figure 7-5: Forces in the front suspension roll plane

Comparison of equations (7.18) and (7.19) concludes that the inclusion of a roll center reduces the total moment transferred to the sprung mass. The moment deference can be regarded responsible for the vertical load transfer forces through the linkages, F_{dzrf} and F_{dzlf} [58, 80]. These forces can be estimated as

$$F_{dzrf} = \frac{M_{xrf} - M_{xrfo}}{t} = \frac{F_{yrf} R_{erf} + F_{dyrf}(z_{rf} + h) - F_{dyrf} h_{rcf}}{t} \tag{7.20-1}$$

$$F_{dzlf} = -\frac{M_{xlf} - M_{xlfo}}{t} = -\frac{F_{ylf} R_{elf} + F_{dylf}(z_{lf} + h) - F_{dylf} h_{rcf}}{t} \tag{7.20-2}$$

For the rear wheels, theses forces are

$$F_{dzrr} = \frac{M_{xrr} - M_{xrro}}{t} = \frac{F_{yrr} R_{err} + F_{dyrr}(z_{rr} + h) - F_{dyrr} h_{rcr}}{t} \tag{7.20-3}$$

$$F_{dzlf} = -\frac{M_{xlr} - M_{xlro}}{t} = -\frac{F_{ylr} R_{elr} + F_{dylr}(z_{lr} + h) - F_{dylr} h_{rcr}}{t} \tag{7.20-4}$$

The lateral slip angle, α, is needed in the calculation of the tire-ground friction forces. Since the kinematic analysis is performed in frame 1, the velocity of each wheel (unsprung mass), $\mathbf{V_{uij}}$, which is obtained in frame 1, should be transformed into frame 2 using the following equation:

$$\mathbf{V_{guij}} = \boldsymbol{R^{-1}}\mathbf{V_{uij}} \tag{7.21}$$

where $\mathbf{V_{guij}}$ is the velocity vector of wheels in frame 2. Then the lateral slip angle, α, can be calculated from Figure 7-6 as follows:

$$\alpha_{if} = tan^{-1}\frac{V_{guify}}{V_{guifx}} - \delta \text{ and } \alpha_{ir} = tan^{-1}\frac{V_{guiry}}{V_{guirx}} \tag{7.22}$$

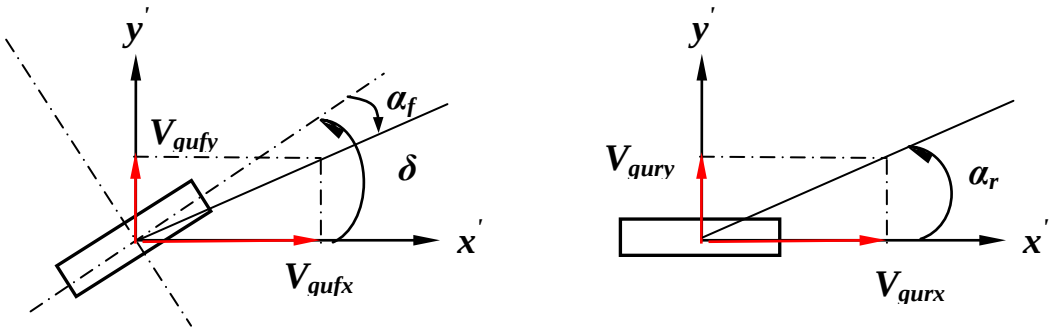

Figure 7-6: illustration of the slip and steering angle

The relative longitudinal slip velocities for the front and rear wheels are

$$v_{rif} = \Omega_{uif}R_{eif} - (V_{uifx}cos\delta + V_{uify}sin\delta) \text{ and } v_{rir} = \Omega_{uir}R_{eir} - V_{uirx} \tag{7.23}$$

Equations of Motion

Based on the kinematic and kinetic analyses, the equations of motions are established for each individual rigid body. Due to different configurations as shown in Figures 7-1 and 7-2, the equations of motions of the PSS and conventional vehicles are different.

The translational motions of vehicle body for the PSS vehicle are described by:

$$m_s(\dot{u} + \omega_y w - \omega_z v) = \sum F_{sxif}cos\delta_f + \sum F_{sxir} + m_s g sin\varphi \tag{7.24-1}$$

$$m_s(\dot{v} + \omega_z u - \omega_x w) = \sum F_{sxif}sin\delta_f + \sum F_{dyij} - m_s g cos\varphi sin\theta \tag{7.24-2}$$

$$m_s(\dot{w} + \omega_x v - \omega_y u) = \sum F_{szij} + \sum F_{dzij} - m_s g cos\varphi cos\theta \tag{7.24-3}$$

For the vehicle body rotational motions of the PSS vehicle, the dynamic equation is

$$\sum \mathbf{M} = \dot{\mathbf{H}} = \frac{\delta \mathbf{H}}{\delta t}^{\cdot} + \boldsymbol{\omega} \times \mathbf{H} \tag{7.25}$$

where **H** is the angular momentum and **ω** is the angular velocity of vehicle body in the frame 1. By the symmetry assumption of the vehicle about the longitudinal axis, *x*, the above equation becomes

$$\begin{Bmatrix} M_x \\ M_y \\ M_z \end{Bmatrix} = \begin{bmatrix} I_{xx} & 0 & I_{xz} \\ 0 & I_{yy} & 0 \\ I_{xz} & 0 & I_{zz} \end{bmatrix} \begin{Bmatrix} \dot{\omega}_x \\ \dot{\omega}_y \\ \dot{\omega}_z \end{Bmatrix} + \begin{Bmatrix} \omega_x \\ \omega_y \\ \omega_z \end{Bmatrix} \times \left(\begin{bmatrix} I_{xx} & 0 & I_{xz} \\ 0 & I_{yy} & 0 \\ I_{xz} & 0 & I_{zz} \end{bmatrix} \begin{Bmatrix} \omega_x \\ \omega_y \\ \omega_z \end{Bmatrix} \right)$$

Or

$$I_{xx}\dot{\omega}_x + (I_{zz} - I_{yy})\omega_y\omega_z - I_{xz}(\omega_x\omega_y + \dot{\omega}_z) = \sum F_{dyij}h_{rcj} + \sum F_{sxif}sin\delta_f(h + z_{if}) + t(\sum F_{szlj} - \sum F_{szrj}) \tag{7.25-1}$$

$$I_{yy}\dot{\omega}_y + (I_{xx} - I_{zz})\omega_x\omega_z + I_{xz}(\omega_x^2 - \omega_z^2) = -\sum(F_{szif} + F_{dzif})(b + x_{if}cos\delta_f) + \sum(F_{szir} + Fdzirc - xir - Fsxifcos\delta fh + zif - Fsxir(h + zir) \tag{7.25-2}$$

$$I_{zz}\dot{\omega}_z + (I_{yy} - I_{xx})\omega_x\omega_y + I_{xz}(\omega_y\omega_z - \dot{\omega}_x) = \sum(F_{sxif}sin\delta_f + F_{dyif})(b + x_{if}cos\delta_f) - \sum F_{dyir}(c - x_{ir}) + (F_{sxrf}cos\delta_f + F_{sxrr} - F_{sxlf}cos\delta_f - F_{sxlr})t \tag{7.25-3}$$

The equations of motion for the wheels in the PSS vehicle are described by the following equations:

Front Wheels:

$$m_{uf}a_{uifx} = F_{xif} + F_{xifc} - F_{sxif}cos\delta_f + m_{uf}gsin\varphi \tag{7.26-1}$$

$$m_{uf}a_{uifz} = \mathrm{F_{zifc}} - \mathrm{F_{szif}} - \mathrm{F_{dzif}} - \mathrm{m_{uf}gcos\varphi cos\theta} \tag{7.26-2}$$

$$\mathrm{I_{uf}}\dot{\Omega}_{uif} = \mathrm{T_{if}} - \mathrm{R_{eif}F_{gxif}} \tag{7.26-3}$$

Rear Wheels:

$$m_{ur}a_{uirx} = F_{xir} + F_{xirc} - F_{sxir} + m_{ur}gsin\varphi \tag{7.27-1}$$

$$m_{ur}a_{uirz} = F_{zij} + F_{zirc} - F_{szir} - F_{dzir} - m_{ur}gcos\varphi cos\theta \tag{7.27-2}$$

$$I_{ur}\dot{\Omega}_{uir} = T_{ir} - R_{eir}F_{gxir} \tag{7.27-3}$$

It should be noted that the longitudinal component of contact force between wheel and ground are passing through the wheel center, and does not contribute to the wheel spin torque in equations (7.26-3) and (7.27-3).

For the conventional vehicle, the longitudinal springs of the front suspensions always remain in the vehicle pitch plane and do not rotate with the wheels in a steering motion, as illustrated in Figure 7-2. The equations of motions differ from those of the PSS vehicle. The translational motions of vehicle body are described by:

$$m_s(\dot{u} + \omega_y w - \omega_z v) = \sum F_{sxij} + m_s g sin\varphi \tag{28-1}$$

$$m_s(\dot{v} + \omega_z u - \omega_x w) = \sum F_{dyij} - m_s g cos\varphi sin\theta \tag{28-2}$$

$$m_s(\dot{w} + \omega_x v - \omega_y u) = \sum F_{szij} + \sum F_{dzij} - m_s g cos\varphi cos\theta \tag{28-3}$$

Body rotational motions:

$$\mathrm{I_{xx}\dot{\omega}_x + (I_{zz} - I_{yy})\omega_y\omega_z - I_{xz}(\omega_x\omega_y + \dot{\omega}_z) = \sum F_{dyij}h_{rcj} + t(\sum F_{szlj} - \sum F_{szrj})} \tag{29-1}$$

$$\mathrm{I_{yy}\dot{\omega}_y + (I_{xx} - I_{zz})\omega_x\omega_z + I_{xz}(\omega_x^2 - \omega_z^2) = -\sum(F_{szif} + F_{dzif})(b + x_{if}) + \sum(F_{szir} + Fdzir)c - \acute{x}\acute{r} - Fsxifh + zif - Fsxir(h + \acute{z}\acute{r})} \tag{29-2}$$

$$\mathrm{I_{zz}\dot{\omega}_z + (I_{yy} - I_{xx})\omega_x\omega_y + I_{xz}(\omega_y\omega_z - \dot{\omega}_x) = \sum F_{dyif}(b + x_{if}) - \sum F_{dyir}(c - x_{ir}) + \sum(F_{sxrj} - F_{sxlj})t} \tag{29-3}$$

The equations of motion for wheels:

$$m_{uj}a_{uijx} = F_{xij} + F_{xijc} - F_{sxij} + m_{uj}gsin\varphi \tag{30-1}$$

$$m_{uf}a_{uifz} = F_{ijz} + F_{zijc} - F_{szij} - F_{dzij} - m_{uf}gcos\varphi cos\theta \tag{30-2}$$

$$I_{uj}\dot{\Omega}_{uij} = T_{ij} - R_{eij}F_{gxij} \tag{30-3}$$

The roll, pitch and the yaw angels can be obtained through an Euler angle analysis with the knowledge of the angular rates of the vehicle by the following equations

$$\dot{\theta} = \omega_x + (\omega_y sin\theta + \omega_z cos\theta)tan\varphi \tag{7.31-1}$$

$$\dot{\varphi} = \omega_y cos\theta - \omega_z sin\theta \tag{7.32-2}$$

$$\dot{\psi} = \frac{\omega_y sin\theta + \omega_z cos\theta}{cos\varphi} \tag{7.33-3}$$

7.3 Overall Dynamics Study Using Adams/car Model

In this study, the proposed PSS concept is implemented to build the virtual suspension models in Adams/car environment. In this section, several simulations are carried out based on the Adams/car models to investigate the overall performance of the PSS vehicle. The investigation includes the suspension kinematics and compliance (K&C) characteristics, the steering performance, a single lane change and an ISO or a double lane change.

7.3.1 Analysis of Kinematics and Compliance (K&C) Characteristics

Prior to the simulation of the full-car models, a suspension analysis in the Adams/car environment is conducted to explore the kinematics and compliance (K&C) characteristics of the PSS distinguishing from those of a conventional vehicle. This analysis can help the understanding of other simulation results presented in this chapter. The main measures in terms of K&C characteristics, such as the camber, caster, toe and kingpin inclination angles; ride rate and afore-aft wheel center stiffness; scrub radius and roll center height, are investigated though suspension analysis for both the PSS and conventional suspension. The definitions of the above mentioned measures are given in the Appendix.

In this analysis, a parallel wheel travel test is first carried out for a PSS assembly and a conventional suspension assembly. The amplitude of the wheel bump and rebound is assigned to be 100 mm. Alothoug the test has been carried out for both the front and rear suspensions, only the test results for the rear is presented herein because the only difference between these two types of suspensions in the rear is that the rigid connection (trailing arm) in the conventional suspension is replaced by a spring-damper strut in the PSS. Any difference of the simulation results is induced by the longitudinal strut. The test setup in Adams/car is illustrated in Figure 7-7. The vertical spring stiffness and damping coefficient are identical between the two types of vehicle suspensions and are the same values of theose used in the analytical model as listed in Table 7-1.

The camber, caster, toe and kingpin inclination angles are illustrated in Figure 7-8. It can be seen that the magnitude of camber angle of the PSS is larger than that of the conventional suspension. The mangnitude of the caster angle of the PSS is smaller than those of the conventional suspension in the bump travel while larger in the rebound travel. The toe angle of the PSS is always larger than that of the conventional suspension in the entire bump and rebound travel. This may be due to the fact that the fore-aft motion of the wheel center in the PSS assembly is larger than that in the conventional suspension assembly due to the soft longitudinal strut.

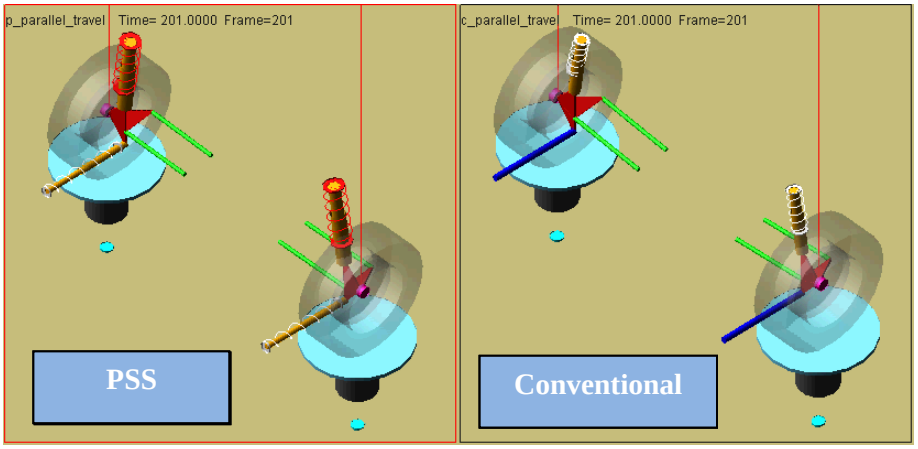

Figure 7-7: Scheme of a parallel wheel travel test in Adams/car

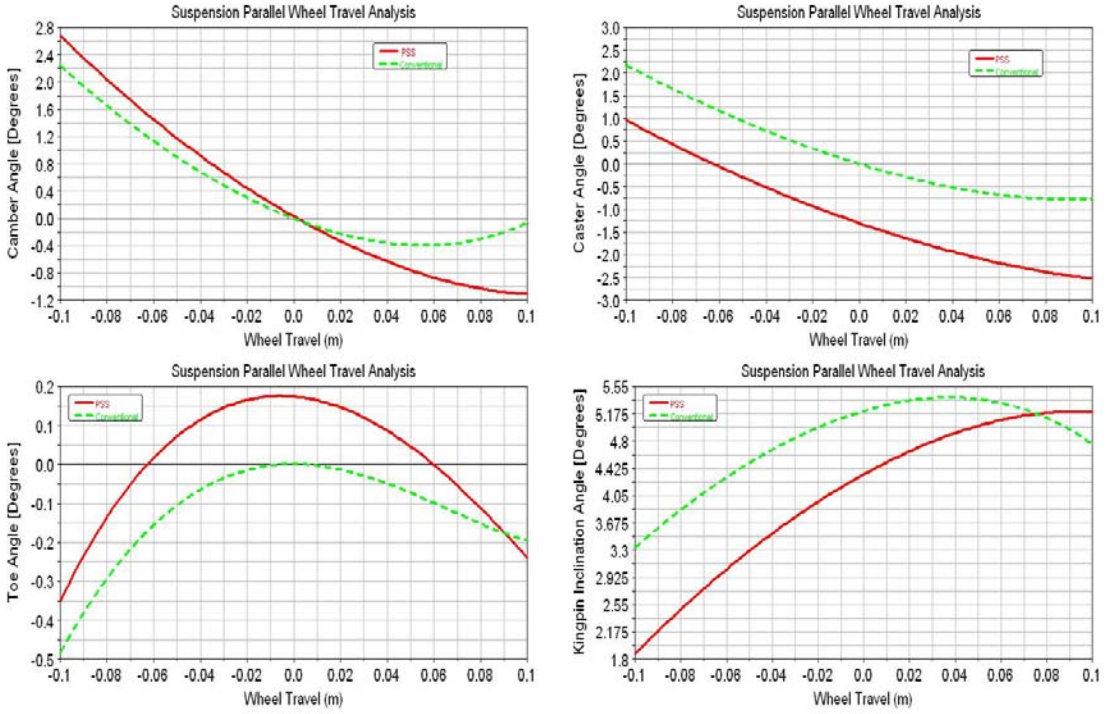

Figure 7-8: Camber, caster, toe and kingpin inclination angles in a parallel wheel travel analysis

Figure 7-9 displays the suspension ride rate and afore-aft wheel center stiffness. The simulation results indicate that the ride rate of the PSS is smaller than that of the conventional suspension. This means that the soft longitudinal strut can reduce the ride rate although the vertical struts in two types of suspensions are completely identical. This is why the vertical acceleration in the PSS vehicle

induced by the road obstacle is slightly smaller than that in a conventional vehicle, as presented in previous chapters. The afore-aft wheel center stiffness of the PSS suspension is significantly smaller than that of the conventional suspension which is mainly provided by the bushings. Therefore, the vibrations in the longitudinal direction can be efficiently isolated, as presented in previous chapters.

Figure 7-10 depcts the roll center height in the parallel wheel travel analysis. The roll center of the PSS is heigher than that of the conventional suspension. This implies that the soft longitudinal compliance may reduce the distance from the vehicle gravity center to the roll center, which means that the roll response of a PSS vehicle may be smaller than that of a conventional vehicle.

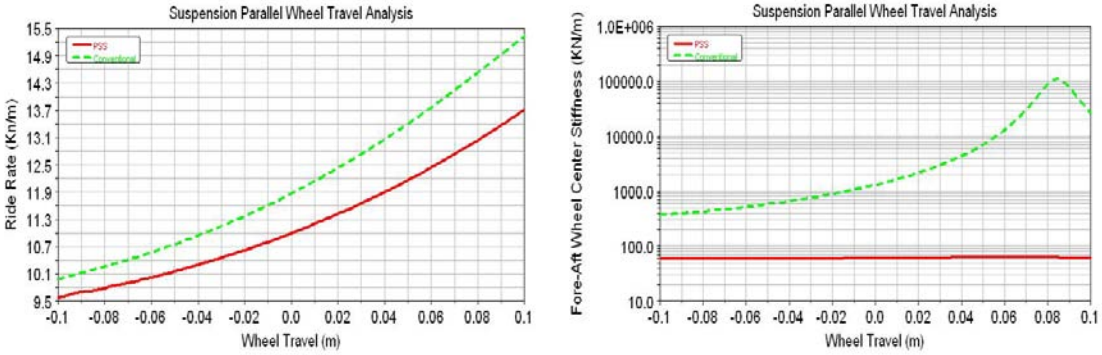

Figure 7-9: Comparison of ride rate and afore-aft wheel center stiffness

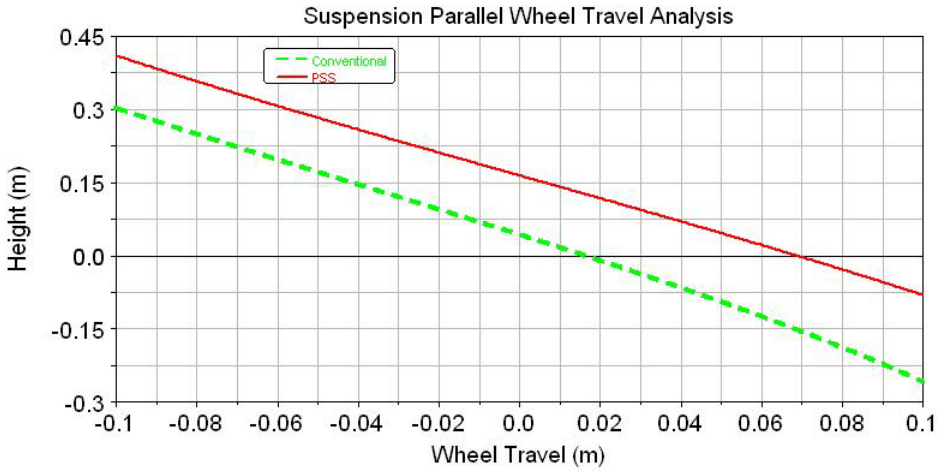

Figure 7-10: Comparison of roll center height in a parallel wheel travel analysis

Figure 7-11 illustrates scrub radius in the parallel wheel travel analysis. It can be seen that the scrub radius of the PSS in a travel analysis is larger than that of the conventional suspension. In the most range of the travel, the scrub radius of the PSS is positive. This implies that the soft longitudinal

compliance can increases the scrub radius. This means that the PSS vehicle may provide greater road feeling and feedback so that drivers can feel when the front tires start to break loose in a corner. However, the PSS may increase the steering effort, steer torque and the kickback on the bumps compared to the conventional suspensions.

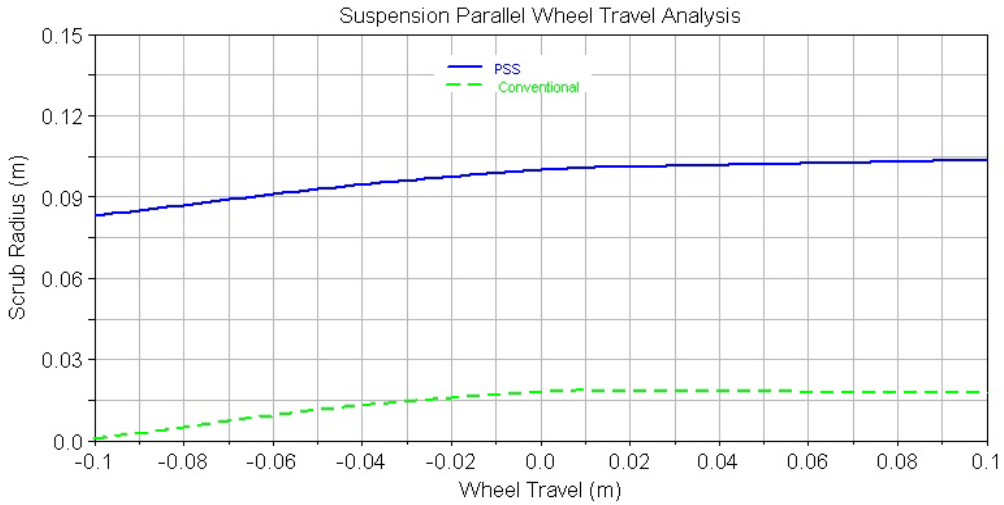

Figure 7-11: Comparison of scrub radius in a parallel wheel travel analysis

A front suspension steering analysis is also conducted. The major results are similar to those of the parallel wheel travel analysis. Two specific sets of the steering analysis measures are the steering ratio and total track. These measures are plotted in Figure 7-12 and 7-13. The results show that steering ratios and the total wheel tracks of the PSS and conventional suspension assemblies are generally very close, although the steering ratio of PSS suspension is slightly less than that of the conventional vehicle when the input at the steering wheel is in the range of -50º ~ -180º, and the total wheel track of the PSS vehicle is slightly larger than that of the conventional vehicle when the magnitude of steering angle input is above 100º. In fact, larger wheel track of the front PSS at large steering angle may be beneficial to the roll stability in a sharp turning because the larger wheel track results in smaller roll response. In generally, the results indicate the new configuration and longitudinal strut in the front PSS have little influence on the steering ratio and the wheel track.

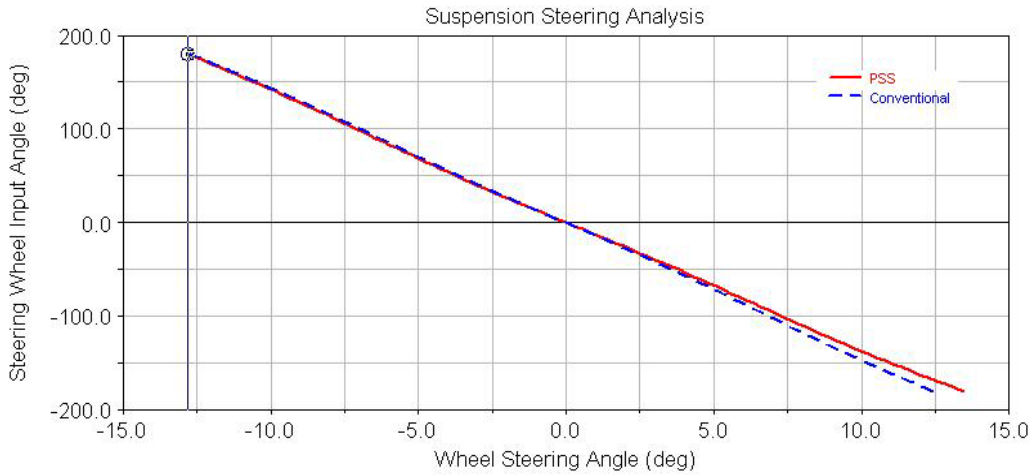

Figure 7-12: Relationship of the steering wheel input angle and wheel steering angle in a suspension steering analysis

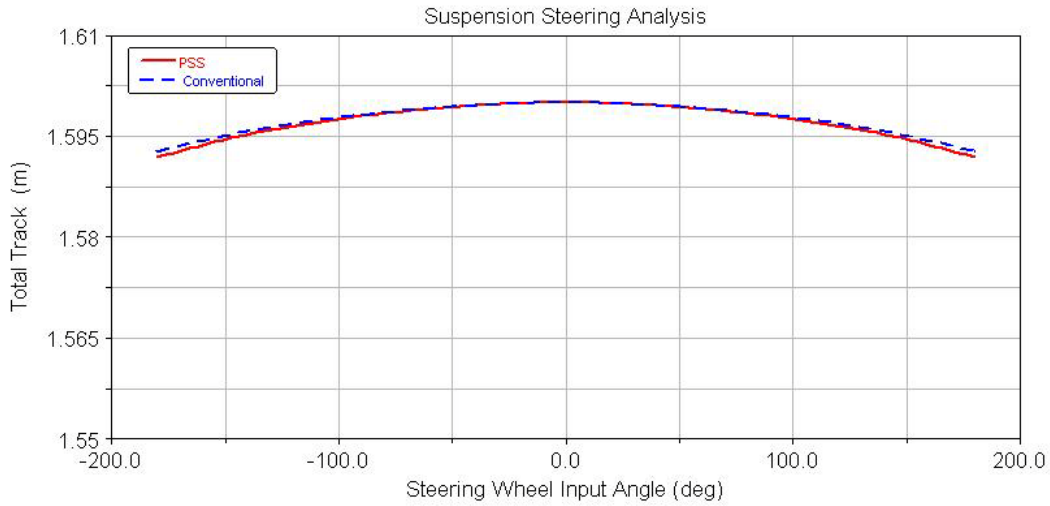

Figure 7-13: Comparison of total wheel-track in a suspension steering analysis

7.3.2 Investigation of Turning Performance

In this study, the dynamic responses of a PSS vehicle to a step steering input at 50 km/h are predicted and compared with those of a conventional vehicle. The step input at steering wheel is 75º (approximately equal to 5º steering angle at front tires) and step duration is 1 second.

Figure 7-14 displays the time history of lateral acceleration response in the step turning manoeuvre. It can be seen that the transient and steady-state responses of the lateral acceleration are generally comparable between the PSS and conventional vehicles. The response of the conventional

vehicle exhibits an approximate 0.05 g overshoot while the response overshoot of the PSS vehicle is very small.

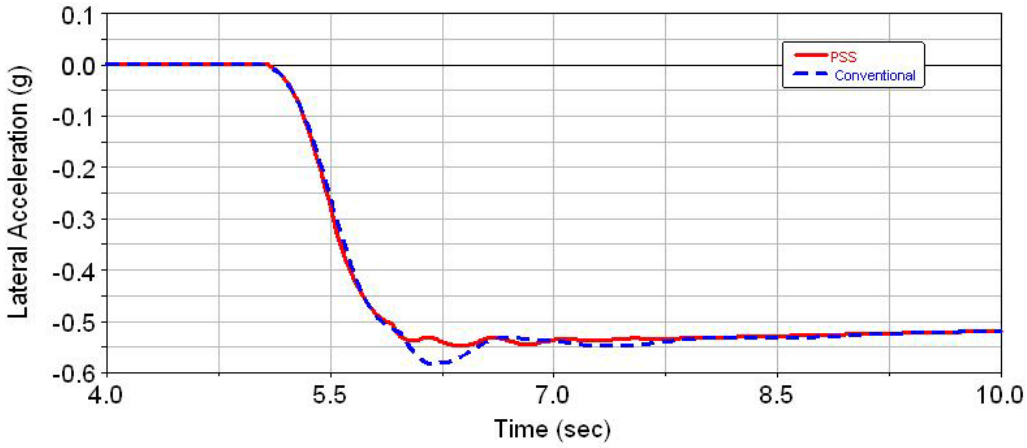

Figure 7-14: Time history of vehicle lateral acceleration response in a step turning

Figure 7-15 depicts the roll angle response and shows that the roll angle of the PSS vehicle is slightly smaller than that of the conventional vehicle after the steering input reaches a constant value. This may related to the smaller distance between the vehicle gravity center and the roll center, as discussed in the suspension parallel wheel travel simulation.

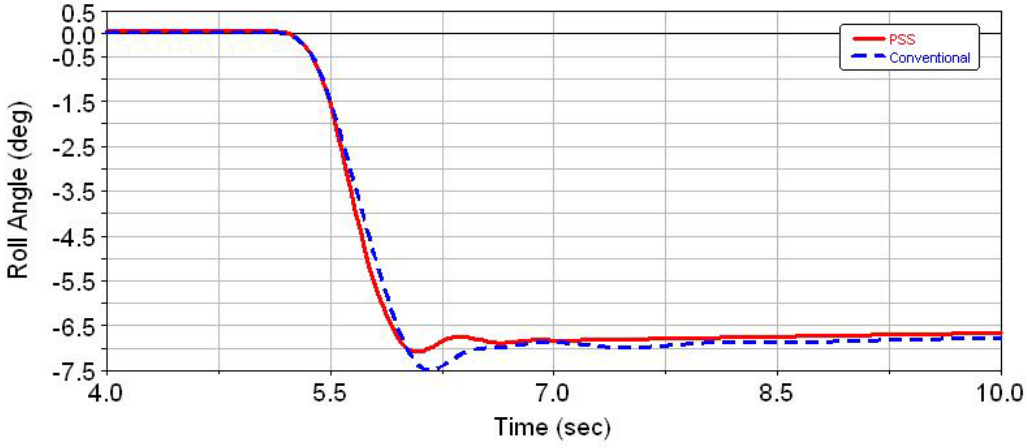

Figure 7-15: Time history of vehicle roll angle in a step turning manoeuvre

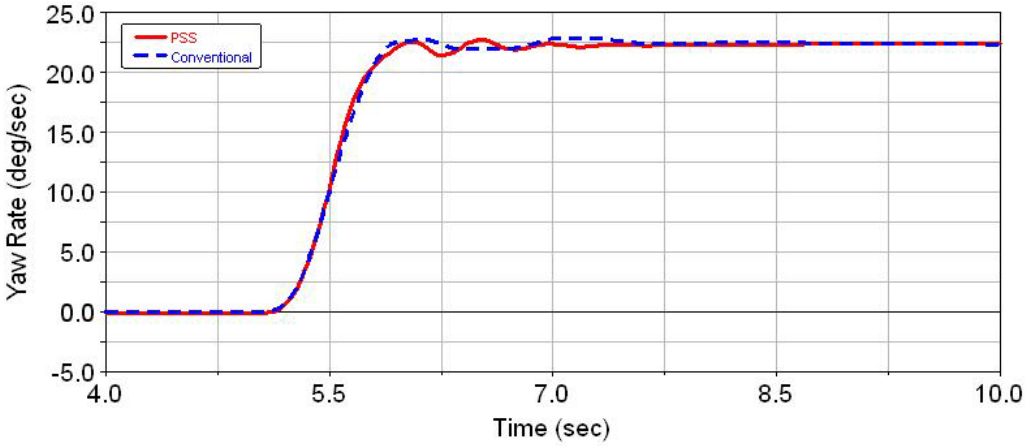

(a) Yaw

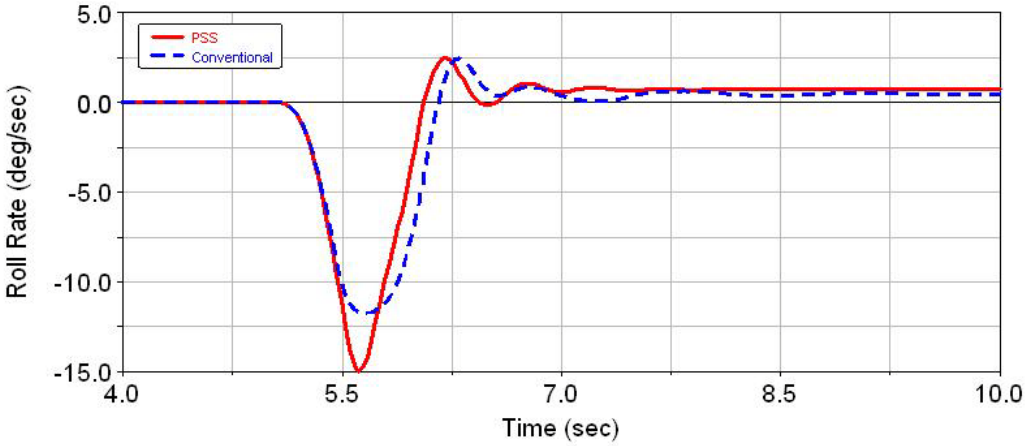

(b) Roll

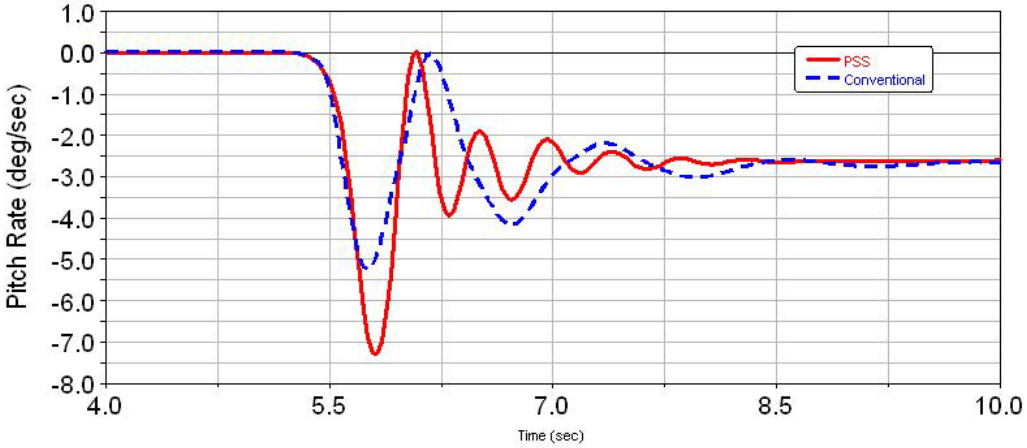

(c) Pitch

Figure 7-16: Vehicle angular velocities in a step turning manoeuvre

The yaw, roll and the pitch rates in this turning manoeuvre are plotted in Figure 7-16. The steady-state angular velocities are generally very close between the two types of vehicles. On the other hand, the transient parts of the angular velocities, especially the roll and pitch rates of the PSS vehicle, are larger than those of the conventional vehicle. The large pitch motion of the PSS vehicle is due to the small anti-dive which is related to the small longitudinal stiffness. Figure 7-16 further shows that the frequencies of the transient angular response of the PSS vehicle are slightly larger than those of the conventional vehicle.

7.3.3 Simulation of a Single Lane Change Manoeuvre

The dynamic behaviour in a single change is simulated at 80 km/h with a magnitude of 30º sinusoidal input at the steering wheel, which is approximately equivalent to 2º at the front wheels. Figure 7-17 depicts the trajectory of the two types of vehicles in such a manoeuvre. It is shown that the PSS vehicle turn about 0.8 m far away laterally than a conventional vehicle in the same operation, which means the PSS vehicle is more sensitive to the sinusoidal steering input. This implies that for a same single lane change, a comparatively small steering input is needed for the PSS vehicle. In addition, it can be found that, before the application of steering command, the conventional vehicle deviate from the straight line. This deviation is due to the accumulation of computational error.

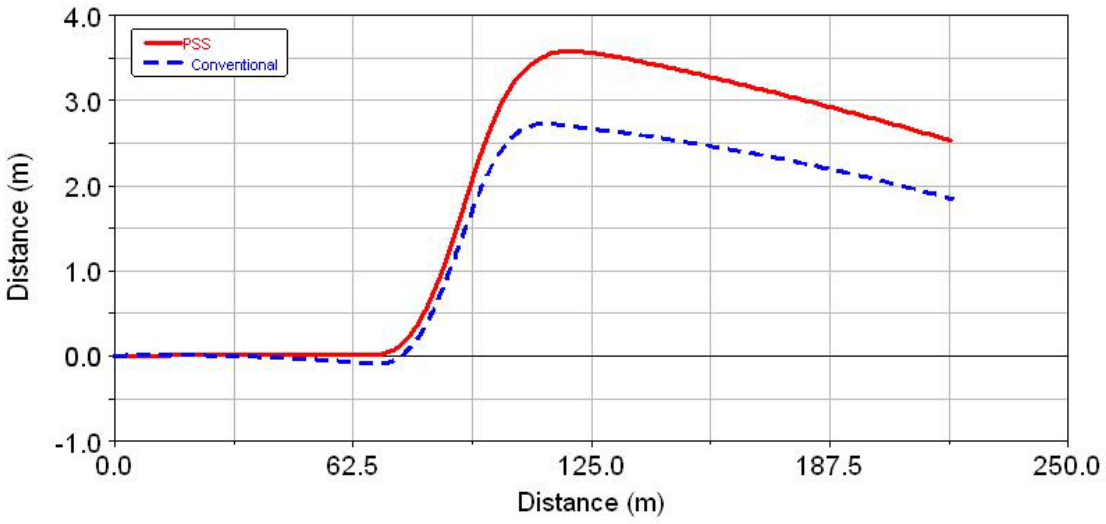

Figure 7-17: Vehicle trajectory in a single lane change manoeuvre

Figure 7-18 and 19 illustrate the yaw velocity and lateral aceleration responses, respectively, in the single lane operation. Consistently to the vehicle trajectory, the manitude of yaw velocity of the

PSS vehicle is slightly larger than that of the conventional veicle. The peak values of the lateral accelration responses of the two types of vehicles are very close. The simulation results also imply that the response frequency of the PSS vehicle is slightly larger than that of the conventional vehicle. The reaction of the PSS vehicle to a lane-change input is slower than that of the conventional vehicle.This point can also be seen in the roll motion response as shown in Figure 7-20.

It is noted that the results of the single lane change simulation using the Adams/car full-car model are not consistent with those obtained in the simulation using a single-track handling model presented in Chapter 6. In the simulation using the single-track model, the results of a single lane change are very comparable between the two types of vehicles. The trajectories of the PSS and conventional vehicles predicted in that simulation almost coincide as seen in Figure 6-18(b), whereas the simulation results by the Adams/car exhibit a certain difference as shown in Figure 7-17. This difference may be related to the model complexity since the Adams/car model is a full-car model and being more realistic, but the single-track model is highly simplified with a number of assumptions. Besides, the accumulation of computational error may play a role in the difference of the lateral position.

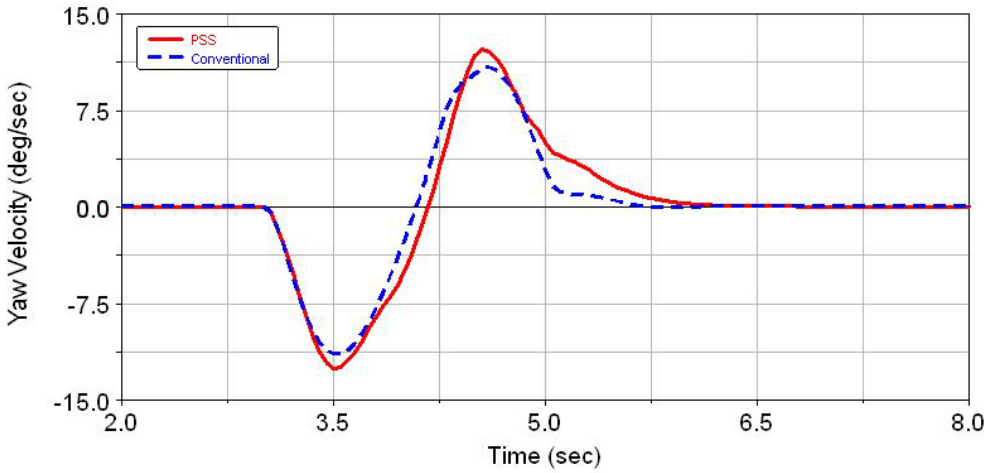

Figure 7-18: Time history of yaw velocity in a single lane change manoeuvre

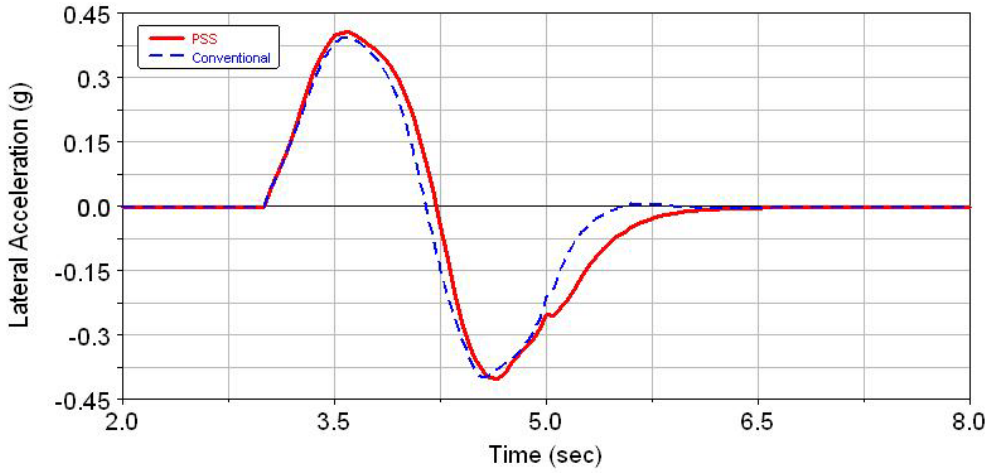

Figure 7-19: Time history of lateral acceleration in a single lane change manoeuvre

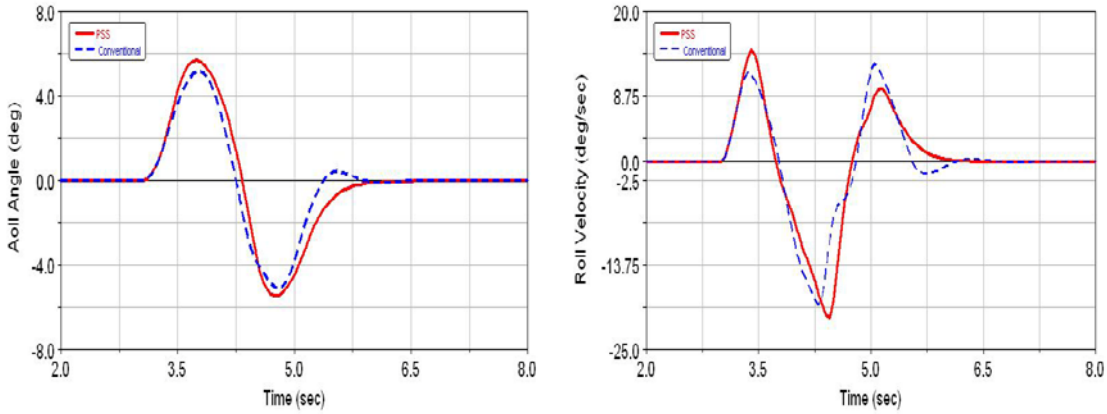

(a) Roll Angle (b) Roll Velocity

Figure 7-20: Time history of roll response in a single lane change manoeuvre

7.3.4 Study of ISO (Double) Lane Change Test

A double lane change course described in ISO-3888 is a performance test in which a vehicle experiences a steering operation to pass a path illustrate in Figure 7-21. The analysis stops after the vehicle travels 250 m. This course test can examine the obstacle avoidance ability of a vehicle, and therefore is important and necessary to be performed. In this study, an ISO lane change is carried out at 100km/h for a PSS vehicle and a conventional vehicle.

The required steering wheel inputs for the two types of vehicles are predicted and plotted in Figure 7-22. As shown, during the first part of lane change, the required steering angle for the PSS

vehicle is smaller than that for the conventional vehicle. In the second part of the lane change, in which the vehicle returns to its original alignment, the required steering demand for the PSS vehicle fluctuates, and is not as smooth as that for the conventional vehicle. Such a result implies that the PSS vehicle responses faster to a steering demand to avoid an incoming obstacle than the conventional one. But at the end of the double lane change, adjustments are needed for the PSS vehicle to return to its original position.

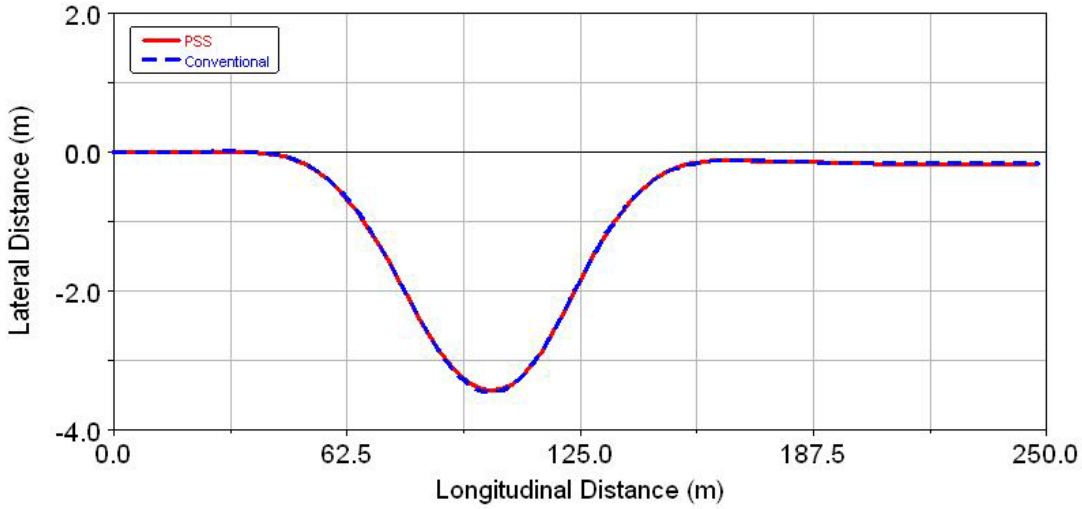

Figure 7-21: Path of a double (ISO) lane change course at 100km/h in Adams/car

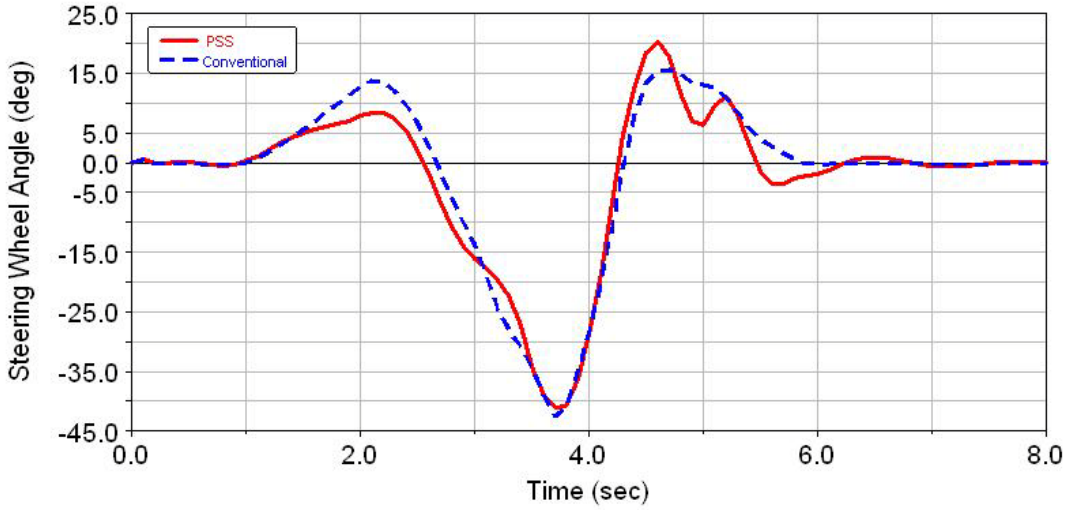

Figure 7-22: The required steering wheel input in a double (ISO) lane change test

The lateral acceleration and yaw velocity responses in the double lane change are illustrated in Figure 7-23 and 24, respectively. It can be seen that these responses of the two types of vehicles are very comparable. The deviation from each other is very trivial and can be negligible. As reflected in the required steering wheel inputs, the yaw velocity of the PSS vehicle has a small fluctuation when the vehicle returns to its original alignment.

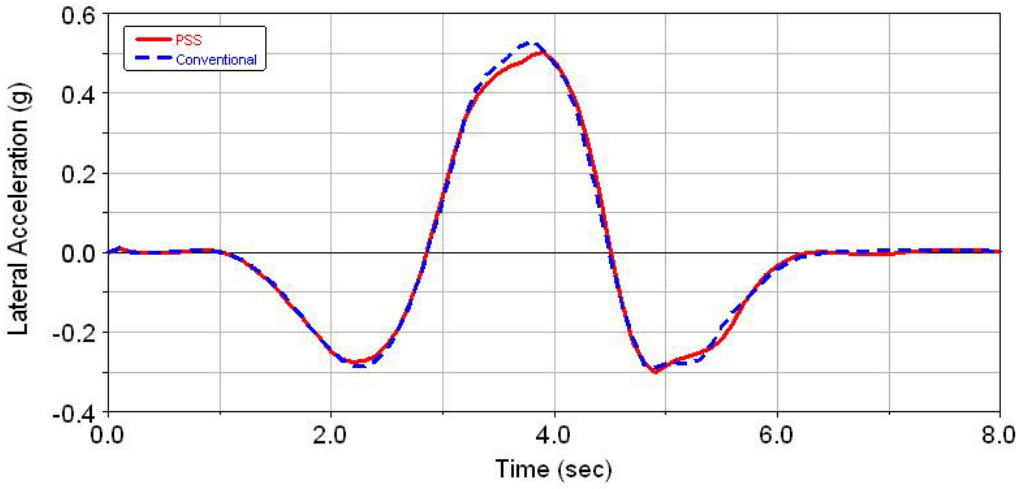

Figure 7-23: Time history of lateral acceleration in a double (ISO) lane change test

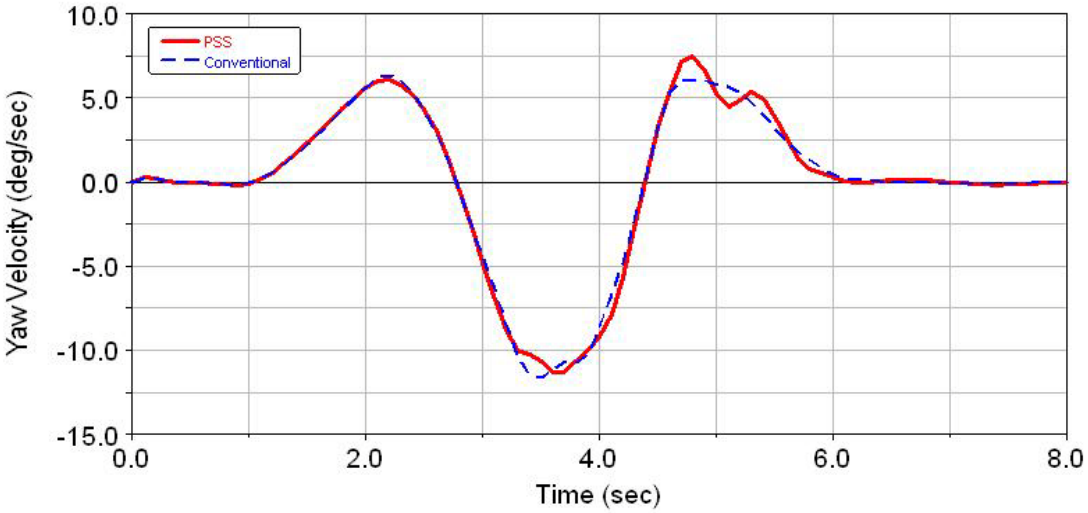

Figure 7-24: Time history of yaw velocity in a double (ISO) lane change test

The roll angle and the roll velocity of the two types of vehicles are investigated as illustrated in Figure 7-25. While the roll angle responses are very close and comparable between the two types of

vehicles, the roll velocity of the PSS vehicle has a slightly large maximum and minimum values compared with those of the conventional vehicle. However, the difference is very small.

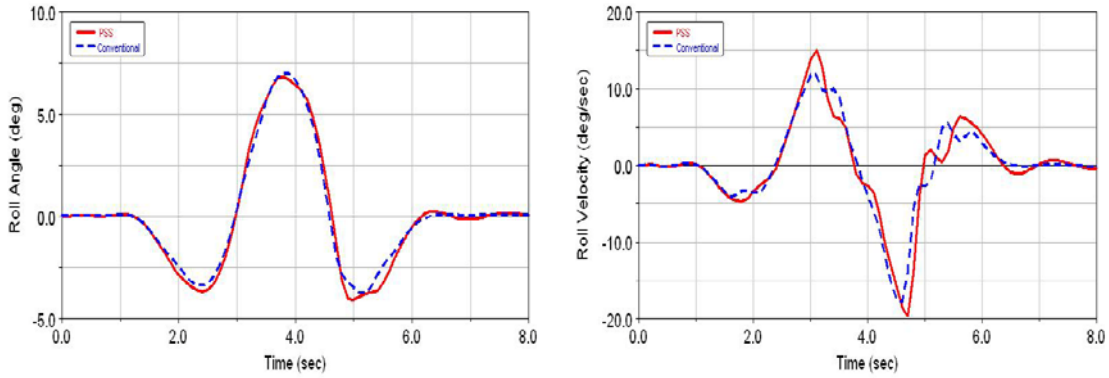

(a) Roll Angle (b) Roll Velocity

Figure 7-25: Time history of roll response in a double (ISO) lane change test

7.4 Validation of the Proposed 18-DOF Analytical Model

The proposed 18-DOF analytical models for a PSS and a conventional vehicle are first validated with a virtual model developed in the Adams/car in a scenario of passing over an obstacle. In this validation, a single 200 mm long and 100 mm deep pothole is assigned to the right side of the road. The dynamic responses of the PSS and conventional vehicles to this single pothole are predicted using the proposed 18-DOF analytical model and the Adam/car one. The simulation speed is 50 km/h and the vehicle parameters used for the simulation are listed in Table 7-1

Table 7-1: Vehicle parameters of a PPS and a conventional vehicle

	PPS	Conventional
Total Mass (kg)	1307	1307
I_{xx} (kgm^2)	800	800
I_{sy} (kgm^2)	1630	1630
I_{sz} (kgm^2)	2000	2000
I_{xz} (kgm^2)	600	600
b (m)	1.0643	1.0643
c (m)	1.4357	1.4357
2t (m) (wheel track)	1.6	1.6

k_{sr} (kN/m)	23.8/2	23.8/2
k_{sf} (kN/m)	35.7/2	35.7/2
c_{sr} (kNs/m)	2.207/2	2.207/2
c_{sf} (kNs/m)	3.311/2	3.311/2
k_{tf}, k_{tr} (kN/m)	175	175
c_{tf}, c_{tr} (kNs/m)	0.5	0.5
$k_{lf(r)}$ /$k_{sf(r)}$		30
$c_{lf(r)}$ (kN.s/m)		2.5
m_{ur} (kg)	35.75	35.75
m_{uf} (kg)	38.184	38.184
h (m)	0.25	0.25
h_{rcf}	0.5	0.5
h_{rcr}	0.5	0.5
I_{ufy} (kgm^2)	2	2
I_{ury} (kgm^2)	2	2

Figure 7-26 illustrates the time history of the vehicle longitudinal and vertical accelerations. It can be seen that, in general, the results from the different models are in fairly good agreement for both the PSS and conventional vehicles. In the longitudinal direction, the acceleration response of the PSS vehicle, as expected, is much smaller than that of the conventional vehicle due to the soft longitudinal strut in the planar system. For the conventional vehicle, the longitudinal acceleration response predicted from the 18-DOF model has a time delay with that predicted from the Adams/car model. After the wheels have passed over the obstacle, the longitudinal acceleration response of the conventional vehicle from the 18-DOF model exhibits notable oscillation. In the vertical direction, the results from both the analytical and Adams/car models show that the acceleration of the conventional vehicle is larger than that of the PSS vehicle. Result deviations between the two types of models are observed for both types of vehicles. The vertical accelerations from the Adams/car models are slightly smaller than those from the proposed 18-DOF analytical models.

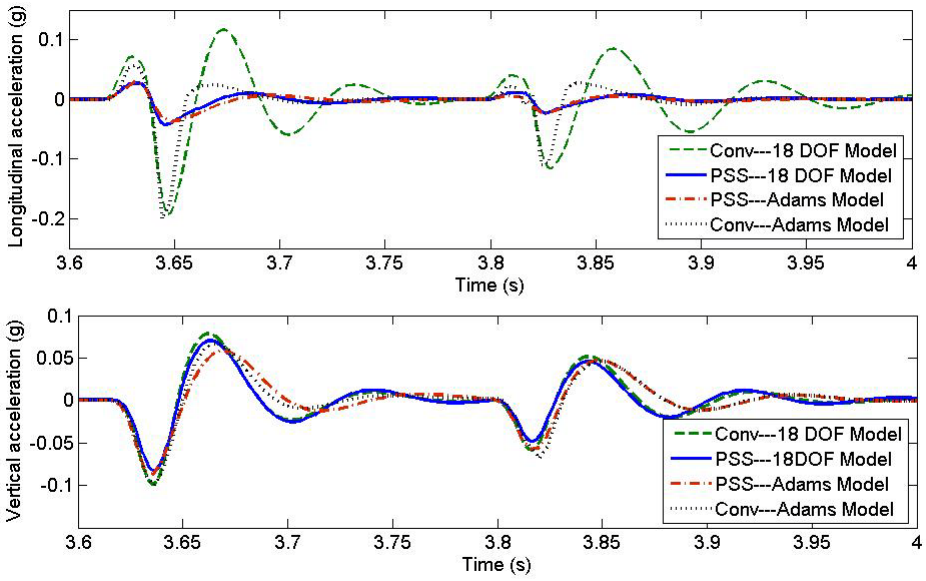

Figure 7-26: Comparison of acceleration responses between the proposed 18 DOF and Adams/car models due to a single pothole

Figure 7-27 displays the responses of the roll and pitch rates obtained from the two types of models. The peak value of the roll and pitch rates for the conventional vehicle predicted by both the 18-DOF analytical model and Adams/car model is slightly larger than those of the PSS vehicle. A time delay is also observed between the results from the 18-DOF analytical and Adams/ car models. Such a delay is due to the small difference of pothole position set in the Adams/car and 18-DOF models. A slight variation between the responses obtained from different models is also observed.

Despite the existence of the deviation between the results for different models, such a deviation is very small and negligible. The results from the 18-DOF model are generally comparable to those from the Adams/car model. The slight differences between the results from different models may be attributed to the bushings used in the construction of the Adams/car model. The suspension rates in the Adams/car also slightly differ from those in the 18-DOF model, although the spring stiffness in the Adams model is assigned as the same values as those in the analytical model, as discussed in Section 7.3. Secondly, the roll centers in the 18-DOF are assumed to be fixed, whereas it is in fact state-dependent in the Adams/car model as shown in Figure 7-10. Furthermore, it is assumed that the suspension longitudinal and vertical struts are completely decoupled in the proposed 18-DOF mathematical model. However, such a coupling cannot be avoided in the Adams/model. In addition,

the camber and toe-in angles, which may play somewhat role in the Adams mode as discussed in Section 7.3, are also completely neglected in the 18-DOF analytical model.

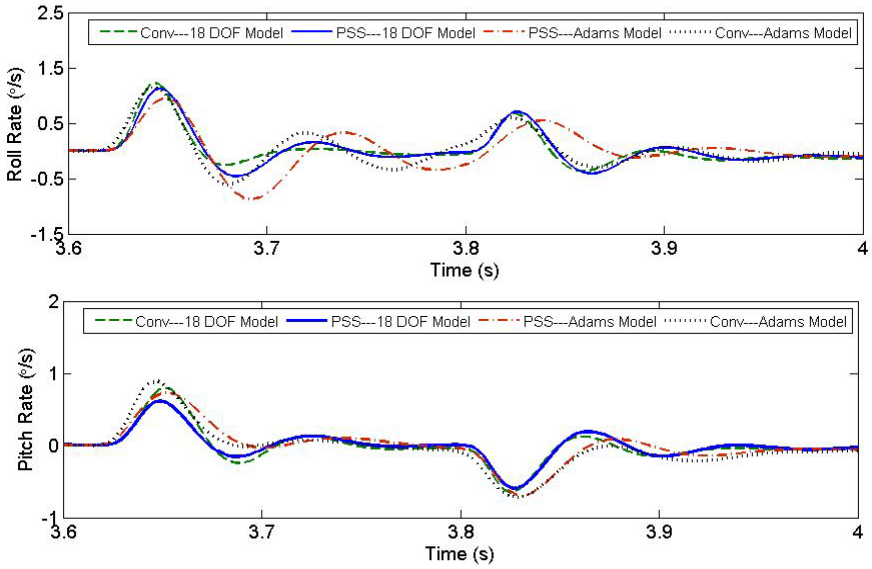

Figure 7-27: Response comparison of roll and pitch rates between the proposed 18 DOF model and Adams/car model due to a single pothole

The proposed 18-DOF models for the PSS and conventional vehicles are also validated with the virtual Adams/car models in the braking and turning scenarios. Figure 28 illustrates the dynamic responses of the PSS vehicle and the conventional vehicle in: (a) a straight line braking at an initial speed of 100km/h, and (b) a turning maneuver at 50km/h. The inputs for these two operations are step signals and the step rising time is 1 second. In order to mitigate the effect of the difference induced by the tire modes on the simulation results, the default parameters of the Adams/car tire model, which is actually a Magic formula model, are modified in line with those used in the 2D Average Lumped LuGre model. Figure 28 indicates that the results from the different models in general have a good agreement with each other for both the PSS and conventional vehicles. In the straight line braking maneuver, the pitch velocity response of the PSS vehicle obtained from the proposed 18-DOF model has a slight time delay compared to that predicted by the Adams/car model. This may be associated with the difference of tire-ground friction models. In the Adams/car model, the tire friction force is calculated by Magic Formula which is essentially a static model. In the 18-DOF model, the tire-ground friction model is a dynamic model in which there is always a time delay between an input and an output. For the conventional vehicle, a slight deviation of the pitch velocity response is observed

between the Adams/car and 18-DOF models. The difference in anti-dive characteristics of the suspension in the two models may contribute to this pitch rate deviation. Meanwhile, the small pitch rate obtained in the 18-DOF model may also be related to the selected value of the longitudinal stiffness for the conventional suspension. This selected value may be different from that of the Adams/car model, which is mainly due to the bushing elasticity and not easy to estimate. The suspension parallel wheel travel analysis implies that the afore-aft wheel center stiffness of the conventional suspension is highly non-linear and varies significantely with the wheel travel, as shown in Figure 7-2. However, in the18-DOF model, it is assumed that the suspension longitudinal spring to be linear and the stiffness to be constant.

The small deviation between the responses obtained from different models is also observed in a turning maneuver as shown in Figure 7-28 (b). The deviations mainly occur at the end of the step rising time. This deviation may be due to the fact that the roll center in the 18-DOF is assumed to be fixed, whereas in fact it is not constant in the Adams/car model.

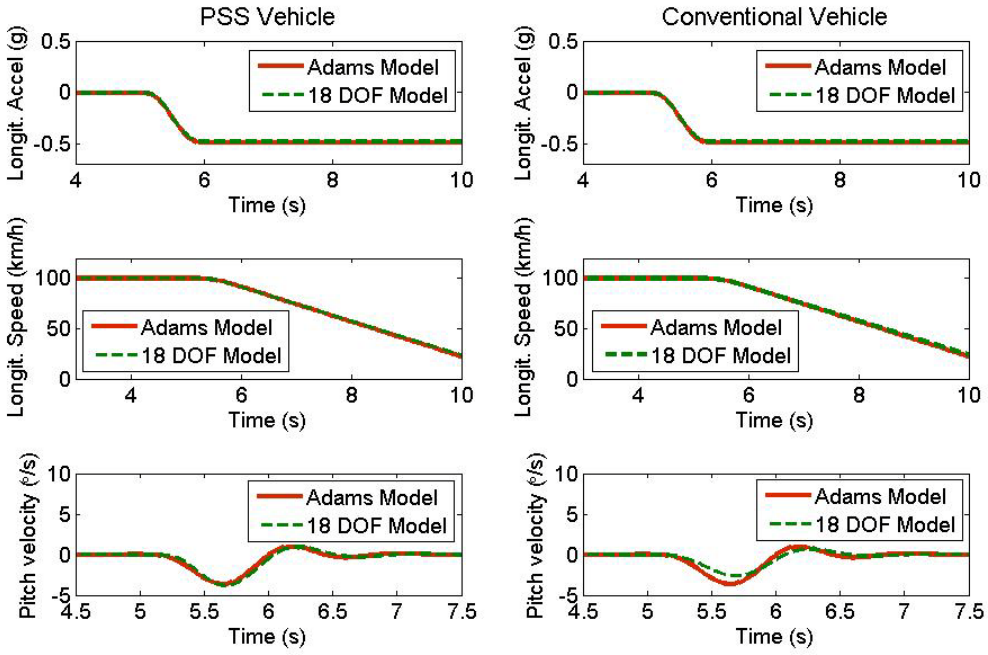

(a) Straight Line Braking (total step braking torque: 1040N.m)

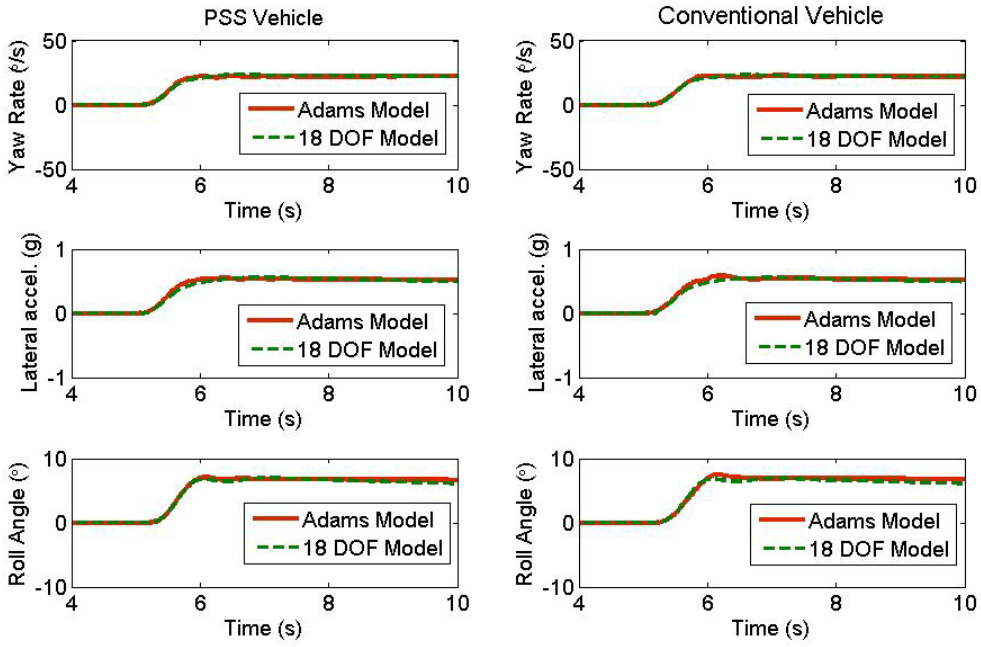

(b) Turning (step steering wheel input: 75º)

Figure 7-28: Response comparison between the proposed 18 DOF and Adams/car models in a straight line braking and a turning manoeuvre

7.5 Investigation of Dynamic Response under Differential Braking

The dynamic response of a PSS vehicle in a differential braking is investigated using the 18-DOF models proposed in Section 2, and the results are presented and analyzed in this section. The body translational acceleration, roll, pitch, and the yaw rate, the roll and pitch angles, and the normal wheel load for a PSS and a conventional vehicle are predicted and compared.

In the simulation, the braking ratio is set such that the nominal braking torque of the front and rear axles is proportional to their static wheel loads. The simulation is carried out on both a straight road and a curved road, namely, straight line braking and brake-in-turn maneuvers. The braking unevenness is set by multiplying the nominal braking torque by a factor 0.9 to one wheel and by a factor 1.1 to the cross wheel. There are totally 2 possible scenarios for the straight line braking and 4 possible scenarios for the brake-in-turn as schemed in Figure 7.29. However, only two scenarios, one for the straight line braking (a) and one for the brake-in-turn (c) are presented in this section.

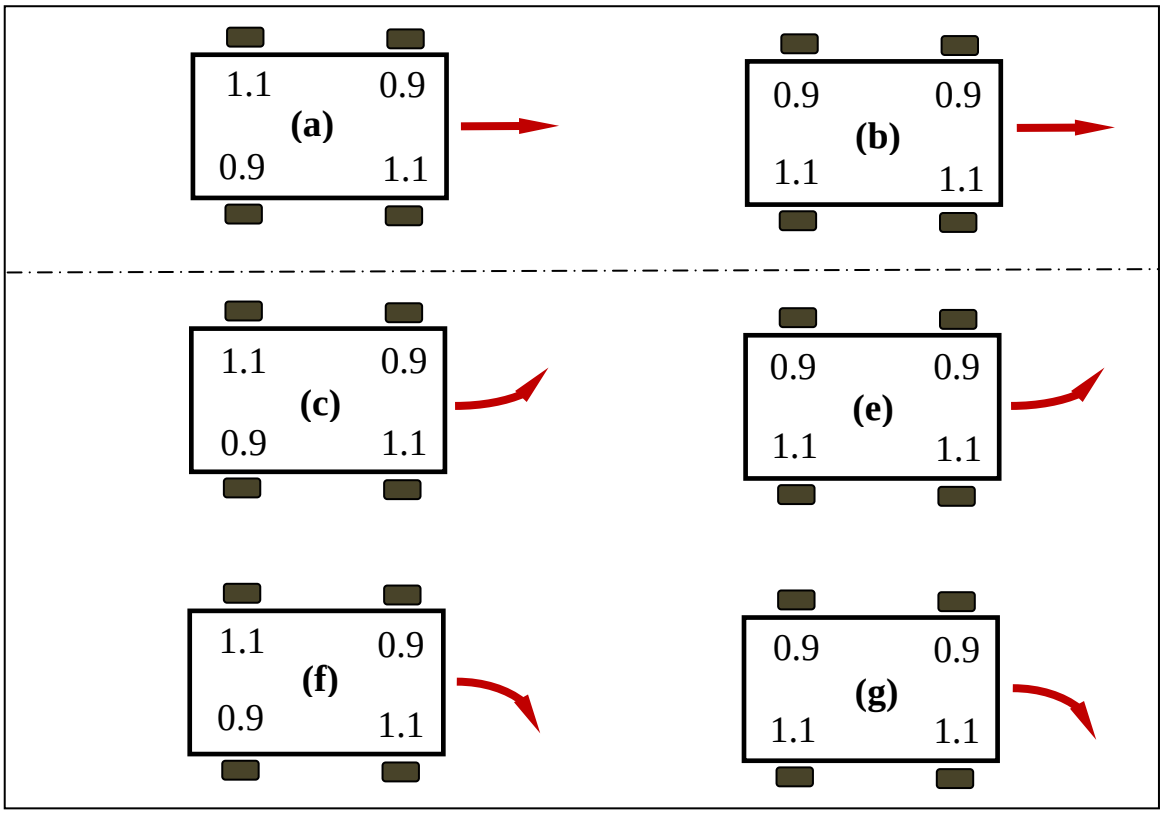

Figure 7-29: Scheme of possible unevenness in a braking manoeuvre (a ~ b for straight line braking; c ~ g for brake-in-turn)

7.5.1 Differential Braking on Straight Road

In this scenario, it is assumed that a trapezoidal braking torque with a maximum of 1000 N.m is applied and distributed to the wheels. The nominal torque applied to each wheel is multiplied by a factor as shown in Figure 7-29 (a). The simulation is carried out at an initial speed of 100 km/h.

The time history of the longitudinal and lateral velocity responses are plotted in Figure 7-30. The results show that the time history of longitudinal velocity of the two types of vehicles coincides while the lateral velocity of the PSS vehicle is slightly larger than that of the conventional vehicle. This slight deviation is also reflected in the vehicle trajectories plotted in Figure 7-31. The deviation may be resulted from the difference of the longitudinal stiffness between the two types of suspensions. It is evident that the tire longitudinal slip can affect the lateral friction force even with the same lateral slip angle, as discussed in Chapter 5. In the braking condition, due to the difference of longitudinal stiffness, the tire longitudinal slip at the contact patch for the two type of vehicles are different, resulting in different lateral friction forces. Such a deviation, however, is so small that can be neglected. It can be concluded that the directional stability of a PSS vehicle in an uneven straight line braking operation is comparable to that of a conventional vehicle. The longitudinal strut in a PSS does not result in a notable influence on the vehicle directional behaviour in straight line braking.

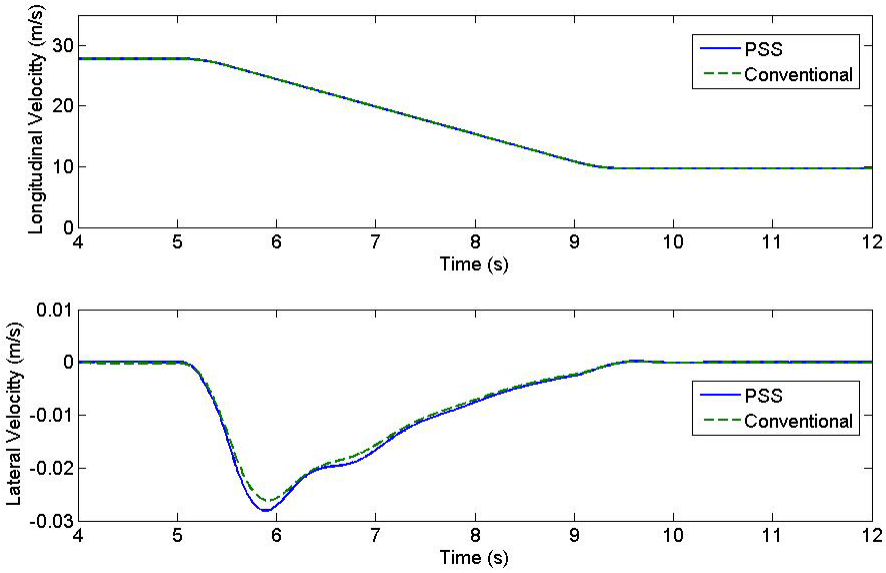

Figure 7-30: Time history of vehicle velocity responses in an uneven straight line braking manoeuvre

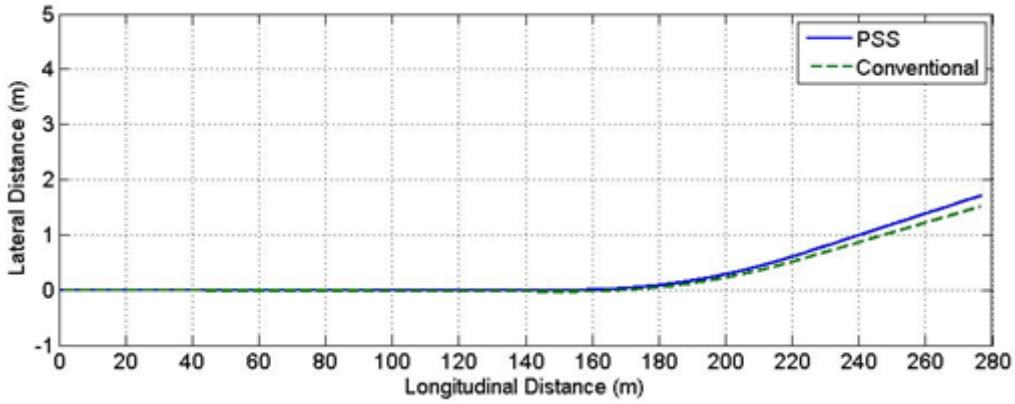

Figure 7-31: Vehicle trajectory in an uneven straight line braking manoeuvre

Figure 7-32 illustrates the time history of acceleration responses. It can be seen that there is no difference in the longitudinal acceleration between a PSS and a conventional vehicles. A small deviation is observed in the lateral and vertical acceleration responses. The difference for the lateral acceleration may be induced by the different lateral friction forces while that for the vertical acceleration may be associated with the pitch motion and braking dive. Since the vertical acceleration at the gravity center of the chassis in such a manoeuvre is caused only by pitch motion than anything else, the magnitudes of the vertical acceleration in both types of vehicles are rather small. It is evident that soft longitudinal connection between the body and tires can induce relatively large pitch motion [100]. This point is also reflected in the pitch velocity and displacement responses illustrated in Figure 7-33 and 7-34, respectively.

The results shown in Figure 7-33 indicate that the pitch rate of the PSS vehicle is larger than that of the conventional one, while the roll and yaw rates of the PSS vehicle are very close to those of the conventional vehicle. As a result, the pitch angle of the PSS vehicle is larger than that of the conventional vehicle as shown in Figure 7-34. The difference of pitch motion is actually caused by the difference in anti-dive and longitudinal stiffness. Even though, the difference of pitch angle is only about half degree, and therefore can be neglected. In other words, the relatively soft longitudinal strut in a PSS has little influence on the roll, pitch and yaw motions of a vehicle.

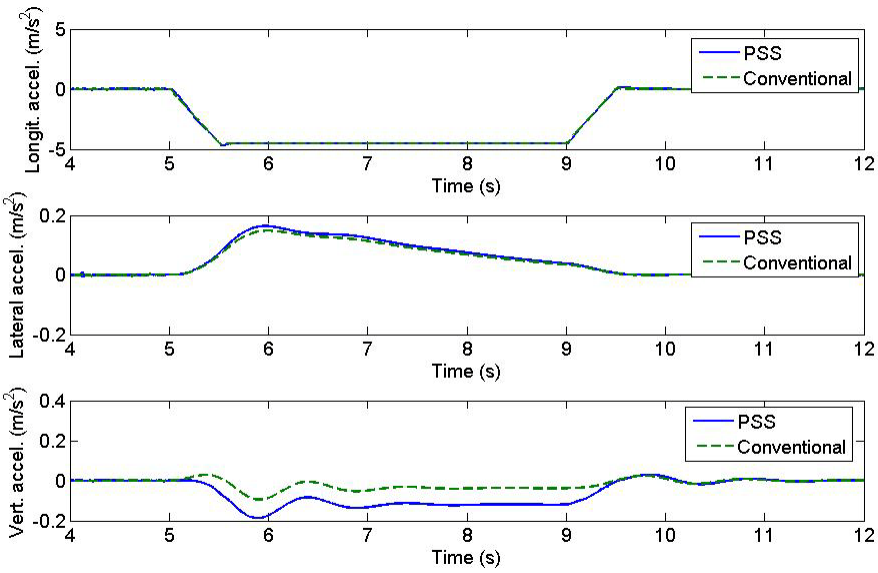

Figure 7-32: Time history of acceleration responses in an uneven straight line braking manoeuvre

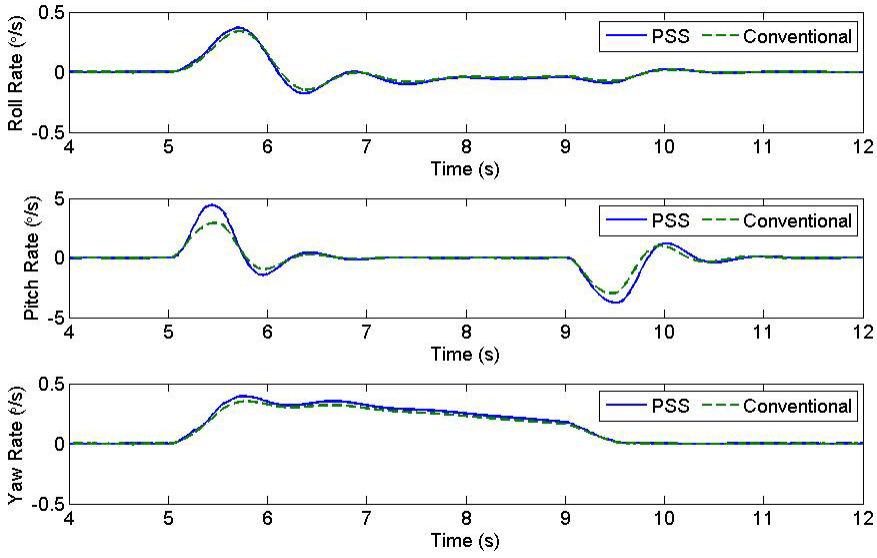

Figure 7-33: Time history of angular velocity responses in an uneven straight line braking manoeuvre

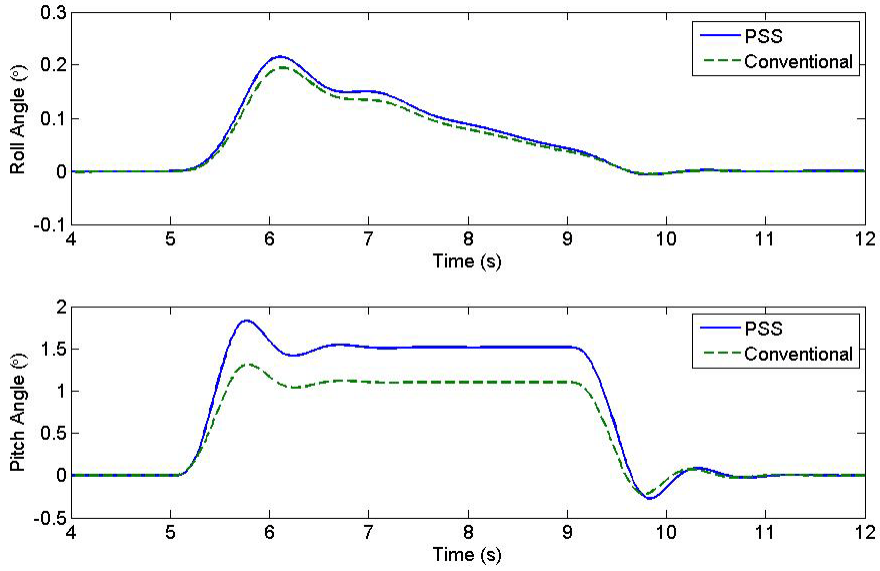

Figure 7-34: Time history of angular displacement responses in an uneven straight line braking manoeuvre

The changes in the normal load at each wheel are displayed in Figure 7-35. In the braking manoeuvre, the load transfer occurs between the front and rear wheels as expected. Such a transfer in a PSS vehicle is about 120 N larger than that of a conventional vehicle in a half *g* straight line braking. The difference in the load transfer is obviously associated with the position change of wheels with respect to the body. For the conventional vehicle, the position changes are very small due to the relatively stiff longitudinal linkage. For the PSS vehicle, however, such changes could be large owing to the soft longitudinal strut. The relatively large pitch motion, and slightly large roll and yaw motions in the PSS vehicle may result from the relatively larger normal wheel load transfer.

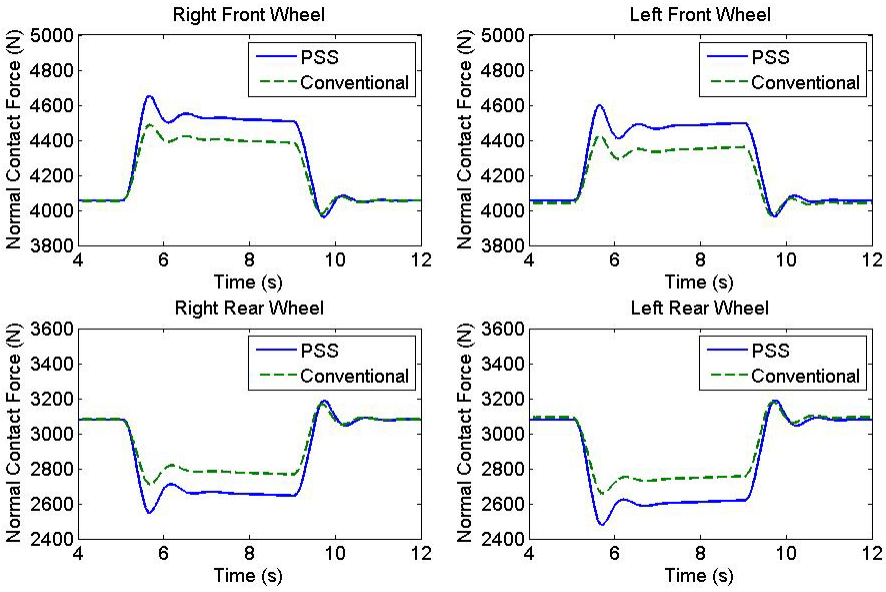

Figure 7-35: Time history of normal wheel load in an uneven straight line braking manoeuvre

7.5.2 Differential Braking in a Turning Manoeuvre

A brake-in-turn manoeuvre is an important scenario in vehicle handling and stability study. The unevenness of braking force in such a manoeuvre may cause some influences on the vehicle directional stability. It is therefore necessary to investigate the dynamic behaviour of a PSS vehicle. In this investigation, it is also assumed a trapezoidal braking torque with a maximum of 1000N.m is applied and distributed to each wheel. The nominal torque applied to each wheel is multiplied by a factor as shown in Figure 7-29 (c). The steering input is a 2° step angle. The braking and steering inputs are applied to the vehicle simultaneously at an initial speed of 100 km/h.

The vehicle trajectory in the differential brake-in-turn is plotted in Figure 7-36. The paths of the two types of vehicles are very close. The path radius of the PSS vehicle, however, is slightly larger than that of a conventional vehicle. This indicates that the PSS vehicle exhibits more understeer characteristic in a differential braking-in-turn manoeuvre. However, this difference is so small that can be neglected.

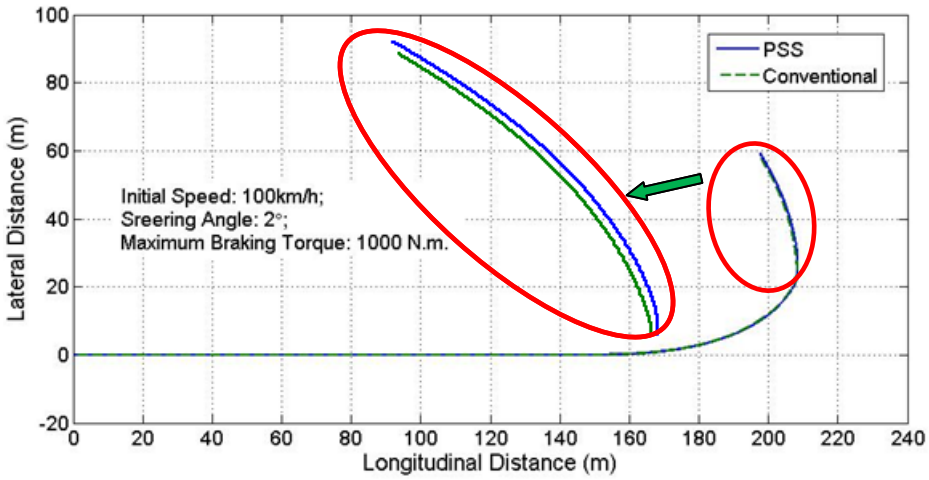

Figure 7-36: Vehicle trajectory in a differential brake-in-turn manoeuvre

The time history of velocity and acceleration responses is illustrated in Figure 37 and 38, respectively. As shown, the longitudinal velocities are very close between the two types of vehicles although there is a small difference of about 0.1m/s, whereas the lateral velocity of the conventional vehicles is slight larger than that of the PSS vehicle during the last half of braking process. The results shown in Figure 38 imply that the acceleration responses along the three orthogonal directions are generally comparable prior to the moment when the braking torque starts to decrease. After this moment, the deviation in the acceleration responses is observed in all the three directions. In the longitudinal direction, the acceleration response of the PSS vehicle changes relatively smooth compared to that of the conventional vehicle. The difference in longitudinal dynamics between the two types of vehicles may be related to the longitudinal dynamic friction. When the braking torque starts to decrease, tire ground friction loses its steady-state and the relative longitudinal slip of tires undergoes successive state changes. Because of the soft longitudinal strut in the planar suspension system, the relative longitudinal slip in the PSS vehicle tires changes milder than that of the conventional vehicle.

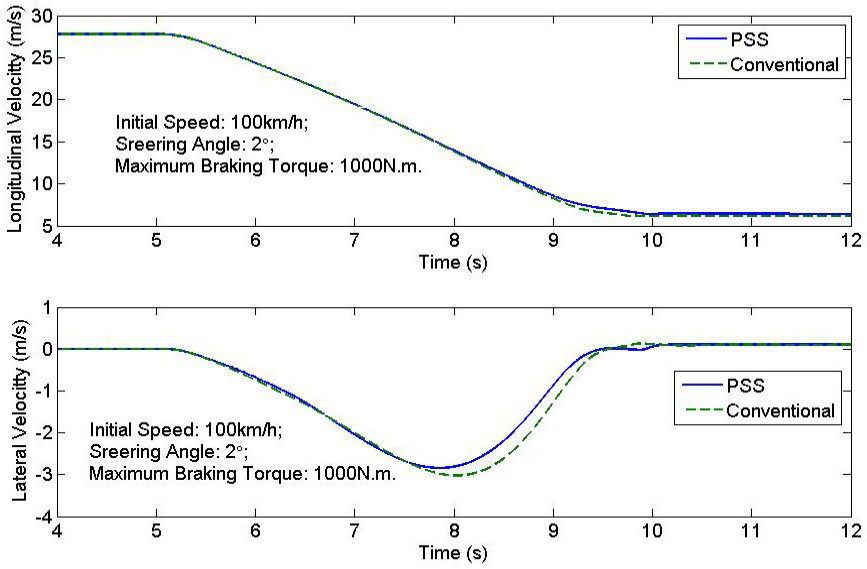

Figure 7-37: Time history of velocity responses in a differential brake-in-turn manoeuvre

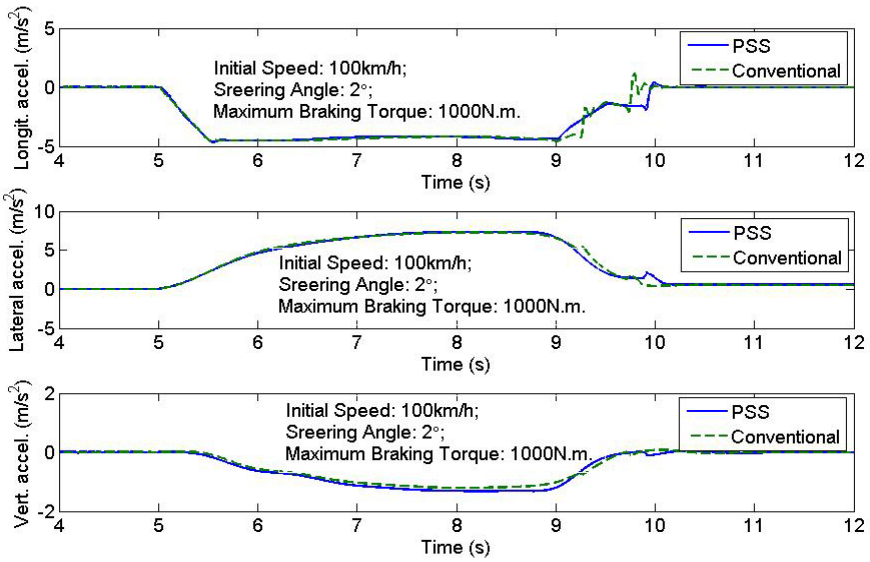

Figure 7-38: Acceleration response in a differential brake-in-turn manoeuvre

Figure 39 shows the time history of vehicle angular velocity in the differential brake-in-turn manoeuvre. Before the braking input starts to decrease, the roll, pitch and the yaw rates of the PSS vehicle are very close to those of the conventional vehicle, except the pitch rate of the PSS vehicle is relatively larger at the beginning of the manoeuvre when the braking torque increases. After the

moment when the braking input starts to decrease, the magnitudes of the roll and pitch rates are close between these two types of vehicles whereas there is a time delay for the conventional vehicle. This time delay may be related to the difference in the longitudinal stiffness of the two types of suspension systems. When the braking torque starts to decrease, the kinetic energy stored in the compressed longitudinal springs of the planar suspension systems can push the wheels back to their original locations, and induce a relative velocity (forward) between tires and ground. However, due to the stiff longitudinal stiffness, the relative motions in the conventional vehicle are not so evident as in the PSS vehicle. Such a relative velocity can reduce the tire slip velocity (backward) defined by equation (5-4). As consequence, the tire friction forces in the PSS vehicle decrease faster than those in the conventional vehicle, so that the PSS vehicle can response earlier in roll and pitch motions.

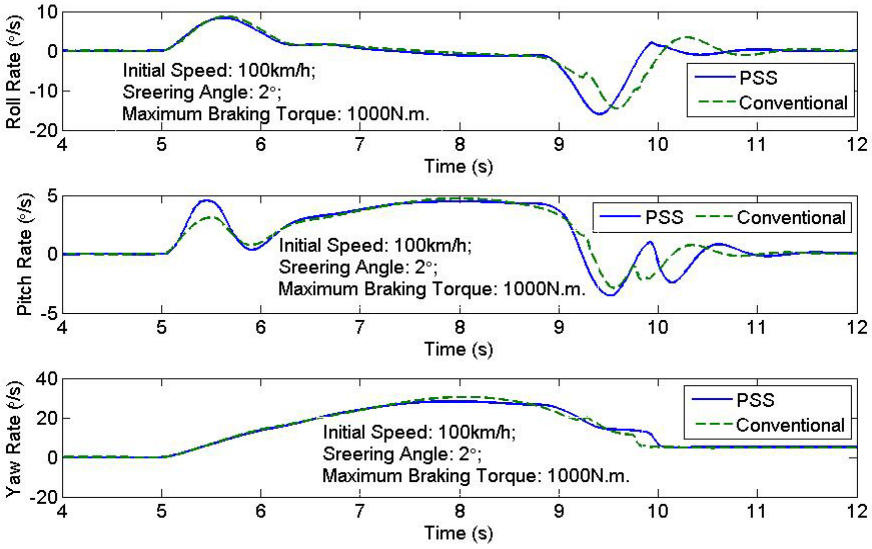

Figure 7-39: Angular velocity responses in a differential brake-in-turn manoeuvre

The time history of the roll and pitch angles is plotted in Figure 7-40. Similar to the uneven straight line braking scenario, the roll responses are very close between the PSS and conventional vehicles, whereas the pitch motion of the PSS vehicle is larger. However, the difference is only about half degree in such a half *g* braking operation while the vehicle is turning.

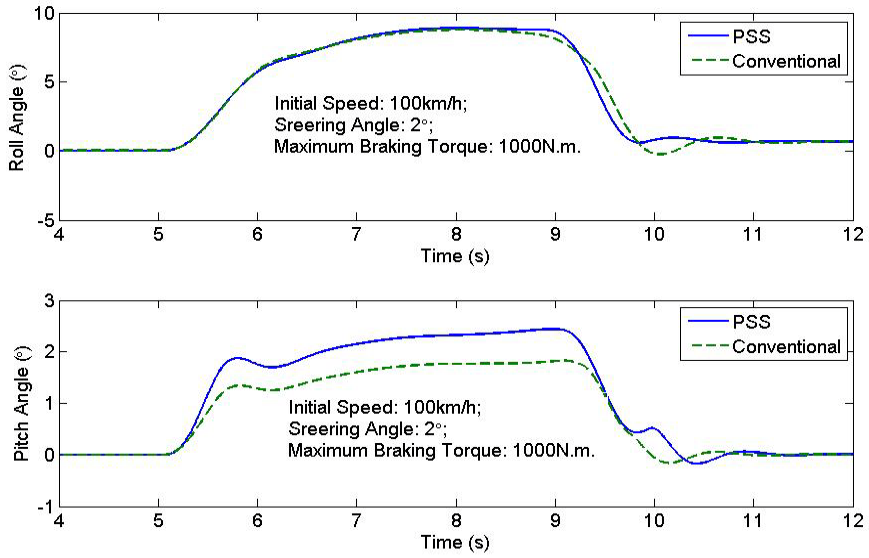

Figure 7-40: Time history of angular roll and pitch angle in a differential brake-in-turn manoeuvre

The suspension longitudinal deflections in the uneven braking-in-turn may be of interest. They are also investigated and plotted in Figure 7-41. As expected, the suspension longitudinal deflections of the PSS vehicle are considerably larger than those of the conventional vehicle. Combined with the results presented previously, a certain amount of longitudinal relative motion between the body and wheels may not be harmful to the vehicle braking, handling and roll performance. A large transient deflection at the rear right wheel takes place when the braking input decreases. Such a deflection exceeds the value of d_r (5cm) in equation (7-13.1), and may challenges the design space. This problem can be easily solved by adding a bumper or stopper for the longitudinal strut in the detailed design, and equation (7-13.1) can be modified with piecewise characteristics in case a stopper for the longitudinal strut is employed.

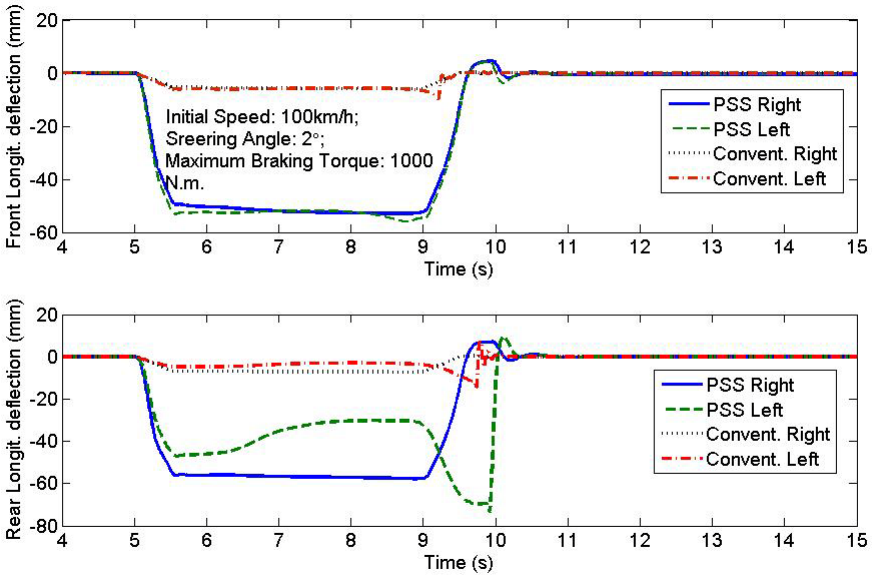

Figure 7-41: Suspension longitudinal deflections

The normal wheel loads at the four wheels are illustrated in Figure 7-42. The results indicate that the normal wheel load can be laterally transferred from the left side to the right side during the brake-in-turn manoeuvre (turn left). The simulation results also show that the increase of the normal wheel at the front right wheel is larger than that at the rear right wheel, while the reduction at the front left wheel is smaller than that at the rear left wheel. This implies that the normal load transfer also occurs between the front and rear duo to the braking. The results further indicate that the normal wheel loads of the PSS vehicle are larger than those of the conventional vehicle at the wheels (front right and rear left) where the applied braking torque is larger. At the moment of 7 second, the difference is about 132N, which is slightly larger than the load transfer in the straight line braking as shown in Figure 7-34 At the wheels (front left and rear right) where the applied braking torque is smaller, the normal wheel load of conventional vehicle is slightly larger. However, the variation in the wheel normal load is very small compared to the magnitude of the wheel load, and, therefore, can be negligible.

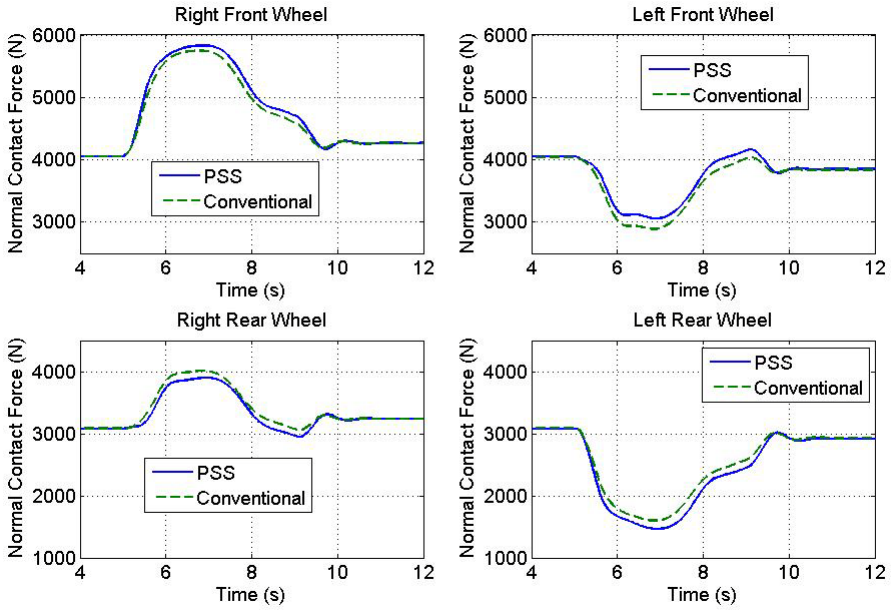

Figure 7-42: Time history of normal wheel load in an uneven brake-in-turn manoeuvre

7.6 Investigation of Dynamic Response due to Asymmetric Potholes

The dynamic behaviors of a PSS vehicle to a pair of asymmetric obstacles are investigated using the proposed models. The simulation is carried out at 50 km/h. Two 200 mm long, 100 mm deep potholes are respectively assigned to each side of the road as shown in Figure 7-43. The distance between the potholes is 1m. The chassis translational acceleration; roll, pitch and yaw rates; roll and pitch angles; and the normal wheel load for the PSS and conventional vehicles are predicted and compared.

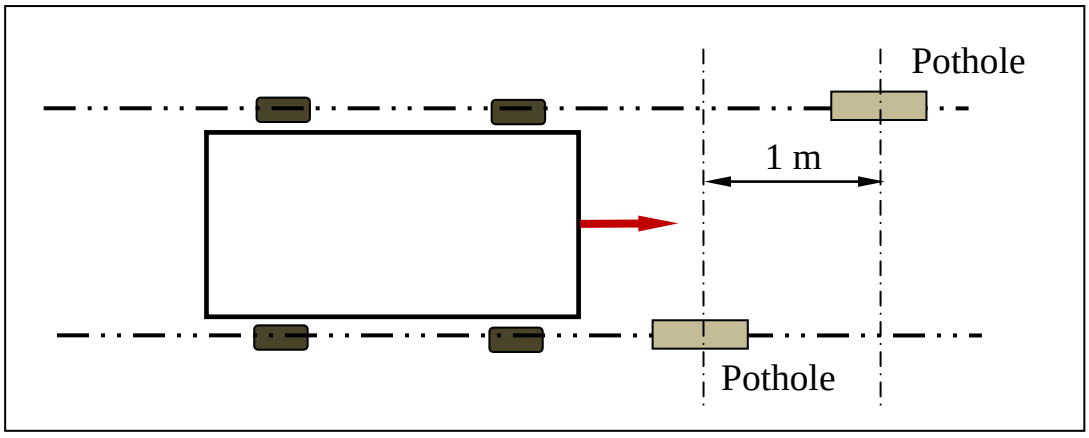

Figure 7-43: Illustration of the pothole positions

Figure 7-44 illustrates the time history of acceleration response. It can be seen that the lateral and vertical accelerations of the PSS and conventional vehicles are comparable, although a small variation is observed in the lateral acceleration response. Four peaks correspond to the impacts when four wheels traverse the potholes. In the longitudinal direction, the acceleration response of the conventional vehicle exhibits oscillations with large magnitudes, whereas that of the PSS vehicle is much small and smooth. The simulation results have clearly demonstrated that the planar suspension system has a significant improvement in absorbing the longitudinal shocks induced by the road obstacles. The acceleration response of the PSS vehicle is very small compared with that of a conventional vehicle in the longitudinal direction. This is the primary advantage of the planar suspension over the existing automobile suspensions.

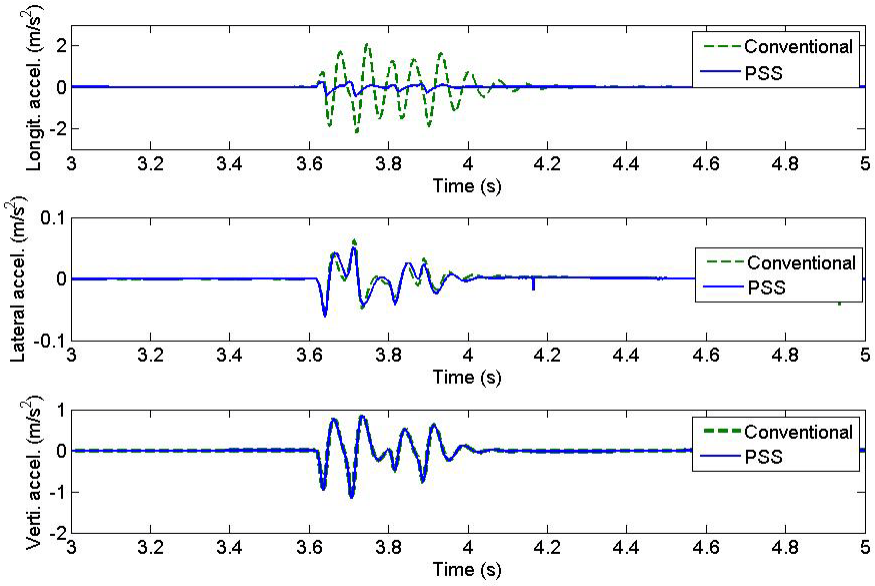

Figure 7-44: Time history of vehicle acceleration responses to asymmetric potholes

The time history of the longitudinal and lateral velocity responses are plotted in Figure 7-45. The results show that the forward velocity of the conventional vehicle oscillates very seriously when the vehicles traverse the asymmetric potholes. Such oscillations, as well as those exhibited in the longitudinal acceleration response, are related to the large longitudinal stiffness in the conventional suspension. On the contrary, the changes of forward velocity in the PSS vehicle are smooth. Due to the obstacle steering effect, the asymmetric potholes induce small lateral velocity. As shown, such small lateral velocities for both types of vehicle are generally comparable.

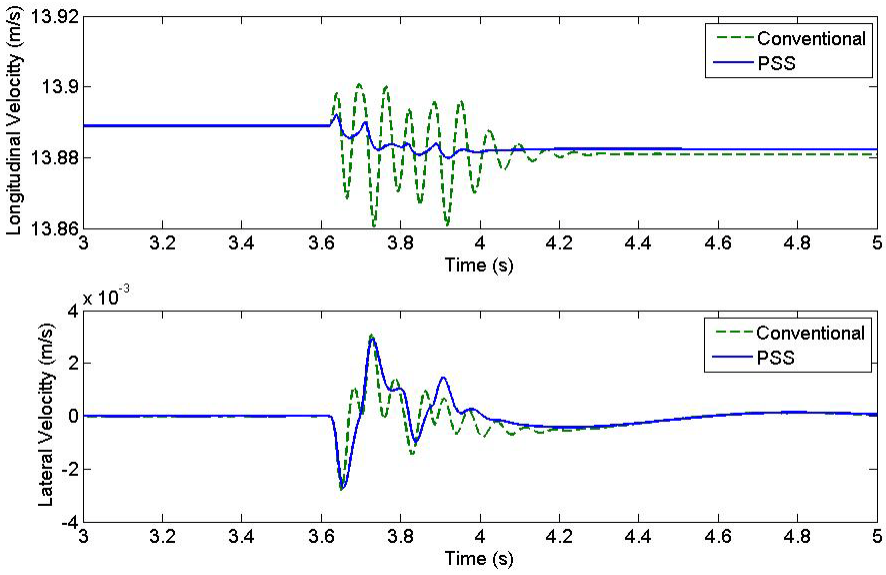

Figure 7-45: Time history of vehicle velocity responses to asymmetric potholes

When vehicles pass over road obstacles, the longitudinal tire-ground interaction forces at four wheels are different and the moments generated by these forces about the vehicle vertical axis, *z*, are not balanced. The unbalanced moment can induce directional deviation. Such a phenomenon is called obstacle-steering effect. The trajectories of the vehicles traversing a single pothole located in the right side, as well as two asymmetric potholes at two sides are plotted in Figure 7-46. It is very interesting to see that the directional deviation of the PSS vehicle due to the road potholes, although not very significant, is smaller than that of the conventional vehicle in this scenario. The small directional deviation of the PSS vehicle may be attributed to the soft longitudinal strut which can provide good capacity of longitudinal impact absorption.

The roll, pitch and the yaw rates of the two types of vehicles due to the asymmetric potholes are plotted in Fig 7-47. As shown, the roll rates of the two types of vehicles are very close. The peak value of the pitch rate for the conventional vehicle is slightly larger than that of the PSS vehicle. But the difference is very small and can be negligible. Fig 7-47 further shows that the yaw rate of the PSS vehicle induced by the potholes is smaller than that of the conventional vehicle. The relative small yaw response of the PSS vehicle is due to the fact that the longitudinal spring damping struts can attenuate the longitudinal impact, whereas the considerably rigid longitudinal connection in the conventional suspension cannot provide sufficient cushion, and, therefore, the longitudinal impact is completely transmitted to the vehicle body. As a consequent, the PSS vehicle has a small directional

deviation as discussed previously. This means that the PSS vehicle has a better ability to stabilize its direction against disturbance of potholes than the conventional vehicle.

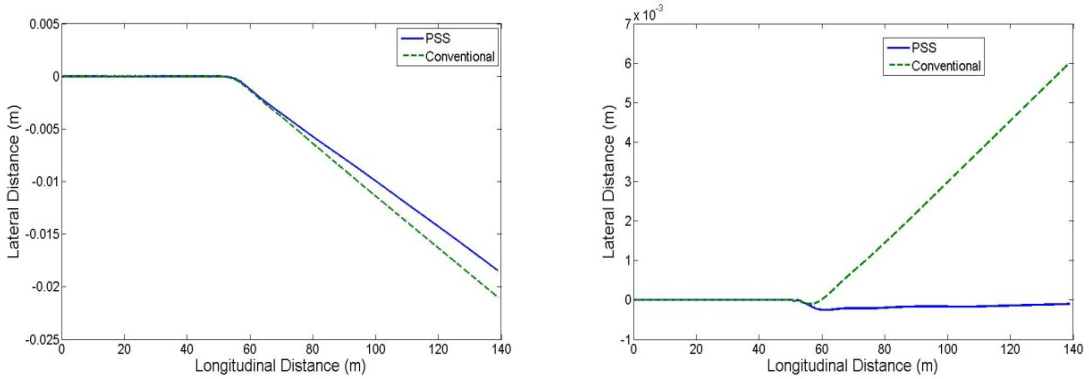

(a) Single Pothole (b) Asymmetric Potholes

Figure 7-46: Vehicle trajectories when experiencing potholes

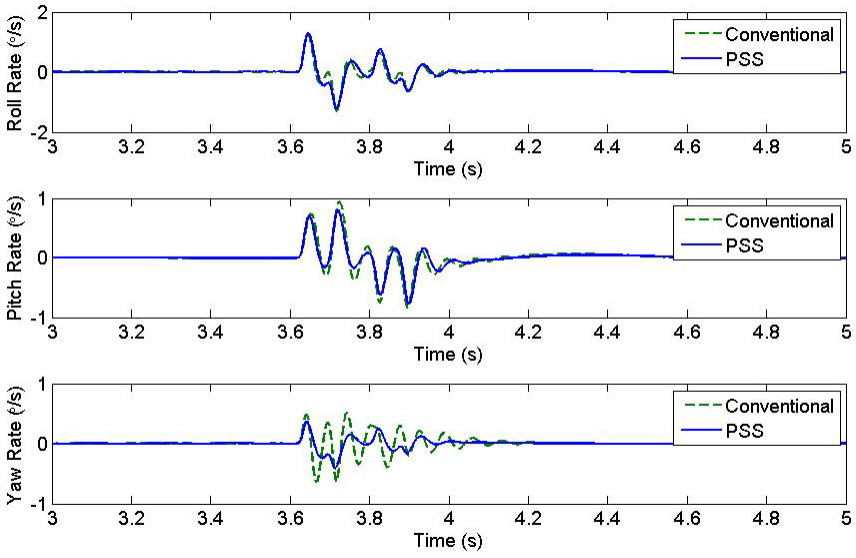

Figure 7-47: Time history of angular velocity responses due to asymmetric potholes

Figure 7-48 displays the response of the roll and pitch angles. The simulation result indicates both the roll and pitch angles induced by the road potholes are very small and can be negligible. The negligible angles are attributed to the vehicle suspension system. Also, the roll and pitch angles for both types of vehicles are very close. There should be no surprise to the pitch response in this scenario when comparing with the results presented before where the pitch of PSS is always larger. In

this asymmetric potholes scenario, the coupling among the different factors such as the right and left sides, the front and rear ends, and different motions may play a more important role in the response.

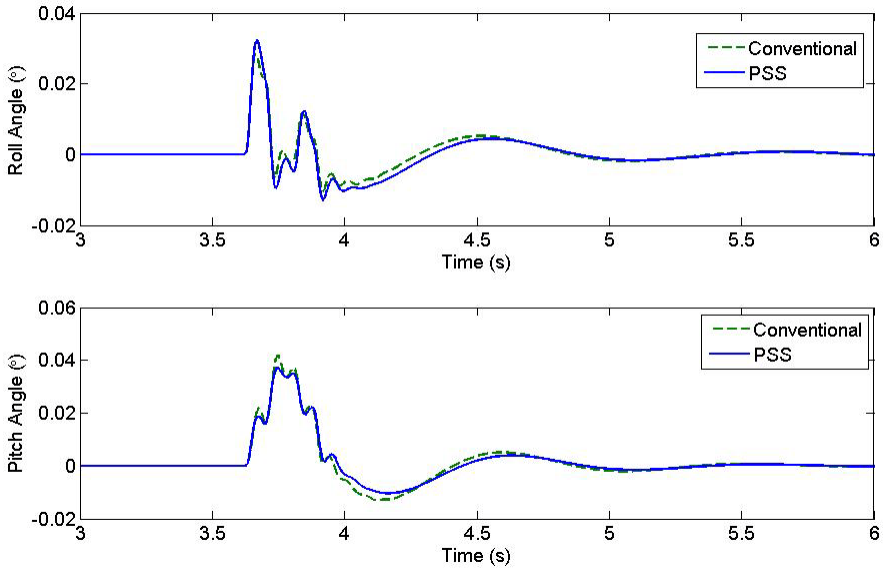

Figure 7-48: Time history of angular velocity responses due to asymmetric potholes

The normal wheel loads at the four wheels are predicted and illustrated in Figure 7-49. The results indicate that the normal wheel loads of the PSS vehicle are slightly larger than those of the conventional vehicle. However, the difference in the wheel normal loads is very small and can be negligible.

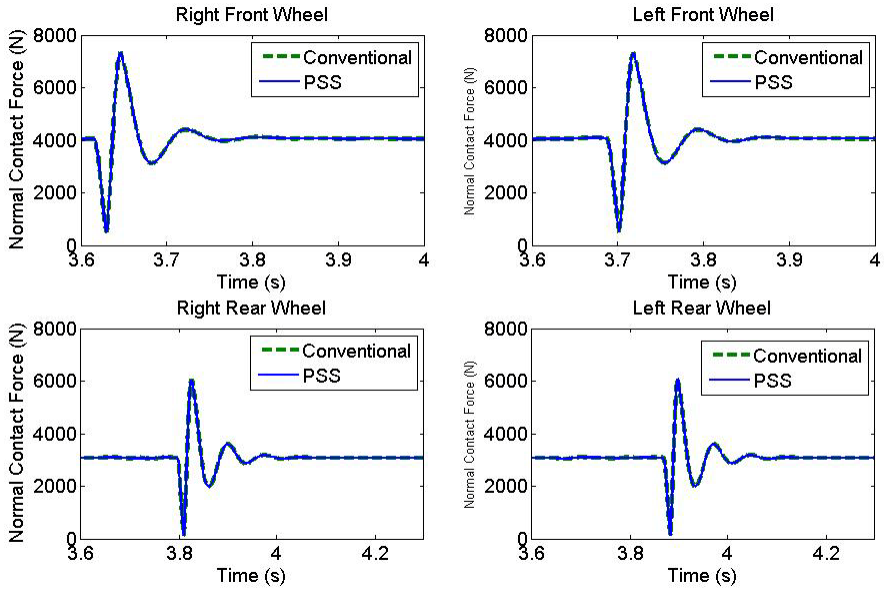

Figure 7-49: Time history of normal wheel load when traversing asymmetric potholes

7.7 Summary

In this chapter, 18-DOF analytical full-car models, as well as the Adams/car virtual models for the PSS and conventional vehicles were developed. The validation between the 18-DOF mathematical and the Adams/car models for both PSS and conventional vehicles were carried out in three scenarios, including passing over a single pothole, braking on a straight road, and turning on a flat road. The 18-DOF model together with a dynamic 2D friction model can account for the effect of the longitudinal elasticity in a suspension system on the total dynamic behaviour of vehicles.

The total dynamics of the PSS vehicle was first studied using the Adams/car virtual models for several basic maneuvers. The simulation results reveal that the PSS system has slightly small ride rate, considerably small afore-aft wheel center stiffness and higher roll center compared to the conventional suspension. The dynamic responses of the two types of vehicles in a step steering, single and double lane changes are general comparable, but small deviations are observed. The results of turning simulation indicate that the PSS vehicle has small roll displacement. In addition, the result also exhibits time delay between the corresponding response of the PSS and conventional vehicles.

The study under differential braking shows that the implementation of planar suspension systems will not deteriorate the roll, pitch and yaw performance of a vehicle. In some cases such as uneven braking-in-turn, the PSS vehicle exhibits, although very slight, more understeer characteristic. The

study of the dynamic response due to the asymmetric road potholes demonstrates that the implementation of PSS can significantly improve the vehicle capacity of longitudinal shock absorption, while the roll and pitch performance are comparable to those of the conventional vehicle. When passing road potholes, the PSS vehicle has a better directional stability. Actually there is no surprise to the investigation results because the “soft” longitudinal strut in a PSS is soft only when the deflection under a threshold value .When the longitudinal deflection exceeds this threshold value, the longitudinal spring becomes as stiff as the longitudinal connection in the conventional vehicle. The possible relative longitudinal motion between chassis and wheels is constrained by this property and thus cannot be too large. It can be concluded from that the small relative longitudinal motion will not change the total vehicle dynamic performance significantly besides its merits as exhibited in this study.

Chapter 8
Conclusion and Future Work

8.1 General

The main objective of this research is to study the dynamic behaviour of a vehicle equipped with planar suspension systems (PSS). The specific objectives are: a) to develop a quarter-car model for preliminary evaluation of ride comfort; b) to develop a half-car pitch plane model for pitch dynamics study; c) to develop a single-track yaw plane model for handling study incorporating with the half-car pitch plane model; d) to develop a full-car model for total dynamics study; and e) to construct virtual models in Adams/car, the most popular commercial software in automobile industry, to reveal the suspension properties and to validate the proposed mathematic models. Unlike the common reported models in which the effect of longitudinal compliance in the suspension system is completely neglected, and the wheels are assumed to be fixed to the vehicle body, the mathematical models developed in this research take into account the relative longitudinal motions between wheels and vehicle body. Therefore, these models can be used to study the influence of suspension longitudinal compliance on the overall dynamics of a vehicle. The radial-spring tire model was modified by adding the tire damping and employed in this study to generate the road excitation forces due to road discontinuities in the vertical and longitudinal directions. A dynamic 2D tire friction model based on the LuGre friction theory was modified and employed to simulate the 2D friction in the tire-ground contact pitch.

This study was focused on the consideration of ride comfort, handling characteristics, traction/braking performance, directional stability and the roll behaviour. The purpose of this study was to gain a total insight on the dynamic behaviour of a vehicle with the proposed planar suspension systems, and to provide a platform to implement the concept of the PSS system in automobiles. In this study, a parallel investigation of the dynamic performance of the same vehicle with conventional suspensions was carried out. The results of this investigation were used as a baseline for the evaluation of the PSS vehicle dynamics. Ride and pitch dynamics of the PSS vehicle were studied using a planar quarter-car and half-car models, respectively, in both frequency and time domains. The ride quality of the PSS vehicle was evaluated using the basic comfort evaluation method provided by ISO 2631, taking into account the chassis bounce, pitch and the longitudinal acceleration. Handling performance was also studied using a single-track yaw plane half-car model. The steady-state

handling characteristics, transient and frequency handling responses in various scenarios were investigated in depth. The total dynamic behaviour when combining the bounce, pitch, roll and the longitudinal dynamics in some important maneuvers, such as single lane change, obstacle avoidance, brake-in-turn, and asymmetric obstacle traversing, was thoroughly investigated. The results obtained in the above mentioned studies were validated by those obtained from the virtual vehicle models constructed in Adams/car environment.

8.2 Highlight of Contribution

From reviewoing literature, it was concluded that the spring-damping element of a typical suspension system is conventionally designed to connect the vehicle's chassis and wheels vertically. This design layout can only provide good isolation of the chassis from vibrations in the vertical direction. The impacts from the ground along the longitudinal direction are entirely transmitted to the vehicle body with little absorption. This study has thus focused on the development of a new suspension system to overcome this limitation to achieve a better longitudinal ride quality without sacrificing other dynamic performance. The main contributions were summarized as follows:

- A novel design layout of automobile suspension was proposed and a longitudinal spring-damper strut was implemented in addition to the vertical one.
- The relative longitudinal motions between the wheels and body were taken into consideration in the development of various mathematical models. The effects of longitudinal suspension compliance on the vehicle dynamics can thus be quantitatively investigated using these models. These effects are rarely reported in the published literature.
- In the formulation of half-car pitch plane model, the tire friction force was taken into account for the simulation of vehicle pitch dynamics in time domain. This friction force in some cases, such as obstacle traversing, can be very large but was neglected in the reported studies.
- The unsprung mass and inertias were taken into account in the formulation of vehicle handling model and full-car model, whereas they were generally neglected in the reported literature.
- Wheel load transfer due to the lateral friction forces developed in the tire-ground contact patch was considered in the formulation of full-car models. This transfer was always neglected.
- The damping of tires was added in the radial-spring tire contact model.

- In order to well capture the transient friction behaviour between the tires and ground, a newly developed dynamic tire friction model was modified. The effective tire rolling radius, contact patch length and normal wheel load are state-dependent instead of constant in this modified tire friction model. These variables are estimated by the radial-spring tire contact model.

8.3 Conclusions

The major conclusions drawn from this dissertation research are summarized below:

- The planar suspension system has smaller afore-aft wheel center stiffness, and thus exhibits good potential to attenuate the impact and isolate vibration due to road excitations, regardless of single or random distributed, in both vertical and longitudinal direction. In addition, the replacement of the rigid trailing arm by a soft longitudinal strut can slightly improve capacity of vibration isolation in the vertical direction.
- The overall ride quality of a vehicle could be improved with a PSS system when the vibrations along the longitudinal direction are taken into account in accordance with ISO 2631, although the soft longitudinal strut can induce slightly larger pitch motion. Significant improvement of shock attenuation can be obtained in the longitudinal direction through the application of a PSS system.
- The handling performance of a PSS vehicle is generally very close and comparable to that of a similar conventional vehicle, although at high frequency the PSS vehicle is more sensitive to the directional excitation than the conventional vehicle, particularly in terms of the lateral acceleration. Therefore, the PSS vehicle needs relatively small steering input for a same single lane change.
- While a PSS vehicle exhibits a similar steady-state handling performance to a conventional vehicle, the application of PSS in vehicles can enhance the understeer trend, i.e. understeer becomes more understeer, neutral steer becomes slightly understeer and oversteer becomes less oversteer. The longitudinal force can enhance the understeer trend of a vehicle with PSS more than that of a vehicle with the conventional suspension.
- Due to small distance between the vehicle CG and the roll center in a PSS vehicle, the roll angle of the PSS vehicle is smaller than that of a conventional vehicle in a turning manoeuvre.

- The implementation of planar suspension systems will not deteriorate the roll, pitch and yaw performance of a vehicle. In some cases such as uneven braking-in-turn, the PSS vehicle exhibits, although is very slight, more understeer character.
- In some cases such as passing road potholes, the PSS vehicle has a better directional stability.
- Due to the implementation of the longitudinal strut in the PSS vehicle, the longitudinal impact applied to the tires by road obstacles can be sufficiently absorbed, and the longitudinal force can be significantly reduced. Therefore, PSS can protect the suspension components (joints, bushings, links and vertical struts), tires and vehicle body from the damage caused by impact.

8.4 Recommendation for Future Work

The dissertation research exhibits a potential to develop the planar suspension system and implement it in ground vehicle design. In view of the potential benefits and promising results of the present study, the implementation of this concept in real automobiles is feasible. A list of further studies that can be undertaken, along with recommendation for research improvement, is presented in the following:

- An optimization needs to be conducted for the suspension longitudinal parameters, the maximum value of allowed suspension longitudinal travel, d_r, and the longitudinal damping coefficient, to make a reasonable comprise between design space, longitudinal vibration isolation, handling and roll dynamics.
- Detailed design should be carried out to implement this idea in real automobile suspension. More attention should be paid on the connection of drive-line, brake-line and steering system to the front wheels so that the control command from the driver can be accurately and timely transmitted to the front wheels.
- A prototype of the PSS should be fabricated after the detailed design. In-lab experiments are necessary to investigate the dynamic performance of the planar suspension system for refining the PSS design.
- The refined PSS should be installed in a vehicle to conduct in-lab and on-road tests in various conditions to further validate the results obtained in this study, and to improve the detailed design of the planar suspension system.

Bibliography

1. J. Reimpell, H. Stoll and J. W. Betzler, "The Automotive Chassis: Engineering Principles**",** *Reed Elsevier and Professional Publishing Ltd*, 2001;
2. H. Kambe and S. Koumura, "Reduction of longitudinal vibration by side-view arrangement of suspension", *Vehicle System Dynamics*, 2008, Vol. 46, supp., pp. 161 ~ 173;
3. D. J. Cole, "Fundamental Issues in Suspension Design for Heavy Road Vehicles", *Vehicle System Dynamics*, 2001, Vol. 35, No. 4~5, pp. 319~360;
4. A. Forsen, "Road-induced longitudinal wheel forces in heavy vehicles". *SAE Transactions*, 1997, Paper No. 973260;
5. R. S. Sharp and D. J. Allison, "In-plane vibrations of tyres and their dependence on wheel mounting conditions". *Vehicle System Dynamics*, 1998, Vol. 29, Supp. 1, pp. 192~204;
6. C. A. Sawyer, "Magneti Marelli Redefines Rear Suspension Design", *Automotive Design and Product*, August 2005. Download from: http://www.autofieldguide.com/articles/080502.html;
7. J. Y. Wong, "Theory of Ground Vehicles", *John Wiley & Sons Inc*, 2001;
8. S. Rakheja and J. Woodrooffe, "Role of suspension damping in enhancement of road friendliness of heavy vehicle", *Heavy Vehicle System, Int. J. of Vehicle Design*, 1996, 3(1-4), pp. 363-381;
9. M. Yokoyama, J. K. Hedrick and S. Toyama, "A model following sliding mode controller for semi-active suspension systems with MR damper", *Proc. of the American Control conference*, 2001, 4, pp. 2652-2657,
10. R. S. Sharp and D. A. Crolla, "Road Vehicle Suspension System Design - a review", *Vehicle System Dynamics*, 1987, Vol. 16, Issue 3, pp.167-192;
11. D. Ammon, "Vehicle dynamics analysis tasks and related tyre simulation challenges", *Vehicle System Dynamics*, 2005, Vol. 43, Supplement, pp.30–47,
12. D. E. Williams and W. M. Haddad, "Active Suspension Control to Improve Vehicle Ride and Handling", *Vehicle System Dynamics*. 1997, Vol. 28, pp. 1-24l
13. Ballo, "Comparison of the properties of active and semiactive suspension", *Vehicle System Dynamics*, 2007, Vol. 45, Issue 11, pp.1065–1073;
14. D. Rhovat, "Survey of advanced suspension developments and related optimal control applications", Automarica, 1997, Vol. 33, No. 10, pp.1781-1817;

15. G. Verros, S. Natsiavas and C. Papadimitriou, “Design Optimization of Quarter-car Models with Passive and Semi-active Suspensions under Random Road Excitation”, *Journal of Vibration and Control*, 2005, 11**,** pp.581–606;
16. D. V. Koulocheris, V. K. Dertimanis and K. N. Spentzas, “Analysis and optimization of a fixed-tank vehicle”, *Forsch Ingenieurwes*, 2006, 70, pp. 171–178.
17. S. Rakheja, A. K. W. Ahmed and X. Yang, “Optimal Suspension Damping for Improved Driver- and Road-Friendliness of Urban Buses”, *SAE TECHNICAL PAPER SERIES*, 1999-01-3728;
18. G. Georgiou, G. Verros and S. S. Natsiavas, “Multi-objective optimization of quarter-car models with a passive or semi-active suspension system”, *Vehicle System Dynamics*, 2007, Vol. 45, No. 1, pp.77–92;
19. M. L. Eugenio and R. S. Barbosa, “Contribution for elastomeric bushing development for the lower control arm of a compact vehicle”, *SAE TECHNICAL PAPER SERIES*, 2007-01-2533 E;
20. Carpiaux, “In-wheel suspension”, United States Patent 6357770, 2002;
21. V. Cossalter, “Frequency-domain method for evaluating the ride comfort of a motorcycle”, *Vehicle System Dynamics*, 2006, Vol. 44, No.4, pp. 339–355;
22. M. H. Kargarnovin, D. Younesian, D. Thompson and C. Jones, “Ride comfort of high-speed trains travelling over railway bridges”, *Vehicle System Dynamics*, 2005, Vol. 43, No. 3, pp173~199;
23. J. P. C. Goncalves and J. A. C. Amberosio, “Optimization of Vehicle Suspension Systems for Improved Comfort of Road Vehicles Using Flexible Multibody Dynamics”, *Nonlinear Dynamics*, 2004, 34, pp. 113–131, 2003;
24. C. Liu and R. Herman, “Road profiles vehicle dynamics and human judgment of serviceability of roads spectral frequency domain analysis”. *Journal of transportation engineering* / March/April 1998/107;
25. A.K.W. Ahmed, “Ground Transportation System”, Encyclopedia of Vibration, ISBN 0-12-227085-1, Academic Press, London, U.K. 2001. pp. 603-620.
26. K. Strandemar and B. Thorvald, “Ride diagram: a tool for analysis of vehicle suspension settings”, *Vehicle System Dynamics*, 2006, Vol. 44, Supplement, pp.913–920;
27. J. Rauh., “Virtual development of ride and handling characteristics for advanced passenger cars”. *Journal of Vehicle System Dynamics*, 2003, Vol. 40, pp: 135–155;
28. ISO 2631, “Mechanical Vibration and Shock ---Evaluation of Human Exposure to Whole-Body Vibration ---Part 1: General Requirements”, 1997;

29. S. L. Koo, H. S Tan and M. Tomizuka, “Impact of Tire Compliance Behavior to Vehicle Longitudinal Dynamics and Control”, Proceedings of the 2007 American Control Conference Marriott Marquis Hotel at Times Square, New York City, USA, July 11-13, 2007;
30. G. Verros and S. Natsiavas, “Ride Dynamics of Nonlinear Vehicle Models Using Component Mode Synthesis”, *Nonlinear Dynamics*, 2002, 34, pp. 113-131;
31. M. W. Sayers and S. M. Karamihas, “Interpretation of road roughness profile data”, Final Report, Contract DTFH 61-92-C00143, Report No. FHWA RD-96-101, 1996;
32. B. R. Davis and A. G. Thompson, “Power Spectral Density of Road Profiles”, *Vehicle System Dynamics*, 2001, Vol. 35, No. 6, pp. 409–415;
33. M. Ambrož, G. Šušterši and I. Prebil, “Creating models of road sections and their use in driving dynamics simulations”, Vehicle System Dynamics, 2007, Vol.45, No. 10, pp.911–924;
34. D. V. Koulocheris, V. K. Dertimanis and K. N. Spentzas , “Analysis and optimization of a fixed-tank vehicle”, *Forsch Ingenieurwes*, 2006, 70, pp. 171–178;
35. X. Liu, X. Guan and J. Zhang, “Simulation of stochastic vibration of maglev track inspection vehicle”, *Mechanical Systems and Signal Processing*, 2007, 21, pp. 1927–1935;
36. G. Thompson and C. E. M. Pearce, “RMS Values for Force, Stroke and Deflection in a Quarter-car Model Active Suspension with Preview”, *Vehicle System Dynamics*, 2003, Vol. 39, No. 1, pp. 57–75;
37. Y. Zhang and A. Alleyne, “A practical and effective approach to active suspension control”, *Vehicle System Dynamics*, 2005, Vol. 43, No. 5, pp.305–330;
38. C. Papalukopoulos and S. Natsiavas “Nonlinear biodynamics of passengers coupled with quarter car models”, *Journal of Sound and Vibration*, 2007,304, pp.50–71;
39. R. S. Sharp, “Wheelbase filtering and automobile suspension tuning for minimizing motions in pitch”, *Proc Instn Mech Engrs, Part D: J Automobile Engineering*, 2002, Vol. 216, No.12, pp.933-946;
40. R. Steven and Z. Liu, “Road vehicle suspension and performance evaluation using a two-dimensional vehicle model”, *Int. J. Vehicle Systems Modelling and Testing*, 2008, Vol. 3, No. 1/2, pp.68-93;
41. S. H. Ju and H. T. Lin, “A finite element model of vehicle–bridge interaction considering braking and acceleration”, *Journal of Sound and Vibration*, 2003, Vol. 303, pp.46–57;
42. S. Hegazy, “Vehicle Ride Comfort and Stability Performance Evaluation”, SAE TECHNICAL PAPER SERIES, 2009-01-2859.

43. K. B. Arıkan, Y. S. Ünlüsoy, I. Korkmaz,and A.O. Çelebi: "Identification of linear handling models for road vehicles", *Vehicle System Dynamics*, 2008,Vol. 46, No. 7, pp. 621 - 645;
44. Q. Qu and Y. Liu, "On Lateral Dynamics of Vehicles Based on Nonlinear Characteristics of Tires", Vehicle System Dynamics, 2000, Vol. 34 , pp.131–141;
45. Lukowski, S., Momot, M., Kraemer, D., and Kunz. K.: "Basic linear theory of handling and stability of automobiles", *Proc. IMechE, Part D: J. Automobile Engineering*, 2009, Vol. 223, pp. 1~10;
46. P. Bolzern, F. Cheli, G. Falciola and F. Resta, "Estimation of the Non-Linear Suspension Tyre Cornering Forces from Experimental Road Test Data", *Vehicle System Dynamics*, 1999, Vol. 31, No. 1, pp. 23 -34;
47. C.-F. Lin, A. G. Ulsoy and D. J. LeBlanc, "Vehicle Dynamics and External Disturbance Estimation for Vehicle Path Prediction", *IEEE TRANSACTIONS ON CONTROL SYSTEMS TECHNOLOGY*, MAY 2000, VOL. 8, NO. 3, pp.508~518;
48. F. Frendo, G. Greco, M. Guiggiani and A. Sponziello, "The handling surface: a new perspective in vehicle dynamics", *Vehicle System Dynamics*, 2007, Vol. 45, No. 11, pp.1001–1016;
49. M. Bouazara, M. J. Richard and S. Rakheja, "Safety and comfort analysis of 3-D vehicle model with optimal non-linear active seat suspension", *Journal of Terramechanics,* 2006, 43, pp. 97–118;
50. C. Kim and P. L. Ro, "An Accurate full car ride model using model reducing techniques", *Journal of Mechanical Design*, 2002, Vol. 124, pp. 697-706;
51. S.-L. Koo, H.-S. Tan and M. Tomizuka, "Impact of Tire Compliance Behavior to Vehicle Longitudinal Dynamics and Control", *Proceedings of the 2007 American Control Conference*, Marriott Marquis Hotel at Times Square, New York City, USA, July 11-13, 2007;
52. M. Azman, P. D. King and H. Rahnejat: "Combined bounce, pitch, and roll dynamics of vehicles negotiating single speed bump events". *Proc. IMechE Part K: J. of Multi-body Dynamics*, 2007, Vol. 221, pp. 33-40;
53. H. E. Tseng, L. Xu and D. Hrovat, "Estimation of land vehicle roll and pitch angles", *Vehicle System Dynamics*, 2007, Vol. 45, No. 5, pp.433-443;
54. J. Song, "Performance evaluation of a hybrid electric brake system with a sliding mode controller". Mechatronics, 2005, 15, pp.339–358;

55. C. Ghike, T. Shim, and J. Asgari, “Integrated control of wheel drive–brake torque for vehicle-handling enhancement”. *Proc. IMechE, Part D: J. of* Automobile Engineering. 2009, Vol. 223, pp.439-457;

56. J. He, D. Crolla, M. Levesley and W. Manning, “Integrated active steering and variable torque distribution control for improving vehicle handling and stability”. SAE, 2004-01-1071;

57. T. Shim, and D. Toomey, “Investigation of active steering/wheel torque control at the rollover limit manoeuvre”. SAE, 2004-01-2097;

58. T. Shim and G. Ghike, “Understanding the limitations of different vehicle models for roll dynamics studies”. *Vehicle System Dynamic*, 2007, Vol. 45, No. 3, pp. 191–216;

59. T. Day, S. Roberts and A. York, SIMON: a new vehicle simulation model for vehicle design and safety research. SAE, 2001-01-0503;

60. D. Moline, S. Vaduri and E. H. Law, “Fidelity of Vehicle Models Using Roll Center Principles”, SAE 2000-01-0693.

61. M. Prado *et. a.*, “Bus handling analysis and experimental validation using the multibody system technique*”*, SAE technical paper series, 2001-01-3966;

62. Sancibrian, Ramon, Garcia, Pablo, Viadero, Fernando, Fernandez, Alfonso and De-Juan, Ana (2009) 'Kinematic design of double-wishbone suspension systems using a multiobjective optimisation approach', *Vehicle System Dynamics*, First published on: 09 December 2009 (iFirst)

63. S.-S. Kim and W. H. Jeong, “Real-time multibody vehicle model with bush compliance effect using quasi-static analysis for HILS”, Multibody Syst Dyn, 2009, 22: 367–382

64. K. Hussain, H. Rahnejat and S. Hegazy, “Transient vehicle handling analysis with aerodynamic interactions”, *Proc. IMechE, Part K: Journal of Multi-body Dynamics*, 2007, Vol. 221, pp.21-32;

65. T. Shim and P. C. Velusamy, “Influence of Suspension Properties on Vehicle Roll Stability”, SAE 2006-01-1950;

66. F. Yu and Y. Lin, “Vehicle System Dynamics” (Chinese), *China Machine Press*, 2005;

67. Gillespie, T.D, ‘Fundamentals of vehicle dynamics’. *SAE Inc.*, 1992, PA, USA;

68. R. S. Sharp and C. Pilbeam, “Achievability and value of passive suspension designs for minimum pitch response”, *Proc. IMechE Conference on Vehicle Ride and Handling*, 1993, London, UK, pp.243-259;

69. M. C. Odhams and D. Cebon, “An analysis of ride coupling in automobile suspensions”, *Proc Instn Mech Engrs, Part D: J Automobile Engineering*, 2006, Vol. 220, pp.1041-1061;

70. J. Edelmann and M. Plöchl, “Handling characteristics and stability of the steady-state powerslide motion of an automobile”, Regular and Chaotic Dynamics, Vol. 14, No. 6, pp.682-692;
71. N. Yu, S. Muthiah and B. T. Kulakowski, “The handling characteristics of a transit bus”, *Int. J. Vehicle Systems Modelling and Testing*, 2007, Vol. 2, No. 2, pp.138-152;
72. T. W. Chu and R. P. Jones, “Analysis and simulation of nonlinear handling characteristics of automotive vehicles with focus on lateral load transfer”, *Vehicle System Dynamics*, 2007, Vol. 46, sppl., pp.17–31;
73. G. Mavros, “On the objective assessment and quantification of the transient-handling response of a vehicle”, *Vehicle System Dynamics*, 2007, Vol. 45, No. 2, pp.93–112;
74. T. W. Chu and R. P. Jones, “Analysis and simulation of nonlinear handling characteristic of automotive vehicles with focus on lateral load transfer”, *Vehicle System Dynamics*, 2007, Vol. 46, sppl., pp:17-31;
75. S. Lukowski, M. Momot, D. Kraemer, and D. Kunz, “Basic linear theory of handling and stability of automobiles”, *Proc. IMechE, Part D: J. Automobile Engineering*, 2009, Vol. 223, pp.1-10;
76. K. B. Arıkan, Y. S. Ünlüsoy, I. Korkmaz and A. O. Çelebi, “Identification of linear handling models for road vehicles”, *Vehicle System Dynamics*, 2008, Vol. 46, No. 7, pp. 621 – 645;
77. F. Frendo, G. Greco and M. Guiggiani, “Critical review of handling diagram and understeer gradient for vehicles with locked differential”. *Vehicle System Dynamics*, 2006, Vol. 44, No. 6, pp.431–447;
78. Lutz, J. Rauh and W. Reinalter, “Developments in vehicle dynamics and the tire model performance test”, *Vehicle System Dynamics*, 2007, Vol. 45, Suppl. pp.7–19;
79. K.B. Arıkan *et. al*., “Identification of linear handling models for road vehicles”, *Vehicle System Dynamics*, 2008, Vol. 46, No. 7, pp.621-645;
80. M. Blundel and D. Harty, “The multibody systems approach to vehicle dynamics”, *ELSEVIER Butterworth Heinemann*, 2004;
81. V. Harth *et. al.*, “A Modelling Approach to Tire-Obstacle Interaction”, *Multibody System Dynamics*, 2000, 11, pp. 23–39;
82. P.W.A Zegelaar and H.B. Pacejka, “The In-Plane Dynamics of Tyres on Uneven Roads”, *Vehicle System Dynamics*, 1996, Suppl. 25, pp. 714-730;
83. V. Harth *et. al.*, “A Modelling Approach to Tire-Obstacle Interaction”, *Multibody System Dynamics*, 2000, 11, pp.23–39;

84. S. Kim, P E. Nikravesh and G. Gim, “A two-dimensional tire model on uneven roads for vehicle dynamic simulation”, Multibody System Dynamics, 2004, 11, pp. 23–39;
85. S. Chae *et. al*., “Dynamics response predictions of quarter-vehicle models using FEA and rigid ring truck tire model”, *Proceedings of IMECE2006 2006 ASME International Mechanical Engineering Congress and Exposition*, November 5-10, 2006, Chicago, Illinois, USA;
86. W. Liang, J. Medanic and R. Ruhl: “Analytical dynamic tire model”, *Vehicle System Dynamics*, 2008,Vol. 46, No. 3, pp. 197–227;
87. E.Velenis, P.Tsiotras, C. Canudas-de-Wit and M.Sorine, “Dynamic tire friction model for combined longitudinal and lateral vehicle motion”, *Vehicle System Dynamics*, 2005,Vol. 43, No.1, pp. 3–29;
88. H. Pacejka and E. Bakker, “The magic formula tyre model”. *Proc. 1st International Colloquium on Tyre Models for Vehicle Dynamics Analysis*, Delft, The Netherlands, 21-22 October, 1991;
89. H. B. Pacejka, “Tyre and vehicle dynamics”, *Elsevier Butterworth-Heinemann*, 2002.
90. N. Balaramakrishna and R. K. Kumar, “A study on the estimation of SWIFT model parameters by finite element analysis”, *Proc. IMechE Part D: J. Automobile Engineering*, 2009,Vol. 223, No. 10, pp.1283-1300;
91. M. Gipser, “FTire – the tire simulation model for all applications related to vehicle dynamics”, Vehicle System Dynamics, 2007, Vol. 45, Suppl, pp.139–151;
92. J. Rauh and M. Mössner-Beigel, “Tyre simulation challenges”, *Vehicle System Dynamics*, 2008,Vol. 46, Supplement, pp.49–62;
93. H. Haga, “Evaluation of tyre models for durability loads prediction using a suspension-on-a-drum environment”, *Vehicle System Dynamics*, 2005, Vol. 43, Suppl, pp.281–296;
94. S. Chae *et. al.*, “Dynamic response predictions of quarter-vehicle models using FEA AND rigid ring truck tire models”, *Proceedings of ASME International Mechanical Engineering Congress and Exposition*, November 5-10, 2006, Chicago, Illinois, USA, IMECE2006-13365;
95. Frazer-Nash Consultancy Limited, “Fork lift truck validation and trials”, *Health and Safety Executive 2006*, 2006;
96. C-K. Chae et al, “A feasibility study on indirect identification of transmission forces through rubber bushing in vehicle suspension system by using vibration signals measured on links”, *Vehicle System Dynamics*, 2006, Vol. 33, pp. 327–349;
97. D. C. Davis, “A Radial-Spring Terrain-Enveloping Tire Model”, *Vehicle Systems Dynamics*, V3,

1974, pp.55~69;

98. J. M. Starkey, “The effects of vehicle design parameters on handling frequency response characteristics.” *Int. J. of Vehicle Design*. Vol. 14, No. 5/6, 1993, pp.497-510;

99. Xia, X. and Law, E. H.: “Linearized Analysis of front and four wheel steering automobiles: understeer, oversteer and handling qualities.” *American Society of Mechanical Engineers, Applied Mechanics Division, Transportation Systems. 1990,* v.108, pp.9-18;

100. J. J. Zhu, A. Khajepour and E. Esmailzadeh, “Pitch dynamic study of a vehicle with a planar suspension system”, *Int. J. Vehicle Systems Modelling and Testing*, 2010, Vol. 5, No.1, pp.18–34;

101. C. Canudas-de-Wit, P. Tsiotras, E. Velenis, M. Basset and G. Gissinger, “Dynamic friction models for road/tire longitudinal interaction”, *Vehicle System Dynamics*, 2003, Vol. 39, No. 3, pp.189–226;

102. A. Eichberger and W. Rulka, “Process Save Reduction by Macro Joint Approach: The Key to Real Time and Efficient Vehicle Simulation”, *Vehicle System Dynamics*, 2004, Vol. 41, No.5, pp.401 – 413.

Appendix A

Definitions of Suspension Kinematics and Compliance (K&C) Characteristics

1. **Camber angle**: the angle measured in the front elevation between the wheel plane and the vertical;
2. **Caster angle**: the angle measured in the side elevation between the steering (kingpin) axis and the vertical;
3. **Toe angle**: the angle measured in the top elevation between the longitudinal axis, *x*, of the vehicle and the line of intersection of the wheel plane and the road surface;
4. **Kingpin Inclination angle**: the angle measured in the front elevation between the steering (kingpin) axis and the vvertical.
5. **Ride rate**: the spring rate of the suspension relative to the body, measured at the tire contact patch. It is different from the "wheel rate" which is defined as the vertical stiffness of the suspension relative to the body, measured at the wheel center. Ride rate is the equivalent rate of the wheel rate and tire rate.
6. **Afore-aft wheel center stiffness:** The stiffness of the suspension in the fore-aft direction relative to the body, measured at the wheel center.
7. **Scrub radius**: the lateral distance in the *y* direction from the point at the intersection of the steering axis (the kingpin axis) and the ground plane, to the line of intersection of the wheel and ground planes.